Thermal Spray of a Drug Delivery System onto Femoral Orthopaedic Implants

Ahmed Chebbi, B.Eng

A thesis submitted in fulfillment of the requirement for the degree

of

Doctor of Philosophy

Supervisor:

Dr Joseph Stokes

School of Mechanical and Manufacturing Engineering

Dublin City University, Ireland

Declaration

I hereby certify that this material, which I now submit for assessment on the programme of study leading to the award of Doctor of Philosophy is entirely my own work, that I have exercised reasonable care to ensure that the work is original, and does not to the best of my knowledge breach any law of copyright, and has not been taken from the work of others save and to the extent that such work has been cited and acknowledged within the text of my work.

Signed: I.D. Number: 53145631 Date: 11/07/2011

Dedication

TO MY BELOVED MOTHER&FATHER

The source of all the good in me

Acknowledgements

First and above all, praise is due to almighty Allah for His everlasting blessing and guidance in conceptualising, developing and completing this project.

I am to the highest degree thankful to my supervisor Dr. Joseph Stokes for his continual support and guidance throughout the duration of this work. His innovative ideas, constructive comments, suggestions and advice throughout the project were much appreciated. I was very fortunate to have been able to work with him since undertaking my final year project degree.

I very much thank the assistance of all the staff in the School of Mechanical and Manufacturing Engineering, in particular Michael Tyrell for the technical support provided throughout the course of my PhD. I extend my gratitude to the staff of other schools and research centers for their technical support on a number of characterisation techniques. I also greatly appreciate the support provided by many of the researchers in the department, in particular the invaluable advice and suggestions of Dr Khaled Ben Younis on the Design of Experiments work. Thanks also to Finbarr O'Sullivan in the National Institute for Cellular Biotechnology for assistance with the *in vitro* experimental work.

I genuinely show gratitude to all my friends and colleagues in DCU for their encouragement and support, in particular Elena Irina Pascu for the numerous scientific discussions during the last year of my work. I cannot forget to be grateful to my office mates Tuty, Aqida, Shadi, Joe and Jack for creating a perfectly pleasant study environment. Thank you as well to my good friend Melanie Braune for all the tedious proof reading.

I offer heartfelt thanks to my loving wife, Faten Ben Ezzedine for her love, continued patience, encouragement and understanding especially during the last stage of my PhD. Special thanks to my family in Tunisia who always believed in me.

Finally, I would like to acknowledge the financial support provided by the Irish Research Council for Science, Engineering and Technology, funded by the National Development Plan, which made this project possible.

Contents

List of Figures

List of Tables

Nomenclature

ALP	Alkaline Phosphatase
Ar	Argon
Ca	Calcium
DDS	Drug Delivery System
DoE	Design Of Experiments
DTA	Differential Thermal Analysis
EMAA	Ethylene Methacrylic Acid Copolymer
FTIR	Fourier Transform Infra-Red spectroscopy
H_2	Hydrogen
He	Helium
N_2	Nitrogen
Ti	Titanium
HA	Hydroxyapatite
P	Phosphate
PCL	Polycaprolactone
PDLLA	Poly-DL-Lactide
PHB	Polyhydroxybutyrate
PHV	Polyhydroxyvalerate
PMMA	Polymethylmethacrylate
Ra	Roughness
SCFH	Standard Cubic Feet per Hour
SE	Secondary Electrons
SEM	Scanning Electron Microscopy
TGA	Thermograviometric Analysis
THA	Total Hip Arthroplasty
UV	Ultra violet
VP	Variable Pressure
XRD	X-Ray Diffraction

Abstract

Thermal Spray of a Drug Delivery System onto Femoral Orthopaedic Implants

Ahmed Chebbi

Hydroxyapatite bioceramics are proven to be good materials for bone replacement and repair applications, due to their similarity in chemical composition to bone. Plasma spraying has been commonly used to apply hydroxyapatite coatings onto metallic implants for use in orthopaedic surgeries. The addition of HA coatings was successful in improving the performance of titanium implants. However, this type of implant has shown some limitations with regards to mechanical (implant loosening) and biological (infections) behaviour. It is thought that local drug delivery would be useful to prevent implant failures that could be treated with therapeutic agents (drug/growth factor). It is hypothesised in this work that polymers proven in drug delivery for other applications could be successfully applied to implants using existing technology in the sector. This research aims to introduce biodegradable materials (polymers) to the existing HA-titanium combination and to bare titanium implants in order to act as a drug-delivery vehicle. The proposed materials (PCL, PMMA and PHBV) consisted of biodegradable and non-biodegradable polymers (used separately or as a composite) that are widely used as drug delivery systems. The method used to apply these drug delivery systems in this project was flame spraying, due to its superior mechanical advantages over other techniques. Taking into account the thermal sensitivity of the chosen polymers and the high process temperature generated by the process, the mains challenges of this study were to obtain viable coatings with regards to all coating properties (chemical, physical, biological) and to control the mechanical characteristics of such coatings by varying the process parameters. Screening tests were conducted to determine the spraying parameters suitable for each polymer, followed by a more thorough Design of Experiments analysis to understand the relationship between three process factors: traverse speed, number of passes and spraying distance, and four coatings properties: thickness, roughness, adhesion and wettability. Chemical, physical, physiological and biological tests were also performed in order to study the suitability of the proposed polymers for such an application. The optimal process parameters to spray the PCL and PHBV matrices were: traverse speed of 0.152 m/s and 0.33 m/s, spraying distance of50 cm and 42.5 cm number of passes of 6 and 14, respectively. Viable polymer composites were obtained with the optimised spraying parameters on bare titanium and on HA coatings. These polymer coatings were not chemically damaged following flame spraying and all physiological and biological indicators suggested that the deposition technique used in this project is well suited for applying polymeric materials on orthopaedic implants for use as bioactive and drug delivery systems.

1 Introduction

The most commonly used synthetic material for bone attachment is Hydroxyapatite (HA). Plasma spraying has been traditionally used to spray HA, which is a bioactive material used mainly because of its calcium to phosphorous ratio being similar to that of bone. However, HA's brittleness and low strength limits its applications in hard tissue implants.

Postoperative complications following total hip replacement are quite frequent; the most common cause of THA failure is aseptic loosening, with infection being the next common cause [1]. Patients receiving orthopaedic prostheses are also at risk of septic arthritis, deep bacterial infections involving implants and bacteraemia [2]. Implant related osteomyelitis has also increased with the increase of joint replacement surgeries. Particularly for the latter, conventional infection treatment was deemed unsuccessful due to the bacterial glycolyx around the non-living bone or material [3]. Generally, increasing evidence suggests that microbial adhesion and subsequent colonisation leading to biofilm development are involved in the aetiology of device-related infections [4, 5]. Continuous delivery of antibiotics appears to be an effective approach to kill bacteria during early stages of colonisation [6]. Therefore, HA coated titanium implants could benefit greatly from an integrated polymer layer acting either as a drug delivery system (for antibiotics, bone growth factors, and so on) or even as bone regenerative agent. In a well-integrated implant in bone, the healing process that takes place immediately after the implantation, leads to a reorganisation and a regeneration of a bone-like structure at the interface [7]. Biodegradable polymers offer the advantage of extending this bone regeneration to the inner parts of the implant.

Recently, attention has been given to the application of HA in combination with polymers. The concept of using polymers as binders for particulate bio-ceramics is to produce composites with improved handling and retention characteristics and to overcome the problem of brittleness associated with ceramic bone repair implants. Due to its osteoconductivity and biocompatibility, HA can be combined with biodegradable polymers to provide drug delivery system (DDS) functionality. Some biodegradable polymers such as polycaprolactone (PCL) and poly lactic acid (PLA) have been found to have potential applications for bone, cartilage repair and also drug delivery. Several other biodegradable

materials (polymers) can be used; including polyhydroxybutyrate (PHB) and its copolymer polyhydroxyvalerate (PHV), polyglycolic acid (PGA), and polymethylmethacrylate (PMMA). Biodegradable materials have the advantage of allowing new tissue to take over load-bearing or other functions without any of the potential chronic problems associated with the presence of bioactive implants. By degrading over time, such polymer coatings can be used to deliver drugs and growth factors to the implantation site and therefore avoid the need to remove the drug carrier.

The main objective of this research was to investigate whether drug-delivery polymers could be incorporated in implant design, using existing technologies. Specifically, this requires the understanding of the relationship for specific drug-delivery polymers between the thermal spraying process parameters (spraying distance, number of passes, traverse speed) and the coating properties (thickness, roughness, adhesion, wettability) in order to be able to control the characteristics of the coatings and customise them according to the desired final application of the implant coating (load-bearing or not). In fact, there is no report of PCL previously sprayed for a drug delivery application and PHBV has never been thermally sprayed. This process investigation stage led to the development of process models for three of the four responses initially investigated. The statistically significant models were then used to optimise the process in order to obtain coatings with high roughness and adhesion, two of the most important factors for orthopaedic coatings.

The newly produced polymer coatings would have a mechanical requirement for adhesion to a base HA coating or bare titanium surface on one side and to encourage cell adhesion on the other side. The aim is to obtain thermally sprayed bio-deposits which will act both mechanically and biologically (as DDS) to accommodate cells and to enhance their growth and tissue regeneration.

The development of such a DDS represents the first step towards the production of the final product. It proves that such a system can effectively be produced from biodegradable polymers, using thermal spraying, in order to obtain superior coating biological and mechanical performances. The following phase of the project would be the drug-polymer attachment and drug release kinetics development. The final product would undoubtedly improve the therapeutic recovery of the patient's post-surgery and to extend the life of the

implant through the use of slow releasing regenerative drugs at the source, a feature that is needed for the treatment of post-operative infections and complications. This research investigates many questions notably the most important being:

- Would the thermal spray process affect the thermal behaviour of the polymer?
- Would the bioactive properties of the coatings be compromised?
- Can polymers be incorporated onto HA coatings via thermal spraying?

1.1 Objectives of the Research Project

The specific objectives of this research project were:

- Phase 1: To identify, analyse, and understand the relationship between a number of flame spraying process parameters and the important coating properties, through the development of process models (using a statistical technique) that relates process variables to relevant coating responses for two biodegradable polymer-based matrices.
- Phase 2: Using the developed models, to optimise the process and to produce novel pure biodegradable polymer coatings, with good physical, chemical and biological properties that offer the potential for improved *in vivo* performance, using the flame spraying technique.
- Phase 3: Using the process models developed during this research project for polymers, and process models previously developed in-house for bioceramics, to produce novel bi-layer coatings with good physical, chemical and biological properties that offer the potential for improved *in vivo* performance, using the flame spraying technique to deposit polymeric materials on previously plasma sprayed hydroxyapatite coatings.

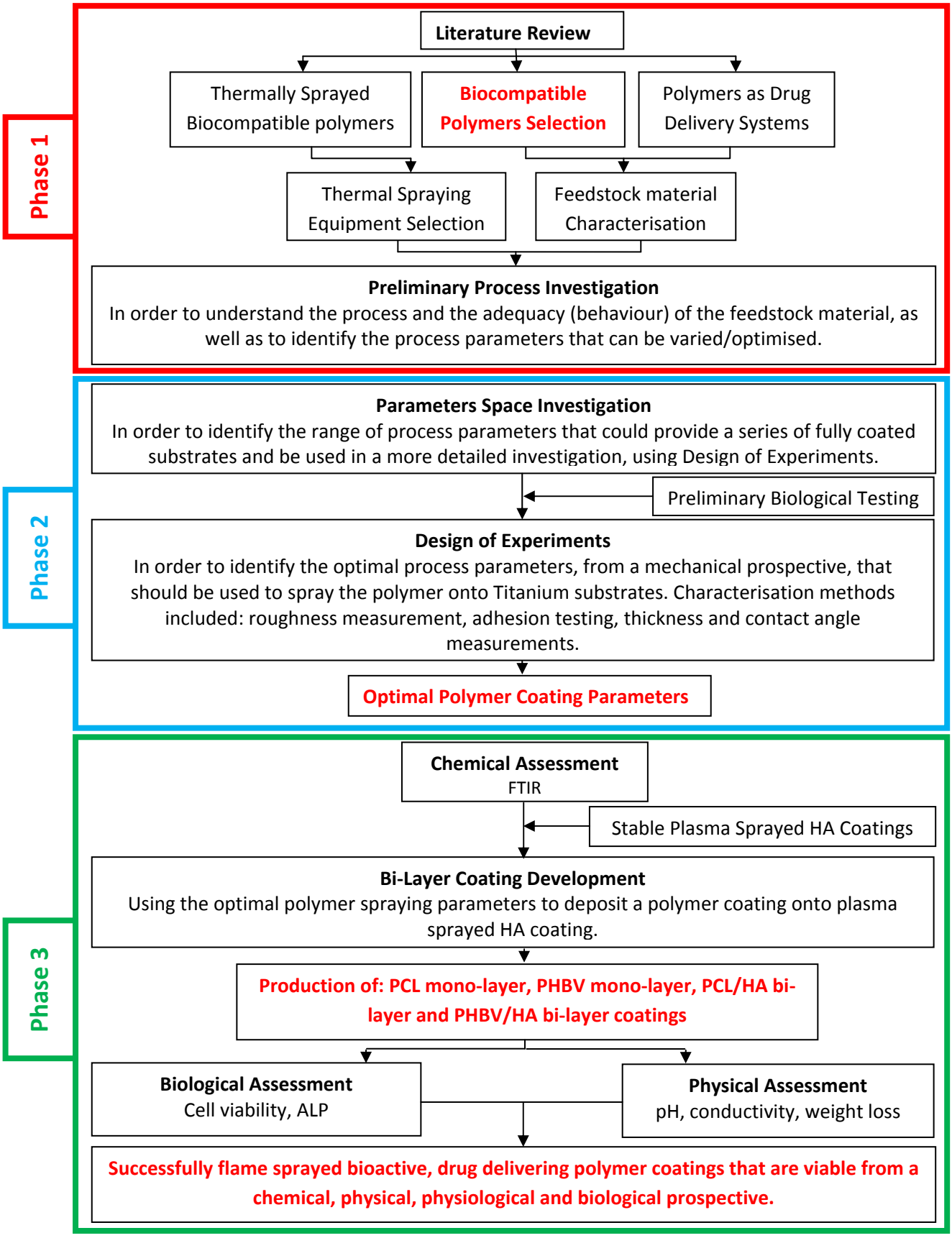
Phase 1
Literature Review
Thermally Sprayed Biocompatible polymers
Biocompatible Polymers Selection
Polymers as Drug Delivery Systems
Thermal Spraying Equipment Selection
Feedstock material Characterisation
Preliminary Process Investigation
In order to understand the process and the adequacy (behaviour) of the feedstock material, as well as to identify the process parameters that can be varied/optimised.
Phase 2
Parameters Space Investigation
In order to identify the range of process parameters that could provide a series of fully coated substrates and be used in a more detailed investigation, using Design of Experiments.
Preliminary Biological Testing
Design of Experiments
In order to identify the optimal process parameters, from a mechanical prospective, that should be used to spray the polymer onto Titanium substrates. Characterisation methods included: roughness measurement, adhesion testing, thickness and contact angle measurements.
Optimal Polymer Coating Parameters
Phase 3
Chemical Assessment
FTIR
Stable Plasma Sprayed HA Coatings
Bi-Layer Coating Development
Using the optimal polymer spraying parameters to deposit a polymer coating onto plasma sprayed HA coating.
Production of: PCL mono-layer, PHBV mono-layer, PCL/HA bi-layer and PHBV/HA bi-layer coatings
Biological Assessment
Cell viability, ALP
Physical Assessment
pH, conductivity, weight loss
Successfully flame sprayed bioactive, drug delivering polymer coatings that are viable from a chemical, physical, physiological and biological prospective.

1.2 Structure of the Thesis

This thesis was structured over a number of chapters as follows.

Chapter 2 presents a complete and detailed review of literature. This chapter introduces the present implant coatings technology and processing techniques. Thermal spraying is explained in detail. Biodegradable polymers previously used as drug delivery systems are comprehensively discussed, with focus given to the polymers used in this project: PCL, PMMA and PHBV. Thermal spraying of some (non-degradable) polymers is explained, showing the challenges of using the flame spraying technique with the polymeric class of materials. Finally, the Design of Experiments technique is introduced.

Chapter 3 reviews the feedstock materials, processing, and characterisation techniques, and equipment used. The flame spraying and plasma spraying equipment used in this work is presented, along with the operating procedures followed for both ceramics and polymers spraying. Finally, every powder and coating characterisation and testing procedure has been outlined and thoroughly discussed. These include statistical analysis methods and procedures as well as mechanical, chemical, physiological, physical and biological testing.

Chapter 4 presents the results and discussions in a systematic and consistent manner. All feedstock materials are characterised and discussed in the first section of Chapter 4. This is followed by the results of a preliminary process investigation discussing how the newly acquired equipment was used with the powders chosen. A more thorough screening stage was performed and discussed with the aim of identifying the ranges of process parameters that could be varied during the optimisation phase. The latter stage was designed using statistical software (Design Expert 7), where the coatings were characterised and the results were used to obtain an optimised set of spraying parameters which allows the spraying of optimised polymer coatings on bare titanium and on HA coated titanium implants.

Finally, the conclusions drawn from this work and the recommendations for future research are presented in chapter 5.

2 Literature Review

2.1 Bone Structure

Bone is a complex and dynamic living tissue, continually engaging in a process called remodelling: the construction of new bone tissue and breaking down of old bone tissue [8]. Bone is a composite made of cells (osteoblasts, osteoclasts and osteocytes), organic elements such as collagen and polysaccharides (for high tensile and flexural bone strength), and inorganic apatite crystals (for stiffness and high compressive strength) [9]. Bone structure is hierarchically organised, which means that bone displays different structural entities at different length scales.

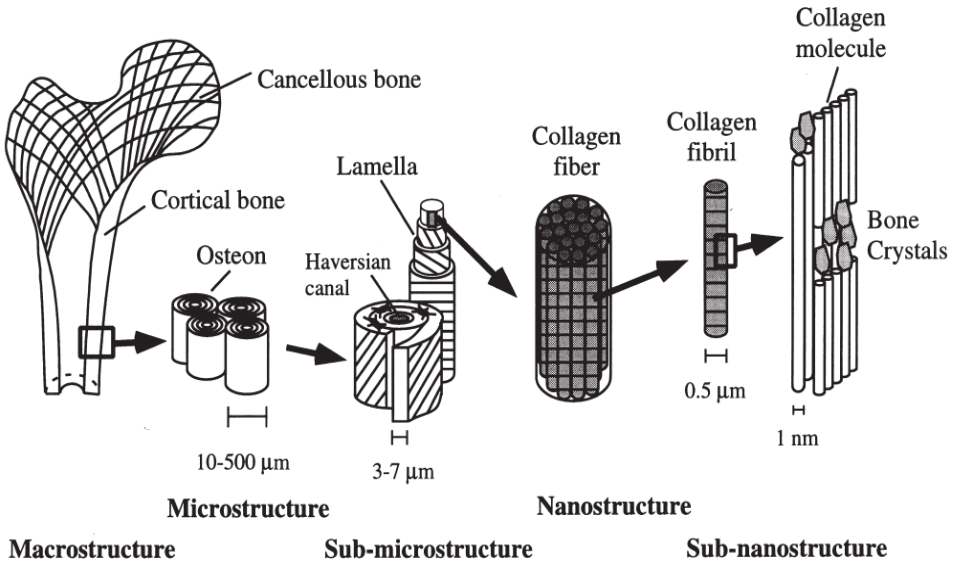

Figure 1: Hierarchical structural organisation of bone [10]

At the macrostructure level, bone is distinguished into the cortical and cancellous types (Figure 1). In cross-section, the end of a long bone, such as the femur, has a dense cortical shell with a porous, cancellous interior. Cortical (compact) bone contains a few spaces and constitutes the strongest form of bone tissue. It is found beneath the periosteum of all bones and makes up the bulk of the diaphyses of long bones [8]. Compact bone provides protection and support and resists the stresses produced by the weight and movement of the human applying it.

Cancellous (spongy) bone does not contain oseteons, in contrast to compact bone. Spongy bone consists of lamellae arranged in an irregular lattice of thin columns called trabeculae. Cancellous bone makes up most of the bone tissue of short, flat, and irregularly shaped bones [8]. Cancellous bone material is generally much more metabolically active; it is remodelled more often than cortical bone, and is therefore 'younger' on average than cortical bone [10]. As a result, even though cancellous and cortical bones may be of the same kind of material, the maturation of the cortical bone material may alter the mechanical properties at the microstructural level.

The mechanical properties of human cortical bone from the tibia, femur, and humerus have been found to vary between subjects, although the density remains the same. In human spongy bone, by contrast, there is no difference in the mechanical properties of the humerus, the proximal tibia, and the lumbar spine [10]. The mechanical properties of cortical bone are much higher than those of spongy bone, such as Young's modulus (0.01-3GPa for spongy bone versus7-30 GPa for cortical bone).A number of factors influence the mechanical properties of cortical bone such as the porosity, the mineralisation level and the organisation of the solid matrix. Typical mechanical properties of human cortical and spongy bone properties are shown in Table 1.

Table 1: Mechanical properties of human femoral (cortical) bone (adapted from [11, 12]**)**

Mechanical properties	Test direction related to bone axis for cortical bone		Spongy bone
	Parallel	**Normal**	**-**
Tensile Strength (MPa)	124-174	49	1.5-20
Compressive Strength (MPa)	170-193	133	2-12
Young's Modulus (GPa)	17-18.9	7-30	0.01-3
Fracture Toughness (MPa $m^{1/2}$)	2-12	8	2
Bending Strength (MPa)	160	-	10
Yield Tensile Strain	0.007	0.004	-
Yield Compressive Strain	0.010	0.011	-

Compact bone composes approximately 80-85% of the human skeleton. It is densely mineralised (80-90%) and thus provides significant mechanical strength and protection [13].

2.2 Orthopaedic Hip Implants

2.2.1 Hip Replacement: An Overview

Orthopaedics is the branch of medicine that deals with the human body's musculoskeletal system. Due to their load bearing functions, hip and knee joints are more prone to fractures and diseases than other parts of the skeletal system. In fact, many degenerative diseases or injuries can impair the normal function of the hip joint leading to pain, muscle weakness and limited movement of the joint. In the past few decades, improved standard of living and healthcare have extended the average life expectancy; as a result, an increasing number of people suffer the pain and loss of mobility associated with degenerative joint diseases. Arthritis is one of the most common causes of hip and knee disorders. The number of people affected by this condition is an estimated 46 million adults in the United States alone [14]. Many types of arthritis exist including osteoarthritis and rheumatoid arthritis. Other joint diseases which may lead to joint replacement include avascular necrosis, osteonecrosis and Paget's disease. Most of these degenerative diseases will eventually require surgery to replace one or both of the damaged surfaces of the hip joint using prosthetic components. The hip joint is a ball and socket joint consisting of two bones, the femur (with its head acting as the ball) and the pelvic girdle (with its acetabulum acting as the socket). Replacement of one half of the joint is known as hemiarthroplasty, whereas replacement of both components is known as Total Hip Arthroplasty (THA) or Total Hip Replacement (THR). THA is by far the most successful and widely used procedure in the treatment of diseased hips. The idea that a diseased hip joint could be treated by surgical procedures in the 20^{th} century is not a revolutionary one. In 1891 Thomas Gluck reported the use of ivory for the replacement of the ball and socket joint of the hip [15]. A full history of the development of arthroplasty of the hip using implants has been provided by Scales [16].

Initial design and development in this area was mainly carried out by orthopaedic surgeons [17]. More recently engineers and orthopaedic surgeons have combined their efforts in designing new hip replacement components. The contribution of cutting edge engineering design tools, such as computation stress analysis, has proven to be highly beneficial in the development of superior joint replacement components.

2.2.2 HA-Coated Hip Implants

Designing hip implants is a challenging and interdisiplinary task whereby mechanical, biological and surgical requirements have to be simultaneously satisfied. Over the years, THA gradually imposed itself as the best treatment for bone degenerative diseases affecting hips (Figure 2).

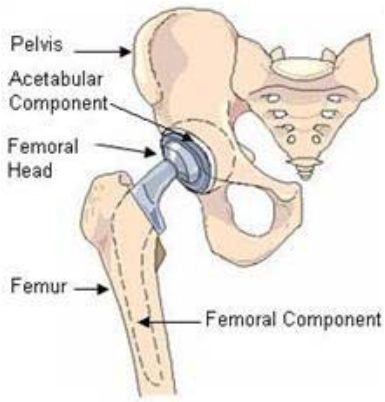

Figure 2: Total hip replacement [18]

In order to restore a normal joint movement, the design of a hip implant must mimic the human hip joint as close as possible. Total hip implants are composed of a femoral component, which fits into the femoral cavity (medullary canal) and an acetabular component which fits into the pelvic socket. The components have two mechanically based functions; to provide for an adequate range of motion and to transfer the joint load onto the bone [13]. Total hip implants could be fixed in place by using a cement (mostly PMMA) to hold the prosthesis in place or by relying on the interaction at the implant-bone interface (bone attachment) for a cementless fixation. Femoral and acetabular components come in different lengths and sizes in order to accommodate patients' anatomical variations. Choosing the correct implant geometry is the first step of a THA and therefore requires thorough preoperative planning. This step is also important in order to decide on the adequate surgical approach and technique to be used. The posterolateral approach is commonly used, with the patient in a lateral (side) position and a posterior dislocation of the hip [19]. The first step in inserting the acetabular component is to dislocate the femoral head from the pelvic acetabulum. The cartilage is then removed from the acetabulum using

a series of special reamers [17]. The smallest size reamer is used first and the size is increased until the acetabular component fits well in the acetabulum and sufficient cancellous bone is exposed. The femoral component is inserted by sectioning the femoral neck and then using a set of tools (reamers, curettes and broaches) to hollow out the femur and shape out the medullary canal to the desired implant geometry. PMMA cements have been used for many years in surgery [20], however in the past few decades, reports of high radiographic failure rates and osteolysis led to a general dissatisfaction with the use of cement for fixation of total joint replacements [21]. Since then, cementless methods have been developed further.

Bioactive fixation is one of three cementless fixation methods; biological and mechanical fixation being the remaining types. The bioactive method also known as surface active bonding can occur with materials having surface active properties [17]. Bioactive materials are known for their osseointegration properties by eliciting a specific biological response at the interface of the material, resulting in the formation of bond between the tissues and material [22]. Bioceramics and hydroxyapatite coated implants in particular, are the most successful of these bioactive materials and have been widely used in orthopaedics [23, 24] and dentistry [25, 26].

Hydroxyapatite successfully became the first choice for bioceramic coatings in medicine due to its composition being similar to that of the mineral phase of bone and tooth enamel. HA-coated implants combine the strength and ductility of metallic implants with the increased biocompatibility and osteoconductivity associated with hydroxyapatite. The advantages HA-coated implants do offer to orthopaedic applications include; a more rapid fixation and stronger bonding between the host bone and the implant, and increased uniform bone in growth and/or on growth at the bone implant interface [23, 27]. The accelerated bony growth through allowing new bone formation from the side of the original bone as well as from the side of the ceramic coating is known as bilateral osteogenesis [28].

Following the insertion of hip implant into the femur, press-fitting provides primary fixation by wedge-like structures fixing the implant securely within the medullary canal. This process, also known as ‘interperiodicum’ [29], occurs with all cementless prosthesis, regardless of the nature of the surface (metallic or ceramic) and will decrease due to the

formation of a fibrous capsule around the implant until it reaches a level of fixation that is not enough to securely fix the stem [28]. This inevitably leads to loosening of the prosthesis. An HA-coated implant, however, provides a secondary fixation between the coating and the bone by chemical bonding. Furlong et al. [30] concluded that the process of bonding osteogenesis could produce stability which is analogous to primary facture healing in healthy cancellous bone, with its potential of permanent physiological union.

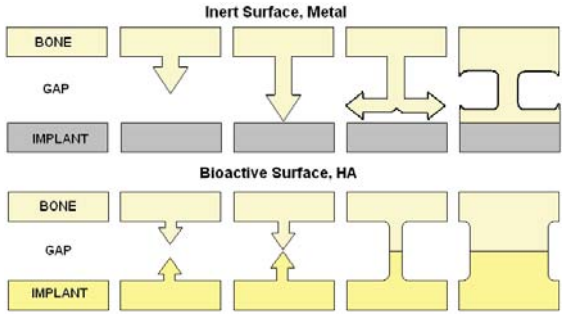

Figure 3: Schematic of bone-implant interface in the case of inert and bioactive surfaces (adapted from [28]**)**

Figure 3compares between bone-implant interface in the case of a metallic implant and an HA-coated metallic implant. In the case of the former, bone growth will only occur unilaterally from the side of the bone surface towards the implant surface with the trabeculae slowly bridging the gap. In the case of HA-coated surfaces, bone grows on both surfaces, closing the gap more rapidly [28, 31]. Additionally, the release of metal ions from the implant is reduced significantly when HA-coated implants are used. Release of these ions triggers an immune response which leads to the formation of a fibrous membrane around the implant. This fibrous layer prevents adequate fixation between the bone and the implant and increases the likelihood of implant failure by reducing the load-bearing capacity of the implant-bone interface. As bone cells grow directly onto the HA coating, a direct chemical bond between the bone and the implant can be formed. Force transmission and mechanical loading conditions play an important role in bone remodelling [32]; this occurs mainly by the direct chemical bonding between HA and bone cells which allow the transfer of forces between the two to occur more efficiently. Bonding of the surrounding bone to the HA coating begins to occur within the first week of implantation [17]. This process is initiated when partial dissolution of the coating starts and calcium and phosphate

ions are released. Proteins and ions activate the surface of the HA coating encouraging the precipitation of HA crystals onto the HA coating, leading to remodelling of the damaged bone.

2.3 Biomaterials

Biomaterials are synthetic materials, which have been designed to mimic the function of a biological material or to induce a specific biological reaction. Biomaterials differ from other classes of materials in their ability to remain in a biological environment without damaging the surroundings and without getting damaged in the process [33]. All biomedical devices/instruments that come in contact with blood or human tissue are made from biomaterials. Depending on specific biomedical application, biomaterials must display the required biological and physical properties. However, the biological properties and behaviour inside the body are more crucial to selecting biomaterials than the mechanical properties. Therefore, the fundamental requirement of any biomaterial concerns its ability to perform effectively with an appropriate host response for the desired biomedical application, that is, the material and the tissue environment of the body (Figure 4) should coexist without having any undesirable or inappropriate effect on each other [34].

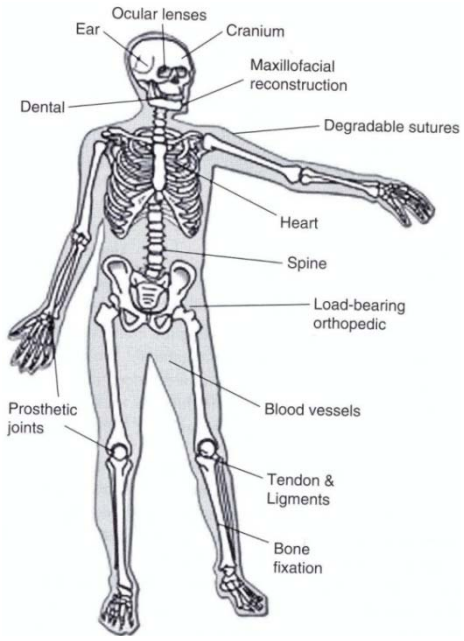

Figure 4: A schematic of the various human body parts, which can be potentially replaced by synthetic biomaterials [34]

Depending on the host response that they trigger, biomaterials properties are classified into three groups: bioinert, bioactive and biodegradable (bioresorbable) (Table 2), with some polymers displaying two of these properties.

Table 2: Biomaterials properties

Biomaterials specifications	Bioinert	Bioactive	Biodegradable
Physiological response	Minimal or no response	Target response	Short/Long term dissolution
Target interaction	Mechanical fixation and support, tissue filling	Chemical reaction	Drug delivery, tissue replacement
Application examples	Bone fixation plates and screws	Bioactive implant coatings	Drug delivery implants, sutures
Biomaterial examples	Titanium	Hydroxyapatite	Polycaprolactone

*Bioinert:*This term refers to any material that once placed in the human body, has minimal interaction with its surrounding tissue and does not release any toxic substance. Examples of these are stainless steel (316L) and titanium alloys (Ti6Al4V). The general mechanism of body response to this type of biomaterials is through a fibrous capsule that might form around the implanted material. Therefore, the biofunctionality of bioinert materials relies on tissue integration through the implant. Most of the materials from this group are used in orthopaedic applications.

Bioactive: This term refers to any material which interacts with the surrounding bone and/or soft tissue, upon implantation within the human body. This interaction occurs through a time dependent kinetic modification of the surface and results in the formation of a biologically active apatite layer on the surface of the implanted material [35]. This layer is chemically and crystallographically equivalent to the mineral phase in bone.

Biodegradable: This term refers to any material that starts to dissolve (resorbed) and is slowly replaced or incorporated by advancing tissue following implantation within the human body. This process varies in duration depending on the type of material and the application. Many of the materials composing this group are polymers (with some bioceramics). Biodegradable materials are very popular as drug delivery systems as they avoid the need for a second operation to remove the drug carriers [36].

2.3.1 Biocompatible Polymers

Biocompatible polymers) are being used in many biomedical as a substitute/support to almost every type of human tissue (Figure 5). Some polymers, however, are more suited to bone applications than others. These include PHB, PCL, PMMA and PHBV. The latter three polymers were used in this project for their successful use as bone replacement materials and features that are explained in the next sections.

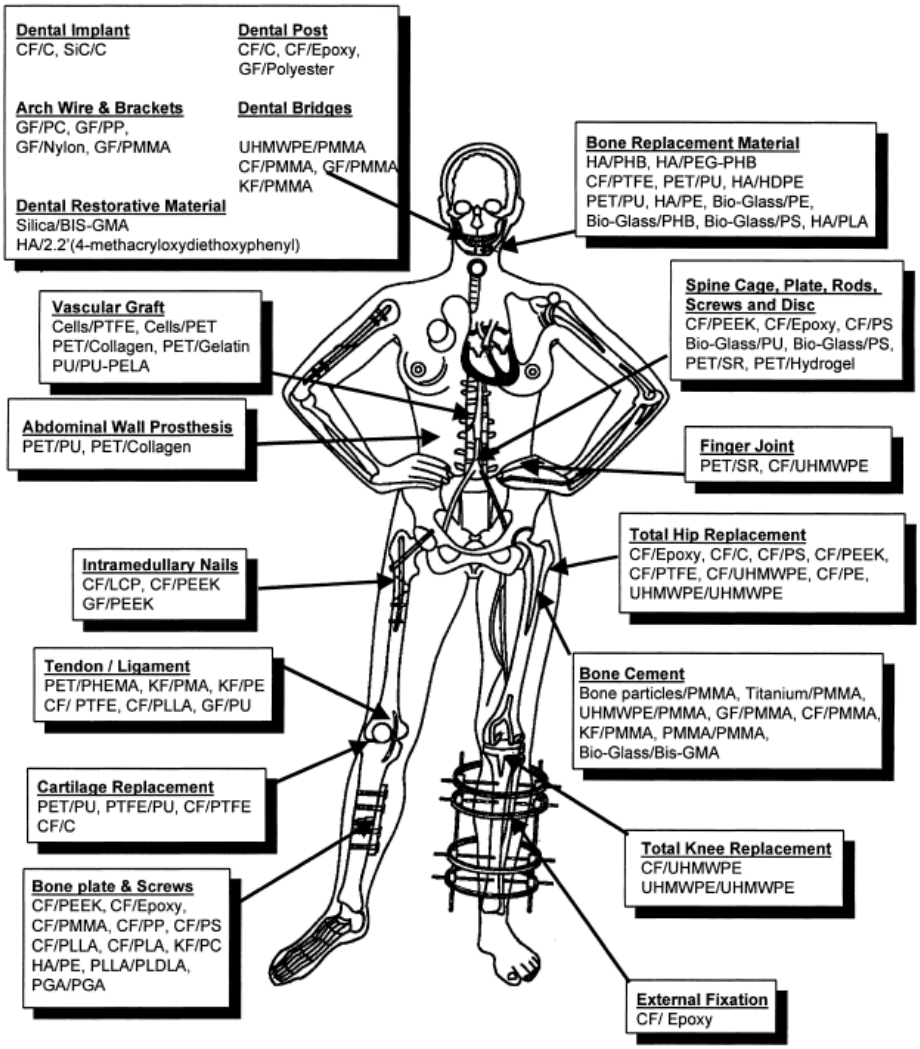

CF: carbon fibers, **C**: carbon, **GF**: glass fibers, **KF**: Kevlar fibers, **PMMA**: polymethylmethacrylate, **PS**: polysulfone, **PP**: poly propylene, **UHMWPE**: ultra-high-molecular weight polyethylene, **PLDLA**: poly(L-DL-Lactide), **PLLA**: poly(L-Lactid acid), **PGA**: polyglycolic acid, **PC**: polycarbonate, **PEEK**: polyetheretherketone, **HA**: hydroxyapatite, **PMA**: polymethyleneterphthalate, **BIS-GMA**: bis-phenol A glycidyl methacrylate, **PU**: polyurethane, **PTFE**: polyetrafluoroethylene, **PET**: polyethyleneterephthalate, **PEA**: poltethylacrylate, **SR**: silicone rubber, **PELA**: block co-polymer of lactic acid and polyethylene glycol, **LCP**: liquid crystalline polymer, **PHB**: polyhydroxybutyrate, **PEG**: polyethyleneglycol, **PHEMA**: poly(20hydroxyethyl methacrylate)

Figure 5: Various applications of different polymer composite materials [37]

2.3.2 Polycaprolactone (PCL)

PCL is a biocompatible, biodegradable, semi-crystalline polymer belonging to the saturated aliphatic polyester group (PGA, PLA, etc.).PCL is prepared by ring opening polymerisation of ε-caprolactone using a catalyst. This polymer melts at 59-64^{o}C with a glass transition temperature (T_g) of -60^{o}C. The crystallinity of the polymer decreases with the increase in polymer molecular weight [38]; polymer with a molecular weight of 5,000 is 80% crystalline whereas the 60,000 polymer is 45% crystalline. The molecular formula of PCL is $C_6H_{10}O_2$(Figure 6).

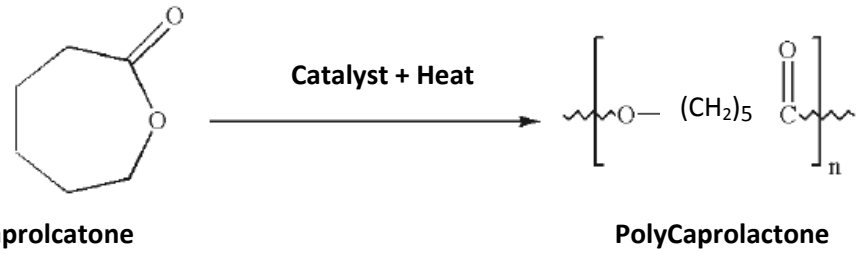

Figure 6: Ring opening polymerisation of Polycaprolactone [38]

PCL degradation, both *in vitro* and *in vivo*, occurs as a bulk process that can be divided into two phases [39]: a hydraulic chain scission inducing a molecular weight loss of up to 5,000, followed by an onset of weight loss. The second phase of degradation is characterised by low molecular fragments and small polymer particles being carried away from the site of the implantation by the solubilisation in the body fluids or by phagocytosis [38]. Complete degradation and elimination of PCL may last for up to 2-4 years, depending on its molecular weight (the larger the molecular weight, the longer the degradation phase). This extended degradation period makes PCL one of the slowest degrading polymers. Its degradation kinetics can be controlled by a number of factors such as crystallinity and porosity [40].PCL is one of the most hydrophobic of all of the commercially available biodegradable polymers. It has good mechanical properties and is widely compatible with various types of polymers (blends, blocks, and so on), which widens its field of applications[41]. As a biocompatible polymer, PCL has shown a non-inflammatory, non-mutagenic response after implantation in animals [38]. However, other studies [42] have shown that there was a moderate inflammation after two weeks of implantation in male wistar rats.

2.3.3 Polymethylmethacrylate (PMMA)

PMMA is a biocompatible polymer from the acrylates group. PMMA is a glassy and atactic polymer, and seeing that its methyl and ester groups cannot be interchanged in a crystal lattice, the material is amorphous and transparent [43]. It has a density of 1.19 g/cm^3 and has very low water absorption. PMMA has a glass transition temperature of 100^{o}C, a melting point of approximately 160^{o}C and a boiling point of 200^{o}C [38], and its molecular formula is $(C_5O_2H_8)_n$ (Figure 7).

PMMA is characterised by a high structural stiffness, along with its glassy nature which can lead to dissipative phenomena when the semi crystalline matrix is subjected to impact [44]. PMMA can be produced through different polymerisation routes. These include, bulk polymerisation, emulsion polymerisation, and solution polymerisation.

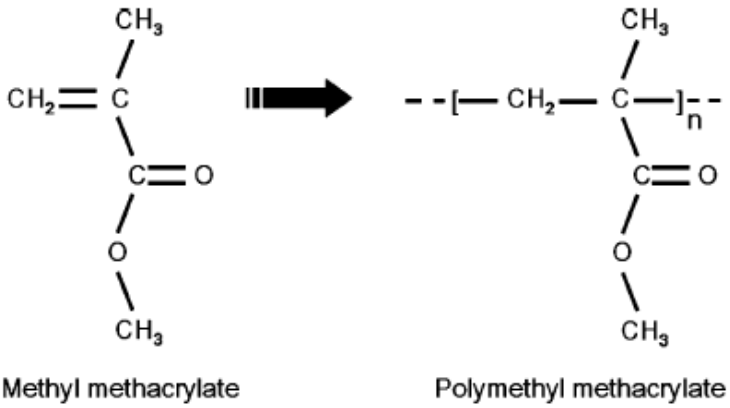

Figure 7: Free radical vinyl polymerisation [45]

Due to its non-degradable and highly biocompatible nature as a polymer, PMMA was widely used in numerous biomedical applications and products from the early stages of biomaterials development, especially in orthopaedics and dentistry. In fact, one of the first uses of PMMA [46] as a biomaterial was for the fabrication of complete denture bases. Since then, having proven its biocompatibility, reliability, low toxicity and versatility, the use of PMMA increased in many areas of biomedical applications. These include intraocular eye lenses, bone cement for implant fixation, bone filling for different cavities and even in cosmetic surgery for wrinkles and scars reduction.

2.3.4 Polyhydroxybutyrate/Polyhydroxyvalerate (PHBV)

PHBV is a copolymer of polyhydroxyalkanotes (PHA). This group of polymers are aliphatic polyesters produced by micro-organism under unbalanced growth conditions. The most common polymer from this group is poly(3-hydroxybutyrate) (PHB). PHB is a semi-crystalline isotactic polymer, has a melting temperature in the range of 160-180^{o}C [47] and a crystallinity ranging from 60 to 90% [48]. In addition to a bacterial synthetic route, several chemical synthetic routes have been developed for PHB synthesis. The main disadvantages of PHB use are due to its tendency to be brittle. This problem can be solved by the synthesis of copolymers of 3- hydroxybutyrate and other hydroxyalkanoates with a relatively low molecular weight and melting point [49] such as the Polyhydroxy valerate (PHV) copolymer.

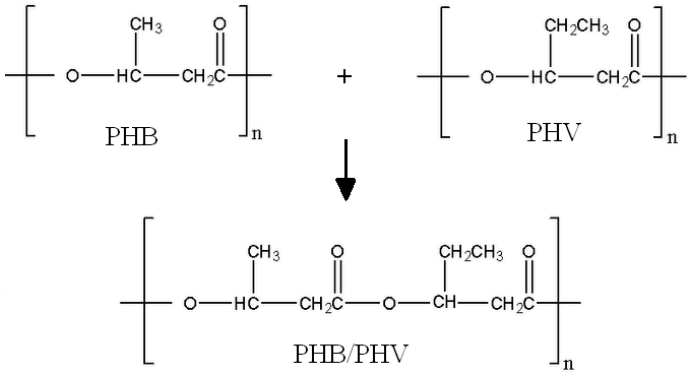

Figure 8: PHBV synthesis

The major advantage of using PHBV copolymer (Figure 8) over the PHB homopolymer is that the copolymer has a lower flexural modulus or level of crystallinity, which makes it tougher and more flexible. The copolymers of PHB and PHBV have similar semi-crystalline properties as PHB alone; however the melting temperature is lower depending on the HV content [50]. The crystallinity and mechanical properties of PHBV can change with the variation of the percentage ratio of the respective monomers [51]. This type of polymers experiences surface erosion, by hydrolytic cleavage of the ester bonds. Copolymers degrade by a multistage process where the greater part of the molecular weight loss occurs before the considerable mass loss [51]. Even though no correlation has been

found between the degradation rate and the amount of PHV in the copolymer, PHBV being less crystalline than PHB undergoes degradation at a much faster rate [50]. This could be explained by the fact that an attack by degrading enzymes is more difficult with highly crystalline polymers [52].

2.3.5 Hydroxyapatite (HA)

HA is a calcium phosphate ceramic being widely used as a biocompatible material for orthopaedic applications. Because of its chemical composition and its artificial origin [28], HA shows no toxicity, no antigenic activity and more importantly no carcinogenic activity. In addition to that, the bone is able to grow on top of the ceramic surface, as if it would be growing on living bone, this is known as osteoconductivity. For the past few decades, calcium phosphate ceramics in general and hydroxyapatite in particular, have been used in dentistry and medicine for applications including dental implants, periodontal treatment, alveolar ridge augmentation, orthopaedics, maxillofacial surgery, and otolaryngology [53].

The chemical formula of HA is $Ca_{10}(PO_4)_6(OH)_2$, with a Ca/P ratio of 1.67, it has crystal hexagonal structure with a space group of $P6_3/m$ (a=b=9.432 Å, c=6.881 Å) [22, 54]. The unit cell contains Ca, PO_4 and OH ions (Figure 9) closely packed together to represent the apatite structure.

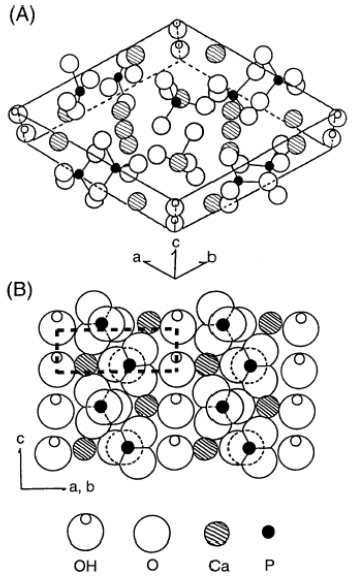

Figure 9: Illustration of a) crystal structure b) ac or bc face of hydroxyapatite [55]

Figure 9 shows how the PO_4 groups acts as the skeletal framework, providing the apatite structure with its chemical stability. OH^- groups can be substituted by either fluoride forming fluoroapatite or chloride forming chloroapatite. The suitability of apatite for ions substitution can be used to modify the hexagonal symmetry and vary the degree of crystallinity or the crystal size which are associated with the increase of stability of the structure and therefore a reduction in solubility [22]. These are essential parameters for tailoring bioceramics to specific biomedical applications.

Various calcium phosphate compounds exist (Table 3). Hydroxyapatite (HA) is of most interest as it is the most similar to the calcium phosphate phase present in bone.

Table 3: Calcium phosphate compounds [56]

Formula	Name	Molar Ca/P	Symbol	Solubility	Acidity	Thermodynamic Stability
$Ca(HPO_4).H_2O$	Dicalcium phosphate dihydrate	1.0	DCPD	+++++	+++++	+
$Ca_4H(PO_4)_3$	Octacalium phosphate	1.33	OCP	++++	++++	++
$Ca_9H(PO_4)_6$	Amorphous calcium phosphate	1.3-1.5	ACP	+++	+++	+++
$Ca_3(PO_4)_2$	Tricalcium phosphate	1.5	TCP	++	++	++++
$Ca_{10}(PO_4)_6(OH)_2$	Hydroxyapatite	1.67	HA	+	+	+++++

These calcium phosphate phases have chemically been well characterised and have not been reported to cause foreign body reactions or other forms of chronic inflammatory responses [57]. The dissolution process of HA results in an increase of the extracellular concentrations of calcium ($[Ca^{2+}]_e$) and phosphorous ($[PO_4^{3-}]_e$), which results in the precipitation of apatites on a substrate ceramic, forming a carbonate apatite crystal layer [58]. The very strong interface between material and bone has been associated to this crystal layer [59]. HA shows the slowest dissolution rate in comparison to other calcium phosphate compounds, which results in almost direct bonding with adjacent bone and tissue. Table 3 also shows that HA has the best thermodynamic stability, which is a valuable feature for any implanted biomaterial where the processing method involves high

temperatures and where chemical degradation needs to be minimised. The comparison of bone composition to that of HA is shown in Table 4.

Table 4: Compositions of bone versus Hydroxyapatite [60]

Constituents (wt%)	Bone	HA
Ca	24.5	39.6
P	11.5	18.5
Ca/P ratio	1.65	1.67
Na	0.7	Trace
K	0.03	Trace
Mg	0.55	Trace
CO_3^{2-}	5.8	-

The properties of calcium phosphate based compounds which make them superior biomaterials include: biocompatibility, similarity in composition to bone, bioactivity and osteoconductivity [61]. Bioactivity, which is the ability of biomaterials to directly bond with bone and thus forming a uniquely strong interface [62], is characterised *in vivo* by the formation of carbonate apatite on the surface of the implanted material due to the partial dissolution of the calcium phosphate ceramic, reacting with the electrolytes in the biological fluid and forming carbonate apatite similar to that of bone [63, 64]. This apatite layer increases integration and incorporation of biomaterials. According to Jarcho et al. [65], a possible explanation for this increase in integration and incorporation could be that hydroxyapatite might have many areas on its surface that meet the electrical and spatial requirements for primary bone bonding. This results in a chemical bonding by which even dense materials become strongly attached to bone despite the fact that there is no in-growth of bone into a dense material [58].

HA is neither osteogenic nor osteoinductive, it is however osteoconductive. Osteoconductive biomaterials provide a template/scaffold for bone in growth. One of the major factors influencing the osteoconductivity is the porosity (macro and micro) of the ceramic material [58]. A large macroporosity (400–600 μm) facilitates infiltration by fibrovascular tissue and revascularisation, leading to bone reconstruction. Some preclinical studies [66, 67] have demonstrated that the combination of calcium phosphate ceramics (oestoconductive only) with osteogenic or osteoinductive substances shows better results in

the treatment of certain bone defects, where osteoconductivity alone is insufficient to achieve solid union. However, this new development is yet to be validated for clinical applications.

Decades of clinical practice have unanimously established that HA coatings are beneficial to orthopaedic prostheses applications in terms of earlier fixation and stability with more bone in growth or on growth being achieved [68]. In fact, most components become stabilised within three months with bone apposition. However, doubts still exist concerning the durability of the fixation, the main concern being the degradability of the HA coating and the disintegrated HA granules, resulting in accelerated wear. HA degradation may also lead to increased osteolysis and potentially the degradation product entering the joint space and damaging the articulating surface [69].

Mechanical properties of HA:

The key properties of hydroxyapatite are its bending strength, tensile strength, and fracture toughness. As shown in Table 5, the large scatter in material properties of bulk and plasma sprayed HA is due to many factors, such as the random strength distribution and the effects of residual microporosity, grain size, ion impurities and other process parameters [70]. With increasing Ca/P ratio, the strength increases, reaches a peak at Ca/P of 1.67, and sharply decreases for Ca/P > 1.67 [71]. Young‘s modulus of bulk HA varies from 11 to 117 GPa, depending on the residual porosity and impurities. Despite its valuable properties as a biomaterial (biocompatibility, bioactivity, osteoconductivity, direct bonding with bone), HA shows poor mechanical properties such as low impact resistance and fracture toughness (~ 1MPa-$m^{1/2}$). The latter is found to decrease almost linearly with increasing porosity [70]. As a result, this severely limits its application in orthopaedics for load-bearing functions. Nonetheless, HA is the most adequate candidate for coating metallic prostheses or filling small bone defects. With regards to implant’s coating materials, the use of HA would result in a combination of the good mechanical properties of metals and alloys with the excellent biocompatibility and bioactivity of HA in promoting bone growth to bond firmly from a mechanical point of view [72].

Table 5: Bone and HA mechanical properties [11]

Property	Spongy bone	Cortical bone	Bulk dense HA	PS HA
Porosity, %	70-95[1]	5-30[4]	~0	1[8]-18[10]
Pore size, μm	500-1500[1]	5-100[1]	-	7[12]
Crystallinity	-	-	-	40-80[2]
Density, g/cm^3	0.1[1]	1.85-2[1]	3.16[5]	1.2[12]-2.8[8]
Compressive strength, MPa	2-12[2]	100-230[2]	500-1000[6]	0.5-3.4[8]
Tensile strength, MPa	1.5[3]-20[2]	50[3]-150[2]	78-196[7]	7-80[2]
Flexual strength, MPa	10[2]	50[2]	115-200[6]	-
Young's modulus, GPa	0.01-3[1]	7-30[2]	11[2]-117[5]	0.28[8]-5.3[3]
Poisson ratio	0.03[1]	0.4-0.6[1]	0.27[5]-0.3[8]	0.28[13]
Elongation at break, %	5-7[2]	1[5]-3[2]	3-4[9]	-
Fracture toughness, MPa-m$^{1/2}$	2[2]	12[2]	1[6]	0.28-1.41[3]

References [1]Kutz [73] [2]Hench et al.[22] [3]Sun et al.[68] [4]Wachter et al.[74] [5]Bronzino [78] [6]Black et al. [81] [7]Legeros [75] [8]Tsui et al.[79] [9]Gibbsons [82] [10]Khor et al.[76] [11]Li et al.[80] [12]Rokkum et al.[83] [13]Yang et al.[77]

Thermal behaviour:

Plasma spraying is the most commonly used processing technique to produce HA coatings. The phase composition of the coating formed by plasma spraying depends on the thermal history of the hydroxyapatite powder as it passes through the flame [54]. When HA powder particles experience high in-flight temperatures, thermal decomposition occurs, changing the balance of phases in each particle. This affects the original characteristics of HA such as phase composition, crystal structure and powder morphology, and results in HA coatings with altered hydroxyapatite properties. The thermal decomposition (Table 6) of HA is sequential and occurs as follows:

1. Water evaporation: HA retains water on its surface and within its pores [84]. The first stage of thermal decomposition being when this water is evaporated.
2. Dehydroxylation: The next stage is for the hydroxyapatite to gradually lose its hydroxyl group (OH^-). This stage is reversed when HA coatings cool down and rehydrate.

3. Decomposition: At a critical temperature, irreversible dehydroxylation occurs. This is known as decomposition. This final stage leads to the formation of other calcium phosphate phases, such as β-tri-calcium phosphate (β-TCP) and tetra-calcium phosphate (TTCP).

One of the main problems related to HA processing is its low stability at temperatures near the sintering range, which could be caused by small deviations in the ideal Ca/P ratio [85-87]. Additionally, numerous other factors affect the thermal behaviour of HA, such as subtle modifications in preparation chemistry, powder surface condition, firing atmosphere and even particles aggregation can promote undesirable decompositions and phase transitions [88]. Gross [54] concluded that heating hydroxyapatite with a water vapour pressure higher than 900 mmHg avoids decomposition. Levingstone [82] reviewed and gathered the thermal effect data of HA as shown Table 6.

Table 6: Thermal decomposition of HA [89]

Temperature	Reaction
25-200^{o}C	Evaporation of absorbed water
200-600^{o}C	Evaporation of lattice water
600-800^{o}C	HA decarbonation
800-900^{o}C	HA dehydroxylates to form oxyapatite (OA)
1120-1470^{o}C	β-TCP, stable up to 1120^{o}C, transform to α-TCP
1550^{o}C	Incongruent melting of HA
1630^{o}C	TTCP melting temperature. Formation of CaO
1730^{o}C	TCP melting temperature

2.3.6 Biocomposites

Composites are materials made from two or more constituent components. Combining two materials (ceramic/ceramic, ceramics/polymer, and so on) is driven by the need to improve material properties or to take advantage of specific properties of two different materials in order to obtain tailored composites (coating, scaffold, implants, to mention a few). Composites generally include a matrix material and an additive/reinforcement material. The

aim of the additive is to impart a much needed physical, mechanical or chemical property to the matrix material and to increase its adequacy to the specific application.

Biocomposites designate materials that are biocompatible. The use of biocomposites is widely developed in many biomedical applications (Figure 5).Polymer based biocomposites are particularly attractive as their mechanical behaviour can be optimised to match the properties of natural bone [90]. Some biocomposite examples and their use are presented below.

HA/PCL:

The porous forms of HA have been used as bone scaffolds to encourage bone in-growth and osteointergration [91]. However, in order to be used effectively as load bearing materials, the mechanical properties of porous HA, such as the brittleness and low strength, should be improved. These properties limited the wider applications of porous HA in hard tissue implants [92, 93]. By adding a layer of HA/PCL biocomposite, the mechanical properties of the scaffold were improved [94], these include the compressive strength and the modulus of elasticity.

HA/PHB:

The use of polyhydroxyalkanoates (PHAs) is rapidly increasing in orthopaedics due to their excellent biocompatibility, slow degradation and good mechanical properties. PHB reinforced with HA proved to be a better choice for bone reconstruction surgery than pure polymer or pure HA [95]. Shishatskaya et al. [96] investigated the physiochemical and biocompatibility of different ratios of PHB/HA composites *in vivo* and *in vitro*. It was found that as the percentage of HA increased, the cohesive force and the surface wettability increased. The crystallinity and the temperature properties of the composite remained the same as those of the polymer with a more hydrophilic surface. It was concluded that PHB/HA composites favourably affect osteogenic cells and are therefore ideal candidates of bone reconstruction applications.

HA/PHBV:

Knowles and Hastings [97] reported that the copolymer PHBV degrades slowly, and therefore can be suitable for implant device applications in bone replacement applications

when it is reinforced with bioactive ceramics particles such as HA.PHBV reinforced with HA was found to have improved osteointegrative properties and interaction with tissue, this was due to the excellent physical-mechanical characteristics of these composites, which are similar to those of bone tissue [98]. Luklinska and Schluckwerder [99] showed that, after one month of implantation, lamellar bone structure has well developed around the HA/PHBV implant surface. At three months, marrow cells were observed in the new bone structure. At six months, the bone layer was compact and continuous around the composite implants.

PMMA/HA:

PMMA has been used as bone cement for a long period of time now. A good way to improve the biocompatibility of bone cement is to include a bioactive component into the composition. Previous studies have evaluated PMMA-based bone cement modified with bioactive components such as gamma-methacryloxypropyl trimethoxysilane and calcium acetate [100]. Another study [46], investigating the effect of HA content on enhancing biocompatibility of dental PMMA/HA composites, concluded that the presence of HA in the material composition leads to an increase of the water absorption and hydrophilic character of the composite, which in turn leads to good cell growth, proliferation and viability on these composite materials.

HA/EMAA:

Although EMAA was not used during this project, mentioning its use helps understanding the importance of combining HA with a biocompatible polymer in order to improve implant performance. Over the past decade, hydroxyapatite coatings have been sprayed on metallic bone implants to improve the bone-implant fixation based on the excellent bioactivity and oseteoconductivity of HA. However, the complex biological and mechanical requirements for implant materials cannot generally be fulfilled by one single material, and pure HA coating systems have shown some limitations induced by the susceptibility to stress shielding of the bone at the bone-implant interface due to the great difference of modulus between the implant (106GPa for Ti-6Al-4V, 8-120GPa for HA) and the bone (7-30 GPa for cortical bone) [101]. Stress shielding affects the normal remodelling of bone and limits the degree of bone restructuring [102]; it also leads to aseptic loosening

of implants and long term implant failure. Hydroxyapatite and EMMA (ethylene methacrylic acid copolymer) composite coatings were produced by a thermal spray technique in order to obtain a coating with optimal combination of biological and mechanical properties of these materials for orthopaedic implants[103].This study concluded that HA/EMAA composite coatings exhibited good adhesion to metallic substrates, increased modulus of elasticity, good toughness, and reasonable dissolution behaviour[103].

PHB/PMMA:

PHB as a microbial polyester is known for its highly biodegradable and biocompatible nature. However, as an implant material, it is brittle and has low abilities for some chemical modifications. Such limitations can be challenged by producing a biocomposite that includes PHB and another element. This was performed through reactive blending with a glassy acrylic powder, PMMA [44]. This study showed promising results from a morphological point of view, the blend not showing macro phase separation, which may be attributed to the compatibility in melt between the two polymers [44]. From a biological point of view, the activity of this composite against some pathogenic microorganisms was found to increase by increasing the amount of PMMA in the blend [44].

Poly(D,L-lactide)/PCL/HA:

Hydroxyapatite can also be useful as bone-filling material; the idea behind using polymers as binders for particulate bioceramics is to produce biocomposites with improved handling and retention characteristics and to overcome the problem of brittleness associated with ceramics bone repair. In a study with Poly(D,L-lactide)/PCL as an HA complement [104] to produce bone-filling material for non-load-bearing applications, a soft, highly flexible and easily shaped composite was obtained. Both, the modulus of elasticity and the yield stress, increased with HA loading, while the percentage elongation decreased. Therefore, these HA/polymer composites are thought to be novel candidates for bone-filling applications due to their unique physical properties and suitable degradation rates.

2.3.7 Titanium (Ti)

Titanium is a silvery, ductile metal with large industrial applications because it is much stronger than aluminium, less dense than iron and almost as corrosion-resistant as platinum.

This metal was discovered in the late 1500's and has been recognised as an element for 200 years, however, this metal has only gained strategic importance from the second half of the twentieth century and is now extensively used in almost all industries: automotive, aerospace, biomedical, construction and so on. This sudden growth in the development and use of Ti was triggered by the discovery by Dr. Wilhelm J. Kroll [105] of a relatively safe and economical method to produce Ti metal in the late 1930's.

Titanium is dimorphic with a transformation temperature of 882±5^{o}C [106]. Below this temperature, the metal is in its α-form: hexagonal closed-pack (hcp) crystal structure with lattice parameters at 25^{o}C of a=2.95404Å and c=4.6833Å. Above 882±5^{o}C, the metal transforms to its β-form: body-centered cubic (bcc) structure with a cell parameter of 3.3065Å at 900^{o}C. At 20^{o}C, Titanium has a density of 4.51 (α) and 4.32 (β), it has melting point of 1668^{o}C and a boiling point of 3262^{o}C [106]. Titanium alloys can be classified as either α, near-α, α+β, metastableβ or β depending on their room temperature microstructure [107].

The main physical advantages of Ti over other metals are its high specific strength, very valuable to the aerospace industry, and its corrosion resistance which is useful to the biomedical industry. Titanium's corrosion-resistant behaviour is based on the formation of a stable, protective oxide layer capable of resisting corrosion by body fluids [105]. This physiological inertness in the human body makes Ti such a key element in designing biomedical products and implants nowadays.

Titanium was first used in the biomedical field (surgery and dentistry) in the late 1950's and is now extensively and routinely accepted by medical professionals at a global scale as the material of choice for prosthetics, inner body devices and other medical instruments. In fact, Steinemann [108] found that the properties of titanium metals are favourable for making surgical implants that are intrinsically safe and damage-tolerant and concluded that titanium is the material of choice for medical applications. The biocompatibility performance of a metallic alloy *in vivo* is closely associated with its corrosion resistance and with the biocompatibility of its corrosion products. Corrosion data shows excellent resistance for titanium and its alloys, though some precautions should be taken in order to optimise their composition [109]. The most common biomedical use of titanium nowadays

is for hip implants. Some material requirements fulfilled by titanium and titanium alloys for such applications are shown in Figure 10.

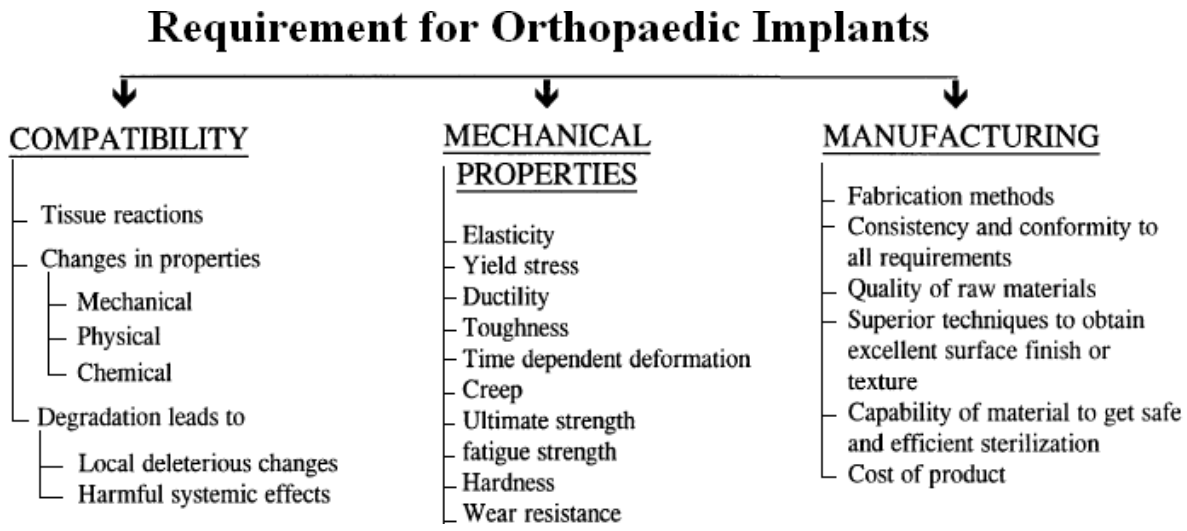

Figure 10: Implant materials requirements in orthopaedic applications [107]

Ti6Al4V alloy, which was originally designed for aerospace applications, is considered as a standardised metallic biomaterial [108]. This titanium alloy is currently used by most orthopaedic implant manufacturers (such as Stryker), especially for hip and knee replacements. Some of the mechanical properties of this alloy are listed in Table 7.

Table 7: Ti6Al4V minimum and average properties at room temperature (adapted from [105]**)**

Ti6Al4V Alloy			
Ti6AL4V Properties Range			
Ultimate tensile strength	900-993MPa	**Hardness**	36 HRC
0.2% yield strength	830-924MPa	**Modulus of elasticity**	113.8GPa
Elongation	14%	**Modulus of rigidity**	42.1GPa
Reduction in area	30%	**Poisson's ratio**	0.342

Recently, new titanium alloy compositions, tailored for specific biomedical applications, have been developed such as Ti-6Al-7Nb [110]. This was developed in response to concerns relating vanadium (in Ti6Al4V alloys) to potential cytotoxicity [109].

2.4 Thermal Spraying

Thermal spraying consists of a number of processes, in which finely decomposed materials are accelerated and propelled, either by process gases or atomisation jets, in a molten or semi molten state towards a prepared substrate to form a coating (Figure 11). The feedstock material may be metallic or non-metallic (polymeric, ceramic etc) and may come in different forms (powder, rod, wire, and cord) depending on the specific process. The heating required to melt and propel the coating material can be generated by three main energy sources: combustion flame, electric arc and plasma arc.

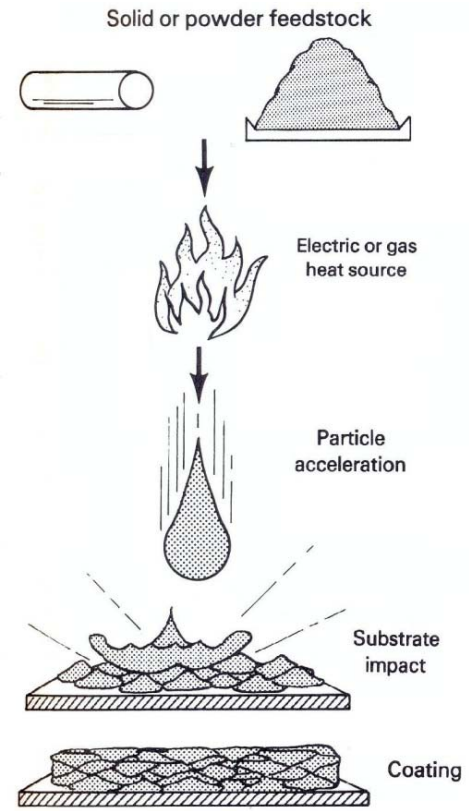

Figure 11: Generic thermal spray process [111]

The earliest thermal spraying experiments were performed in the late 1800'sleading to M.U Schoop (Zurich, Switzerland) presenting his first patents (1882 to 1889) [111]. Schoop's first patents described how a stream of molten lead and zinc particles impinging on a substrate could build-up as a protective coating to avoid corrosion. The first process used

lead and tin wires as coating material, which were fed into a modified oxy-acetylene welding torch. This process was then developed furthermore to also work with powders.

Nowadays, a large number of industrial sectors rely on thermal spray processes and coatings. This is due to the versatility of the process and to a number of advantages it has to offer to every industry. The main advantages of thermal spraying are:

- The significant choice of materials that can be used to produce coatings.
- The ability to apply coating without significant heating up of the substrates, which in turn allows the use of a wide range of substrate materials.
- The ability to strip off and recoat worn or damaged coatings without changing the parts properties or dimensions.

As a result, the introduction of thermal spraying to industry improved: wear resistance, heat resistance, clearance and dimensional control, corrosion and oxidation resistance, electrical properties and so on.

The main disadvantage of thermal spraying is the line-of-sight nature of the process. This means that contours and complex shapes require deviations from spraying normal to the surface ($90^{o}\pm20^{o}$) [111]and generally compromise their material properties.

Thermal spray processes can be divided in four main groups, with each one of these groups offering various alternatives (Figure12).

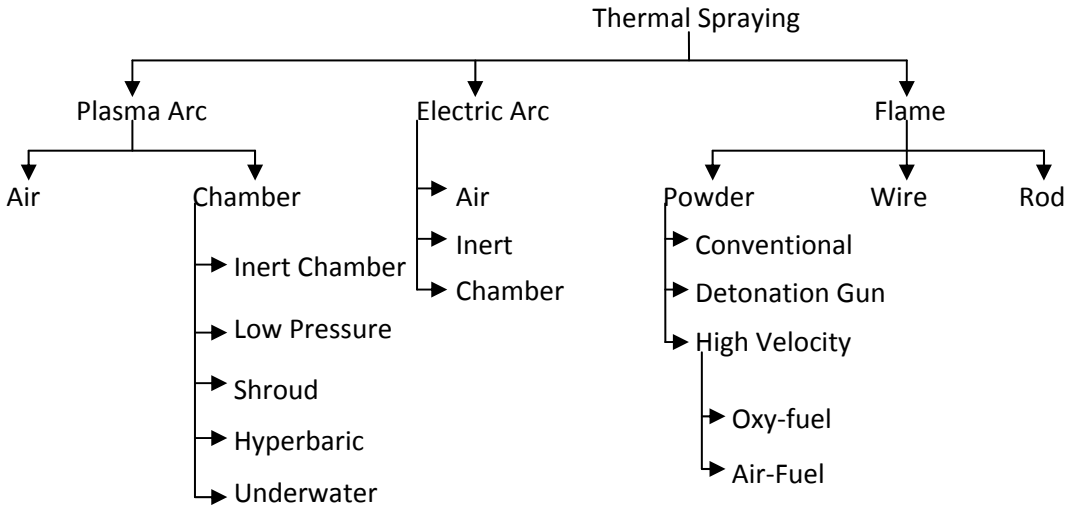

Figure 12: Thermal spray processes and subsets (adapted from [111]**)**

Table 8 shows a comparison of the most used thermal spray processes in industry. The difference between these processes can be divided into three main outputs:

- Jet characteristics
- Particle feed characteristics
- Coating characteristics

Table 8: Thermal spray process comparison [111]

	Attribute	Flame spray	HVOF	Detonation gun	Wire arc	Air plasma	Vacuum Plasma
Jet	*Jet temperature, K*	3500	5500	5500	>25,500	15,000	12,000
	Jet velocity, m/s	50-100	500-1200	>1000	50-100	300-1000	200-600
	Gas flow, sLm	100-200	400-1100	N/A	500-3000	100-200	150-250
	Gas type	O_2,acetylene	CH_4,C_3H_6, H_2,O_2	O_2,acetylene	Air,N_2,Ar	Ar,He,H_2, N_2	Ar,He,H_2
	Power input, kW equiv.	20	150-300	N/A	2-5	40-200	40-120
Particle feed	*Particle temperature (max), ^oC*	2500	3300	N/A	>3800	>3800	>3800
	Particle velocities, m/s	50-100	200-1000	N/A	50-100	200-800	200-600
	Material feed rate, g/min	30-50	15-50	N/A	150-2000	50-150	25-150
Coating	*Density range (%)*	85-90	>95	>95	80-95	90-95	90-99
	Bond strength, MPa	7-18	68	82	10-40	<68	>68
	Oxides	High	Moderate to dispersed	Small	Moderate to high	Moderate to coarse	None

In all thermal spraying processes, the structure and the deposit efficiency of the coating are affected by the interaction of the powder particle velocity feed rate and the flame [111]. Deposit efficiency decreases rapidly if the raw material is not properly heated, thus the coating will contain trapped, unmelted or partially melted particles. If the particle velocity

is too low, some powder may disintegrate, resulting in coating deterioration and elevated operating costs [111].

2.4.1 Flame Spraying

Process characteristics:

Flame spraying uses the chemical energy of combusting fuel gases to generate heat of up to approximately 3000^{o}C. The highest combustion temperatures are generated by a combination of oxygen and acetylene, which is the main fuel type used. Propylene can also be used; however, the downside of this fuel gas is that it requires twice as much oxygen to obtain the same flame temperature as acetylene, thus increasing the likelihood of oxide formation on the coating.

Feedstock materials are generally stored in a hopper that either could be an integral part of the gun or connected to it via hoses. A suction effect is created at the gun hopper orifice by the fuel gas flow in order to carry the powder into the oxygen/fuel gas stream, where the powder is melted and the particles/droplets are accelerated towards the substrate surface by expanding gas flow and air jets. A typical gun cross section is illustrated in Figure 13.

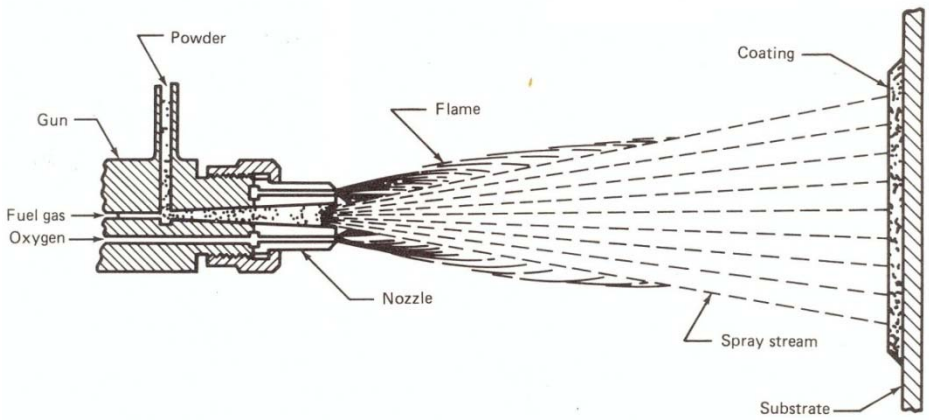

Figure 13: Cross section of a powder flame spray [112]

Coating characteristics:

Due to the relatively lower particle velocities and temperatures generated by flame spray [112], the coatings produced have generally lower adhesive strength, lower overall cohesive strength, and a higher porosity than coatings obtained by other thermal spray processes.

Flame spray processes typically yield coating densities ranging from 85 to 98% [111]. These lower densities coatings have been shown to result from the low jet temperatures and velocities of this process. For metal spraying, the oxidising condition of the flame spray process induced oxide inclusions in the metal deposit; this is explained by the high degree of droplet/atmosphere interaction. In polymer spraying, a very dense, well-bonded surface layer is obtained; a structure due to the post fusing, or coincidental with deposition.

2.4.2 Atmospheric Plasma Spray

Process characteristics:

Plasma is known as the fourth state of matter. It is produced when a gas is exposed to a very high energy input (electric discharge); gas molecules can then dissociate into atoms that are ionised, losing an electron of the outer shell and becoming ions. When electrons and ions recombine, a high amount of energy is set free releasing heat and light. On average, plasma is electronically neutral, because any charge imbalance would result in electric fields that would tend to move the charges in such a way as to eliminate the imbalance [113].Plasma spraying uses powders as the feedstock and plasma (hot ionised gas) as the heat source. Plasma torches generate controllable temperatures well in excess of the melting range of almost all substances. Sulzer Metco suggests that the 9MB plasma gun can generate temperature of up to 16,000^{o}C.A section view of a typical plasma torch is shown in Figure 14.

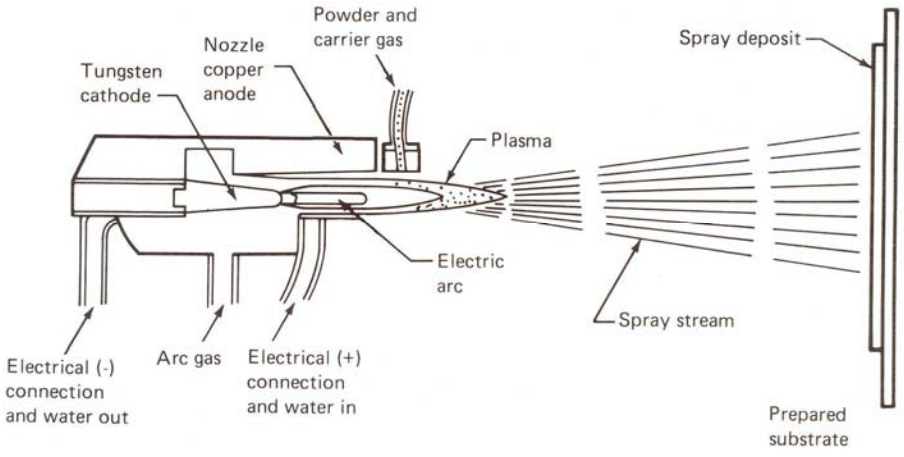

Figure 14: Sectional view of plasma torch [112]

During plasma spraying, one gas or a mixture of gases are passed through an electric arc between a coaxially aligned tungsten cathode and an orifice in a copper anode. Tungsten is used because it has a high melting point and is a good thermionic emitter (continually emitting electrons to maintain the arc discharge).When the gas passes through the nozzle, it is heated and ionised, producing a plasma. As the plasma exits the gun [112], disassociated molecules recombine and liberate heat. The powder is introduced externally into the plasma plume, where it is melted and propelled onto the work piece by a very high velocity stream. The plasma-forming gases generally used are: Nitrogen (N_2), Argon (Ar), both primary, and Hydrogen (H_2), Helium (He), both secondary. The type of gas used depends on the requirements of specific applications. Mono-atomic gases (Argon and Helium) have lower enthalpies than diatomic gases (Nitrogen, Hydrogen). Argon is widely used for its inert nature which protects the powder particles and electrodes from the environment; it is also a relatively cheap and an easily ionised gas. When argon is used to produce plasmas, a large arc current is required to allow materials to melt. This results in extremely high gas velocities and therefore reduced particle residence times in the plume, preventing adequate melting of materials such as ceramics (high melting points). This is where a secondary gas (Hydrogen or Helium)comes into play in order to increase the heat content to an adequate level. Commonly used gas combinations, in ascending order of enthalpy are: Ar, Ar/He, Ar/H_2, N_2, N_2/H_2.The numerous process characteristics are not only controlled by the gas mixtures but by a number of other inputs. These are shown in Figure 15.

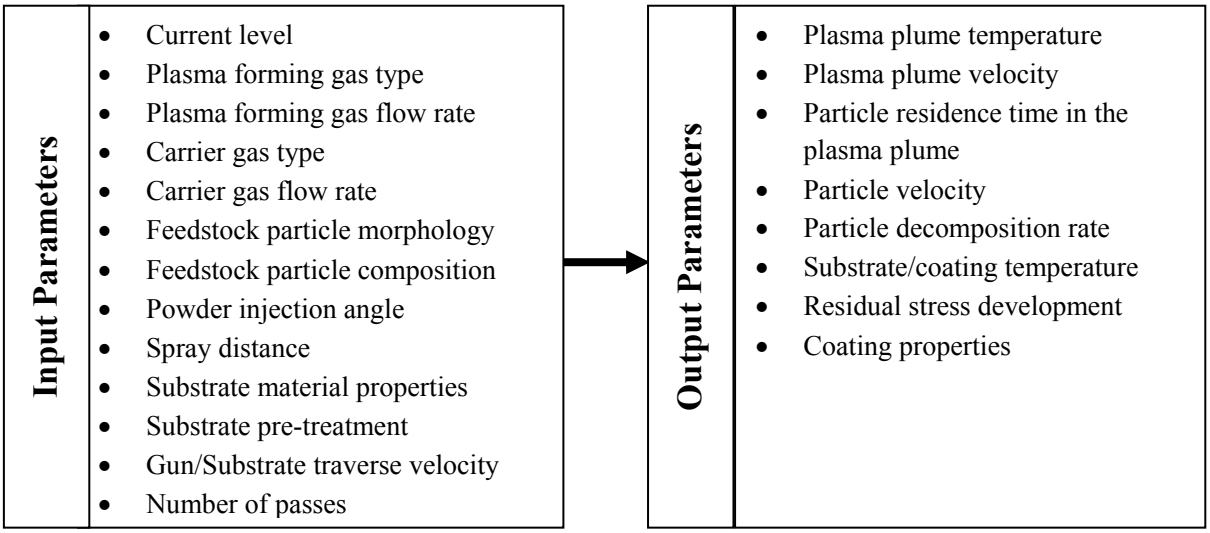

Figure 15: Input and output parameters

Coating characteristics:

As previously mentioned, during plasma spraying, the expanding hot gas jet created by a plasma arc entrains feedstock particles, heats and accelerates them towards the substrate, where they impact, deform and re-solidify to form a coating. The particles flatten, cool down and solidify so rapidly that the next impinging particulates hit already solidified splats or lamellae [114]. Successively impacting particles cause lamella to build-up, forming the coating. Generally, each pass of the plasma torch produces a coating layer about 5 -15 lamellae thick [89]. Between the depositions (passes), reactions between the surface of the deposited layer and the surrounding environment may occur; these include water absorption or oxide inclusion. Cooling of the layer also occurs. The number of layers applied depends on the required coating thickness.

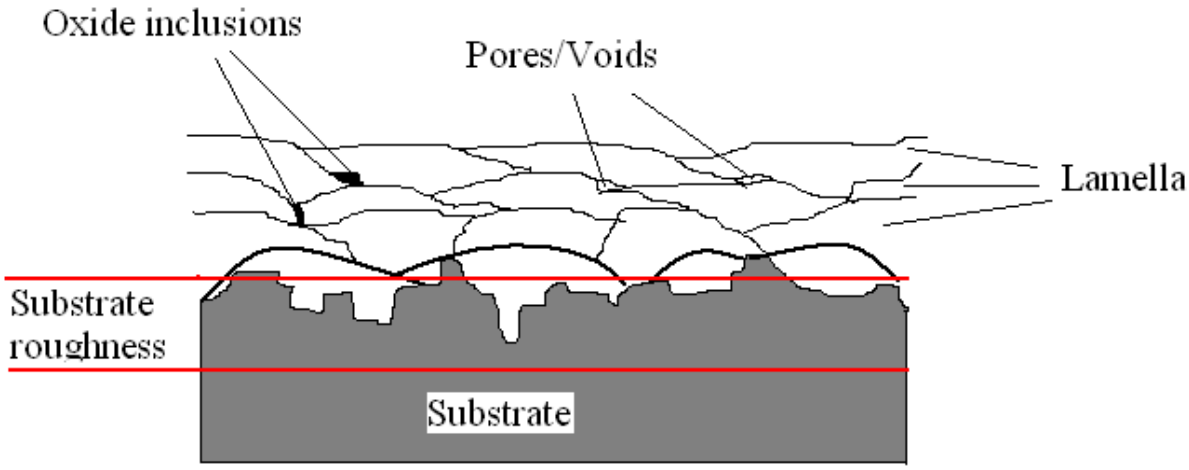

Figure 16: Typical cross section of a plasma sprayed coating

Plasma coatings are characterised by a high degree of particle melting and high particle velocity, which results in deposit densities and bond strengths higher than other thermal spray processes. Depending on the melting temperatures of the particle relative to the plume temperature, the particle may be molten, semi-molten or solid when it impacts the substrate; this has a considerable influence on the coating formation and the appearance of pores/voids between lamella (Figure 16). Ideally, all particles should be in a molten state in order to ensure the desired coating properties. The degree of particle melting depends on the amount of heat to which the particles are exposed, which in turn depends on a number

of factors: the heat content in the plasma flame plume, the location of the particles within the plume, the velocity of the particles and the particle size.

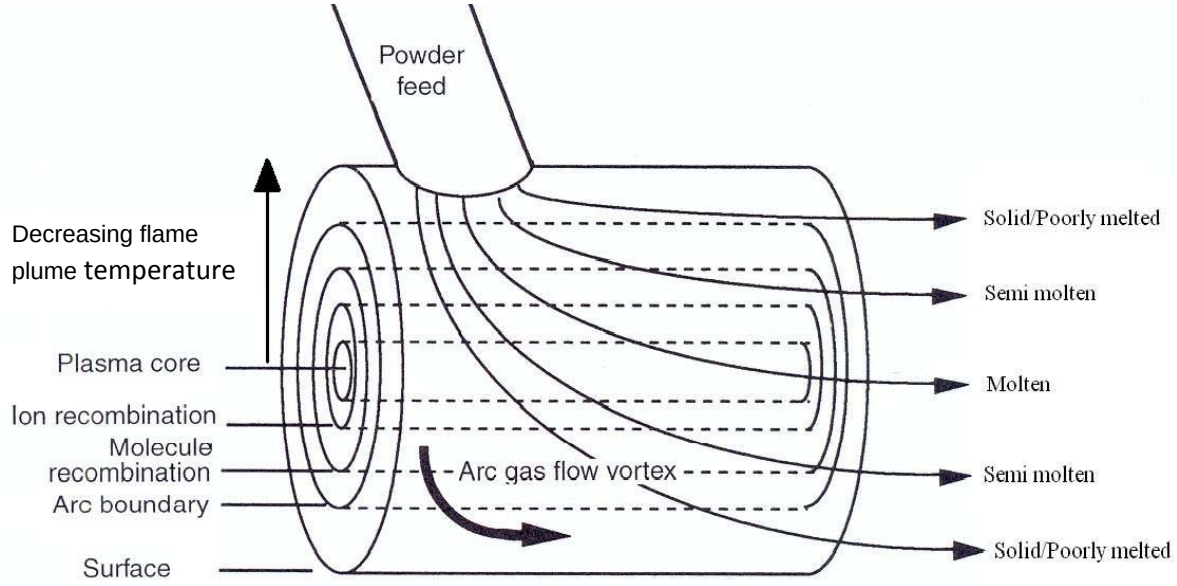

Figure 17: Influence of particle trajectories along the jet on the degree of melting (adapted from [111]**)**

Figure17, shows how the plume section with the highest temperature (plasma core) induces full melting of the feedstock particles. On the other hand, the plume boundaries with a much lower temperature, produces particles that are poorly melted or remained solid.

The trajectories of the particles along the jet are greatly influenced by the carrier gas type and velocity/flow rate. When the powder particles are radially injected perpendicular to the plasma jet, the velocity of the carrier gas and its initial momentum at impact with the plume will determine the particles trajectories. In order for the particles to follow the ideal trajectory (molten particle in Figure 17), the carrier gas flow rate should inject feedstock particles into the plasma jet at a momentum similar to that of the plasma jet [89]. Inert gases (argon and nitrogen) are mostly used as carrier gases because they prevent chemical changes to the feedstock particles. The choice of the carrier gas can also affect the trajectories of the particle. Leung et al. [115]found that nitrogen has a gas momentum value that is 37% greater than that of argon. In the case of helium, it was 10% less than argon for the same flow rates used.

2.5 Properties of Thermally Sprayed Coatings

2.5.1 Plasma Sprayed HA for Orthopaedic Coatings

Many methods have been used to deposit HA coatings on metallic implants, including dip-coating sintering [116], electrophoretic deposition [117], solution deposition [118], immersion coating [119], ion-beam sputter coating [120] and thermal spraying. Plasma spraying is the most successful method to apply HA coatings on metallic implants, and it is therefore the most commonly used technique of HA coatings formation for clinical applications. Extensive research has been conducted in the area of plasma sprayed HA coatings [54, 68, 76, 79, 80, 89, 121-123]. International standards BS ISO13779-1:2000 [124] and BS ISO13779-2:2000 [125] regulate the properties of hydroxyapatite powders and coatings for implant applications. Both the structure and the composition of the HA coatings are significantly modified from the feedstock powders. Therefore, from a materials science perspective, the physiological response of the coating does not necessarily reflect the exact characteristics of the feedstock [68]. The outcome of plasma sprayed hydroxyapatite is influenced by three main factors: feedstock powders, implant metals, and spray parameters. The quality of HA coatings is assessed with regards to a number of outputs, including, purity (chemical composition), crystallinity, Ca/P ratio, porosity (microstructure), thickness and surface roughness [126]. Variations of these properties can lead to different bioactivity, durability and mechanical properties of the coating, such as cohesive and bond strength, tensile strength, shear strength, Young's modulus, residual stress and fatigue life [68]. Tsui et al. [79], suggested that the ideal HA coating for orthopaedic implants should be highly crystalline with low porosity, it should also have strong cohesive strength, good adhesion to the substrate with a high chemical and phase stability.

Purity and Crystallinity:

Following plasma spraying, the purity and the crystallinity of the HA coating decrease in comparison to the feedstock due to the decomposition of HA at high temperatures and the rapid cooling rate that follows. The coating crystallinity is determined by the degree of particle melting and the solidification time of the lamellae, highly amorphous coatings dissolve quicker. It is important to control the phase purity and crystallinity of HA coatings

due to the variation in dissolution properties between different calcium phosphate phases. A faster dissolution rate means a supersaturated environment is created, allowing physiologically produced HA to precipitate on the coating and enhance bone in growth, however, this also leads to the resorption or degradation of the coating [127]. It is therefore detrimental to predict the properties of HA coatings by effectively designing the purity and the crystallinity of HA. This is achievable by strictly controlling both the spray parameters and the quality of the original feedstock powder [68]. Gross et al. [54] proposed a model for phase formation in plasma sprayed HA coatings.

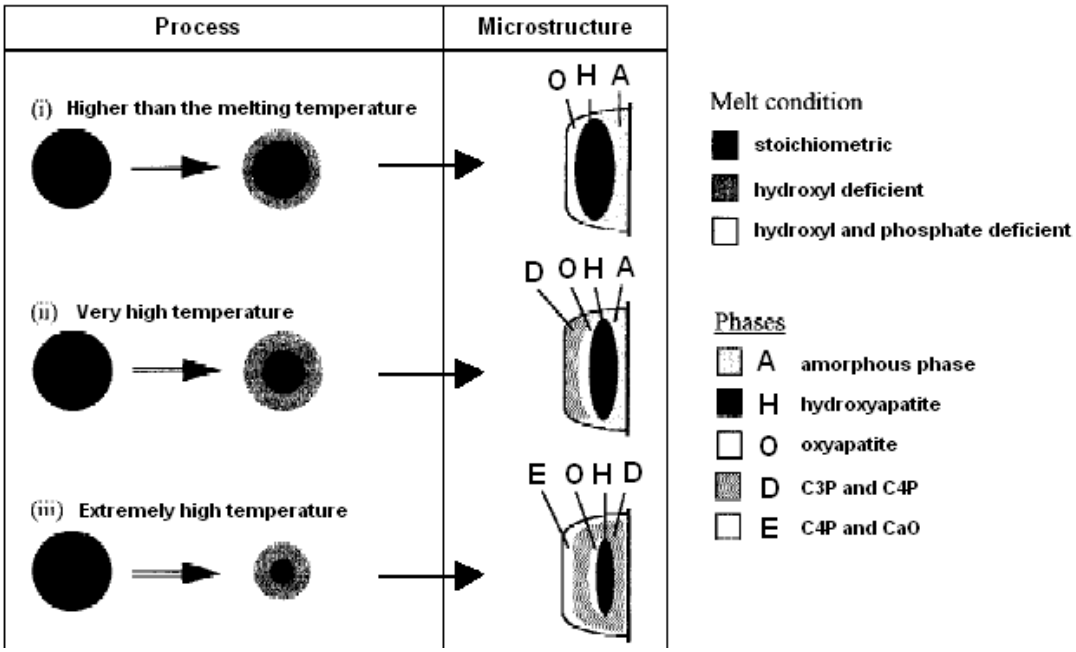

Figure 18: Phase formation model for plasma sprayed HA coatings [54]

The process stage (Figure 18) shows the different melt chemistries as a function of particle temperature. The microstructure column depicts the possible phases that can be formed in lamellae. The unmelted portions generally retain their crystalline structure after cooling down, melted particles on the other hand become amorphous or recrystallise to nanocrystals according to the varying cooling rates [123]. It is thought that the amorphous phase of HA coatings is metastable, possesses a higher internal energy and tends to release the distortion [128]. This led Sun et al. [123] to conclude that the amorphous phase exhibits a higher dissolution compared with the crystalline HA phase when immersed in solution.

Microstructure and porosity:

These two characteristics highly influence the performance of HA coatings. The degree of porosity depends on the melting degree of the in-flight particles when they impinge on the substrate surface. Dense coatings are obtained when highly molten material flow over the surface and fills gaps and pores. Porous coating microstructures form when the particles are at a semi-molten state. Porosity can be controlled by varying the particle solidification time [89] through changing spraying parameters, such as the temperature of the plasma flame/plume and the level of substrate heating. When spray parameters are varied, the state of the original particles can change to different forms: well flattened splats, accumulated splats, spheroidised splats, partially melted particles or even unmelted particles [68]. These microstructural features lead to different levels of porosity in HA coatings. Coating porosity usually decreases with increasing input power level [79]. This is due to the fact that, when particles are fully melted, a lower porosity content is obtained. Pores are also formed when oxygen, nitrogen and hydrogen are released as the temperature of the material decreases on the substrate and the solubility of these materials is reduced accordingly [129]. The nature of the porosity is very important as it controls the specific area of the implant in contact with the physiological medium and, therefore, influences physiochemical interactions at the implant-host interface [79]. Porous coatings allow greater degree of coating dissolution for bone substitution; they also allow greater penetration of bone cells and greater levels of cell attachment [130]. On the other hand, a high degree of porosity affects the mechanical properties of a coating negatively. Heimann [131], reported that dense coatings reduce the risk of bonding degradation on HA coatings, such as cracking, spalling and delamination, during *in vivo* contact with aggressive body fluids.

Roughness:

Coating roughness generally indicates the degree of particle melting within the plasma flame. Smoother coatings usually imply that the particles reach a more fluid state within the plume, which makes them more viscous and enables them to spread out to a greater degree on impact with the substrate [132].Partially melted particles were found to give rise to large undulations due to their inability to flatten on the substrate surface; this resulted in higher coating roughness[133].Surface roughness of HA coatings affects the dissolution and bone in growth on the surface of the coating [68]. Niederauer et al. [134] showed that surface

roughness for bioceramics coatings improved surface wetting properties. These properties can directly affect cell attachment via enhanced formation of focal contacts, or indirectly through selective adsorption of serum proteins required for cell attachment. Deliglianni et al. [135] also concluded that surface roughness, along with crystallinity and surface chemistry, affects cellular response, enhancing cell adhesion and proliferation. This may also be explained by the fact that, as the coating roughness increases, the coating and body-fluid interface increases as well, which in turn increases the dissolution rate and apatite precipitation. The degree of roughness can be controlled through varying feedstock powders and spray parameters [79].

Thickness:

The thickness of HA coatings affect the mechanical properties as well as the resorption of the bioactive coating [68].Coating thickness mainly depends on three factors: the number of spray passes; the powder feed rate and the deposition efficiency [89]. The coating thickness increases when the number of spray passes and the powder feed rate increases. According to De Groot et al. [136, 137], in order to avoid fatigue failure and brittleness, occurring with thick coatings (~100 μm), an optimum thickness of 50 μm would perform better in that regard. This lower thickness of coating would still provide reasonable coating resorption and consistent bone growth. Good resorption properties are known to provide better protection for the bone from the metal-ion release caused by titanium substrates. The correct compromise between resorption and mechanical properties is thought to be in the range of 50-75 μm, as most manufacturers for commercially used orthopaedic implants are using this level of thickness.

Mechanical Properties- Bonding Strength:

The bonding strength of a coating is a combination of adhesive (at the coating-substrate interface) and cohesive (within the coating layers) strength. Whereas adhesive strength typically depends on coating structure, residual stresses and surface roughness of the substrate, the cohesive strength is influenced mostly by the microstructure of the coating (crystallinity, porosity and lamellar structure).

a) Adhesive Strength:

The mechanism of coating adhesion is a complex one and several theories about it exist, but not all adhesion behaviours have one single coherent explanation [121]. Nonetheless, it is well known that four main factors seem to influence the formation of a coating-substrate adhesion, these are, chemical interactions, metallurgical processes, mechanical anchorage, and van der Waals physical interaction forces [138, 139].Partly due to the surface roughness of the substrate, the lower layer of the HA coating is not fully in contact with the substrate. In fact, lower lamellae interlock with the substrate through areas known as 'welding points' or 'active zones' [140]. The most important mechanism for coating adhesion is mechanical anchorage, with its level being linearly dependent on the average surface roughness [141]. Van der Waals forces also play an important role in coating adhesion; these forces occur between atoms of the lamellae and the substrate when the field of atom attractions (0.5nm) is reached [140].

According to Yang and Chang [142] the adhesive conditions are thought to be influenced by the mechanical interlocking between the HA coating and the substrate as well as the residual stresses in the HA coating. Previous studies have shown that the compressive stress produces a tensile stress in the normal direction to the plane of the coating; this in turn promotes delamination of the coating by acting on any pre-existing flaws and defects [143, 144]. Residual stresses occur near the coating-implant interface, when following plasma spraying, the coating rapidly solidifies. This is due to the mismatch of thermal expansion coefficients of the coating and the substrate [145]. The thermal expansion coefficient of metallic substrates is higher than that or ceramic coating (HA in this case), this generates a compressive residual stress after the cooling of the coating. These compressive stresses can induce the coatings to debond [144]. Eberhardt et al. [146] indicated, that in order to obtain a reasonable prediction of the residual stresses in HA coatings, the coating's Young's modulus needs to approach 5.5 GPa. Sergo et al. [147]concluded, that the existence of residual stresses in HA coatings can alter the concentration of supernatant species in solution, tensile stresses enhancing dissolution, and compressive stresses impeding dissolution. Only a few previous studies [77, 79]were able to quantify and predict the magnitude of residual stresses in ceramics coatings; this is due to the complex behaviour and generation mechanism of residual stresses. Residual stresses

generation is influenced by many factors such as the substrate temperature, the plasma flame temperature, spraying parameters, the feedstock powder properties and the coating thickness.

b) Cohesive Strength:

As previously mentioned, cohesive coating strength depends on the cohesion of particles within the coating, the factors influencing this internal interaction include the crystallinity, porosity and densification of coating, which translates on the Young's modulus of coating [148]. Yang et al. [149], showed that the area fraction of cohesive failure seems to be correlated with the porosity content in the HA coatings, indicating that the increase in porosity weakens the cohesive strength of the coating. However, Yang and Chang [150]also suggested that this effect might be interpreted by the effect of decreasing residual stresses. Therefore, the bond fracture mode of HA coatings should be considered as a function of the level of porosity and the residual stresses, rather than the individual effects of each.

Summary:

Ideally, and according to the observations of previous research on hydroxyapatite coated metallic substrate, HA coatings should have a high degree of crystallinity, chemical purity and phase stability, high cohesive strength, good adhesion to the substrate and a low degree of porosity. This type of combinations is very difficult to obtain, however, a balance of all these coating characteristics could be achieved by varying the spraying parameters. Levingstone [89] optimised plasma sprayed HA coatings as shown in Table 9.

Table 9: Summary of the effects of factors variation on the response [89]

Factor		Roughness	Crystallinity	Purity	Porosity	Thickness
A-Current		↑	↑	↑	↑	↑
B-Gas Flow Rate		↓	↓	↑	↓	↓
C-Powder Feed Rate				↓	↓	↑
D-Spray Distance			↓	↓	↓	↓
E-Carrier Gas Flow Rate			↓	↓		↑
Interaction of Factors	**A*B**	↑	↑		↓	
	A*D		↓	↓	↑	↓
	B*C			↓		↓
	B*D			↑	↓	
	B*E		↑			↑
	D*E			↓		

A general agreement exists on what some but not all of the coating characteristics of HA coatings should be. Purity should be as high as possible (95%-97%) with a Ca/P ratio of 1.67 [151]. Crystallinity varies greatly from one study to another and there is no agreement on its percentage within the coating. Nonetheless, according to the ISO standard specification (ISO 13779-2:2000) [125], in order for an HA coating to have sufficient mechanical properties *in vivo*, the crystalline content should be higher than 45%. The same standard states, that the adhesion strength should not be less than 15 MPa, a strength already surpassed by HA coated titanium substrates at the moment (28 MPa) [149]. The porosity of commercially available HA coatings usually vary from 1% to 10% and could go up to 50% [83]. HA coatings generally vary in thickness from 50 μm to 200 μm [68]. The optimal value for coating roughness has yet to be determined. The optimal spraying parameters obtained by Levingstone [89]are shown in Table 10.

Table 10: Plasma spraying parameters for the production of stable HA coatings

Current	Gas Flow Rate	Powder Feed Rate	Spray Distance	Carrier Gas Flow Rate
750 A	104.84 SCFH	19.99 g/min	70.01 mm	10 SCFH

2.5.2 Thermally Sprayed Polymers

Thermal behaviour of ceramic and metallic particles/coatings with various thermal spray techniques have been thoroughly investigated over the previous decades with little consideration given to polymers. Many studies[152, 153] have examined droplet impact behaviour (mainly for metallic powders), a property upon which depend almost all coating characteristics; and although similar in principle to spraying polymer powders, the heating and splatting behaviours of polymer and metallic particles are fundamentally different. In fact, molten polymeric and metallic particles have different impact flow characteristics; they also have significantly different thermal properties and solidification kinetics. The use of polymers is increasing in many applications such as electrical insulation, wear resistance, and bioactive surface, and more research is undertaken in order to understand the thermal behaviour of polymer during thermal spraying processes. Thermally sprayed polymer coatings offer the advantage of the mechanical strengths of thermal spraying and the

multifuncionality of polymer composites. Thermal behaviour of polymer particles is very different from that of other materials; this is mainly due to their much lower melting and decomposition temperatures in comparison to metals and ceramics along with a much smaller thermal conductivity and liquid range [154]. Advantages and disadvantages of using thermal spray processes for polymer deposition are shown in Table 11.

Table 11: Advantages and disadvantages of polymer thermal spraying over solvent-based techniques (adapted from [155]**)**

Advantages	Disadvantages
Solventless deposition of coatings without the use of volatile organic compounds (VOCs) in contrast with dip coating	Lower deposition efficiency
The ability to coat large objects area	Lower surface finish quality
The ability to apply polymer coatings with high melt viscosity	Higher process complexity with a narrow processing window due to the relatively low polymer melting and degradation temperatures
The ability to produce "ready-to-use" coatings with limited post-deposition processing (such as oven drying) in contrast with electrostatic deposition and wet spraying	

Due to this high thermal sensitivity combined with the extremely high temperature levels generated by thermal spray processes, the processing window is expected to be much narrower than with other materials and the process control needs to be more precise. This is crucial in order to avoid the degradation of the polymer which is known to deteriorate the properties of polymers. Degradation typically occurs by the mechanisms of chain scission or oxidation. Chain scission occurs when the polymer is heated to a temperature at which the vibrational energy at certain points of the macromolecule is greater than the bond energy [43]. This type of a reaction can reduce the melt-viscosity and may also affect mechanical properties such as toughness and strength. Oxidation may also occur at elevated temperatures in the presence of oxygen where hydroperoxide formation will be higher, therefore causing a greater degree of chain scission [156]. This degradation mechanism can

affect the chemical structure of the polymer, thus, modifying its properties. The processing window has an upper temperature limit equal to the degradation temperature T_d, and a lower temperature limit equal to the melting temperature T_m, which makes the optimal processing window specific to each polymer.

Decomposition of in-flight particles: The thermal conductivity of most engineering polymers are less than $0.5 Wm^{-1}K^{-1}$[157],thus, large temperature gradients develop within polymer particles in the flame due to this high internal heat conduction resistance (low thermal conductivity). In practice this means that the surface of the particle reaches its thermal decomposition temperature very early in the flame/plume (after 50 μs of entering the plasma jet for a PMMA particle [154]), while the core of the particle remains solid until a very late stage of the process. As a result, the degree of in-flight particle melting is reduced, affecting the coating properties. The surface layer of the polymer particle is therefore constantly decomposing with a mass loss of the in-flight particle, within the flame.

Decomposition within the deposited layers: After deposition on the substrate, the coating layers continue receiving heat from two sources [43]: the solidifying splats and the tail-end of the flame as it traverses across the surface during the spraying process. The latter source has the greater heating effect on the deposited coating layers, mainly because the temperature of the splats do not exceed the polymer decomposition temperature and the exposure time of the coating to the flame is much greater than that of the splats. As a result, the exposure time is thought to play an important role in determining the effect of the flame on the deposited layers. The slower the traverse speeds, the larger is the effect on the coating. Zhang et al. [43] suggested that substantial thermal degradation of the polymer coating occurred at low traverse speeds and choosing the correct traverse speed is a crucial parameter for the thermal spraying of polymer coatings. The value of this critical speed would obviously depend on other operating parameters such as spraying distance and substrate cooling conditions, along with the type of thermal spraying process used and the decomposition temperature of different polymers.

Microstructure: Ivosevic et al. [155] showed that, with no substrate pre-heating, most of the larger polymer splats (>100 μm) exhibited a characteristic "fried-egg" shape with a large,

nearly hemispherical, core in the centre of a thin disk (Figure 19). This shape confirms the existence of a large radial difference in the flow properties of the molten particle surface of polymer droplets (Nylon-11 in this case) and the largely unmelted core. The large radial temperature profile causing this splat formation mechanism is characterised by a low temperature, high viscosity core and a high temperature, low viscosity surface. The same study suggests that pre-heating the substrate to the polymer melting temperature would help to flatten the hemispherical splats. This was attributed to post-deposition flow activated by surface tension, visco-elastic effects and/or residual stress after the initial "fried-egg" splats were fully melted by the pre-heated substrate [155].

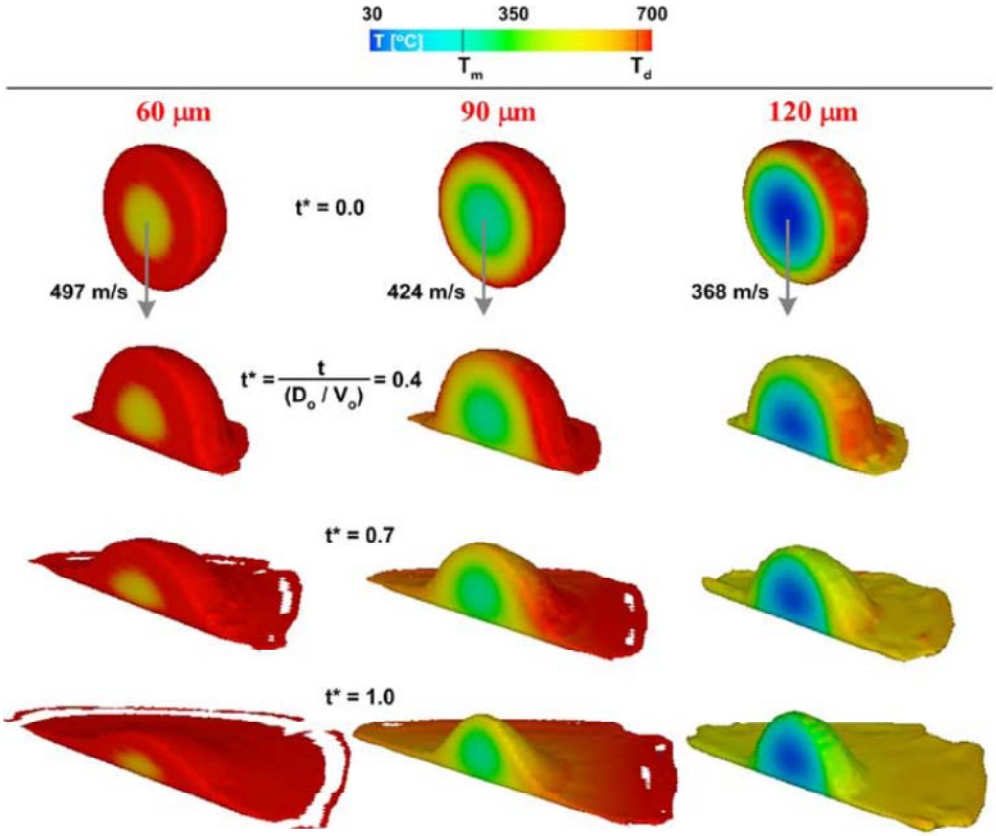

Figure 19: Cross-section of predicted three-dimensional spreading splats for 60, 90 and 120 µm diameter particles [155]

Particle trajectories within the flame/plume can also affect the microstructure of the coating. In fact, a high quality coating microstructure (low porosity) can be obtained when

the mean particle trajectories cross the jet axis. This can be achieved by increasing particle temperature and applying higher velocity which ensures good contact with the substrate and higher bond strength of the coating [111].

Porosity: Porosity with polymer coatings is generally dependent on the nature of the substrate surface, polymer melt viscosity, and decomposition products. In polymer coatings, a substantial amount of porosity was observed [158]. This is due to the low thermal conductivity of polymers, which makes it difficult to completely melt particles without inducing noticeable chemical decomposition of the material. Liao et al. [158]believed that the flattening of in-flight polymer particles was quite low due to the unmolten particle core, which resulted in an increase of porosity within the coating. Bao and Gawne [159] indicated after fracture surface studies that cracks were initiated at pores; such a mechanism can reduce tensile properties. As previously mentioned, substrate preheating can be an option in order to increase the density of the coating. In fact, using a regular flame spray process in order to preheat the substrate and spray the polymer results in denser coatings [158]. This could be explained by the lower flame enthalpy of the oxy-fuel flame spray when compared to the plasma plume and the smaller blow force when compared to an HVOF flame; these specifications make the fusion process occur easily, if the spray parameters are correctly chosen and controlled.

Despite extensive research, the relationship between pore structure, material properties and the type of tissue in growth is still unclear [160].

Mechanical properties: The fusion process of molten particles on previously deposited layers can produce high levels of residual stress due to the rigidity of certain polymers (such as PEEK) and to the thermal coefficient mismatch [158]. Sufficient splat coalescence is required to achieve high coating strength, toughness, and hardness. Poor coalescence is the result of poor particle melting and thus low splat elongation ratio [161]. Brogan and Berndt [161, 162] were able to identify two temperature thresholds for sufficient particle coalescence in spray formed EMAA (Ethylene Methacrylic Acid Copolymer) coatings. However, their proposed model can be applied to other polymer coatings. The lower temperature threshold required for producing a viscous flow to coalesce polymer particle

and to obtain maximal density was estimated to 160°C. Below this temperature, the solidification is faster and the low deformation of semimolten particles following impact on the substrate lead to many defects formation. The flow of accumulating splats is not sufficient to fill the defects, which results in porous coatings [163], with its negative effect on the mechanical performance of the coating. At 160°C[161], the polymer chains having insufficient time to effectively diffuse across the splat boundaries, producing a weak coating-substrate interface, which is the precursor to early mechanical failure. A second threshold was identified at 216°C, during which significant polymer chain diffusion occurs across the splat boundaries, this results in higher ultimate tensile strength, elongation at break, and toughness [164]. Above the second threshold, the gaseous products released during the spraying process can decrease the strength, toughness and hardness of the polymer coating.

Adhesion: Adhesion between sprayed particles and the substrate or previously deposited lamellae is possible since the outer surface of the particle is melted to some extent. Effective contact between the coating and the substrate can only be achieved with a correct flow of particles over the substrate's rough surface. Ideally, the droplets should flow into the irregularities of the substrate and the consequent intimate contact provides an adherent coating [165]. This depends upon the degree of fusion, the velocity of the particles at impact, and the substrate surface condition. Therefore, the particle flow upon impact is critical to obtain good coating adhesion. On the other hand, inadequate flow leads to interfacial voidage. Bao et al. [165] showed that preheating the substrate provides an appreciable improvement in the adhesion of polymer coatings (polyamide 11 in this case). Plasma spray deposition and thermal spray in general involve rapid cooling that restricts the particle flow on the substrate. Preheating the substrate is motivated by the fact that the increase in substrate temperature reduces substantially the polymer splats cooling rate, thus, improving their flow and increasing the true area of contact between the coating and the substrate, which results in enhancement of the coating-substrate adhesion. Preheating is also removes the moisture present on the surface of the substrate, which improves the condition of the surface furthermore. The spraying distance and the plasma arc power in the case of plasma spraying, can improve the adhesion of polymer coatings [165].

Summary: Zhang et al. [154] theoretically showed that polymers are unique in developing large temperature gradients that accelerate the degradation of the surface of the particles and the coating layers. However, the degradation can be limited by controlling the spraying distance, the torch traverse speed and the plasma gas composition (when a plasma gun is used). The required process window for thermally sprayed polymers derives from the need to maximise splat flow and minimise polymer decomposition. Liao et al. [158] concluded that the regular flame spray technique was more suited to thermally spray polymers. Where plasma spray was used, the coatings remained porous with a noticeable degradation level due to the extremely high process temperature and where HVOF (High Velocity Oxy-Fuel) was used, thermal degradation remained low, but dense and smooth coatings were not obtained due to high velocity impact of particles on the substrate. Ivosevic et al. [155] concluded that the optimal thermal spray process for polymers should have a low gas temperature (~100-500^{o}C) to prevent overheating of the polymer particles, a high gas velocity to provide high kinetic energy for good flattening of the high melt viscosity particles and a sufficiently long dwell time for uniform particle melting.

A large particle size or molecular weight distribution tends to facilitate the formation of numerous heterogeneities within the coating microstructure, creating voids, a range of splat aspect ratios, and degraded material [111]. Therefore, a fairly narrow particle size range is preferable in order to control and reduce the large temperature differences in heating of the individual particles [164]. A typical thermal spray powder size for polymers ranges from 45 to 180 μm. However, experimental results [166, 167] show that coating produced from an optimal particles size of less than 100 μm exhibited greater tensile strength, increased wear resistance, and higher density. The experimental and theoretical observations referred to above are applicable to all types of thermal spray processes even though different mechanisms of heat generation are used.

2.6 Polymer Based Drug Delivery Systems

Across all medical disciplines that require delivering a therapeutic agent locally and subcutaneously, removal of the drug carrier seems to be a major drawback. Therefore, using biodegradable polymers as drug delivery systems is becoming the most popular technique as it excludes the need for a second operation to remove the carrier.

Biodegradable polymers in general [50] and for orthopaedic applications [36, 51] in particular have been extensively reviewed. Giavaresi et al. [36] reported that a literature search of scientific publications (MEDLINE[1]), showed that polymers were used to develop drug delivery systems for musculoskeletal pathologies to carry proteins and growth factors for bone regeneration (54% of papers found through MEDLINE search), antibiotics to treat mainly osteomyelitis (22%), antiresoptive (5%) and antineoplastic (4%) drugs. Additionally, multifunctional devices combining mechanical functions and drug delivery have been investigated to improve bone tissue regeneration, fixation and augmentation (15%).Along with excluding the need for a second operation, biodegradable polymers for drug delivery have the advantage of avoiding systemic side effects, assuring high local levels of the drugs, and avoiding the need for recurrent injections or intravenous maintenance [168]. One of the most important complications of currently used polymers is the occurring reaction to rapidly degrading materials [36]. The rate of degradation is thought to be influenced by many factors such as: molecular weight, cyrstallinity, porosity and site of implantation. The same factors seem to have an influence on the degree and the morphology of the induced fibrous tissue around the implant.

Garvin and Hanssen[169] reported that in experimental settings, systems for local drug delivery have been shown to be successful without the need for supplemental parenteral antibiotic therapy. Additionally, local drug delivery would minimise the risk of systemic toxicity that is currently associated with long-term parenteral treatment with antibiotics [170]. The polymers selection for the proposed application and for implantable biomaterials in general should be performed, taking into account some important aspects [171] as:

- The material should not invoke a sustained inflammatory or toxic response upon implantation in the body
- The degradation time of the material should match the healing or regeneration process
- The material should have appropriate mechanical properties for the indicated application and the variation in mechanical properties with the degradation should be compatible with the healing or regeneration process
- The degradation products should not be toxic, and should be able to get metabolised and cleared from the body

[1]MEDLINE Search Strategies: From 1972 to 2004 (“Bone and Bones” [MeSH] OR “Cartilage” [MeSH]) and (“Drug delivery system” [MeSH] and “Polymers” [MeSH])

A review of carriers used for local antibiotics delivery is shown in Table 12.Following a comprehensive literature review, two biodegradable polymers (PCL and PHBV) were used as primary coatings matrix and another biocompatible polymer (PMMA) was required in order to overcome some process limitations associated with PHBV. The biodegradable polymers used in this project were preferred to other polymers as they were found to be the most used materials in applications combining both orthopaedic use and drug delivery use. PHBV was extensively investigated as drug delivery system [47, 172-175]. Similarly, PCL was thoroughly studied by many researchers as a drug carrier [39, 94, 176].

Table 12: Antibiotics drug delivery systems [177]

Carrier system	Antibiotic released
Non-biodegradable	
Acrylic bone cement	Oxacilin, Cefazolin, Gentamicin, Fucidin, Cephalosporin
Cement of BIS-GMA/TEGDMA resin	Cephalexin
Plaster of Paris pellets/beads	Teicoplanin, Gentamicin, Fucidin
Polymethylmethacrylate (PMMA) beads	Gentamicin, Tazocin, Vancomycin
Polymethylmethacrylate (PMMA) cement	Vancomycin
Biodegradable	
Collagen-gentamicin sponge	Gentamicin
Hydroxyapatite blocks	Vancomycin, Gentamicin, Arbekacin
Hydroxyapatite cement	Vancomycin
Nano-HA-PHBV/PEG-GM microsphere	Gentamicin
Bone cement	Ciprofloxacin
Hydroxyaptite-β-tricalcium phosphate composite	Gentamicin
β-tricalcium phosphate-chitosan scaffold	Gentamicin
Chitosan bar	Gentamicin, Vancomycin
Apatite-wollastonite glass ceramic blocks	Cefmetazole, Isepamicin sulphate
Bioglass reinforced plaster of Paris, hydroxyapatite and sodium alginate	Cephazoline
Polylactide and /or polyglycolide implants	Gentamicin, Ciprofloxacin, Vancomycin, Tobramycin, Sodium fusidate
Poly(acrylic acid) and gelatin crosslinked	Gentamicin or Vancomycin
Polyanhybride and polylactide blend	Ofloxacin
Polycaprolactone	Tobramycin
Polyanhybride implants (Septacin)	Gentamicin
Injectable gelling polymer	Gentamicin
Fibrin clots / sealant	Arbekacin, Tobramycin, Ciprofloxacin
Fibrin gel (Vanco-AB-FG) with bone marrow-derived mesenchymal stem cells (BMMSCs)	Vancomycin
Dilactate polymers	Teicoplanin, Tobramycin, Sulperazone, Ciprofloxacin, Pefloxacin
Bone xenograft	Gentamicin
Bone graft / demineralised bone matrix	Tobramycin
β-tricalcium phosphate	Gentamicin, Vancomycin
Calcium sulfate	Tobramycin, Daptomycin
Calcium sulfate with demineralised bone matrix (DBM)	Vancomycin
Calcium phosphate cement (CPC)/injectable CPC	Gentamicin, Teicoplanin
Biomedical polyurethanes	Flucloxacillin, Ciprofloxacin, Fosfomycin, Gentamicin
Fibres	Tetracyline
Cross-linked hyaluronic acid (HA) gel	Gentamicin
Monoolein-water gels	Gentamicin

2.6.1 Polymer-Drug Attachment

Although polymers and copolymers of lactic and glycolic acids are more commonly used for delivering drugs locally, due to their safe and more importantly authorised use for human applications, more biodegradable polymers are being investigated in order to broaden the range of materials that can be used as drug delivery systems. These materials include polymers from the PHAs family and PCL.

In order to produce a polymer-antibiotic compound in a form that is suitable for thermal spraying, spherical particles or microspheres have to be produced. Entrapment of drugs into polymers is known as microencapsulation. Various techniques are available for the encapsulation of core materials [178]; these are divided into three types: chemical methods, physic-chemical methods and physic-mechanical methods. From the later type, two techniques are mainly used for the production of polymeric compounds that encapsulates antibiotics used for orthopaedic treatments: the emulsion solvent evaporation method and the spray drying method.

Emulsion solvent evaporation:

This process is the most frequently used microencapsulation method. It has been applied for the production of PHB and PHBV microspheres [179], PLGA microspheres [180], and PHBV/PCL microspheres [181]. Figure 20shows the preparation steps for emulsion solvent evaporation.

In the final stages of this method [178], the coat encapsulation material (polymer) shrinks around the core material (drug) and encapsulates the core. Following the preparation method described above, DSC data [179] showed that changes in melting temperature from the commercially available PHB and PHBV polymers to their resultant microspheres were not significant, which was an encouraging factor in light of their use in thermal spraying applications. The same study led to the production of PHBV microspheres characterised by a volume mean diameter ranging from 31 to 390 μm, with the size of these particles found to be influenced by all processing conditions. Such a flexibility in powder production would undeniably offer a larger processing window when it comes to thermal spraying.

Using the same technique, Simioni et al. [181] obtained drug-loaded PHBV/PCL microspheres with particles having a spherical form and an average size of 30 µm.

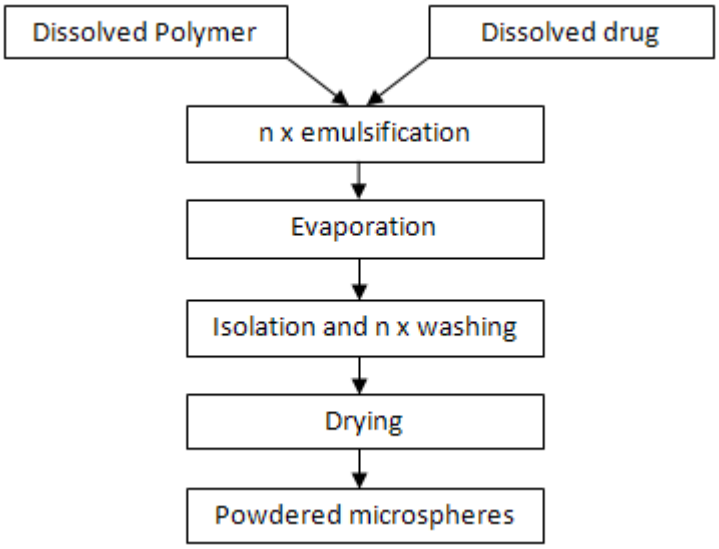

Figure 20: Microsphere preparation using the emulsion solvent evaporation technique

Spray drying:

Spray drying has been widely used in the production of drug-loaded microspheres [182-184]. This one-step method has good control on process parameters [184]. The mixture to be sprayed can be solvent emulsion, suspension, or dispersion. Figure 21 shows the preparation steps for the spray drying technique.

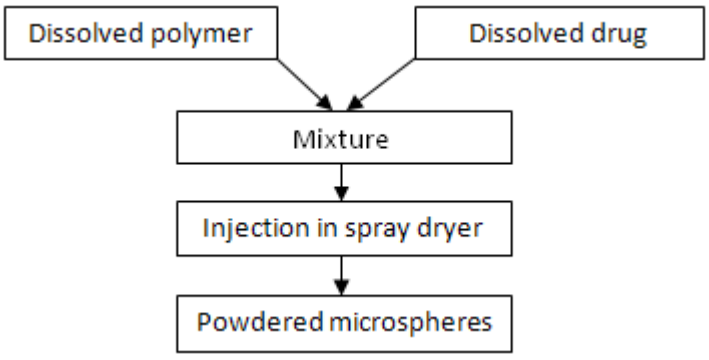

Figure 21: Microsphere preparation using the spray drying technique

Drying of the particles is achieved through the atomisation of the polymer/drug emulsion, which is sprayed through a nozzle into a hot drying medium (air). Schnieders et al. [182] showed that using the spray drying method resulted in a monomodal particle distribution with spherical morphology and smooth particle surface, demonstrating that the antibiotic was completely entrapped with the polymer matrix. It was also found that the drug release was controlled by a combination of pore diffusion and PLGA erosion, although the release mechanism generally depends on the type of polymers used. The same study showed that the distribution of gentamicin (antibiotic) in the polymer microspheres did not affect the glass transition temperatures. From a strictly physical aspect, the addition to drug-loaded polymer microspheres to an HA cement matrix for orthopaedic applications, did not affect the mechanical performance of the cement [182].

Using spraying drying, Patel et al. [184] obtained microspheres with an average particle size of up to 26 μm. This powder characteristic could, none-the-less, be varied by changing the molecular weight of the polymer and the amount of drug to be entrapped. Prior et al. [183] compared between the spray drying and the solvent evaporation methods for the production of PLGA microspheres and found that both methods produced comparable microsphere size distributions. However, encapsulation efficiency was significantly higher with spray drying than with solvent evaporation.

2.6.2 Polymers for Drug Delivery Purposes

Along with some aliphatic polyesters, polyhydroxyalkanoates such as PHB and PHBV, and polycaprolactone are the most important biodegradable polymers with frequent application as biodegradable products in prosthesis and controlled drug release products [185].

PCL :

Polycaprolactone offers a wide range of benefits; the most important of them are its superior osteoinductive potential, low degradation time, good mechanical properties and low emissions of harmful products [51]. The semi-crystalline nature of this polymer extends its resorption time to more than two years because of the closely packed macromolecular arrays which retard fluid ingress [160]. Due to this slow degradation (2~3

years), high permeability to many drugs, and non-toxicity, PCL was initially investigated as a long term drug/vaccine delivery vehicle [50]. Sinha et al. [39] are extensively working on the development of various micro and nano-sized drug delivery vehicles based on PCL. Kim et al. [94] used PCL as a coating component to improve the brittleness and low strength of HA scaffolds, as well as to effectively entrap drugs for local delivery. Microporous PCL and HA-filled PCL materials were found to provide a favourable surface for attachment and growth of primary human osteoblasts in cell culture [176]. Ciapetti et al. [186]also concluded from the ultrastructural findings of their study support the observation that the PCL-based polymers are capable of promoting osteoblast growth and maintenance of their phenotype. In converging conclusions, Coombes et al. [176] suggested that the low resorption of precipitation cast materials based on PCL encourages their use as long-term delivery systems for bioactive molecules such as growth factors and hormones and their extended-residence encourages cell growth and tissue development. Iooss et al. [187] studied PCL microparticles as drug carriers in conjunction with biphasic calcium phosphate granules for injectable bone substitute applications; the *in vitro* release study showed that this type of composite can be efficient for drug delivery systems with osteoconduction properties. According to Jameela et al. [188], the governing factor controlling drug release is diffusion across the polymeric matrix; therefore drug delivery starts quickly with PCL while the polymer itself degrades very slowly. Such a property guarantees the physical integrity of implants that contain PCL. Due to all the characteristics mentioned above, polycaprolactone was therefore used for three main applications in this study: improvement of mechanical properties, encouraging cellular growth, and local drug delivery. As opposed to other polymers, thermal spraying of PCL is not a well investigated technique. However, Garcia Alonso [11] proved that PCL can be deposited without major degradation, even though it has a low melting temperature (60^{o}C) and the thermal spraying technique used was low energy plasma spraying, which generally has a higher plume temperature than HVOF and flame spray.

PHBV:

It has been reported that complete resorption of PHA polymers *in vivo* takes from several months up to 2-2.5 years, depending on the form of the item and on the implantation site [6,

95].PHBV is very particular for the bone tissue engineering applications. It has been demonstrated that a potential component bone tissue adaptation response can be produced with no verification of an undesirable chronic inflammatory response after implantation for periods of up to 12 months [51]. A unique property of PHBV is its piezoelectricity, which was claimed to induce bone reformation in load-bearing sites [172]; this makes it a potential candidate for orthopaedic applications since electrical stimulation has been known to promote bone healing [50]. It was found that the mass loss of this polymer follows zero-order release kinetics and this property along with its hydrophobic nature confirms that this polymer undergoes surface erosion. This degradation property makes PHBV an ideal candidate for developing long term drug delivery systems capable of achieving zero-order drug release [50].Therefore, PHBV may be a potential biodegradable candidate for long term implants. The crystallinity and mechanical properties of PHBV can be changed by varying the ratio of the respective monomers (PHB/PHV) [51].It was found by Rossi et al. [189] that increasing the HV content led to an amorphous structure, which resulted in increased water absorption. This accelerates the dissolution of the drug crystals and therefore a faster release rate. It can be also possible to control the drug release rate by controlling the concentration of the antibiotic crystals in the polymeric matrix. Rossi et al. [189] proved that PHBV/gentamicin (antibiotic) complexes eradicate *Staphylococcus aureus* and gentamicin-resistant *Staphylococcushaemolyticus* adhering to the substrate surface and showed no adverse effects on blood cell integrity. Shishatskaya et al. [96] reported that PHBV and other PHA polymers can be successfully used as matrices for culturing osteogenic cell *in vitro*. The major disadvantages of the PHA polymers group are their limited availability and time consuming extraction process from bacterial culture that requires a proper extraction set-up. There is no literature available for PHBV thermal spraying, which implies that little or no work at all has been performed using this technique to obtain PHBV coatings, hence lies the novelty of the research.

PMMA

The major drawback of PMMA as a drug delivery system comes from its non-biodegradable nature, which requires the removal of the polymer from the implantation site upon completion of their task. Nonetheless, antibiotic impregnated beads [190] have been used in the treatment of chronic osteomyelitis for the past few decades. PMMA is

considered to be an effective method for providing sustained high concentrations of antibiotics locally when used for treatment of bone and soft tissue infections [191]. PMMA can be used in two forms; as an antibiotic-impregnated bone cement applied in arthroplasties, and as antibiotic-impregnated bead chains for musculoskeletal infections [192]. PMMA augmentation was also used for improving screw fixation or as a filling material in cases of severe bone loss. PMMA has relatively poor adhesion to bone [193], however, its implantation into the cancellous bone improves the ultimate mechanical strength of the bone cement composite. PMMA can also be used to fill bone defects particularly in the metaphyseal areas. De Giglio et al.[194] investigated PMMA coatings on titanium implants as barriers against ions release and concluded that the presence of PMMA coatings produces a decrease in ion release from the substrate, it was also found that an annealing treatment considerably reduced the ion dissolution rate, leading to very efficient protective coatings. PMMA have been thermally sprayed (plasma spray) [43, 154, 165], and it was found that adequate spraying parameters can avoid degradation of the polymer coatings and facilitate control over coating properties.

2.6.3 Heat-Stable Antibiotics

From Table 12 and a thorough review of literature, a small numbers drugs appear to be the preferred choice for antibiotic treatment in orthopaedic applications. These are tetracycline hydrochloride [94], gentamicin [195] and tobramycin [196] with PCL as a drug carrier; and sulbactam[172] with PHBV as drug carrier. As the novelty of this project lies in using a thermal spraying technique to produce drug-eluting coatings, it is of primary importance to establish that the drugs/growth factors that could potentially be used are able to sustain the thermal effects caused by the production process.

Tobramycin:

Tobramycin belongs to the family of aminoglycoside antibiotics. Dash and Suryanarayanan [197] performed a thermomicroscopic analysis on tobramycin by connecting a differential scanning calorimeter and a thermograviometric analysed to a thermal analysis operating system. This study revealed two main occurrences: melting was observed at approximately 163^{o}C and crystallisation at about 195^{o}C. It was concluded, following thorough

characterisation, that no appreciable sample decomposition even after heating up to a temperature of 224^{o}C.

Gentamicin:

Wang et al. [198] investigated the thermal stability of gentamicin in order to determine whether the heat might destroy the antibiotics during the manufacturing process antibiotic-loaded polymer beads. Their thermal stability test consisted in incubating the antibiotic in an oven for 30 minutes at various temperatures up to a maximum of 100^{o}C, before testing the bioactivity of the drug. The study suggested that gentamicin was rather stable up to 100^{o}C. TGA data for gentamicin sulfate showed a thermal decomposition starting at 220^{o}C and proceeding stepwise until 330^{o}C [199].

Tetracycline hydrochloride:

Fernandes et al. [200] studied the thermal decomposition of some chemotherapic substances including tetracycline hydrochloride. It was concluded that the latter was a thermally stable agent up to a temperature of around 200^{o}C.

Sulbactam-cefoperazone:

No literature was found on the thermal stability of sulbactam, which implies that this antibiotic feature was not investigated thoroughly.

2.7 DoE Experiments

Design of Experiments (DoE) is a statistical method (Appendix-A) that aims at analysing/understanding how variable parameters in any given process affect the characteristics of the final product. The advantage of this technique in industrial as well as research applications is its cost and time reduction properties. However, the versatility of this technique also allows more thorough analysis to be conducted using more experimental runs, regardless of the time constraint. In fact, DoE allows the operator to obtain a large amount of information while undertaking a minimal number of experiments. Statistical design of experiments refers to the process of planning the experiment so that appropriate data can be collected and analysed by statistical method (mainly software tools) resulting in

valid and objectives conclusions [201].When the problem involves data that are subjected to experimental errors, statistical methods are the only objective approach to analysis. In this context, the parameters to be varied are termed “factors”. The different possibilities for each factor are termed “level”, and the measured output is termed “response”. Factor levels could be either quantitative (nominal) or qualitative (categorical). The influence of a specific factor on any given response can be evaluated by contrasting the average response when the factor was not changed with the average result when it was changed. Responses are represented as a polynomial regression equation of the following form:

$$Y = b_0 + \sum b_j X_j + \sum b_{ij} X_i X_j + \sum b_{ijk} X_i X_j X_k \qquad \textbf{(Eqn.1)}$$

where i, j and k vary from 1 to the number of variables; coefficient b_0 is the mean of the responses of all the experiment; b_i coefficient represents the effect of the variable X_i and b_{ij} and b_{ijk} are the coefficients of regression which represent the effects of interactions of the variable X_iX_j and$X_iX_jX_k$ respectively.

The DoE method can be applied to any subject area either in industry or in academia; it offers wide range of statistical methods/approaches to solve problems, the main ones being factorial experiments, Box-Behnken, etc. The choice of a specific method is dictated by the the aims of the experiments, the number of factors being investigated, and the number of responses analysed.

2.7.1 Factorial Experiments

Factorial experiments are most efficient in studying the effects of two or more factors [201]. This type of experiment implies that in each complete trial of the experiment all possible combinations of the levels of factors must be investigated. A two level factorial experiments with k factors is termed 2^k experiment, a simple example would be a 2^2 experiment, which would be used to investigate the effect of two factors at two different levels for any given responses. Such an experiment would involve 4 experiments as shown in Table 13, where -1 and 1 are the minimum and maximum ranged values for a particular factor.

Table 13: 2-factors, 2-levels factorial experiment

Run	F1	F2
1	-1	-1
2	-1	1
3	1	-1
4	1	1
5	0	0

The effect of each factor is defined as the change in response generated by a change in the level of the factor. In order to eliminate errors that are caused by factors un-accounted for in the experiment such as different batches of materials or machine operators and lab conditions, the experiments are randomised. In order to improve the process stability furthermore, 3 to 6 centre points can be added to factorial designs. These points represent the centre values for all factors and are coded "0" in the case of the example shown in Table 13. In cases where the response values did not yield an adequate model, transformations to all values may be needed to meet the assumptions that make the model valid. Transformations apply a mathematical function to all the response data.

2.7.2 Response Surface Methodology

Response Surface Methodology (RSM) is a series of techniques used to develop, improve and optimise processes, either by maximising or minimising the process responses. The RSM technique used for this project is the miscellaneous technique, which allows 3-level factorial designs to be analysed (-1, 0, 1), as well as special case designs such as hybrid, pentagonal, hexagonal, etc. This technique is useful when more than two factors are being analysed. Having a larger number of experiments also gives the opportunity to compare how different process responses interact with each other by manually plotting them.

Even though this research produced a large number of experiments, this DoE technique was preferred as time was not a constraint and the large combinations of factor levels (experiments) generated, covered more of the design space being investigated, which was

crucial in a project that aims at investigating a new processing technique for biodegradable polymers.

The statistical package used in this research generates a number of possible solutions based on the optimisation criteria chosen. The software indicates the desirability of each solution (1 being the most desirable and 0 the least). Based on the desirability value and the levels of responses predicted for each solution, an optimal set of process parameters can be chosen.

Summary:

The aim of this literature review was to establish that even though HA coated implants have undeniably improved the success rate of hip implantations, the need for an improved coating performance of orthopaedic femoral implants still exists, both in terms of mechanical performance and bioactive properties such as drug delivery. Biocompatible polymers such as PMMA and biodegradable biocompatible polymers such as PCL and PHBV are seen as the ideal candidates to deliver the improvements targeted by this project. The deposition techniques of such coatings, via thermal spraying, were then discussed and shown to have succeeded with a number of polymers in the past. Therefore the challenge of this project is to combine the use of the flame spraying technique with the bioactive properties of the chosen biocompatible polymers in order to obtain a drug delivery polymer coating. This is used in conjunction with plasma sprayed HA to form an HA/Polymer bilayer orthopaedic coating, which retains the advantages of a ceramic coating while providing a mean to deliver antibiotics or growth factors to the implantation site without the need to remove the drug carrier.

3 Equipment, Materials and Procedures

3.1 Thermal Spraying Equipment

3.1.1 Flame Spray Equipment

Powder flame spray guns are usually lighter and more compact than other types of thermal spraying equipment. Powders in this process were fed into the spray nozzle by gravity from an integral powder canister directly mounted on top of the torch. The powder feed rate was controlled by a pinch valve (or a lever valve) that allowed the powder to flow into the gas stream by gravity and by a suction effect created by the gases flowing into the torch.

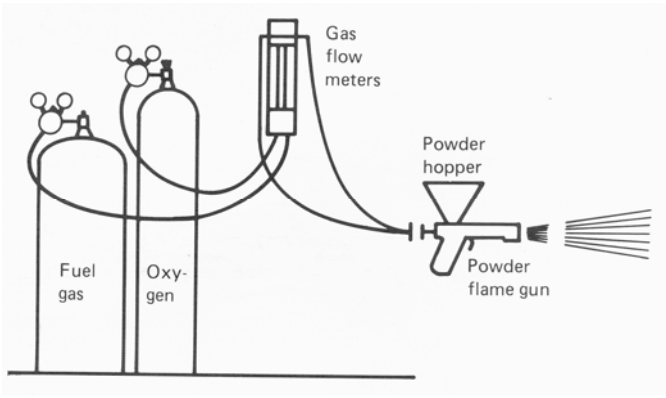

Figure 22: Typical installation of a powder flame spray process [112]

The key components of a typical flame spray system as shown in Figure 22 are:

- Acetylene and Oxygen supplies
- Gas hoses
- Gas regulators for oxygen and fuel
- Gas flow meters for oxygen and fuel control
- Flashback arrestors at the gun and regulators
- Flame spray gun a handling extension, a torch body and a detachable nozzle
- Spray material delivery system
- Extraction booth
- Operator safety equipment: ear muffs, welding glasses, gas and particle masks.

Equipment used:

For the purpose of this project, an IBEDA Mini Spray Jet flame gun (Figure 23) was purchased. This flame gun uses oxygen and acetylene gases for combustion; it uses a particle size range from 10 to 100 microns. The gun maybe hand-held or machine mountable. Due to its lower cost, in comparison to other thermal spray guns, this gun has a limited number of controllable parameters. The oxygen regulating valve has to be fully open during operation whereas the fuel regulating valve can be set to three different positions: neutral flame (stoichiometric mixture of oxygen and fuel gas), oxidised flame (excess oxygen) and reduced flame (excess fuel gas). A powder "dosing" slide allows the diameter of the inlet orifice to be changed, which controls the powder feed rate depending on the average size of the powder being sprayed; four different diameters are available, referenced as 1 to 4, where 1 was the smallest orifice. Operating pressures used were: oxygen 2.5 Bar and acetylene 0.7 Bar. This flame gun also includes an extra powder inlet to allow the operator to use an external powder feeding system for better process controllability, if required or air maybe connected to the current set up to fluidise the powder for increased flowability.

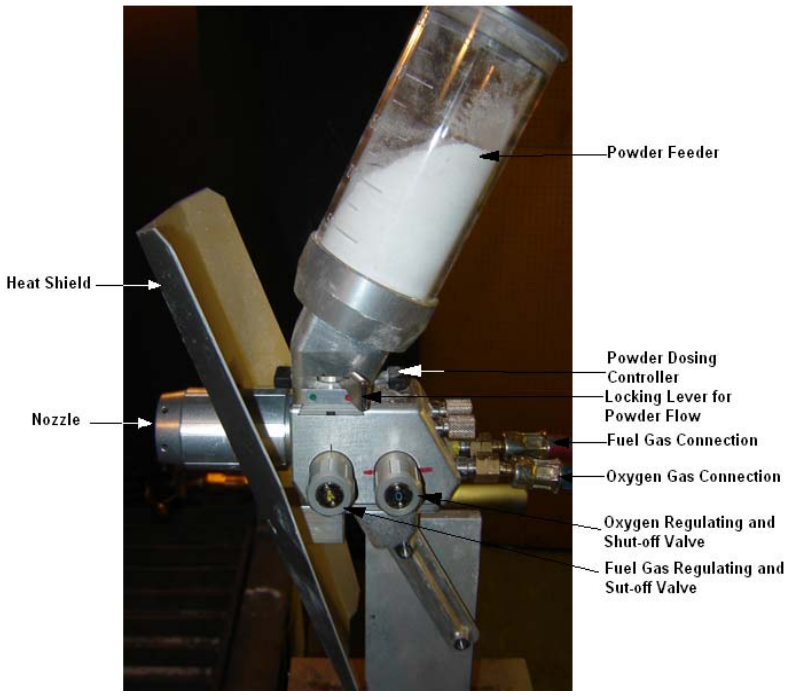

Figure 23: Ibeda MiniSprayJet Flame Spray System

3.1.2 Flame Spray Procedure

Spraying Procedure:

Although there may be limitations in the range of gas and powder flow rates that can be chosen, the choice of powder (melting and boiling temperatures, etc.), its shape and size and other parameters like spray distance, traverse speed (via a linear traverse unit) and number of passes, depicts a limited researched process worthy of optimisation.

The ranges of spraying parameters were set before the spraying based on literature recommendations; these included the spraying distance (0.2-0.4m), the gun traverse speed (0.152-0.254m/s) and the number of passes (6-14). The change in process parameters is discussed in details in chapter 4.

Prior to the deposition of polymers, the substrate samples were pre-heated according to the melting point of the feedstock material. Preheating involved passing the flame of the gun in front of the sample for a "polymer-temperature related"(melting) specific number of passes. The temperature of the substrate was measured using a thermocouple device. Initial problems regarding powder flow and blockage delayed the experimental work. However, this issue was overcome by placing a vibrating device inside the powder cartridge to keep the powder flowing (a concept taken from the plasma powder feed system). Additionally, prior to the PCL/PMMA parameters range selection and due to the low melting temperature of PCL powder and to the fact that following a prolonged storing, moisture may have affected its ability to flow, the powder matrix demonstrated some blocking of the orifice inside the flame gun, which directly affected the suction effect of the oxygen flow. Therefore, the manufacturer suggested the use of compressed air to increase the suction effect. This feature also creates an air-foil effect in the plume that protects the powder from the flame, allowing the powder to melt through latent heat only.

Safety equipment:

Thermal spraying is a hazardous process in many aspects; these include the exposure to ultraviolet light, to noise, fumes and dust generated during the process. Therefore operators are required to use personal protection if the spraying is done in an open booth set-up, which is the case in this project.

- **Ultraviolet light from the plasma arc:** UV light can cause partial or total blindness if the cornea gets burnt. Eye protection using specific welding masks must worn at all times. UV lights are also known to damage the skin, and therefore, wearing an overall is required during the spraying process.
- **Noise:** Thermal spray guns can reach a maximum noise level of 127/128dB (especially with plasma guns) which is considerably more than what humans can tolerate. Physical effects of exposure to excessive noise include tinnitus and a progressive loss of hearing due to the damage of the sensory mechanism in the ear. Other than physical damage, excessive noise can cause stress, difficulties in communication and a lack of concentration. Operators are required to use ear plugs and ear muffs at all times during the spraying process, and limit the exposure time.
- **Fumes and dust:** Thermal spraying generates fumes and dust that might vary in toxicity depending on the material being sprayed. Inhalation of such fumes/dust can lead to respiratory diseases and irreversible bodily damage. An extraction system with the appropriate duct work is needed to clear the harmful gases and particles from the facility and to filter remaining products to the atmosphere. The operator is also required to wear the appropriate face mask which includes a particle filter and a gas filter component.

3.1.3 Plasma Spray Equipment

Equipment:

Plasma spraying is considered to be the most complex and most versatile of all thermal spray processes. The key components of a typical plasma spray system as shown in Figure 24 are:

- Gas supply and gas hoses
- Gas regulators for plasma gases and powder carrier gases
- Main control unit comprising gas flow meters and controls, electric controls for arc current and voltage
- Plasma gun comprising a torch body, anode (nozzle)/cathode, gas injector and powder injector
- Current power generator

- Water-cooling circuit and water cooled power cables (also used to cool the gun)
- Powder hopper
- Extraction booth

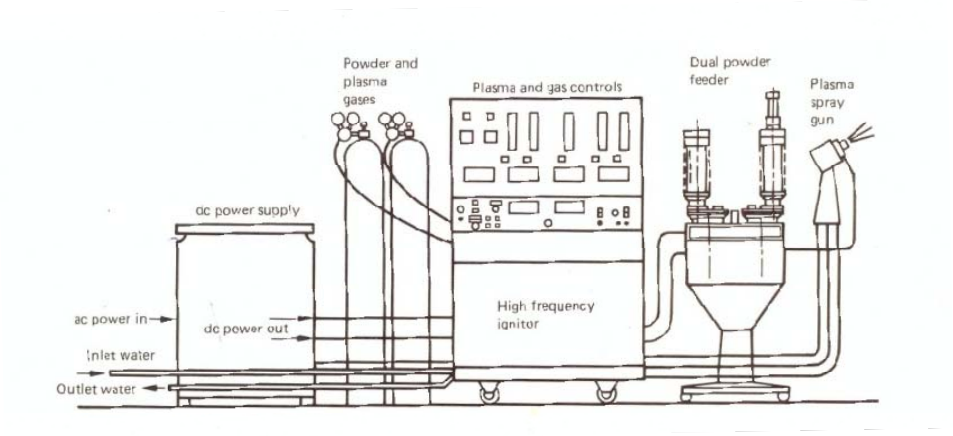

Figure 24: Complete installation of a plasma spray system [112]

In order for the system/gun to generate high temperatures, high power levels are required, therefore, water cooling of the power cables and gun was essential. The plasma spray equipment used for this project is the Sulzer Metco atmospheric 9M plasma spray system. The equipment is located in a purpose built, sound-proof room in the National Centre for Plasma Science and Technology (NCPST) in Dublin City University. This plasma spray system consists of three main units: the plasma gun (9MB), the powder feeder (9MPE) and the control unit (9MCE). The plasma laboratory set-up is shown in Figure 25.

Figure 25: Plasma Spray System

9MB Plasma gun:

The Sulzer Metco 9MB-Dual plasma spray gun (Figure 26) comprises of a 9MB63 electrode, a 3M7-GH nozzle and a closed-loop cooling system to avoid over-heating of the gun parts. The gun has a machine mountable base assembly which allows the gun to be mounted directly onto the extraction booth (current system) or onto a traverse unit. The radial powder injection was located just outside the nozzle, which means that powder was introduced into the spray stream externally perpendicular to the plume direction. The benefits of an external injection are: avoiding the blockage of the nozzle, reducing the risk of contamination and elimination of cleaning and maintenance problems. Some of the main features of the 9MB-Dual plasma gun, according to the Sulzer Metco product data sheet [202], are listed below:

- High powder capabilities: up to 80kW
- High heat output capabilities: up to 16,000^{o}C plasma temperatures (when hydrogen is used as a secondary gas)
- High plasma gas velocity: in excess of 3,050 m/s
- High particle velocities: up to 610 m/s
- Dual gas capability: operates with either Argon or Nitrogen as primary plasma gas

Figure 26: Sulzer Metco 9MB Plasma Gun

Control unit:

The 9MCE plasma control unit (Figure 27) allows the operator to control the main process parameters from two separate panels: (a) a gas flow control panel to control the plasma gas ratios and flow rates, and (b) an electrical control panel to control the arc current. A d.c. electrical energy supply provides power to the system. The 9MCE control unit allows

spraying to be carried out using two plasma forming gases, a primary gas and a secondary gas. The primary plasma forming (Argon) gas flow rates were set to a pressure of 5.17 Bar (75 psi). The secondary gas flow rates could be set to a pressure of 3.45 Bar (50 psi), however, no secondary gas was used in this project. The control unit also controls the powder feeder to start feeding powder to the gun once the ignition has been initiated.

Figure 27: Sulzer Metco 9MCE Control Unit

Powder feeder:

The Sulzer Metco closed-loop 9MPE powder feeder controls the carrier gas flow rate, the vibrating air device (which aids powder flowability), and the coating material feed rate. The feedstock powder is stored in a hopper (Figure 28). The powder is carried from the hopper to the plasma gun using a fluidised bed system via a carrier gas (Argon) to entrain the powder particles and to carry them to the desired location. A weight loss metering system

(via a load cell) provides a continuous closed-loop adjustment of the powder feed rate. The powder carrier gas pressure is set at 5.17 Bar (75 psi).

Figure 28: Sulzer Metco 9MPE Closed-Loop Powder Feeder

Extraction booth and sample mover:

The samples to be sprayed are mounted on a fixture, which is fixed itself is fixed to a traverse unit. The traverse movement is controlled by pneumatic regulators (Appendix-B), with compressed air provided by compressor unit (Figure 25) located underneath the extraction booth. The spraying is performed inside an extraction booth (Figure 25) in order to prevent fumes and dust generated by the process from leaking in the room.

3.1.4 Plasma Spraying Procedure

A plasma equipment operating manual was prepared by the previous plasma spray operators [11, 89] based on optimised observations in the deposition of HA. This project followed the same procedure. The operating instructions are divided into a number of

separate sections. These include: 9MCE control unit start-up, extraction system start-up, purging and gas flow rate set-up, current set-up, powder hopper set-up, powder feeder testing and start-up, sample mover start-up and system ignition. After spraying, a feeder cleaning procedure was required. Following the operation manual allows the easy and effective detection of any system fault prior to ignition and prevents the operator from carrying out the remaining instructions, which was therefore vital to the safety of the operator and the facility itself. The detailed step-by-step instructions are provided in Appendix-C.

Equally this thermal spraying technique is hazardous with high temperatures, welding light and toxic fumes generated, in addition to the high level of noise caused by the extraction system. Therefore, the same safety precautions taken for the flame spraying were also applied during plasma spraying. These included wearing the necessary protective kit: ear plugs and ear muffs, the adequate welding mask, gas and particle masks, protective coveralls and gloves.

3.2 Feed Stock Powders

3.2.1 Polycaprolactone (PCL)

The PCL material used to produce the polymer coatings was supplied by Sigma Aldrich Co. (product #440744) in the form of granules. It was then cryogenically milled using 300 μm solid composites and spun-off (conducted by the Fraunhofer Institute, Germany) and finally sieved to under 150 μm in DCU. Some of the PCL properties provided by the supplier are shown in Table 14.

Table 14: PCL properties provided by Sigma Aldrich

Property	Value
Linear formula	$(C_6H_{10}O_2)_n$
Appearance	White to off-white beads
Form	Crystalline
Density	1.1445 (at 25^{o}C)g/cm^{3}
Melting point	60^{o}C
Melt index	1.00g/10min (at 125^{o}C and 44psi, ASTM D1238-73)

3.2.2 Polymethylmethacrylate (PMMA)

The polymethylmethacrylate powder used for this project was supplied by Goodfellow. The mean particle size was 40 μm. The material properties provided by the supplier are shown in Table 15.

Table 15: PMMA properties provided by Goodfellow

Property	Value
Appearance	White powder
Density	1.19 g/cm^3
Tensile strength	80MPa
Flammability	HB (auto-extinguishes)
Upper working temperature	50 to 90^{o}C
Limiting oxygen index	17-20%

This powder was not specifically produced for thermal spraying as it is the case for most polymer powders. PMMA powder was selected based on the fact that this polymer is already widely used for orthopaedic applications. Although it is not biodegradable, it is biocompatible and thus used to fulfil the function of a drug carrier.

3.2.3 Polyhydroxybutyrate/Polyhydroxyvalerate (PHBV)

The polyhydroxybutyrate/polyhydroxyvalerate polymer used in this project was supplied by Goodfellow. The properties provided by the manufacturer were limited. The information available in the product's MSDS are shown in Table16.

Table 16: PHBV properties provided by Goodfellow

Property	Value
Composition	98% PHB, 2% PHV
Appearance	White to beige
Melting point	150-180^{o}C
Density	1.25g/cm^3
Stability and reactivity	Stable in dry air at room temperature (20^{o}C)
Crystallinity	Semi-crystalline thermoplastic
Manufacturing process	Biological fermentation

3.2.4 Hydroxyapatite (HA)

The hydroxyapatite powder used during this project was supplied by Plasma Biotal Limited under the brand name CAPITAL 60-1. CAPITAL hydroxyapatite is a high purity, crystalline, synthetic bone mineral which is chemically stable at 1300^{o}C in air. It retains a highly crystalline structure. As opposed to the polymer powders used, the hydroxyapatite powder was produced specifically for thermal spray applications. According to the particle characterisation results supplied by the manufacturer, the average particle size for the CAPITAL 60-1 batch was 46.18 μm. The main elemental components and their limits are shown in Table 17. The calcium (CaO) and phosphorus (P_2O_5) ratio was found by gravimetric analysis to be equal to 1.33±0.05 corresponding to 1.68 (Ca/P) and a bulk density of 1.30±0.1 g/ml^3.

Table 17: List of elemental components and limits

Element	Formulae	Concentration
Calcium	CaO	54.5-55.2%
Phosphorus	P_2O_5	41.0-41.2%
Silicon	SiO_2	0.6% max
Carbon	CO_3^{2-}	1.5%max

3.3 Substrates

Two types of substrates were used during this project. Preliminary tests for familiarisation with the new flame spray equipment and the polymer powders involved spraying on rectangular aluminium coupons 50 mm x 20 mm x 2 mm in size to reduce cost. Titanium alloys (Ti6Al4V) (supplied by Impact Ireland) were then used for the remainder of the experimental work in order to mimic as closely as possible commercially available titanium orthopaedic implants. The Ti6Al4V substrate materials used were in form of discs, 10 mm in diameter x 2 mm in thickness, cut from a 10 mm diameter Ti6Al4V rod. Prior to the spraying process, the discs were prepared following the procedure described in the next section. A substrate holder was designed by the previous operator (Figure 29) of the plasma spray equipment to allow multiple sample deposition and to facilitate sample removal. The

design consisted of an aluminium L-shaped plate with two stainless steel clamping bars attached to the front. The clamping bars can be moved up and down by adjusting the screws at the back of the holder. Notches were cut into the clamping bars to allow secure fixation of the titanium alloy discs.

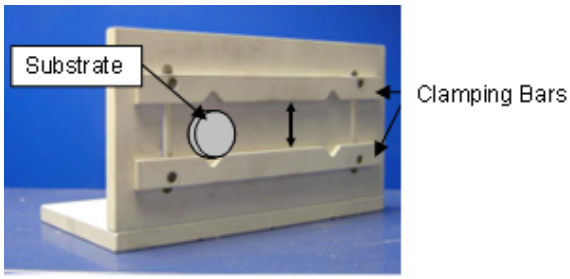

Figure 29: Sample holder [82]

3.4 Substrate Preparation

The bonding of thermally sprayed coatings is mostly mechanical in nature rather than metallurgical or chemical [203]. Thus, the condition of the substrate surface has a major effect on the overall adhesion of the coating, and an adequate surface wetting by the substrate is necessary. This is achieved predominantly by surface treatment (surface roughening) and in some cases by substrate preheating. Surface treatment was performed by grit blasting, which acted both mechanically by roughening the surface and chemically by removing any oxide layers, to create a very active substrate surface. Molten particles hitting the substrate are known to conform to the surface roughness, producing mechanical interlocking. This in turn affects the adhesion and peel strength of the coatings. The grit blasting, involved propelling high velocity irregular grit particles at the surface of the substrate. During this process some of the grit material can be embedded on the surface of the substrate; therefore the grit material should be biocompatible in order to avoid adverse effects on the quality of the coating *in vivo*, and applied at an angle not perpendicular to the substrate. Thus, grit blasting of the substrate was done using pure white alumina oxide, 500 μm (mesh 36) in size; Al_2O_3 is the most commonly used material for grit blasting of titanium implants [204]. Following recommendations from Amada and Hirose [205], grit blasting was performed using a blasting angle of 75^o and a blasting pressure of 5 Bar. Every test piece was grit blasted for 2 minutes to ensure a good surface roughness. Following this

physical roughening, the substrates were cleaned to remove any traces of grit material, grease and other contamination. According to the cleaning procedure described by Levingstone [89], the substrates were treated with compressed air to remove surface alumina particles. This was followed by placing the samples in an ultrasonic bath with a dilute acetone solution for 5 minutes. Finally, the samples were rinsed with water, dried with compressed air and stored in sealed bags to avoid recontamination.

Substrate preheating was also performed on the Ti samples pre-polymer spraying. The surfaces were heated up to the melting temperature of each polymer and in case of a polymers composite, the surface was heated up to its lower melting temperature. Preheating the surface increased particle melting and therefore the cohesion of the coating.

3.5 Surface Analysis

Substrate surface and coating roughness:

The surface roughness (Ra) of the grit blasted titanium disks and final coatings were determined using a Mitutoyo Surftest 402 surface roughness tester. This equipment consists of a stylus that was displaced over the surface of the substrate/coating. Prior to measuring the samples, the accuracy of the roughness tester was checked using a calibration block and a percentage error of 0.01% was found, which was within the ±0.3% acceptable threshold for errors. The roughness measurements of the coatings were obtained by running the stylus across the coated surface three times, following three different lines at 120^{o} angles from each other (Figure 30) in order to be as representative as possible of the roughness variation that could occur at the coating surface. The average Ra values of these measurements were taken as the roughness value for each sample.

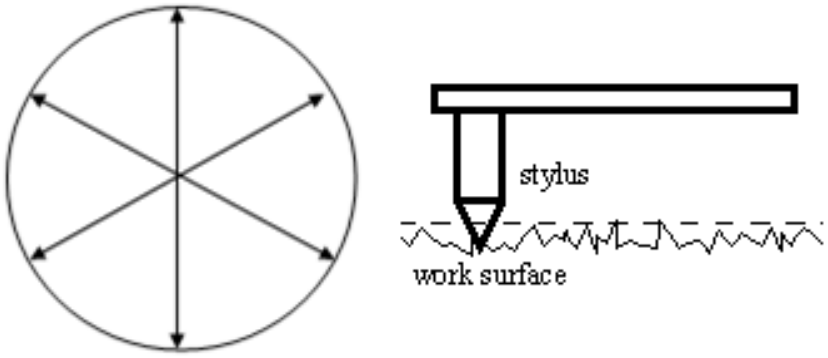

Figure 30: Stylus movement (right) and direction of pass (left) across the coating surface

3.6 Powder Characterisation

3.6.1 Powder Morphology

The polymer and HA powder morphologies were studied using a Scanning Electron Microscope (ZEISS *EVO LS15*). The SEM uses a beam of highly energetic electrons to examine objects on a very fine scale. SEM examination can yield valuable information about the topography of coatings/surfaces, the morphology of particles/powders and the composition/ratio of compounds within a coating. When a sample is bombarded with electrons [206], the strongest region of the electron energy spectrum is due to secondary electrons (SE). Secondary electrons are produced when an incident electron excites an electron in the sample and loses most of its energy in the process. This excited electron migrates towards the surface of the sample, undergoing elastic and inelastic collisions until it reaches the surface. If it has sufficient energy it will then escape. The SE mode in an SEM produces high resolution images with a large depth of field which yields images with 3D appearances. Therefore, the SE mode is the preferred option for topography related studies. Often, operators also use the SEM for the examination of surface roughness, coating porosity and the thickness of each sample's cross-section. Prior to the SEM examination, some sample preparation steps were required. Due to the non-conductive nature of the materials used in this project, electrical charging of the powder sample occurs during electron irradiation. In order to avoid this problem and to increase the signal and surface resolution, the sample was coated with a layer of gold. The first step in this process was to fix the powder to an aluminium stud that fits both the SEM stage holes and the gold coater apparatus, using conductive double-sided tape. Excess powder was then removed by blowing compressed air onto the sample surface; to prevent loose powder particles in the SEM chamber during vacuuming. The sample was then placed into the chamber of an *Edwards Scancoat* gold sputtering coater where a nanometric layer of gold was deposited on the sample powder for 80 seconds. This pre-examination step insured that there was electrical conductivity in the sample.

Alternatively, a Variable Pressure (VP) mode can be used to study non-conductive samples. This mode allows the reduction of the operating pressure by letting Nitrogen in the chamber (using a secondary pump). Nitrogen neutralises the negative ions on the sample surface and

therefore avoids pre-coating the samples with gold. The gold coating technique was mostly used in this research, except where specified, due to the unavailability of the VP mode. Studying the powder morphology was a crucial step in understanding the coating formation when using thermal spray processes as the shape and size of the feedstock powder affects the parameters used in order to obtain the desired coating characteristics.

3.6.2 Particle Size Distribution

The particle size analysing system worked on a laser diffraction principle using Mie theory, and Fraunhofer analysis. When powder particles are passed through a laser beam, the latter is scattered onto a detector array. An algorithm is then used to determine the particle size, which depends on the intensity of light dispersion, where the dispersion angle is inversely proportional to the particle size. The particle size distribution can affect some of the process parameters and the characteristics of the final coatings; therefore it is a key characterisation step towards understanding the coating formation.

Particle size was performed using the Malvern Mastersizer particle size analyser. This apparatus uses a single lens laser diffraction system with a small helium neon laser of the order of 2 milliWatts power to measure the size of particles. Prior to the analysis, 0.5 g of powder was mixed with 30 ml of a dispersant solution. The suspension was stirred and then placed in an ultrasonic bath for 5 minutes. The dispersant solution used consisted of 1 g of sodium hexametaphosphate in 1000 ml of de-ionised water. This was prepared according to the standard BS ISO 14887[207]. Particle size analysis was then carried out in accordance with BS ISO 13320-1:1999 [208].

3.6.3 Powder Density

The densities of feedstock powders were determined by using helium pycnometry. This technique approximately measures the true density of particulate materials. The density measured by helium pycnometry is a prerequisite for air permeability. Helium pycnometry works by forcing helium into voids of a pre-weighted sample; the helium is able into flow in the smallest voids and pores and can therefore be used to measure the volume per unit weight of the powder sample. The Micromeritics AccuPyc 1330 pycnometer used in this research determines the skeletal density and volume of a sample by measuring the pressure

change of helium in a calibrated volume. The AccuPyc works by measuring the amount of displaced helium. The pressures observed upon filling the sample chamber and then discharging it into a second empty chamber allows the computation of the sample solid phase volume. Gas molecules rapidly fill the tiniest pores of the sample, thus only the truly solid phase of the sample displaces the gas. The accuracy of this apparatus was within 0.03% of reading plus 0.03% of nominal full-scale sample chamber volume [209]. The testing parameters are shown in Table 18.

Table 18: Parameters used for the helium pycnometry

Parameter	Value
Purge fill pressure	19.5psig
Run fill pressure	19.5psig
Equilibrium rate	0.005psig/min
Run precision	Yes
Full scale	0.05%
Sample size	1 g

3.6.4 Powder Thermal Behaviour

Thermograviometric analysis (TGA) and Differential Thermal Analysis (DTA) of the HA and polymer powders was carried out in order to determine their thermal behaviour and expected melting and decomposition temperatures. The analysis was carried out using the Stanton Redcroft Differential Thermal Analyser/ Thermal Gravimetric Analyser.

- The DTA technique measures the temperature difference between a sample and an inert reference sample, while the two substances undergo identical thermal cycles. The DTA produces a curve that provides data on the transformations that have occurred to the sample such as glass transitions, crystallisation, etc.
- The TGA is used to determine the changes in weight of a sample in relation to the change in temperature. The resulting TGA curve provides information about degradation temperatures, absorbed moisture content, solvent residues, etc.

The equipment used in this study was capable of heating the sample up to a temperature of 1500 ºC. For this project, two settings were used, depending on the feedstock powder

(polymer, ceramic). A 20 mg sample of the HA powder was heated in a platinum pan at a rate of 10 ºC/min up to a temperature of 1450 ºC[89]. The powder was then cooled down to room temperature at a rate of 10 ºC/min. A 10 mg sample of each of the polymer powders was heated in the same alumina pan at a rate of 5^{o}C/min up to a temperature of 530^{o}C. The sample was then cooled down to room temperature at the same rate (5^{o}C/min) [11].

3.6.5 Powder Composition

Two distinct techniques were used to determine the composition powders and coatings. X-ray Diffraction (XRD) was used to determine the phase content of the HA powder and coatings; while Fourier Transform Infra-Red (FTIR) spectroscopy was used to determine the composition of the polymer powders and coatings. X-ray diffraction is a versatile, non-destructive technique that provides detailed information about the phase composition, the structural imperfections and the crystallographic structure of natural and manufactured materials. The XRD apparatus used was the Bruker D8-Advance Diffractometer. The parameters used are shown in Table 19.

Table 19: XRD scan parameters for HA powder

Parameter	Value
Scan type	Locked couple
Range	20-60(^{o}2θ)
Scan speed (sec/step)	0.02sec/step
Incident beam divergence	5
Increment	1.0^{o}
Receiving slit	0.2^{o}

XRD scans of the HA powder were carried out in accordance with ASTM F 2024-00, “The standard practice for X-ray determination of phase content of plasma-sprayed hydroxyapatite coatings” [210]. Prior to starting the scans, the sample powder was spread out on a glass slide using a double sided tape or a coated sample mounted on the rig. The slide was then attached to the XRD plate in the same way.

After the scan was completed, the Bruker Diffract Plus EVA software was used to analyse the resulting XRD patterns. Phase identification was possible by matching the obtained patterns with standard diffraction patterns provided by the EVA software in the Joint

Committee on Powder Diffraction Standard files (JCPDS).Powder purity results were obtained from the XRD patterns using the following Eqn. 2[89]:

$$\text{Purity (\%)} = \frac{\Sigma Ac - \Sigma Ai}{\Sigma Ac} x100\% \quad \textbf{(Eqn. 2)}$$

where Σ*Ac* is the sum of areas of all crystalline peaks and Σ*Ai* is the sum of the area under the non-HA peaks.

Fourier Transform Infra-Red (FTIR) spectroscopy was used to determine the composition of the polymer powders. FTIR spectroscopy enabled the identification of compounds and sample compositions. This technique was based on the principle that molecules absorb specific frequencies (resonant frequencies) that are characteristic to their structure. In order to obtain interferograms for each sample, a beam of IR light was guided through an interferometer and then through the sample. The IR spectrum is then obtained by performing a Fourier transformation of this signal. A Perkin Elmer *Spectrum GX* FTIR apparatus was used for this project.

3.6.6 Powder Crystallinity

Powder crystallinity can be calculated by a number of techniques varying in complexity and accuracy. The Rutland method is commonly used due to its accuracy and relative simplicity [11, 79, 89], using XRD data.

$$\text{Crystallinity (\%)} = \frac{\Sigma Ac}{\Sigma Ac + \Sigma Aa} x100\% \quad \textbf{(Eqn. 3)}$$

where Σ*Ac* is the sum of the areas of all HA crystalline peaks and Σ*Aa* is the sum of the area under the amorphous peak.

3.7 Process Modelling

As the thermal spraying technique was a novel method of applying biodegradable polymers for drug delivery purposes, it was important to use the DoE technique for two reasons. Firstly, to determine the influence of process factors on a number of coating properties that directly affect the mechanical integrity of the coating as well as physical properties that directly affect the interaction between the coating and the living tissue following implantation. Secondly, following the process investigation step, the use of DoE allowed for the optimisation of the parameters in order to obtain the best possible responses

statistically (Appendix-A) that would guarantee optimal coating strength and biological interaction.

The list of parameters to be varied was narrowed down to three factors due to the following process limitation and issues:

- The powder related parameters were not taken into account as the feedstock materials were provided by external suppliers with an unchanged set of powders properties. Investigation of the powder parameters is not a concern at this stage. However, such an investigation will be required following the polymer-drug attachment stage.
- The substrate related parameters were not taken into account as evidence from the literature review was sufficient to decide on a certain level of coating roughness and the need for a pre-heating step for flame sprayed polymer powders.
- The oxygen/acetylene flow rates were not taken into account as the flame gun used did not allow for a controlled variation of the gas flow rates.

Therefore, taking into account the limitations mentioned above and the information gathered from the literature review, three factors were varied for the purpose of statistical analysis, these were: the gun traverse speed (A: equipment input was inches per second, ips), the spraying distance (B: measured in centimetres, cm), and the number of passes (C: across the substrate face).

As for the responses to be characterised and then optimised, fours coating properties indicators were chosen for the following reasons:

- Coating thickness was found to affect the mechanical integrity of the coating as well as to affect the drug release kinetics in DDS.
- Coating roughness was found to affect the osteoblast cellular attachment on bone implants and is therefore a critical response.
- Coating adhesion was considered to be one of the most important characteristic of any coatings in general and thermally sprayed coatings in particular.
- Coating wettability was an indicator of the hydrophilicity/hydrophobicity of implant surface and therefore an indicator of the suitability of any surface for osteoblast cellular attachment. Coating wettability was determined by via contact angles measurements.

Design Expert 7 (supplied by Stat-Ease Inc) was used during the DoE part of this project. This software has a user-friendly interface that allows the operator to quickly set-up experiments, analyse the data, graphically display the results and finally determine the optimal process parameters. The experimental design used was the miscellaneous 3-level factorial design (3^3) with 5 midpoint repeats. Although this model is the most time-consuming, it was chosen because it offers a more comprehensive study of all parameters interaction, where every single parameter set is tested. It is typically used when the material/process combination is novel and requires an in-depth analysis, which was the case in this project. This model consisted of 31 experiments in sample order, with the parameters variation given in Tables 41 (PCL/PMMA) and Table 54 (PHBV/PMMA).It is useful to note that the gun traverse speed were given in inches per second (ips) in addition to the SI unit (m/s) as it is only possible to input the value of speed to the traverse control unit in ips.

3.8 Coating Characterisation

3.8.1 Coating Morphology

The surface morphology of the coatings and of the polished cross-section of the coating/substrate was examined using the ZEISS *EVO LS15* scanning electron microscope. The scanning parameters were varied according to the material specifications in order to obtain the best possible image. A thin layer of gold was deposited onto the surface of the coatings due to their non-conductive nature. In the case of the polished cross-sections, the conducting path was provided by a copper tape connecting the coating/sample to the aluminium SEM stage. The VP mode was alternatively used. Images of the coating surfaces were taken using a Canon 50mm focal lens camera.

3.8.2 Cross-Section Metallographic Preparation

In order to study the thickness and porosity, the coatings had to be studied through their cross-sectional areas. Therefore, metallographic techniques were used to prepare cross-sections of coatings/substrates. Prior to analysing their cross-section, the coated samples were sectioned using the Buehler *IsoMet 1000* precision saw. The samples were then placed in circular moulds (cross-section facing down) and mounted using a two-part clear resin (EPO-KWICK) with 5 parts of resin to 1 part of hardener. Clear resin was found to facilitate microscopic analysis of the samples by easily distinguishing the polymer coating

from the resin. The samples were then left to cure for 24 hours at room temperature. Knowing that the polymers used have relatively low melting temperatures, cold mounting was preferred in order to avoid damage to the polymer coatings that hot mounting could provoke. The next step was to grind and polish the specimens using the Buehler *MotoPol 2000* Grinder/Polisher.

3.8.3 Coating Thickness

Thickness measurements were performed using the Fischersope Multi 760C apparatus. This equipment combines a number of non-destructive test methods used to analyse coatings and material properties. The Fischerscope system operates according to the selected test method by using specific probes and corresponding calibration protocols. The test method used for the purpose of this project was the Eddy current method for measuring non-conducting coatings on non-ferrous metals. The probe corresponding to this method was the TA.3.3 probe. The thickness readings were obtained by placing the probe perpendicular to the coating surface and then pushing down to trigger the magnetic field. These steps were repeated five times and an average value for thickness was recorded.

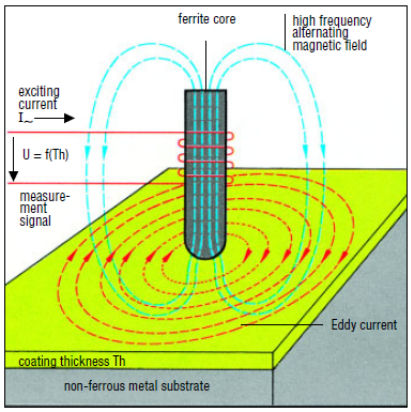

Figure 31: Fisherscope probe, principle of measurements [211]

As shown in Figure31, a high frequency magnetic field induced Eddy currents into the conductive substrate material [212]. The magnitude of these currents depended on the distance between the probe coil and the substrate material (i.e. the coating thickness). The measurement signal which determined the thickness was derived from the reflected impedance change in the probe coil as a function of the Eddy currents generated in the substrate material.

3.8.4 Coating Adhesion

Three coating adhesion methods were considered and tested during this project. The first two methods were the Rockwell C adhesion and Scratch adhesion test. However, these methods did not yield significantly accurate and reliable results, which was mainly due to the relatively high thickness of the coatings and the nature of the coatings themselves (elastic).

The only known and commonly accepted method to compare the adhesion of a set of coatings was the pull-off adhesion test. The pull–off test consisted of an apparatus which provided a tensile force to pull off a coating from its substrate. For the purpose of this project, a *Sebastian Five* (Quad Group, Inc.) pull-off adhesion machine was used to determine the interfacial adhesion between the coating and the substrate. This test allowed the direct measurement of the bond strength between the coating and the substrate.

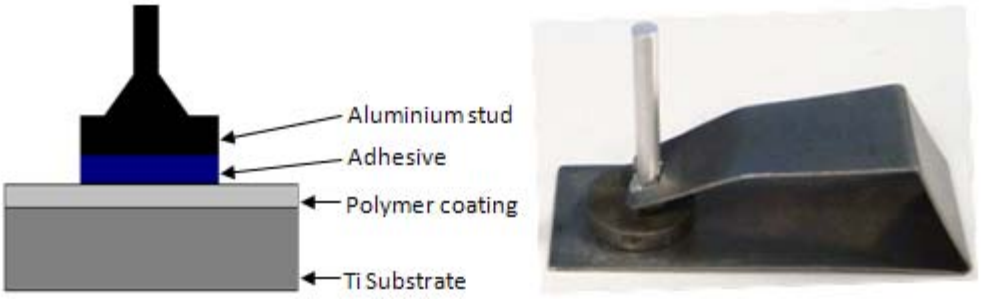

Figure 32: Pull-off stud for adhesion testing

One of the limitations of this test is that the studs usually come pre-coated with a high curing temperature epoxy, which would not be suitable for polymer coatings with low melting temperatures. Therefore a number of room temperature curing adhesives were tested. These included: ARALDITE 2005 (Huntsman adhesives, Inc.), a high shear and peal strength two-parts epoxy paste that was widely used in many studies, three Alpha cyanoacrylate Ester adhesives (Palm Labs, Inc.) with different viscosities (5cP, 100cP, 1500cP) and a commercial range cyanoacrylate (Capitol Essentials).These adhesives were cured at room temperature for 24hours, which made them suitable for usage with polymer samples and therefore avoided any coating damage that high temperature curing could induce.

Bare aluminium pull studs (supplied by Quad Group, Inc.) having 3.4 mm in diameter were coated with a layer of adhesive by using a thin brush. The studs were then secured perpendicular to the face of the coated samples using a fixture (Figure 32). The coated sample and the pull stud fixture were left to cure for 24 hours at room temperature. After removing the fixture, each sample was then inserted into the pull off tester platen and gripped. The force limit was set to the maximum value and the force rate was set to one third of the force range(2.7-3.18 kg/sec). When the test began, a constant load was applied, pulling down against the platen support until failure occurred. The instrument recorded the highest value of force applied before failure. This value indicated the bond strength between the coating and the substrate.

It very important to keep in mind that the adhesive testing performed in this project was considered as a qualitative study for comparing coatings obtained using different settings. The reason for this is that the results of these adhesion tests also depended on some test parameters [213], which were not accounted for in this research. An example of this is the fact that the values obtained with most of the adhesives depended upon the test rate used as the viscoelasticity of the adhesive had an influence on the test result. In order to perform a quantitative analysis, a custom-made adhesive would have had to be prepared and an optimisation of the procedure would have been required.

3.8.5 Coating Wettability

Wettability is a very crucial material property for implantable orthopaedic coatings. In fact, previous studies have shown that cell adhesion is significantly influenced by the water contact angle [214]. One method to quantitatively compare the wetting of different coatings by a liquid is to measure the contact angle. This feature is geometrically defined as the angle formed by a liquid at the intersection of three boundaries: liquid, gas and solid.

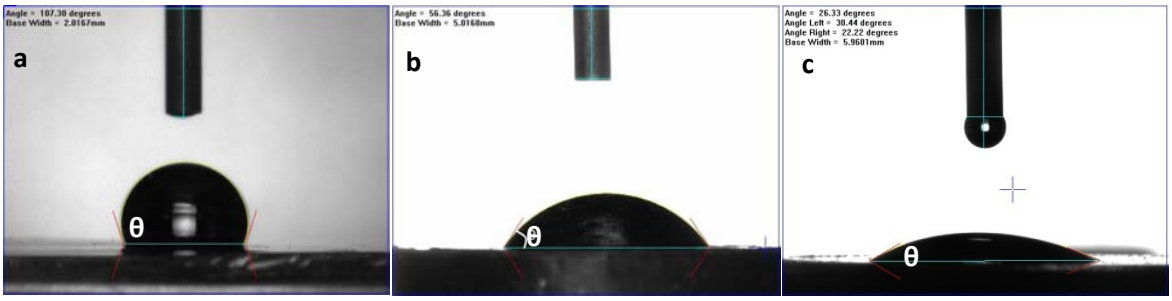

Figure 33: Contact angle θ of red tangent at the three phase boudary

It is widely accepted that low contact angles (less than 90^{o}) (Figure 33b and 33c) indicate that the liquid spreads/wets well on the coating surface which implies that the coating is hydrophilic, whereas a high contact angle (more than 90^{o}) (Figure 33a) indicates that the liquid poorly wets the coating surface, making the coating hydrophobic. Material hydrophobicity generally induces poor cell adhesion.

The contact angle measurements were performed using a contact angle goniometer which is comprised of a monochrome camera and a motor-actuated 10ml syringe. Deionised water was used as the wetting liquid. After placing the samples in front of the camera and underneath the syringe, the liquid is pushed down until a droplet was placed on the surface. The static contact angle was then measured by using software. Three measurements were made and then averaged for each sample.

3.8.6 Coating Composition

Fourier Transform Infra-Red (FTIR) spectroscopy was used to determine the composition of the chemical state of the polymer coatings following flame spraying. FTIR spectroscopy enables the identification of compounds and sample compositions. This technique is based on the principle that molecules absorb specific frequencies (resonant frequencies) that are characteristic to their structure. In order to obtain interferograms for each sample, a beam of IR light is guided through an interferometer and then through the sample. The IR spectrum is then obtained by performing a Fourier transformation of this signal. Spectra of powders and coatings were then plotted against each other in order to determine if polymer-specific peaks had disappeared or if new peaks had appeared in the coatings. A Perkin Elmer *Spectrum GX* FTIR apparatus was used for this project.

3.8.7 Coating Degradation

The degradation properties of biomaterials are of primary importance to the biomaterials selection and design. In fact, the degradation rate affects (to different extents) process responses such as cell growth, tissue regeneration, drug release and host response [215]. The degradation rate must occur in equilibrium with bone regeneration for an effective load transfer and to avoid implant loosening. Figure 34 shows the correlation between the degradation time of the orthopaedic coatings and the builing up of bone tissue.

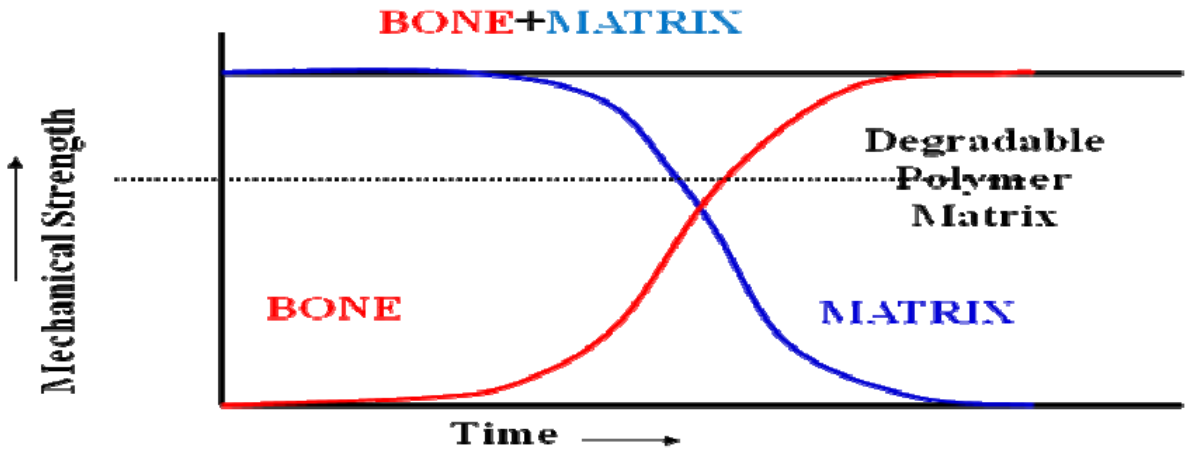

Figure 34: Idealised equilibrium between degradation rate of bone scaffold and bone regeneration [216]

Thorough and lengthy degradation studies are crucial in any drug-release related application. However, seeing that the current project does not cover the pharmacological aspect of the DDS and only deals with the design of the release vehicle, the *in vitro* degradation tests only covered an initial period of 28 days, where the mechanical integrity of the DDS is under the highest risk.

Degradation tests were conducted in order to investigate the rate of dilution and the weight loss of the optimised polymer coatings, the HA coatings and the polymer/HA bi-layers. Hydrolytic degradation was performed in phosphate buffer solution (PBS) of pH = 7.4 at 37^{o}C. Samples with similar (as close as possible) and known coating weights were placed in vials containing 70ml of PBS. The vials were incubated in a water bath at 37^{o}C, and every 7 days for 4 weeks one sample of each coating type was removed from the jar, left to

dry for 24 hours and weighed. Weight changes were calculated at each time period as follows:

$$\% \text{ weight change} = \frac{Wf - Wo}{Wo} x100\% \qquad \textbf{(Eqn. 4)}$$

where W_f and W_o, respectively represented the weights of the coatings prior to immersion in solution and following testing. The results were then plotted and analysed. Phosptate buffer solution (PBS) was used in this work as is it usually the case in biological research, in order to mimic the osmolarity and ion strength of the human body and therefore helped to maintain a constant pH. Following sample weighting, SEM images were taken of the coatings at different points of the degradation time.

3.8.8 pH and Conductivity

The responses of bone tissue/cells to changes in pH constitute a homeostatic mechanism that aids in maintaining systemic acid-base balance [217]. This was conducted through constant buffering to keep normal pH levels in the cell organism by accepting or releasing H^+. Therefore the level of pH *in vivo* is crucial for the wellbeing of cells and the cellular growth. In fact, precise control and maintenance of pH in the blood and extracellular matrix is required because the machinery of cells is very sensitive to changes in H^+ concentration; cell formation requires pH levels to be in the neutral range of 7.3-7.4[217].Disruption to such levels of pH can have detrimental effects on cells, thus jeopardising the bone formation process by a number of phenomena such as denaturising and digesting proteins and losing enzymes functions.

pH and conductivity levels were performed in de-ionised water and the values were measured using a handheld Hanna HI 98311 pH, EC and TDS meter (Hanna Instruments, Inc). The accuracy of the apparatus at 20^{o}C was ±2%f.s (EC/TDS).

3.9 Biological Testing

In order to investigate the *in vivo* response of the various powders and coatings produced in this project, a cell culture study was conducted. This also allowed for the comparison of polymers to each other in order to choose the most suitable DDS for the intended application.

3.9.1 Powders Biological Assessment

Powders extract preparation:

All four feedstock powders (HA, PMMA, PCL, PHBV) were tested for biocompatibility. The powder samples were sterilised using a Harrick plasma steriliser with a 15 mA DC applied to the RF coil. The powder cytotoxicity was investigated by contacting cell cultures with the extracts of the tested materials. For this purpose, powder extracts (for PCL, PMMA, PHBV, HA) at a 10% concentration (additional 1% concentration for HA) of the powder in cell culture medium were prepared in aseptic conditions. Powders were incubated in the medium for 24 hours in standard culture conditions (prior to use).

Cells and medium:

Human osteoblasts (HOB) obtained from Promocell were used to examine cell behaviour in contact with the feedstock powders. Osteoblasts are mononuclear cells of mesenchymal origin, responsible for bone formation and remodelling. The cells were thawed from a frozen stock and cultured in osteoblast growth medium (Promocell) supplemented with 10% heat inactivated foetal calf serum and penicillin-streptomycin 10ml/L under standard culture conditions (37^{o}C and 5% CO_2). The medium was substituted every day. Passage number four was used for this experiment (biochemical assays).For this study, cultures of 2000 cells/well in a 96-well plate, were prepared. The testing procedures for this study were performed according to ISO 10993-5 [218].

Assays:

For the preliminary biological study, cell proliferation WST-1 and alkaline phosphatase ALP assays were used.

- Cell proliferation assay WST-1: A premixed WST-1 reagent (Clontech) provided a method to measure cell proliferation based on the enzymatic cleavage of the tetrazolium salt to a water-soluble formazan dye. The HOB cells were cultured in the flat bottomed 96-well plateat the density of 2000 cells/well, with the previously prepared extracts (24 hours, 37^{o}C, 5% CO_2). Cell cultures with an unmodified, basic cell medium were used as a control. After 24 hours of incubation, 10µl of premixed WST-1 reagent was added to each well (1:10 final dilution). The plate was then incubated for two hours in standard culture conditions. Finally, the plate was thoroughly shaken for 1 minute and

the light absorbance at 450nmwas monitored using a multiplate reader (Infinite 200 NanoQuant microplate reader).

- Alkaline phosphatase (ALP) assay: The ALP activity was measured using a colorimetric test at pH 10.4 in glycine 0.1M buffer (0.1m glycine, 1mM $MgCl_2$, 1mM $ZuCl_2$) with a 5mM p-Nitrophenylphosphate (p-NPP) as a reagent. To perform the assay, culture media (extracts) were removed from the culture plate by flicking the plate upside down onto a paper tissue. Then, the cells were washed with PBS by shaking the plate. After PBS was removed, the prepared substrate solution was added into each well (100 µl/well). Cells with the reagent solution and the addition of TritonX100 (TritonX100 triggers the cell membrane lysis) were incubated for 2 hours in standard culture conditions. The reaction was then stopped by adding 1M NaOH to each well (50 µl/well). The amount of alkaline phosphatase was determined colorimetrically by using a multiplate reader. Absorbance was measured at 405 nm.

3.9.2 Coating Biological Assessment

a) Preliminary biological assessment

As mentioned in the introduction of this thesis, the biological assessment was an essential part in investigating the viability of flame sprayed biocompatible polymers for an orthopaedic application. A biological assessment was performed following the DoE study in order to identify which of the optimised polymer spraying parameters yielded enhanced biological response. However, as a precautionary measure to make sure that the processing technique was not totally destructive, a preliminary biological assessment was performed prior to starting the DoE study. During this assessment, a cell proliferation (WST-1) study was carried out, in which three samples from each type of coating (PCL/PMMA and PHBV/PMMA) were compared to bare Ti discs and a reference (growth medium). The parameters used to spray the sample in each case were mid-range parameters. Human osteoblasts were seeded on the sprayed discs for three and five days following the same procedure used for the powder biological testing.

b) Post-DoE biological assessment

This second biological assessment was carried out to make sure that the optimised polymer coating obtained and the polymer/HA bi-layer coatings performed well for cell viability as

well as alkaline phosphatase. The procedure for the ALP assay was the same as for the previous biological assessments of this work (*section 3.9.1*). The summary of the final coating biological assessment is shown in Table 20.

Table 20: Cell culture test summary

Surface	Tests	Incubation
Titanium	Cell Viability (XTT)	3 days
HA	Alkaline phophatase	7 days
PHBV/PMMA(C1)		
PCL/PMMA(C2)		
HA/C1		
HA/C2		

The cell viability XTT assay is quite similar to the WST-1 assay as it is also based on tetrazolium salt. The XTT assay kit (Sigma-Aldrich) with 1% PMS was reconstituted as per the manufacturer's instructions. XTT was added equal to 20% of the culture media volume and the plates incubated for 4 hours. The assay can be shortened to 2 hours in most cases, however, incubating for 4 hours increases sensitivity for low cell numbers. 3 x 100µl of XTT supernatant was transferred to 96 well plated and read at 450 nm.

4 Results and Discussions

4.1 Materials Characterisation

4.1.1 Substrate Material

Following the grit blasting and the cleaning of the substrates, the roughness of ten randomly selected titanium discs were measured using the surface profilometer following the procedure outlined in section 3.4.2.The roughness results are given in Table 21. The grit blasting and the subsequent cleaning procedures previously mentioned were thoroughly followed for every single titanium disk in order to ensure consistent results, and therefore to avoid any bias to the DoE results.

Table 21: Substrate surface roughness

Sample	*R_a value (µm)*				
	1	**2**	**3**	**Average**	**SD**
1	3.0	3.5	3.1	3.2	0.2
2	2.8	2.8	3.1	2.9	0.1
3	3.2	2.7	2.7	2.8	0.2
4	2.9	2.9	2.9	2.9	0.0
5	2.7	2.8	2.9	2.8	0.1
6	2.8	3.4	3.2	3.1	0.3
7	3.2	2.8	2.7	2.9	0.3
8	3.4	2.8	2.8	3.0	0.1
9	3.3	3.3	3.5	3.3	0.1
10	3.3	3.2	3.1	3.2	0.1
Average				**3.0**	**0.1**

The average surface roughness found was 3 µm. This value corresponds to the roughness values suggested by Yang and Chang [150] which provides the requirement for high coating adhesion without generating excessive oxidation of the micro surface of the Ti-alloy during grit blasting. The standard deviation recorded was 0.1 µm. This is less than the 1.0 µm standard deviation reported by Bahbou et al. [219]. Therefore, the roughness testing indicates that the procedure followed was repeatable and produced a roughness level suitable for thermal spray applications. Similar roughness values were measured and

implemented by Levingstone [89]. Further increase in substrate roughness could promote splat instability during thermal spraying, resulting in radial jetting and breakup, and producing more irregularly shaped splats [220].

4.1.2 Polycaprolactone (PCL) Powder

Powder morphology:

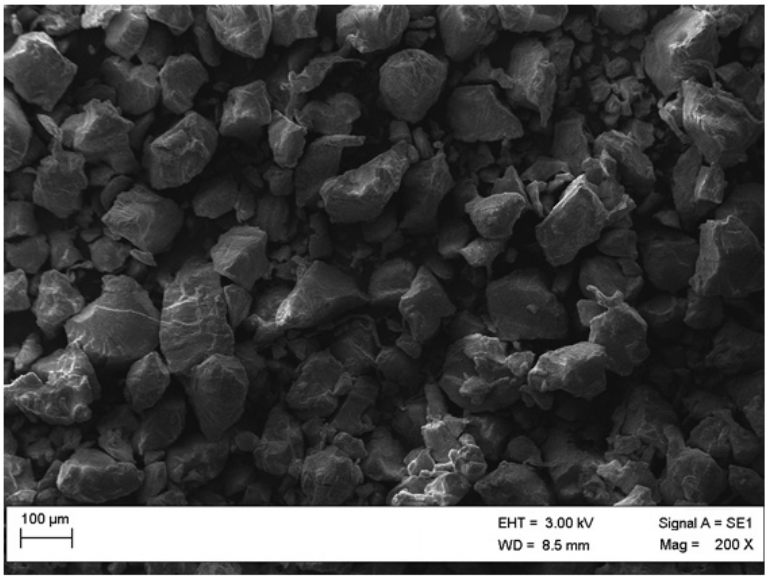

Figure 35: PCL powder morphology

The PCL powder consists of highly irregular and angular morphology particles (Figure 35), as a result of the cryogenic milling method used to reduce the powder size. Such characteristics can cause the powder to be heated unevenly during flame spraying and in turn, lead to the introduction of process variability. Additionally, irregular powders with poor flowability can cause blockages in the powder feeding system. Ideally, flame spray feedstock materials should have totally or partially round morphologies which offer an increased flowability; size distribution being another important factor [70]. However, seeing that thermal spraying of biocompatible polymers is not widely used, PCL specifically made for flame spraying was not available, thus this powder was used.

Particle size distribution:

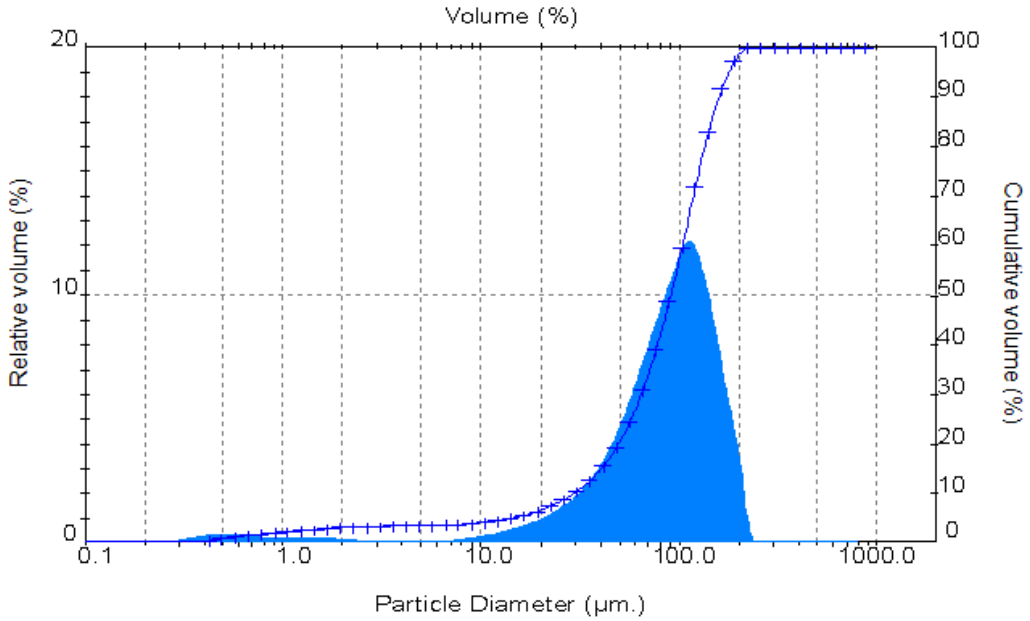

Figure 36: Particle size distribution for PCL

Table 22: Particle size data for PCL

D[4, 3]	D[3, 2]	D(v, 0.9)	D(v, 0.5)	D(v, 0.1)
92.7 µm	15.08 µm	158.8 µm	90.76 µm	29.25 µm

Where D[4,3]: volume mean diameter, D[3,2]: surface area mean diameter, D(v,0.9): 90% of the volume distribution is below this value, D(v,0.5): 50% of the volume distribution is below this value, D(v,0.1): 10% of the volume distribution is below this value.

The PCL particle size distribution appeared to follow a Gaussian distribution (Figure 36) with an average particle size of 92.7 µm (Table 22). The small cluster on the left-hand-side of the distribution graph may have been caused by the de-agglomeration of finer particles during testing, or due to the processing and size reduction technique. The main particle size range varied between 10 µm and 110 µm. This was deemed an acceptable size distribution range to allow a reduced degree of particle melting within the flame.

Thermal behaviour:

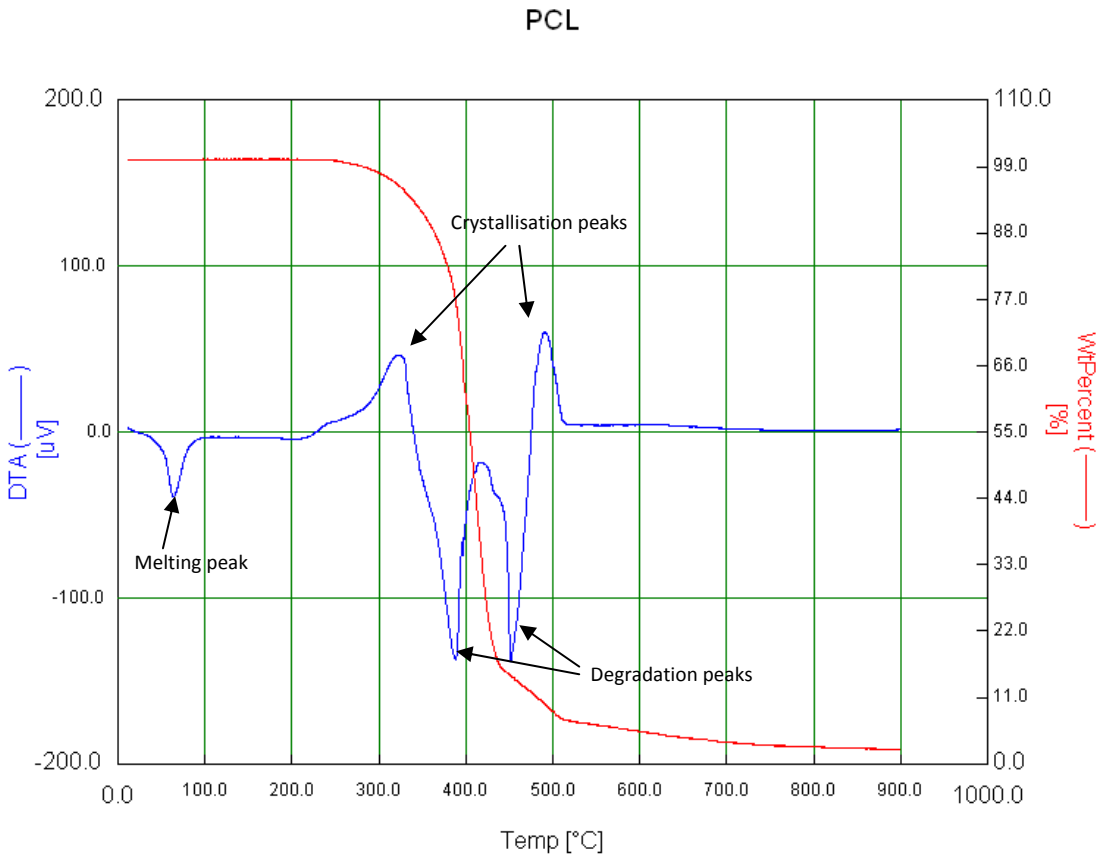

Figure 37: TGA and DTA of PCL powder

The first peak of the DTA curve (melting peak) indicated a melting temperature of approximately 60°C. The following peak represents a crystallisation step, whereas the following peaks were degradation peaks. The TGA (weight loss) curve started to decline at approximately 260°C, which indicated that the degradation of polycaprolactone began at this temperature. A large difference between melting temperature and decomposition temperature for polymers is an important requirement when thermal spraying is used [221]. According to Figure 37, the difference between melting and decomposition temperatures for PCL was equal to 200°C, which is a precursor for low polymer degradation during flame spraying. Thermal conductivity of polymers is not commonly investigated and thus only two conductivity values were found for PCL; 0.203W/mK [222] and 0.4 W/mK [223].

Powder density:

The average density for the PCL sample powder using helium pycnometry was found to be 1.1868 g/cm^3 (Table 23).

Table 23: PCL density values from the helium pycnometer

Den[1]	Den[2]	Den[3]	Den[4]	Den[5]	Den[6]	Den[7]	Den[8]	**Average**
1.1903	1.1884	1.1894	1.1875	1.1859	1.1839	1.1848	1.1842	**1.1868 g/cm^3**
Dev[1]	Dev[2]	Dev[3]	Dev[4]	Dev[5]	Dev[6]	Dev[7]	Dev[8]	**Average**
0.002	0.0001	0.0011	0.0008	0.0024	0.0000	0.001	0.0004	**0.0009 g/cm^3**

4.1.3 Polymethylmethacrylate (PMMA) Powder

Powder morphology:

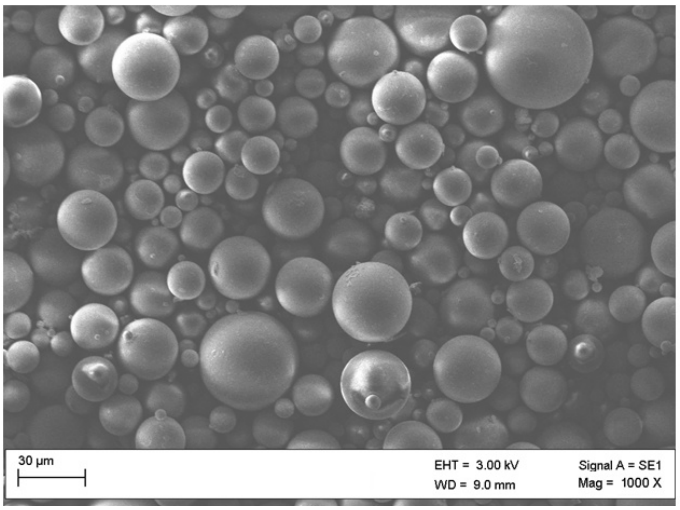

Figure 38: PMMA powder morphology

The SEM image (Figure 38) of the as-received PMMA powder clearly shows that the powder has a spheroidal shape. Even though having a relatively small average particle size, implying a larger contact surface area between particles, the shape of this PMMA powder suggested good flowability for powder injection in the gun. This was confirmed in the preliminary spraying as no blockage occurred at any stage of the process when PMMA was sprayed alone.

Particle size distribution:

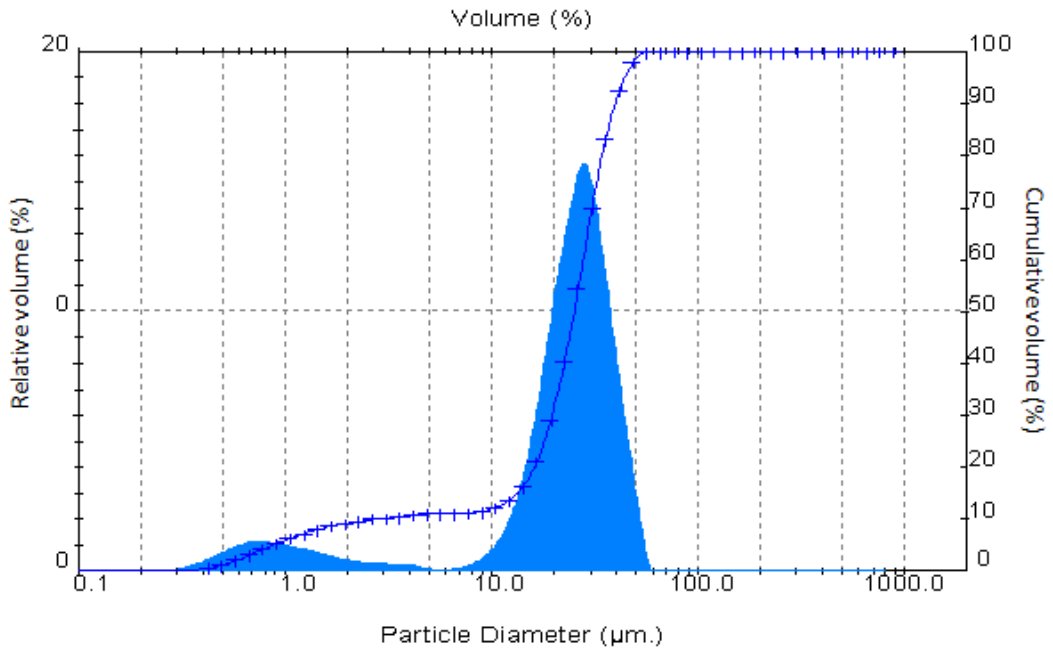

Figure 39: Particle size distribution for PMMA

Table 24: Particle size data for PMMA

D[4, 3]	D[3, 2]	D(v, 0.9)	D(v, 0.5)	D(v, 0.1)
24.52 µm	6.02 µm	34.49 µm	25.08 µm	2.02 µm

The PMMA particle size distribution followed a Gaussian distribution (Figure39) with an average particle size of 24.52 µm (Table 24). This value confirms the manufacturer's range for the average particle size: 25-30 microns. The small bump on the left-hand-side of the distribution graph may have been induced by the de-agglomeration of finer particles during testing. The main range of particle size varied between 10 and 60µm. This fell into the lower limit for thermally sprayed polymer powders. It was, however, deemed suitable for this application due to its circular morphology and its availability.

Thermal behaviour:

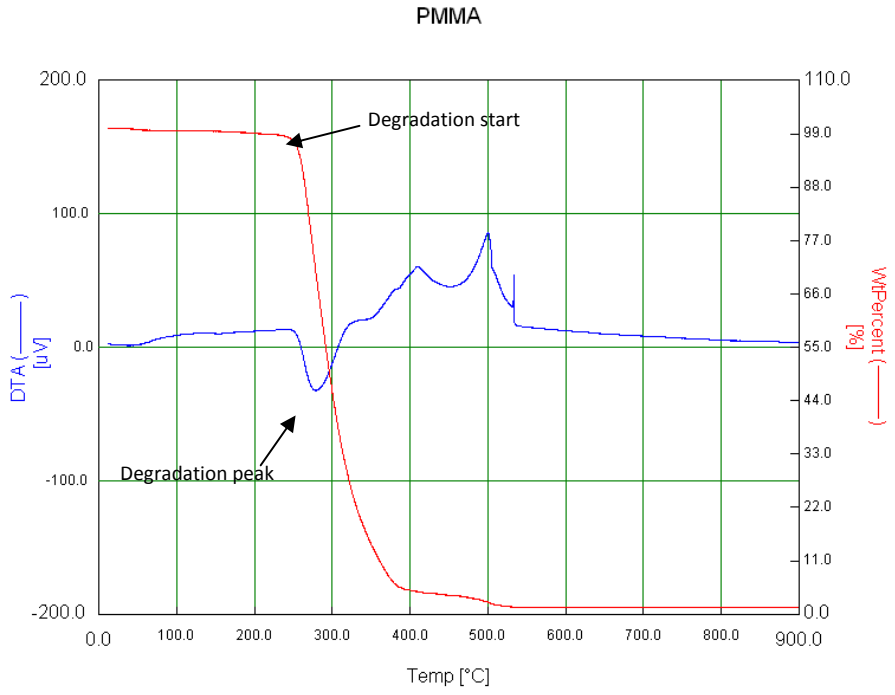

Figure 40: TGA and DTA of PMMA powder

According to the TGA and DTA curves, degradation of PMMA began at 230°C.Despite the experiment being repeated a number of times; the melting peak was not clearly identified for this powder. Taking into account literature approximations for PMMA melting temperatures (~160°C), the approximate difference between the melting and decomposition points for PMMA was equal to ~70°C. From literature, the thermal conductivity of the PMMA was found to be 0.193 W/mK[224].

Powder density:

The average density for the PMMA sample powder using helium pycnometry was found to be 1.2781 g/cm^3 (Table 25).

Table 25: PMMA density values from the helium pycnometer

Den[1]	Den[2]	Den[3]	Den[4]	Den[5]	Den[6]	Den[7]	Den[8]	**Average**
1.2803	1.2799	1.2801	1.2801	1.2782	1.2739	1.2766	1.2757	**1.2781 g/cm^3**
Dev[1]	Dev[2]	Dev[3]	Dev[4]	Dev[5]	Dev[6]	Dev[7]	Dev[8]	**Average**
0.0006	0.0002	0.0004	0.0004	0.0016	0.0013	0.0014	0.0005	**0.0008 g/cm^3**

4.1.4 Polyhydroxybutyrate/Polyhydroxyvalerate (PHBV) Powder

Powder morphology:

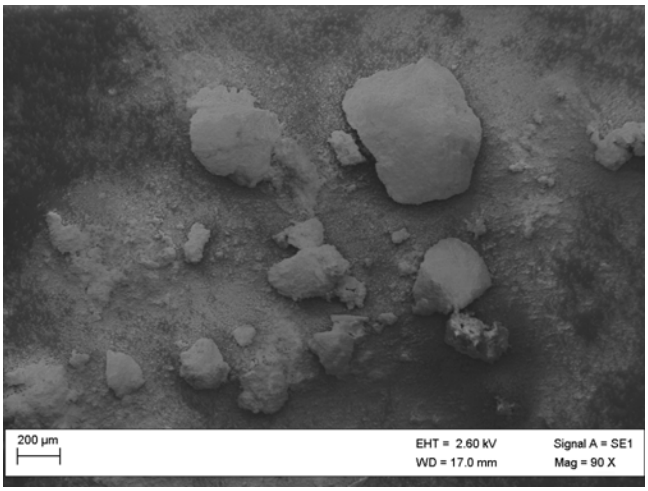

Figure 41: PHBV powder morphology

The morphology was very irregular and very inconsistent in size (Figure 41). The type of production technique used to obtain this powder morphology was not provided by the manufacturer.

Particle size distribution:

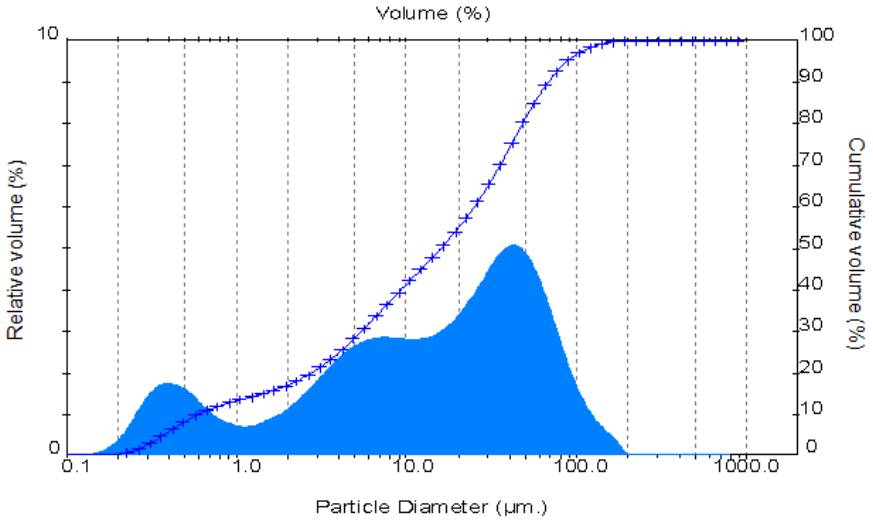

Figure 42: Particle size distribution for PHB98%/PHV2%

Table 26: Particle size data for PHB98%/PHV2%

D[4, 3]	D[3, 2]	D(v, 0.9)	D(v, 0.5)	D(v, 0.1)
27.05 µm	2.28 µm	67.73 µm	15.92 µm	0.59 µm

The particle size analysis revealed a multimodal particle size distribution with average diameters appearing within three ranges, approximately, 0.1 µm-1 µm, 1 µm-10 µm, and 10 µm-100 µm. Figure 42shows the particle size distribution was fitted to three Gaussian curves. Multimodal type distribution may be the result of attrition (fracture of large particles into smaller ones) during processing or blending of two or more distinct particle streams. Large particle ranges are not ideal in thermal spraying application as they can produce large temperature differences in heating of the individual particles, which in turns leads to numerous heterogeneities within the final coating microstructure. However, it is possible to manipulate the process in order to adapt it (to some extent) to the powder used. In fact, the PHBV powder used in this project was the only available powder form for the chosen polymer, and knowing the valuable features of this polymer for the proposed application, it was necessary to investigate it regardless of the technical difficulties that may arise. The mean particle size obtained from the particle sizing experiment was 27.05 µm (Table 26).

Thermal behaviour:

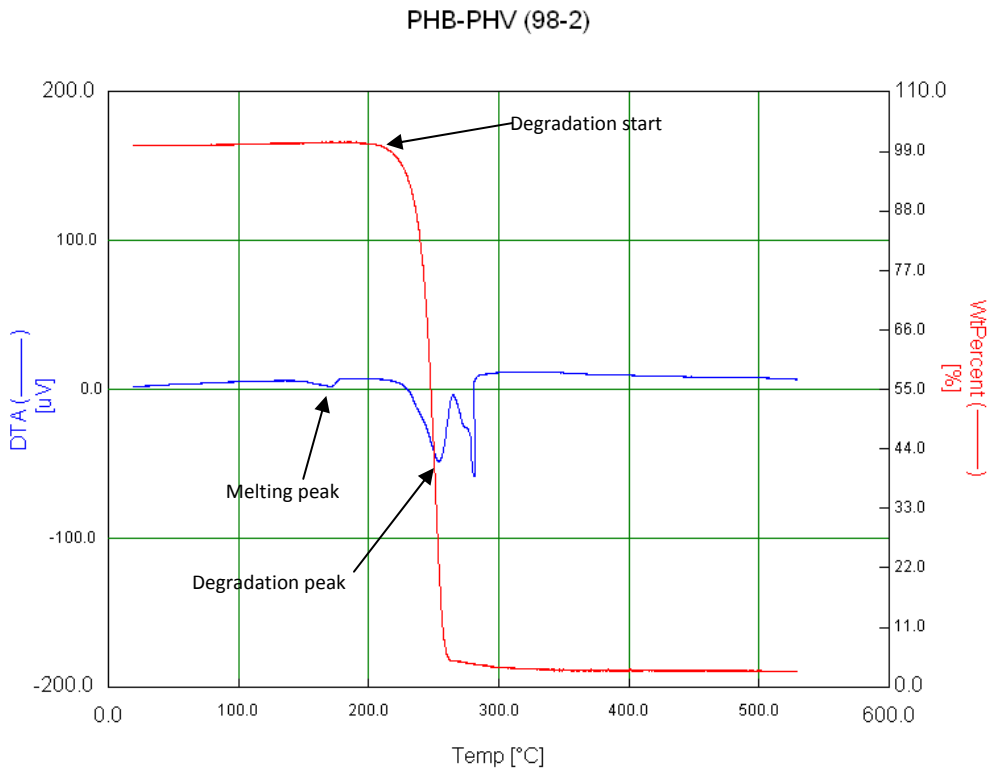

Figure 43: TGA and DTA of PHBV powder

The first peak appearing in the DTA curve occurred at a temperature of 170^{o}C, represents the melting temperature of this polymer. The TGA curve on the other hand indicated that degradation of PHBV began at approximately 220^{o}C, which graphically translates into a sharp decrease of percentage weight loss. According to Figure 43, the difference between melting and decomposition points for PHBV was equal to 60^{o}C. Thermal conductivity of PHBV, according to the supplier, was equal to 0.15 W/mK.

Powder density:

The average density for the PHBV sample powder using helium pycnometry was found to be 1.3287 g/cm^3 (Table 27).

Table 27: PHBV density values from the helium pycnometer

Den[1]	Den[2]	Den[3]	Den[4]	Den[5]	Den[6]	Den[7]	Den[8]	**Average**
1.3374	1.3364	1.3334	1.3313	1.3271	1.3237	1.3217	1.3186	**1.3287g/cm^3**
Dev[1]	Dev[2]	Dev[3]	Dev[4]	Dev[5]	Dev[6]	Dev[7]	Dev[8]	**Average**
0.0356	0.0345	0.0316	0.0295	0.0252	0.0219	0.0199	0.0168	**0.0268 g/cm^3**

The density of thermally sprayed feedstock materials is a very important factor as it affects the in-flight velocity and the degree of melting of powder particles. The densities of all polymeric materials were close to each other: PCL = 1.187 g/cm^3, PMMA = 1.278 g/cm^3, PHBV = 1.3287 g/cm^3. The higher standard deviation observed with the PHBV density may be due to the processing technique of this polymer, which could cause variation in the molecular weight within the same batch. The density is also an important factor when blending of two or more powders is required (as shown in the next sections) as a large difference in densities could results in heterogeneous mixing. PMMA having a density mid-way from PCL and PHBV suggested that it could perform well as an additive to either polymer. The values obtained for all polymers were much lower than the density observed with the HA powder (next section): 3.25 g/cm^3.

4.1.5 Hydroxyapatite (HA) Powder

Particle size distribution:

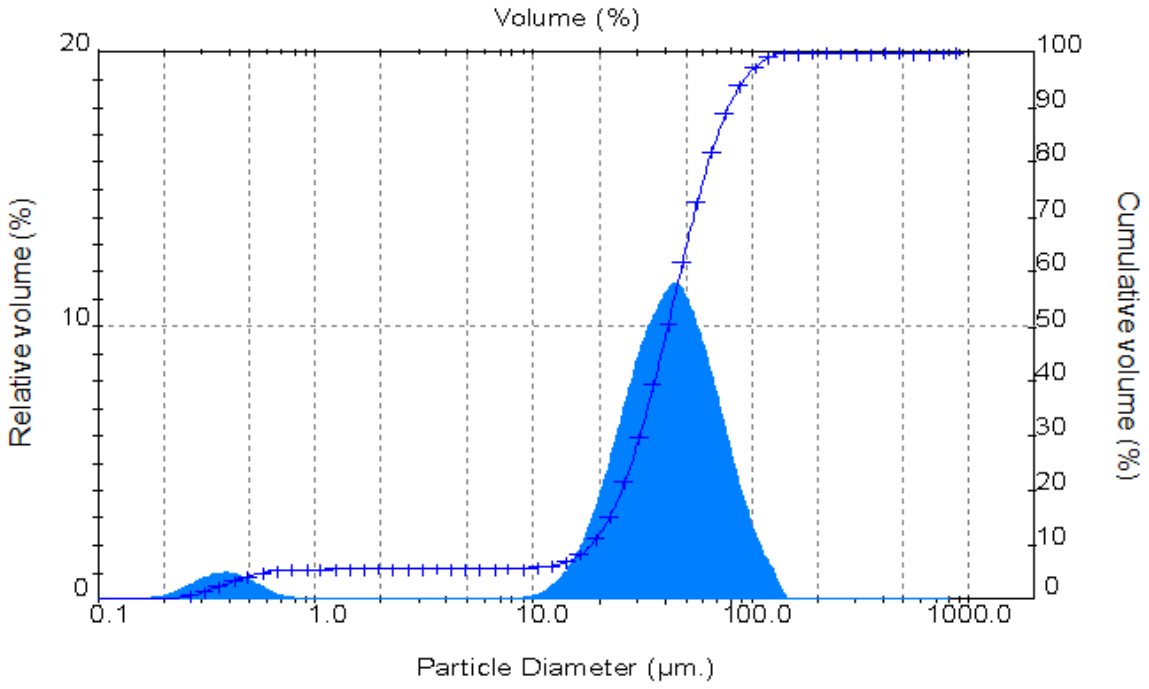

Figure 44: Particle size distribution for HA

Table 28: Particle size data for HA

D[4, 3]	D[3, 2]	D(v, 0.9)	D(v, 0.5)	D(v, 0.1)
44.83 µm	5.49 µm	78.3 µm	41.26 µm	18.24 µm

The average particle size was found to be 44.83 µm (Table 28), which was very close to the value given by the supplier, 46.18 µm. Therefore, the HA average particle size falls within the 20-45 µm range, as stated by Kweh et al. [225] producing dense, good quality coatings. The particle size distribution analysis results for hydroxyapatite (Figure 44) also indicates that the size of the particles falls within two separate clusters, one between 0.2 and 0.9 µm (small cluster) and the other between 10 and 110 µm (large cluster). The particles in the smaller cluster are more likely caused by deagglomeration of the larger HA agglomerates [11]. The particles falling in the large and narrow cluster fit ideally with the desired application (plasma spraying). When most of the particles are found within a narrow range,

improved process parameters are expected; the most important one being less variation in the degree of melting of particles within the plasma plume.

Powder morphology:

The SEM images in Figure45 show that the Captal 60-1 HA powder consisted of a mix of particles with spherical morphology and particles with irregular morphology. The latter appeared to be an agglomeration of smaller particles rather than single highly irregular particles. Irregular shaped powder presents a number of problems such as poor flowability within the powder feeding system, uneven particle melting and flow instability during spraying, all of these introducing process variability [89]. However, the percentage of irregular particles in the powder appeared to be low, with most of the powder consisting of spherical particles, (due to the spray drying production method used). Therefore Captal 60-1 was deemed suitable for plasma spraying. Additionally, the same powder was successfully used for previous research [89] with the same equipment and no issues relating to powder morphology were raised.

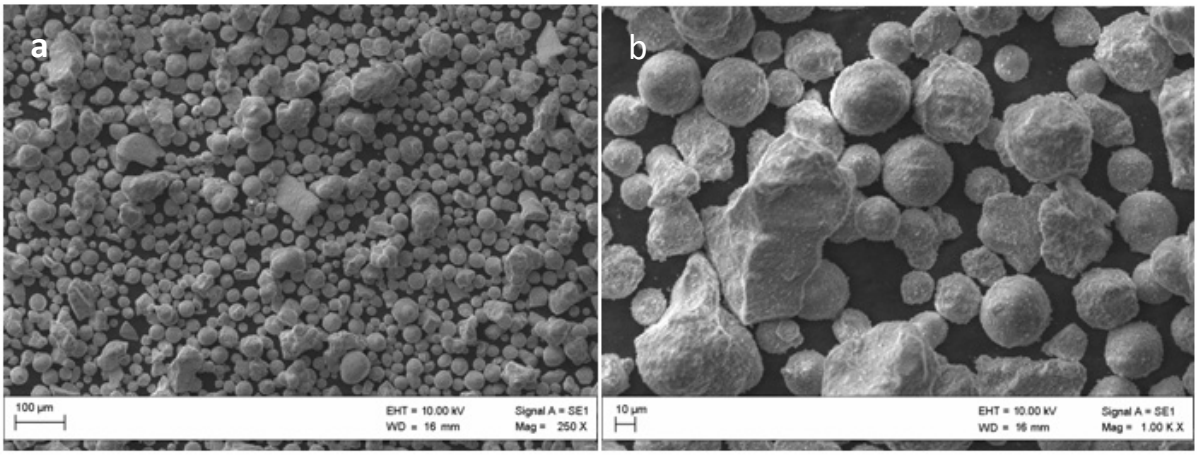

Figure 45: HA powder morphology: a) at Mag=250X; b) at Mag=1000X

Powder density:

The average density value for the HA powder found using helium pycnometry was 3.25 g/cm^3 (Table 29). This value fell within the range of 3.08 and 3.47 g/cm^3 of commercially available HA as investigated by Kehoe [70], and was higher than the minimum density value of 3.05 g/cm^3 required by the FDA for HA powders used for coated femoral implants

applications [226]. Higher density of hydroxyapatite powders plays an important role in preventing the inclusion of human fluid into the interfacial area between the HA coating and Ti implants in hip joint replacements [70].

Table 29: HA density values from the helium pycnometer

Den[1]	Den[2]	Den[3]	Den[4]	Den[5]	Den[6]	Den[7]	Den[8]	**Average**
3.3076	3.2952	3.2824	3.2524	3.2525	3.2367	3.2135	3.2118	**3.25 g/cm^3**
Dev[1]	Dev[2]	Dev[3]	Dev[4]	Dev[5]	Dev[6]	Dev[7]	Dev[8]	**Average**
0.0742	0.0619	0.0491	0.0190	0.0191	0.0033	0.0199	0.0216	**0.033 g/cm^3**

Powder composition:

Figure 46 shows the XRD pattern for the CAPITAL-60 hydroxyapatite powder. Both powder crystallinity and purity were derived from the XRD patterns (for powders and coatings) using Eqn.2 and 3. The crystallinity and purity of the powder used in this project were both higher than 95% (99.5% and 99% respectively).

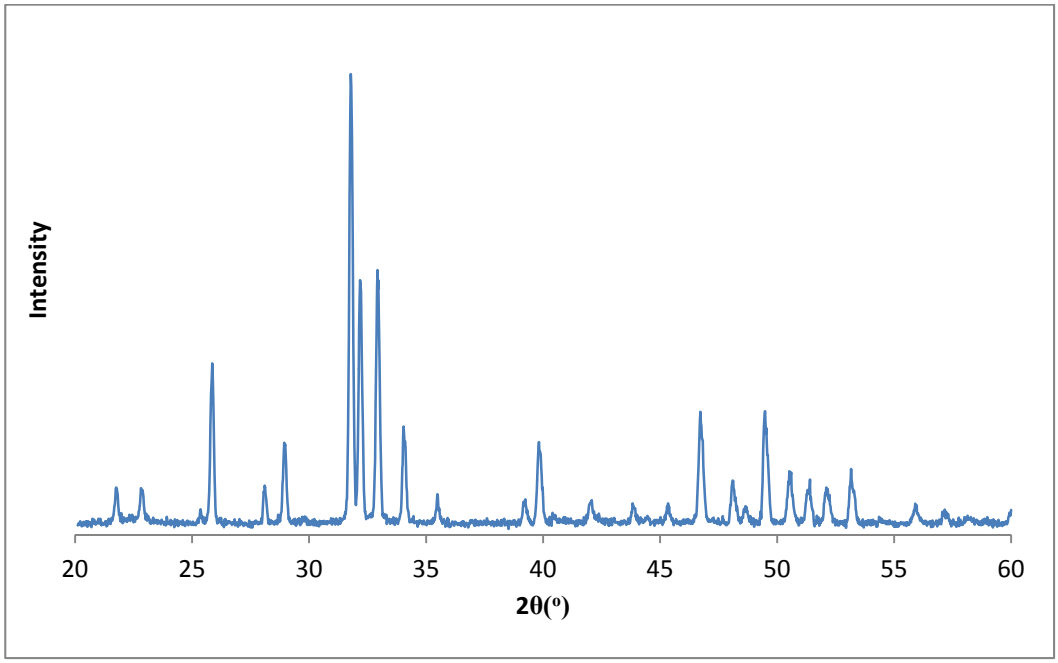

Figure 46: XRD pattern of CAPITAL 60 HA powder

4.2 Preliminary Process Investigation

Due to the relatively low velocity and the rapidly decreasing jet temperature, the spray distance for conventional flame spraying should be less than 40cm [227] in order to avoid particle re-solidification before impact. On the other hand "fried egg" shaped type splats can form if the spray distance is lower than 20cm, as the particles' dwell time can be too short, which then leads to particles been molten only at their periphery[155]. Therefore spray distances between 20 and 40cm result in a more uniform heating and disc shaped splats [164].

For the purpose of this initial process investigation, the gun traverse speed was initially set in the range of0.152m/s (6ips) to 0.254m/s (10ips). The number of passes was varied from 6 to 10 and finally to 14 passes.

4.2.1 PCL Screening

During the screening tests, it was noticed that powder with highly irregular morphology (PCL) resulted in poor particle flowability within the powder cartridge and the flame gun. In fact, after a few passes, the particles started clogging the exit of the powder cartridge, which led to the spray plume becoming unpredictable with interruption of powder injection and sudden bursts of particles before a complete blockage of the powder outlet occurred. Every time a spray interruption occurred, the Ti samples became unusable and had to be discarded, in addition to the fact that the powder-to-coating yield was deemed very poor. In practical terms, this meant that to obtain a coated sample with the desired number of passes, 4-5 attempts were required, implying that 4-5 Ti discs and 4-5 times the amount of powder were wasted. None-the-less, some coatings were obtained (Figure 47).

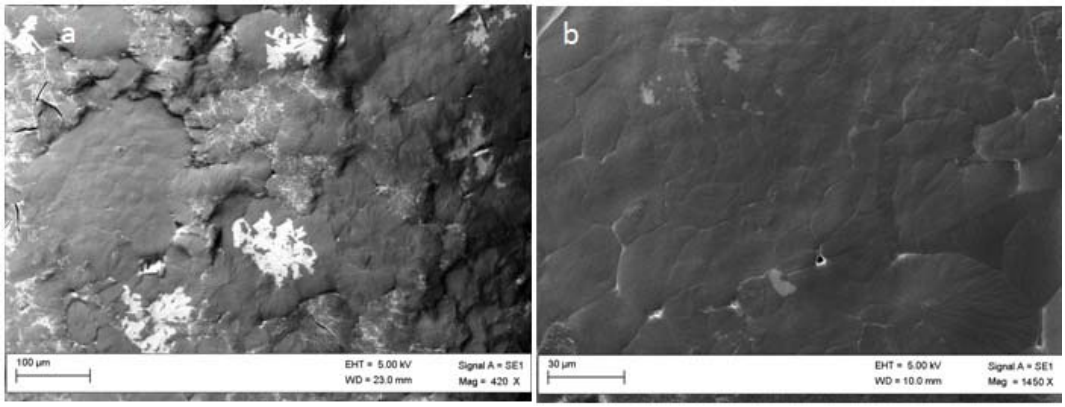

Figure 47: PCL coating morphology: a) at Mag=420X; b) at Mag=1450X

In an attempt to solve the problem related to PCL's morphology and its flowability issue, a pneumatic vibrator, supplied by the gun's manufacturer, was fitted to the base of the powder cartridge. However, this option did not have the desired effect on the spraying results. In fact, the blockage was less frequent but it was still occurring in an unpredictable manner and the coating yield was still poor. An even larger powder orifice (4) was selected with no noticeable improvement. Taking into account that PCL is very expensive to purchase and to grind down to a powder form, the alternative solution was to combine (by mixing powders) PCL with a another biocompatible polymer, PMMA, having excellent flowability in order to obtain a biocompatible matrix and therefore solve the powder feeding issue. Even though this PCL/PMMA matrix was not totally biodegradable, it could still perform its drug delivery purpose.

4.2.2 PMMA Screening

After the first screening of the PMMA flame sprayed coatings, the following images (Figure 48) were obtained. The initial spraying parameters were: 35cm spray distance, gun traverse speed at 0.254 m/s (10ips), 6 passes and the use of the largest orifice for powder flow input.

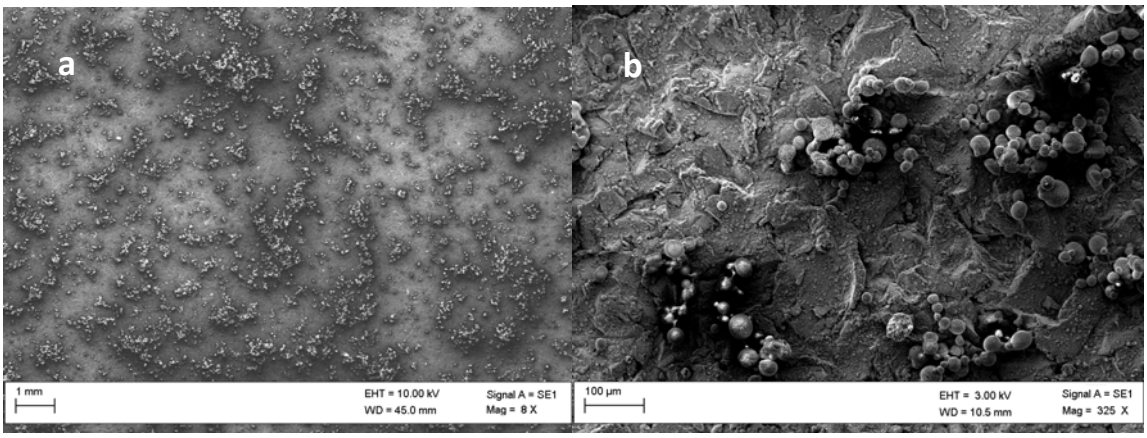

Figure 48: Substrate following PMMA thermal spraying: a) at Mag=8X; b) at Mag=325X

Figure 48a clearly shows that a proper coating was not obtained as patches of agglomerated un-molten/partially molten powder particles were present on the surface of the substrate. This can be explained in two different ways. Either not enough coating material was able to reach the substrate, implying that most of the particles disintegrated in-flight or the particles were not molten enough and hence bounced off the substrate.

According to findings of Zhang et al. [43], the first explanation seems more probable. In fact, due to the low thermal conductivity of polymers and PMMA in this case(less than 0.5 W/m K for most engineering polymers [228] contrary to HA = 1.2 W/m K [229]), a rapid temperature increase at the particle surface would have been experienced, and this, together with its low thermal decomposition temperature, would have led to a mass loss of the in-flight particles within the flame. Knowing that the maximum particle size for this powder is 25-30 microns, the possibility of particles evaporating in flight is likely to have happened. Ivosevic et al. [155] indicated that the surface temperature of a 30 µm polymer particle (Nylon-11) under HVOF conditions was more than twice as high as the upper degradation limit, which confirms that such small particles will most likely fully degrade during spraying.

Figure 48b shows how the particles agglomerated on the substrate. This can be explained by another observation made by Zhang et al. [43]. Due to the low thermal conductivity of polymers and PMMA in this case, a large temperature gradient may develop within the particle. This results in a reduction of the degree of melting of in-flight particles. Practically, this means that the particle surface reaches its thermal decomposition

temperature long before the centre of the particle starts melting, which leads to the decomposition of the surface layer of the particle and correspondingly to a reduction in the particle size. This process causes particles to stick to each other in-flight to form the agglomerated entities observed on the sample. It is important to note, however, that this process probably affected the largest particles of powder, those which could sustain the rapid thermal decomposition of the surface and that it was more likely to occur at the outer boundary of the spray flame where temperatures were lower than at the centre of the spray pattern. This agglomeration could also be explained by the fact that the largest orifice for powder flow was selected. Too much powder could have led to a lack in melting for the particles less exposed to the flame/heat. Finally, all the samples had a dark appearance, thus indicating that too much powder was feeding into the system.

In order to overcome the problem encountered during the first screening test, a number of parameters were varied:

- The traverse speed was reduced from 0.254 m/s (10ips) to 0.203m/s (8ips) and then to 0.152m/s (6ips) in order to increase the contact time between the flame and the sample in order to try to increase the powder deposition efficiency.
- The spray distance was decreased from 35cm to 30cm and then to 25cm.
- The powder flow orifice was reduced from position 3 to position 2 and then to position 1 (smallest size). According to the gun manufacturer the orifice size should be varied depending on the particle size, knowing that the particle range for this gun is approximately from 10 to 100 microns.
- The number of passes was augmented for some samples in order to try to increase the powder deposition efficiency.

The first visual observation was a reduced (shorter and narrower) shape of the flame which resulted in less oxidation as the samples were not dark in colour anymore. This was thought to have been caused by the reduction of the powder inlet orifice diameter, which is the only variable parameter that directly affects the thermal spraying process, leading to a reduction of powder influx in the flame, thus decreasing the size of the plume. SEM images of various samples were taken and it was observed that the only parameter that seemed to affect the final result was the spraying distance.

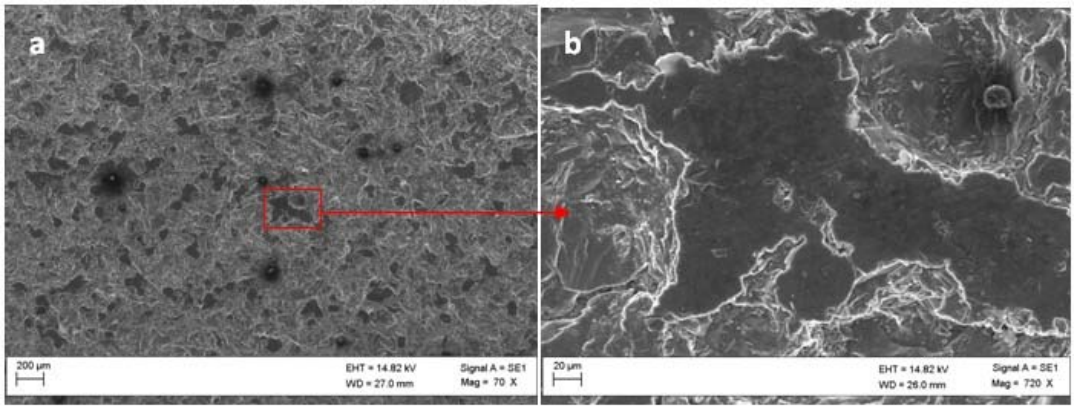

Figure 49: Substrate following PMMA thermal spraying: a) at Mag=70X; b) at Mag= 720X

The sample shown in Figure 49 corresponds to the following spraying parameters: traverse speed= 0.152m/s (6ips), SD= 25cm, 24 passes and powder orifice 1. The only noticeable improvement was that most of the particle agglomeration had been replaced by very small dispersed areas of coatings which were probably caused by the heat effect of the flame tail. This was also observed by Zhang et al. [43]. During the spraying process the deposited/substrate receives heat from two sources: the solidifying splats and the tail-end of the flame as it scans the surface in the normal course of the spraying procedure. Thus the heating effect of the flame can be much higher for two reasons: the flame had a much higher temperature than the splats and the particle exposure time to the flame was much longer than that to the splats (24 passes as opposed to the once off strike of the splat).

4.2.3 PCL/PMMA Screening

In order to minimise the amount of non-degradable biocompatible powder in the matrix as much as possible, incremental ratios of PMMA powder were added until it was possible to spray polymers for at least 30 seconds without interruption (caused by blockage), which would guarantee that the longest run (slowest traverse speed and highest number of passes) could be performed without spray interruption. A threshold of 30 seconds was chosen as the minimum spraying duration for the parameters to be deemed acceptable. Table 30 shows the powder volume ratio (while trying to maximise the PCL quantity) and the orifice tested before obtaining the optimal ratio for acceptable powder flowability. For each powder ratio a few runs were tested and timed and the average time before blockage was recorded.

Table 30: Screening study for the optimal powder orifice and PCL/PMMA ratio

Powder Orifice	PCL:PMMA 90:10	PCL:PMMA 80:20	PCL:PMMA 70:30	PCL:PMMA 60:40	PCL:PMMA 50:50
Orifice 1	< 5 seconds	< 5 seconds	< 5 seconds	< 5 seconds	< 10 seconds
Orifice 2	< 5 seconds	< 5 seconds	< 10 seconds	< 10 seconds	< 10 seconds
Orifice 3	< 10 seconds	< 10 seconds	< 20 seconds	< 25 seconds	>30 seconds
Orifice 4	< 15 seconds	< 15 seconds	< 20seconds	< 25 seconds	> 30 seconds

Table30 summarising the results of this thorough screening stage, showed that the minimum amount of PMMA to be added to PCL in order to guarantee an un-interrupted spraying stream, and therefore no material waste, should be at a volume ratio of 50:50. In fact, all ratios tested prior to the latter resulted in spraying interruption and orifice blockage. Table 30also shows that powder orifice 4 or 3 should be used to avoid any unwanted blockage during spraying.

Following the preliminary test for the optimal powder ratio and orifice size, PMMA and PCL powders were mechanically mixed at a volume ratio of 50:50. This was done in order to solve flowability problems related to using only PCL. It is also important to note that a composite polymers coating could offer increased advantages as a drug delivery layer. In fact, PMMA, being non-biodegradable in nature, would solve issues that might arise from fast or uncontrolled degradation of PCL-only coatings if such degradation affects the mechanical integrity of the coating before osteointegration is complete; whereby PMMA would provide additional mechanical support while PCL degrades over time.

Furthermore, in order to avoid any random blockage at the powder orifice injection point, the powder cartridge was removed and the orifice cleaned following every run. Although tedious and very time consuming, this step considerably reduced the risk of unpredictable blockage.

After a couple of runs with an additional larger powder orifice (4), it was noticed that the number of samples with a dark appearance was unusually high. The second largest powder orifice (3) was then selected. Figure50 shows the difference in colour between a bare Ti disc, a sample obtained with orifice 4 and a sample obtained with orifice 3. Note that the spraying parameters were randomly chosen and were identical for the coated samples.

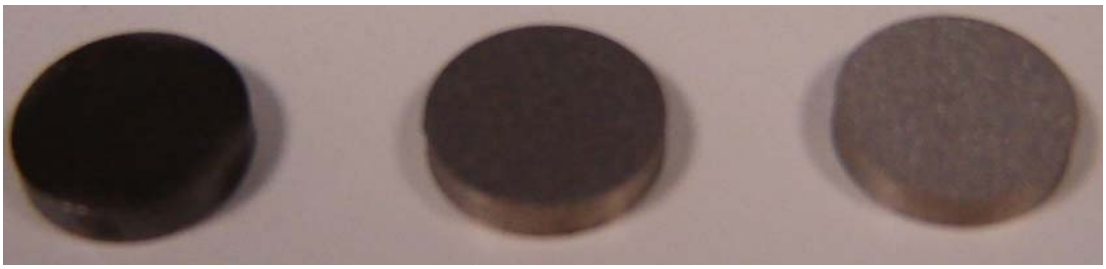

Figure 50: From left to right: orifice 4 used, orifice 3 used, bare Ti disc

The first visual observation was the dark colour of the first sample. This was also observed during the PMMA spraying (orifice 3), which implies that a high in-flow of PMMA in the plume caused a more pronounced dark appearance. The second visual observation was that of the second coated sample (orifice 3), although showing a brighter appearance, it looked to be a thinner coating

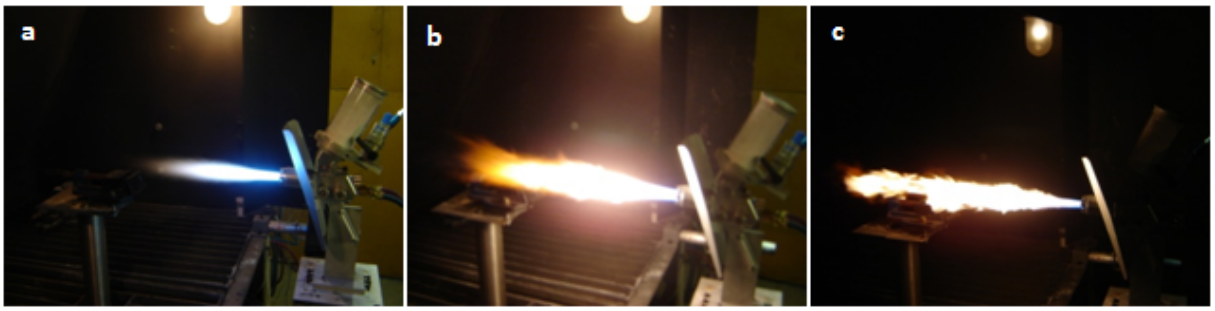

Figure 51: Plume appearance with: a) Neutral flame; b) powder orifice 3 used; c) powder orifice 4 used (excess powder)

Figure 51c shows that when powder orifice 4 was used, a reduced flame was formed. This type of flame usually indicates an excess fuel gas, which was not the case this time around. The extended flame tail also played a role in darkening the appearance of the coatings.

The SEM examination of the clear sample (orifice 3) confirmed the initial visual observation, which was, that a very thin layer which did not cover the Ti rough morphology. In fact, the proportion of polymer (white arrows in Figure 52) to substrate shows that little or no coating was obtained using the mid-range parameters and powder orifice 3.

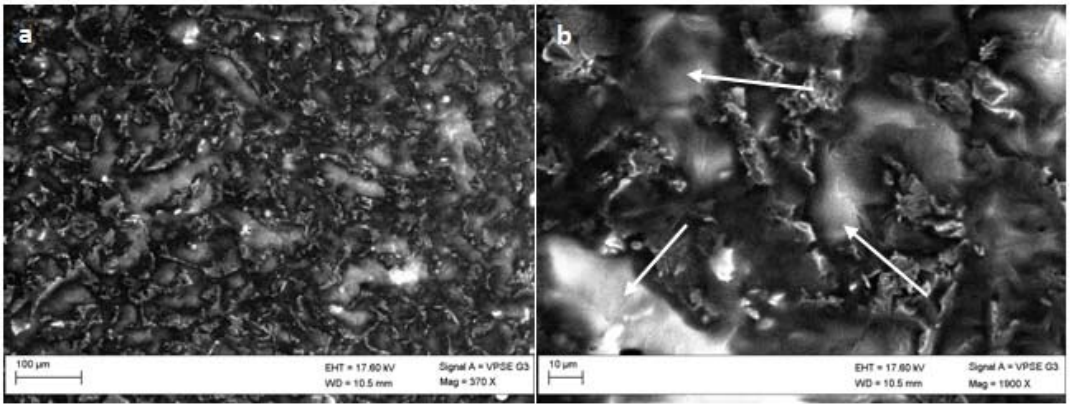

Figure 52: PCL/PMMA coating using powder orifice 3 at: a) Mag = 370 X; b) Mag = 1900 X

Therefore, the spraying ranges would have to be changed accordingly in order to maximise the powder to coating yield, as conducted in the next phase of the project.

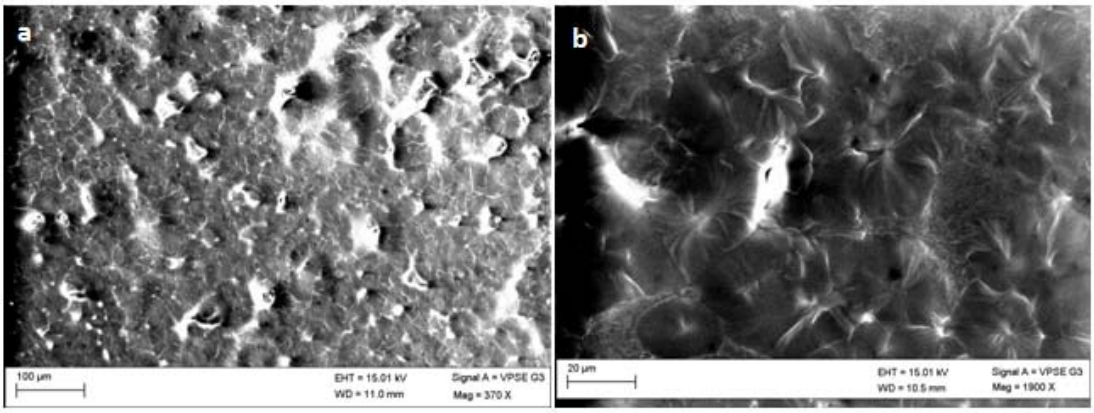

Figure 53: PCL/PMMA coating using powder orifice 4 at: a) Mag = 370 X; b) Mag = 1900 X

The SEM examination of the darkened sample (powder orifice 4), confirms that a coating was formed (Figure 53). When compared to the PCL-only coating, previously examined under the SEM, the PCL/PMMA displayed more roughness, which was a desirable effect when it comes to cell adhesion following implantation. The final powder flow rate obtained when PCL/PMMA was flowing without interruption (orifice 3) was: 15 g/min.

4.2.4 PHBV/PMMA Screening

It was clear from the powder characterisation stage that the PHBV powder would not be easy to spray using the in-house equipment because of its morphology, and that an additive

may be needed to improve its flowability. In fact, based on its very irregular morphology and the particle size distribution, PHBV was the least flowable powder used in this study. A preliminary study was performed to find out which powder ratio and orifice size should be used for a continuous flame spraying sequence of at least 30 seconds.

Table 31: Screening study for the optimal powder orifice and PHBV/PMMA ratio

Powder Orifice	PHBV:PMMA 90:10	PHBV:PMMA 80:20	PHBV:PMMA 70:30	PHBV:PMMA 60:40	PHBV:PMMA 50:50
Orifice 1	< 5 seconds	< 5 seconds	< 5 seconds	< 5 seconds	< 5 seconds
Orifice 2	< 5 seconds	< 5 seconds	< 5 seconds	< 5 seconds	< 10seconds
Orifice 3	< 5 seconds	< 10 seconds	< 10 seconds	< 10 seconds	< 15 seconds
Orifice 4	< 15 seconds	< 15 seconds	< 20seconds	< 20 seconds	> 30 seconds

Following this extensive screening stage, it was clear that the particle size of the PHBV powder caused considerable spraying disruptions. The most effective way to spray PHBV/PMMA composite without spray interruption and therefore without powder, gas and substrate waste, required a volume ratio of 50:50 PHBV/PMMA (Table 31) along with the largest powder inlet orifice available in the gun. The first coatings obtained with randomly chosen spraying parameters looked more viable (transparent coating covering the entire substrate surface, without darkened areas).

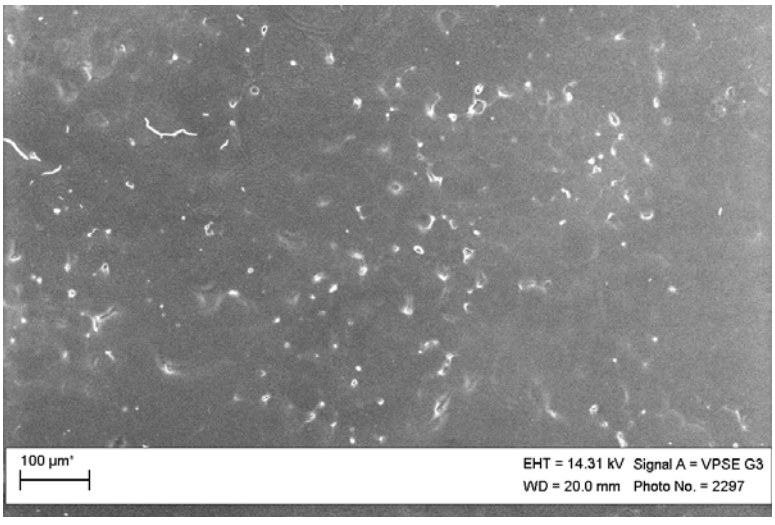

Figure 54: PHBV/PMMA coating morphology at Mag=100X

SEM examination of the PHBV/PMMA coating (Figure 45) confirmed the initial visual observations, whereby the surface of the substrate was fully covered with a polymer layer and no major defects were visible. This was an encouraging result in light of the more thorough investigation to follow in order to optimise the spraying process. It proves that despite the fact that the polymer powders were not suited for such an application and the major flowability problems that come with it, it was still possible to obtain viable polymer coatings. The final powder flow rate obtained when PHBV/PMMA was flowing without interruption (orifice 4) was: 35 g/min.

4.3 Parameter Space Investigation

The aim of this screening process was to identify the range of parameters that would be investigated furthermore for a DoE study in order to obtain the optimal process parameters. As previously discussed, the destructive nature of the process used and the potentially fast thermal degradation of the feedstock materials makes it a challenge to obtain a series of fully covered coatings across a range of parameters, that neither contain partially melted powder particles nor fully degraded powder. The screening stage began by choosing a range of parameters based on literature, and taking into account the new polymer matrix, seeing that specific polymers behaved differently when flame sprayed depending on their particle size, melting temperature, thermal conductivity and so on. The following ranges of parameters were chosen as an initial point for this parameter space investigation stage:

- Spraying distance: 20 cm-40 cm
- Gun traverse speed: 0.152 m/s-0.254 m/s (6 ips-10 ips)
- Number of passes: 6-10 passes

Using these baseline parameters, a one-factor-at-a-time approach was used in order to re-adjust the spraying ranges and therefore to accommodate the process parameters to the polymer matrices used in this project. During this parameter space investigation, six different types of coatings for PHBV/PMMA and four different coatings for PCL/PMMA were observed with different levels of damage and particle melting. In order to facilitate the analysis of coating viability and the suitability of each parameter space, classification charts were made (Figure 55 and Figure 56) with levels of damage or viability being coded.

4.3.1 PCL/PMMA Parameters Range Selection

The colour coding shown in Figure 55 corresponds to the viability of the coating: green-highlighted coatings were deemed viable with the parameters used being suitable, whereas red-highlighted coatings indicate that the state of the coating was unsatisfactory and the set of parameters used was not suitable.

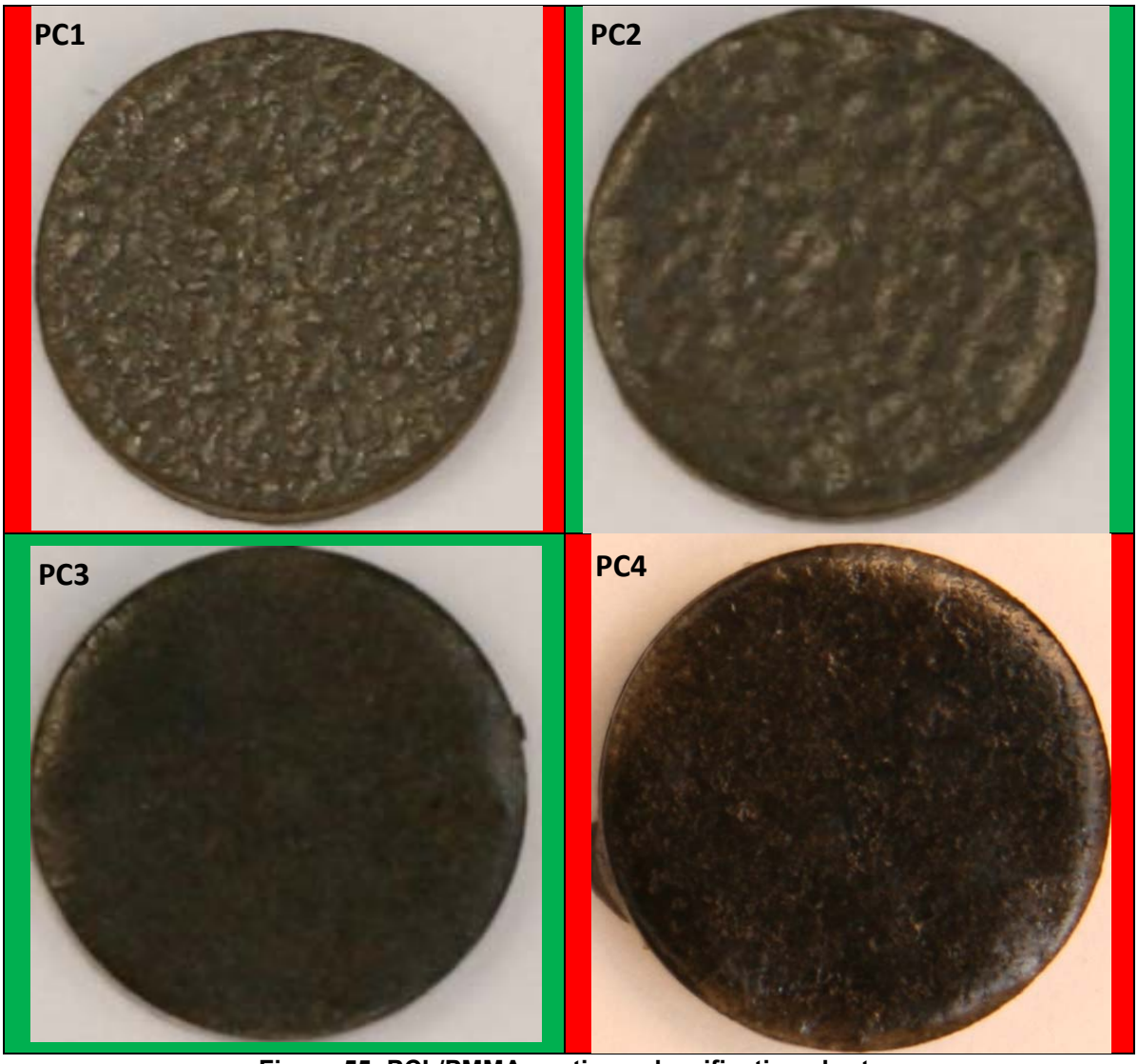

Figure 55: PCL/PMMA coatings classification chart

The descriptions of the coating types (PC: Polymer Coating) shown in Figure 55 were as follows:

- **PC1**: Level of coverage insufficient leading to superficial coverage of the substrate surface, with the roughness of the sand blasted titanium still clearly visible. This type of samples was deemed non-viable as it does not even qualify as a coating.
- **PC2**: Fully covered substrate with a transparent and thin-looking polymer coating, where the roughness of the substrate affects the roughness of the coating surface. This type of coating was deemed viable as full coverage of the coating was obtained, regardless of the apparent thickness.
- **PC3**: Fully covered substrate with a transparent and thick-looking polymer coating. This type of coating was also deemed viable and is in fact the best possible coating that could be obtained with the flame spraying technique.
- **PC4**: Fully covered substrate with a dark polymer coating. The increased level of oxidation may have compromised the chemical integrity of the polymer. This type of coatings was deemed non-viable as the degree of chemical degradation was likely to be enhanced.

a) Varying the spraying distance:

Table 32: Spraying distance screening for PCL/PMMA

Process parameter	Spray distance	Traverse speed	Number of passes	Coating type observations
Minimum	20 cm	0.203 m/s	8 passes	**PC4**
Mid-range	25 cm	0.203 m/s	8 passes	**PC4**
Mid-range	30 cm	0.203 m/s	8 passes	**PC3**
Mid-range	40 cm	0.203 m/s	8 passes	**PC3**
Mid-range	45 cm	0.203 m/s	8 passes	**PC3**
Maximum	50 cm	0.203 m/s	8 passes	**PC3**

As shown in Table 32, due to the length of the flame (50-55 cm), spray distances of less than 30cm resulted in coatings with a darker appearance, which could only be a physical feature, with the chemical state of the coating being fine. Despite this, the lower end of the spraying distance range was taken at 30 cm. Clear coatings with an excellent compact appearance were obtained up to a spraying distance of 50cm. Due to size limitations of the

extraction booth and to avoid having the flame outside the extraction zone, 50cm was taken as the upper limit of the spray distance range. Therefore, the spraying range went from 20-40 cm to 30-50 cm with a mid-point distance at 40 cm. As opposed to the PHBV/PMMA matrix and following visual and microscopic inspections, none of the PCL/PMMA coatings showed traces of un-melted particles, which is a precursor to good mechanical coating integrity.

b) Varying the traverse speed:

Seeing that all the coatings obtained from the spray distance screening had a very good appearance, it was decided to expand out the limits of the spraying range for the remaining two parameters (traverse speed and number of passes).

Table 33: Traverse speed screening for PCL/PMMA

Process parameter	Spray distance	Traverse speed	Number of passes	Coating type observations
Minimum	40 cm	0.101 m/s	8 passes	**PC4**
Mid-range	40 cm	0.152 m/s	8 passes	**PC3**
Mid-range	40 cm	0.203 m/s	8 passes	**PC3**
Mid-range	40 cm	0.355 m/s	8 passes	**PC3**
Mid-range	40 cm	0.406 m/s	8 passes	**PC2**
Maximum	40 cm	0.457 m/s	8 passes	**PC1-PC2**

As shown in Table 33, a traverse speed of 0.101 m/s (4ips) was too slow and resulted in a coating that could be classified by the PC4 type. The exposure time of the substrate holding fixture was very high and resulted in ignition of the aluminium fixture by the tail-end of the flame as the polymer deposited onto the fixture. From a traverse speed of 0.152 m/s (6ips) and up to 0.406 m/s (16ips), excellent coatings were obtained. Above a spraying velocity of 0.406 m/s, parts of the substrate were left exposed and full coverage was lost. Therefore, the range of traverse speed almost doubled going from 0.152-0.254 m/s (from literature) to the much wider range of 0.152-0.406 m/s.

c) *Varying the number of passes:*

In an attempt to push the process to extreme parameter limits, the screening for the number of passes initiated at 2 passes. However, this resulted in partially un-coated substrates. The same result was observed after 4 passes (Table 34).

Table 34: Number of passes screening for PCL/PMMA

Process parameter	Spray distance	Traverse speed	Number of passes	Coating type observations
Minimum	40 cm	0.279 m/s	2 passes	**PC1**
Mid-range	40 cm	0.279 m/s	4 passes	**PC1**
Mid-range	40 cm	0.279 m/s	6 passes	**PC2**
Mid-range	40 cm	0.279 m/s	8 passes	**PC3**
Mid-range	40 cm	0.279 m/s	10 passes	**PC3**
Mid-range	40 cm	0.279 m/s	12 passes	**PC3-PC4**
Maximum	40 cm	0.279 m/s	14 passes	**PC4**

PC2 and PC3 type coatings were then obtained from 6 passes up to 10 passes without overheating of the coatings. After 12 and 14 passes, the samples began to overheat and the coatings burnt-off partially or completely. Therefore, following this screening stage, the spraying range for the number of passes remained between 6-10 passes.

It is important to note that the coatings obtained within the final ranges were of high quality without the presence of totally or partially unmelted particles, and the structural damage they may incur. Table 35 summarises the initial (based on literature) and final (based on this study)results of the screened parameters for the PCL/PMMA matrix.

Table 35: Initial spraying range versus Final spraying range PCL/PMMA

Parameters	Literature Range	Experimentally Established Range
Spraying Distance (cm)	20-40	30-50
Gun Traverse Speed	0.152-0.254	0.152-0.406
Number of Passes	6-10	6-10

4.3.2 PHBV/PMMA Parameters Range Selection

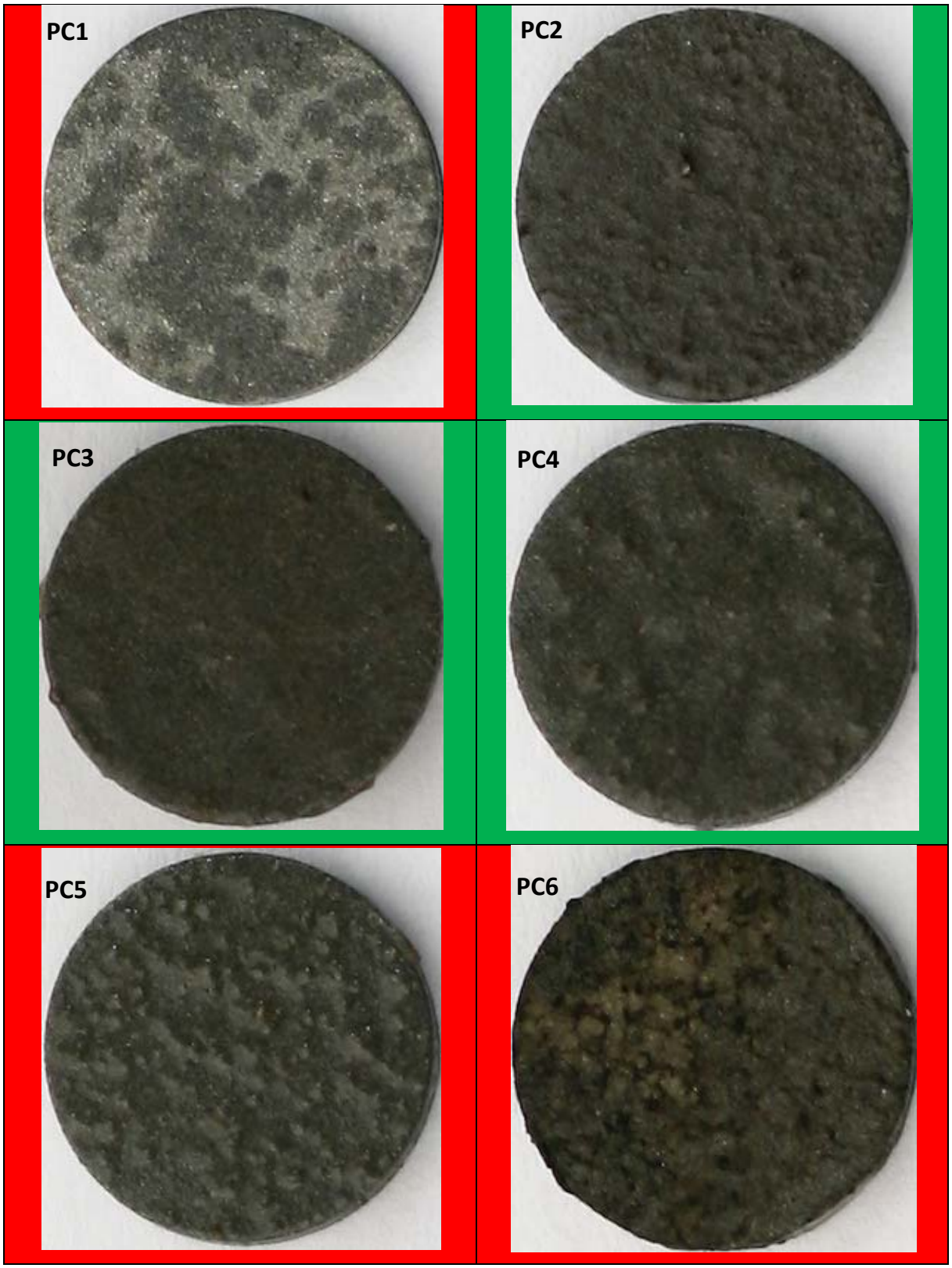

Figure 56: PHBV/PMMA coatings classification chart

The colour coding corresponds to the viability of the coating: green-highlighted coatings were deemed viable and the parameters used suitable, red-highlighted coatings indicate that the state of the coating was unsatisfactory and the set of parameters used was not suitable. The descriptions of the coating types(PC: Polymer Coating) shown in Figure 56 were as follows:

- **PC1**: Level of coverage insufficient leading to dispersed splats of polymer without full coverage of the substrate surface. This type of samples was deemed non-viable as it did not even qualify as a coating.
- **PC2**: Fully covered substrate with transparent and a thin-looking polymer coating, where the roughness of the substrate affected the roughness of the coating surface. This type of coating was deemed viable as full coverage of the coating was obtained, regardless of the apparent thickness.
- **PC3**: Fully covered substrate with a transparent and a thick-looking polymer coating. This type of coating was deemed viable and was in fact the best possible coating that could be obtained with the flame spraying technique.
- **PC4**: Fully covered substrate with a transparent polymer coating. The presence of some dispersed partially melted particles was noticed, adding roughness to the coating surface. This type of coating was deemed viable as a low number of partially melted particles do not compromise the integrity/cohesion of the coating.
- **PC5**: Full coverage of the substrate with a high percentage of totally un-melted powder particles. Such a coating characteristic may compromise the integrity/cohesion of the coating and therefore make the coating non-viable.
- **PC6**: Low level of coverage, with a totally carbonised substrate surface. This type of coatings was deemed non-viable as total degradation of the polymer was almost certain.

This chart was a very useful tool in narrowing down and shifting the parameters ranges in order to obtain the most viable coatings.

a) *Varying the spraying distance:*

It was decided to re-adjust the spraying distance range first, as this parameter was thought to have the largest influence on the structure of the final coatings; a flame that is too close to the coating would have a disintegrating effect, whereas a flame that is too far away would result in an undesirable morphology such as partially melted or totally un-melted particles. After igniting the flame and analysing its shape/amplitude, it was clear that using the 20cm-40cm range would be problematic, since the length of the flame was approximately 45cm. This meant that any deposited polymer would probably be burnt off by the tail-end of the flame. Therefore, knowing that the latter source of energy has the greater heating effect on the deposited coating layers[43], it was decided that the starting range would be 40 cm-50 cm, while taking the mid-range values for traverse speed (0.203 m/s- 8ips) and number of passes (8 passes). The resulting coatings were as follows:

Table 36: Spraying distance screening for PHBV/PMMA coatings

Process parameter	Spray distance	Traverse speed	Number of passes	Coating type observations
Minimum	40 cm	0.203 m/s	8 passes	**PC6**
Mid-range	42.5 cm	0.203 m/s	8 passes	**PC4**
Mid-range	45 cm	0.203 m/s	8 passes	**PC3**
Mid-range	47.5 cm	0.203 m/s	8 passes	**PC3**
Maximum	50 cm	0.203 m/s	8 passes	**PC5**

Following this first run (Table 36), it was found that the two ends of the range (40 and 50 cm) were not able to produce viable coating; thus the range of spraying distance had to be reduced furthermore to 42.5cm-47.5cm in order to increase the likelihood of a DoE (next step) producing as much coated substrates as possible. All coatings obtained within the new range resulted in fully covered substrates with a transparent looking polymer coating. Therefore the small processing window for the spraying distance parameter proved the difficulty experienced in processing a bio-degradable polymer using this flame spray thermal spraying process.

b) Varying the gun traverse speed:

The exposure time was thought to play an important role in determining the effect of the flame on the deposited layers. The slower the scanning speeds, the larger their effect on the coatings. Substantial thermal degradation of the polymer coatings occurred at low traverse speeds and therefore, choosing the correct traverse speed was a crucial parameter for the thermal spraying of polymer coatings [43].The initial range for the gun traverse speed was0.152 m/s-0.254 m/s (6ips-10ips). For the screening, mid-range values were taken at a spraying distance of 45cm and at 8passes.

Table 37: Traverse speed screening for PHBV/PMMA coatings

Process parameter	Spray distance	Traverse speed	Number of passes	Coating type observations
Minimum	45 cm	0.152 m/s	8 passes	**PC6**
Mid-range	45 cm	0.203 m/s	8 passes	**PC4/PC5**
Mid-range	45 cm	0.228 m/s	8 passes	**PC2/PC3**
Mid-range	45 cm	0.254 m/s	8 passes	**PC2/PC3**
Mid-range	45 cm	0.279 m/s	8 passes	**PC3**
Maximum	45 cm	0.330 m/s	8 passes	**PC4**

The initial range of traverse speed did not yield the desired results (PC5 and PC6), with the exception of the highest value (0.254 m/s and 0.228 m/s) as shown in Table 37. Therefore, with the aim of reducing the exposure time of the tail end of the flame on the substrate surface, the range for the gun traverse speed was moved to higher levels going from 0.152 m/s-0.254 m/s (6 ips-10ips) to 0.228 m/s-0.330 m/s (9 ips-13 ips). Overlapping the speed between the mid-range point and the maximum/minimum points was done in order to enlarge the process window for traverse speed and therefore to provide a clearer picture during the DoE analysis.

c) Varying the number of passes:

Similarly to the traverse speed parameter, the number of passes directly affects the exposure time and therefore has a great influence on the structure and appearance of the

final coating. As the range of traverse speed increased following the screening stage, the exposure time was reduced. This can compromise the production of fully covered substrates, thus, the number of passes were increased also. For this reason, the screening stage for the number of passes included a larger parameter window as shown in Table 38.

Table 38: Number of passes screening for PHBV/PMMA coatings

Process parameter	Spray distance	Traverse speed	Number of passes	Coating type observations
Minimum	45 cm	0.279 m/s	6 passes	**PC1**
Mid-range	45 cm	0.279 m/s	8 passes	**PC2/PC3**
Mid-range	45 cm	0.279 m/s	10 passes	**PC3**
Mid-range	45 cm	0.279 m/s	12 passes	**PC3/PC4**
Mid-range	45 cm	0.279 m/s	14 passes	**PC3/PC4**
Maximum	45 cm	0.279 m/s	16 passes	**PC6**

Table 38, shows that the most suitable process window for the number of passes were 10-14 passes. At lower pass numbers the exposure time was too low and limited amount of coating material hit the target, whereas at higher pass numbers the exposure time was too high, resulting in coating degradation.

This screening stage furthermore confirmed the difficulty of processing biocompatible polymers using flame spraying. It also indicated how narrow the process window was for this type of materials to be thermally sprayed, where two extra passes proved crucial to the integrity/structure of the coating. Table 39 summarises the initial (based on literature) and final (based on this study) results of the screened parameters for the PHBV/PMMA matrix.

Table 39: Initial spraying range versus Final spraying range for PHBV/PMMA

Parameters	Literature Range	Experimentally Established Range
Spraying Distance (cm)	20-40	42.5-47.5
Gun Traverse Speed	0.152-0.254	0.228-0.330
Number of Passes	6-10	10-14

The spraying parameters for all ranges were wider for PCL/PMMA than those observed with PHBV/PMMA. Thus the process does have a wide parameter range in terms of producing coatings depending on each powder material used.

4.4 Preliminary Biological Testing

4.4.1 Powder Biological Testing

Preliminary biocompatibility tests (WST-1, ALP) were conducted in order to confirm that the polymers chosen for this project met the biological criteria and that they were suitable candidates for the proposed application.

The results of the PHBV powder investigation were not taken into account as the powder particles formed an opaque extract and therefore the results of the analysis were not reliable (colorimetric test). This problem could be overcome in future stages by filtering the extracts prior to incubation. For this study, a one-time interval (24 hours) was selected, as this initial work only focused on preliminary confirmation of the feedstock materials biocompatibility.

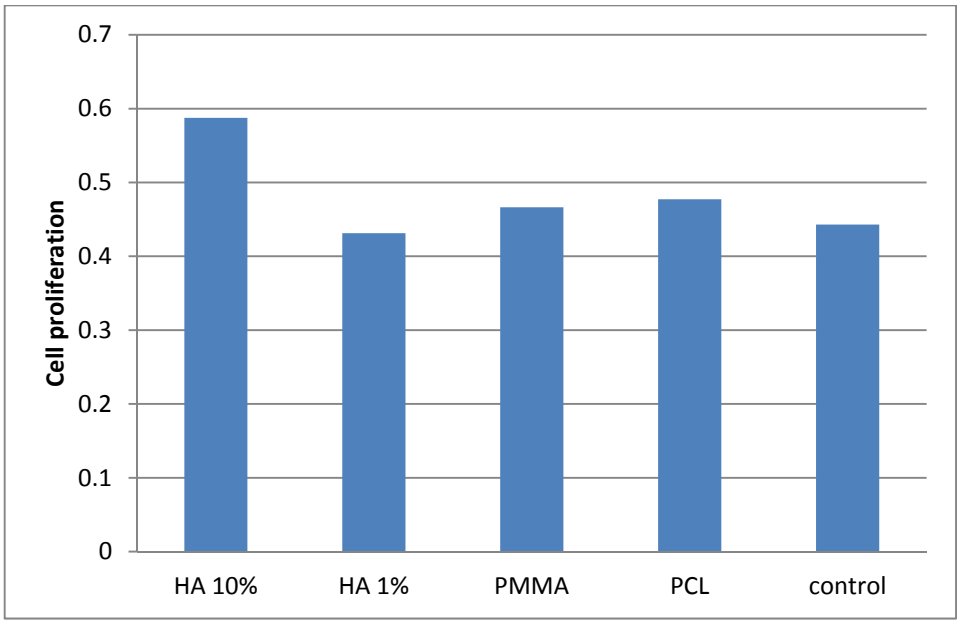

Figure 57: Cell proliferation assay results

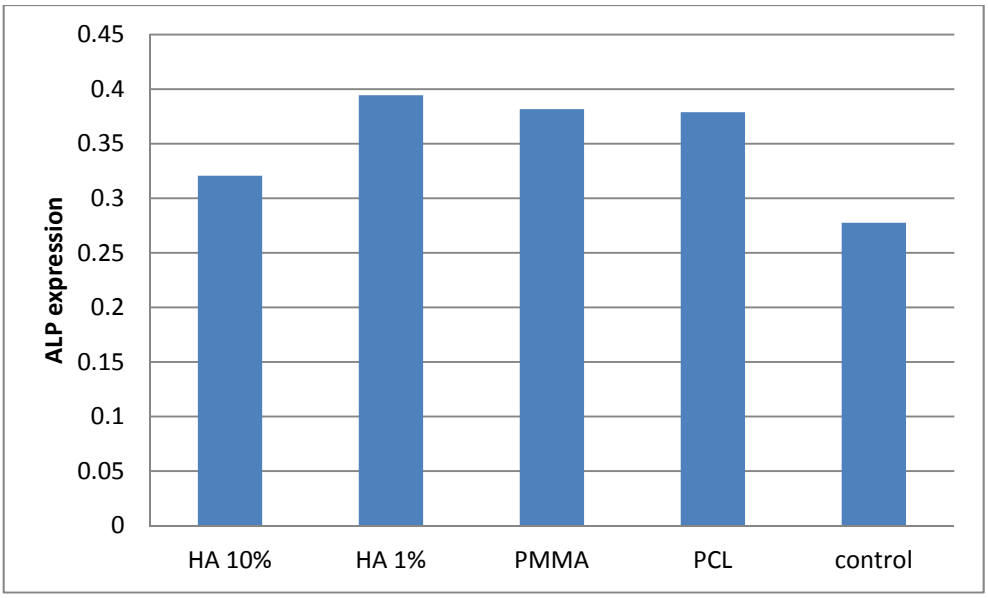

Figure 58: Alkaline phosphatase assay results

After a 24 hours incubation period, the cell proliferation (Figure 57) of all tested materials was higher than for the control material, which indicated that at this stage of the experiment, the materials did not show any cytotoxic effect on the human osteoblasts. The ALP activity (Figure 58) of the tested materials was also higher than that for the control, thus showing that in contact with extracts, cells tend to differentiate and possibly mature into osteocytes, forming bone. This was an encouraging result in light of the future use of these materials.

4.4.2 Coating Biological Testing

After the cell proliferation study was carried out, the preliminary biocompatibility testing results showed that the thermal spraying technique used did not considerably affect the biocompatibility of polymers. In fact, Figure 59 shows that both biodegradable polymers (PHBV/PMMA and PCL/PMMA) performed better than the reference material after three and five days. The optical density of the PHBV-based seeded well almost doubled from after five days, while it increased slightly for PCL-based well.

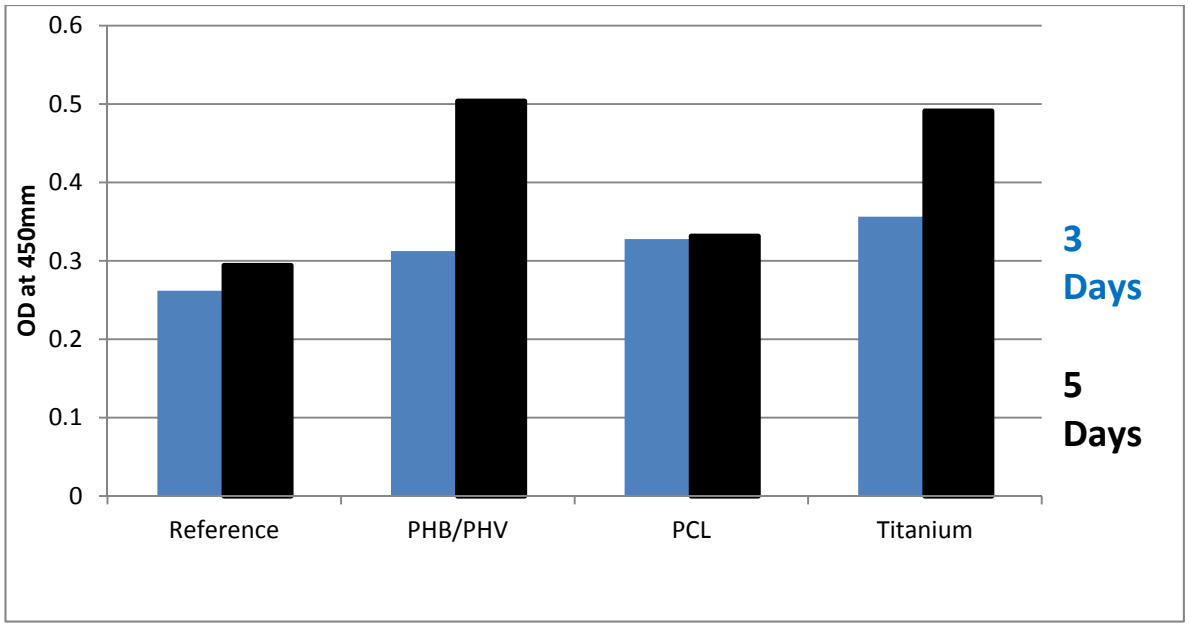

Figure 59: Cell proliferation study for the preliminary coating assessment

The results of this study were encouraging in light of the intended DoE study and the more thorough biological assessment that was to follow. It proved that at this stage, thermally sprayed biocompatible polymers could still perform well despite their exposure to extreme temperatures.

4.5 Response Surface Methodology Study

4.5.1 Coating Adhesion

A low curing temperature adhesive (Araldite 2005) was used. Unfortunately, after curing at room temperature for 24 hours, the samples tested failed at the coating-stud interface. The average shear strengths of this adhesive are characterised by high shear and peal strength (21-30 MPa depending on the coating material), based on metallic materials. It was then decided to use cyanoacrylate (superglue), as this was a low curing temperature adhesive and was tested by the pull-off tester manufacturer with results of 8.27-13.79 MPa on aluminium to aluminium contacts. The samples cured using cyanoacrylate yielded similar results to the araldite 2005 samples, where the failure occurred at the coating-stud interface. In addition to this, three more adhesives with different viscosities were donated by PALM LABS, Inc and tested for this project. The bond strength for each sample was tested for a

series of samples obtained using the same machine parameters and test conditions, and the result is shown in Table 40.

Table 40: Adhesives selection for pull-off testing

Test Results	Araldite 2005	Commercial Cyanoacrylate	Surface Insensitive Cyanoacrylate (1500cP)	Surface Insensitive Cyanoacrylate (100cP)	Surface Insensitive Cyanoacrylate (5cP)
Failure point	stud/coating interface	stud/coating interface	Cohesive failure	Cohesive and adhesive failure	Cohesive failure
Bond strength (kg/cm^2)	4.5	8.7	12.1	22.7	7.1

It was concluded that the alpha cyanocrylate esters supplied by Palm Labs was the most suitable adhesive for this application. Three types of failures occurred overall: a bond failure at the stud/coating interface with the coating left undamaged, a cohesive failure where the coating was partially/superficially pulled-off (Figure 60) and an adhesive failure where some areas of the coating were totally pulled-off the substrate (Figure 61). It was interesting to note that for all the adhesives tested, none of which resulted in an exclusively adhesive failure.

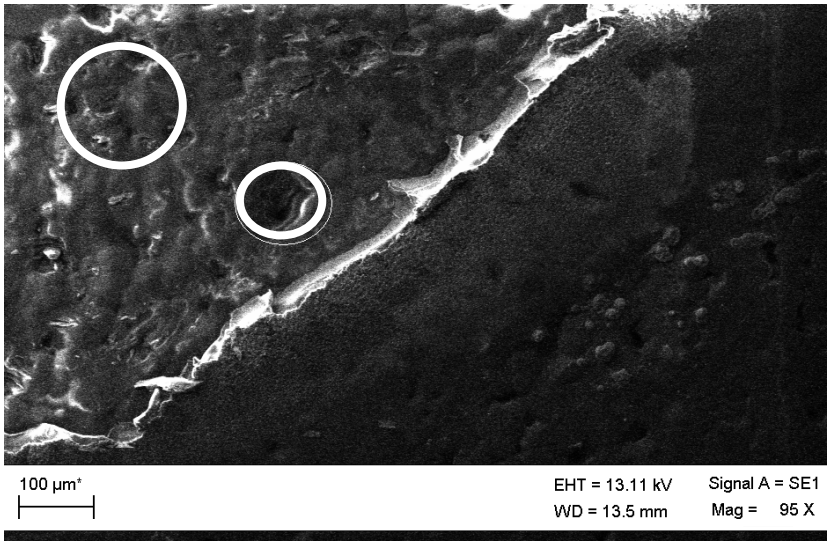

Figure 60: Pull-off test area showing cohesive failure

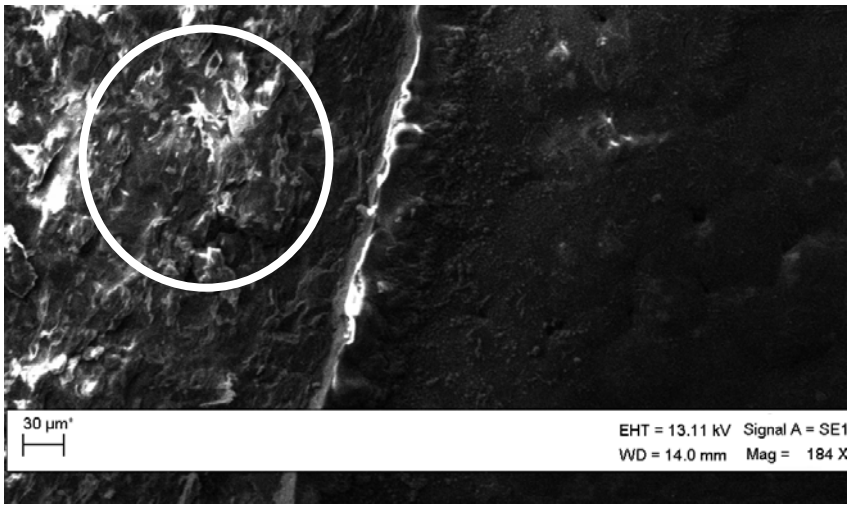

Figure 61: Pull-off test area showing adhesive failure

Figure 60 shows the separation line between the un-tested area (right-hand side) and the area where the adhesive/stud was applied to the coating (white circles). The bond strength recorded for this particular sample was 25 kg/cm^2. The thicker line separating both sides was the result of excess adhesive that slipped beneath the stud under compression. Thus one can assume that the coating was still present in the tested area with minor degradation (encircled area) seeing that the rough topography which characterises the sand-blasted Ti (that can be seen in Figure 61) was not clearly visible. The latter observation indicates that the bond strength of the adhesive was not strong enough to cause either adhesive or cohesive failure, the higher value obtained does however show that this formulation of adhesives (Surface Insensitive) performed better than the previously tested ones and that it was worth experimenting with the lower-end viscosity of the Surface Insensitive brand, as shown later.

4.5.2 DoE Layout for PCL/PMMA

Based on the results of the screening stage and the parameters space investigation, it is now possible to use the DoE technique in order to optimise the PCL/PMMA coatings with respect to the chosen coating characteristics. Table 41 summarises the experiments (Runs) to be carried out during this PCL/PMMA DoE study. The coatings obtained from each run were then characterised with regards to thickness, roughness, adhesion and contact angle, respectively.

Table 41: PCL/PMMA DoE layout

Std	Run	A:Traverse speed(ips(m/s))	B:Spraying Distance(cm)	C: Number of Passes
1	**9**	6(0.152)	30	6
2	**19**	11(0.279)	30	6
3	**7**	16(0.406)	30	6
4	**3**	6(0.152)	40	6
5	**5**	11(0.279)	40	6
6	**16**	16(0.406)	40	6
7	**11**	6(0.152)	50	6
8	**29**	11(0.279)	50	6
9	**1**	16(0.406)	50	6
10	**17**	6(0.152)	30	8
11	**21**	11(0.279)	30	8
12	**2**	16(0.406)	30	8
13	**24**	6(0.152)	40	8
14	**10**	11(0.279)	40	8
15	**30**	16(0.406)	40	8
16	**15**	6(0.152)	50	8
17	**6**	11(0.279)	50	8
18	**14**	16(0.406)	50	8
19	**26**	6(0.152)	30	10
20	**20**	11(0.279)	30	10
21	**31**	16(0.406)	30	10
22	**32**	6(0.152)	40	10
23	**13**	11(0.279)	40	10
24	**4**	16(0.406)	40	10
25	**23**	6(0.152)	50	10
26	**8**	11(0.279)	50	10
27	**25**	16(0.406)	50	10
28	**12**	11(0.279)	40	8
29	**28**	11(0.279)	40	8
30	**22**	11(0.279)	40	8
31	**18**	11(0.279)	40	8
32	**27**	11(0.279)	40	8

4.5.3 PCL/PMMA Thickness Model Validation

Table 42: Thickness measurements for the PCL/PMMA RSM study

Std	Run	T1(µm)	T2(µm)	T3(µm)	T4(µm)	Average(µm)	SD(µm)
9	**R1**	31.1	49.3	48.6	44	43.25	8.43
12	**R2**	118	124	96.4	85.4	105.95	18.12
4	**R3**	125	121	131	118	123.75	5.62
24	**R4**	129	91.1	107	119	111.52	16.32
5	**R5**	129	141	149	111	132.5	16.52
17	**R6**	114	89.1	80.4	110	98.37	16.21
3	**R7**	87.5	84.9	72.7	98.6	85.92	10.63
26	**R8**	98.9	110	104	128	110.22	12.69
1	**R9**	67.6	69	59.2	45.5	60.32	10.79
14	**R10**	118	114	138	129	124.75	10.87
7	**R11**	162	151	126	157	149	15.98
28	**R12**	141	111	112	104	117	16.39
23	**R13**	140	152	158	138	147	9.59
18	**R14**	64	64	59.7	40	56.92	11.46
16	**R15**	162	170	140	153	156.25	12.87
6	**R16**	70.2	75.5	79.1	71.1	73.97.	4.13
10	**R17**	88.4	90.2	122	124	106.15	19.49
31	**R18**	125	116	165	138	136	21.34
2	**R19**	115	120	104	91.8	107.7	12.53
20	**R20**	92.6	103	106	94.5	99.02.	6.49
11	**R21**	136	147	125	138	136.5	9.04
30	**R22**	117	148	129	124	129.5	13.28
25	**R23**	115	107	94.1	79.4	98.87	15.58
13	**R24**	118	132	118	116	121	7.39
27	**R25**	122	129	114	102	116.75	11.59
19	**R26**	123	118	120	119	120	2.16
32	**R27**	162	152	158	150	155.5	5.51
29	**R28**	118	124	133	125	125	6.16
8	**R29**	73.9	98.2	126	116	103.52	22.85
15	**R30**	104	107	103	103	104.25	1.89
21	**R31**	77.3	86.4	99.2	104	91.72	12.15
22	**R32**	164	165	143	163	158.75	10.53

The backward selection method was used to automatically eliminate insignificant model terms in order to study the main effects on thickness (thickness measurements in Table 42). An inverse squared transformation was required in order to obtain the adequate model. Factors/interactions with p-values of less than 0.1 (90% confidence interval) were included in the model. The ANOVA table and model statistics are shown in Table 43.

Table 43: ANOVA table for the PCL/PMMA thickness model

Source	*Sum of Squares*	*Mean Square*	*F Value*	*p-value Prob>F*	*Significance*
Model	7.561E-003	5.040E-004	21.51	<0.0001	Significant
Significance					
A-Traverse Speed	1.348E-003	1.348E-003	57.50	<0.0001	
B-Spraying Distance	3.474E-005	3.474E-005	1.48	0.2410	
C-Number of Passes	8.018E-004	4.009E-004	17.11	0.0001	
AB	1.247E-003	1.247E-003	53.20	<0.0001	
AC	2.690E-004	1.345E-004	5.74	0.0132	
BC	1.634E-004	8.168E-005	3.49	0.0554	
A^2	4.936E-004	4.936E-004	21.06	0.0003	
B^2	6.849E-004	6.849E-004	29.23	<0.0001	
ABC	1.624E-003	8.118E-004	34.64	<0.0001	
A^2C	3.464E-004	1.732E-004	7.39	0.0053	
Residual	3.750E-004	2.344E-005			
Lack of Fit	*2.860E-004*	*2.600*E-00	*1.49*	*0.3551*	*Not significant*
Pure Error	*8.900E-005*	*1.780*E-005			
Cor Total	7.936E-003				
R^2	0.9527				
Adjusted R^2	0.9084				
Predicted R^2	0.7297				
Adeq Precision	20.658				

The ANOVA table for the thickness model shows a p-value of <0.0001. This indicates that the model was significant at more than a 99.99% confidence level. The lack of fit was also not significant, indicating that the model adequately fit the data.

The R^2 value was equal to 0.9527, which is above 0.6 and as close as possible to 1 indicating a good model adequacy. Similarly, the Adjusted R^2 and Predicted R^2 values fit the constraints of being as close as possible to 1 and within 0.2 of each other. In this model, these values were 0.9084 and 0.7297 respectively, with a difference of 0.1787. Finally, the Adequate Precision value, which should be greater than 4 for a good model adequacy, was equal to 20.658. Therefore, having the R^2, Adequate Precision, Adjusted R^2 and Predicted R^2 values all exceeding the required thresholds; it is possible to conclude that an adequate and relatively precise model has been developed.

The ANOVA table shows that the polymer coating thickness was affected by all the process parameters (factors) tested: traverse speed (A), spraying distance (B), number of passes (C) as well as by all possible interactions. The ANOVA table also showed values of "Prob>F" less than 0.0500 for all models terms except factor B (spraying distance) and BC, which furthermore confirmed the significance of these factors and the interaction between them. Factor B had a "Prob>F" value of 0.2410, which indicated that the influence of this factor on the coating thickness was very limited in comparison to other factors/interactions. Analysis of the F-values indicates that the effects of the factors/interactions can be classified by order of amplitude starting with the largest effect as follows: A-traverse speed > AB > ABC > B^2> A^2> C-number of passes > A^2C > AC > BC > B-spraying distance.

The mathematical model for coating thickness was given in terms of coded factors (Eqn. 5) or actual factors (Eqn. 6-8).The coded factors model uses the coded low and high levels (-1 and 1) from the experimental design and can be used to quickly calculate the desired response (thickness in this case) at one of the experimental points. The actual factors model takes in account the differences between the levels of the factors and the difference in effects, meaning that the response value can be calculated at any factors level values (spraying distance, traverse speed, number of passes), within the range of the experiment. More information on factor coding can be found in Appendix A.

Final equation in terms of coded factors for PCL/PMMA coating thickness:

$1/\sqrt{(\text{Thickness})}(1/\sqrt{\mu m}) =$ + 0.087
+ 8.652E-003 * A
+ 1.389E-003 * B
+ 6.030E-004 * C[1]
- 1.076E-004 * C[2]
+ 0.010 * AB
+ 3.954E-003 * AC[1]
+ 1.293E-003 * AC[2]
- 1511E-003 * BC[1]
+ 4.205E-003 * BC[2]
+ 8.723E-003 * A^2
+ 0.010 * B^2
+ 0.013 * ABC[1]
+ 2.921E-003 * ABC[2]
+ 0.010 * A^2C[1]
- 2.584E-003 * A^2C[2] **(Eqn. 5)**

Final equation in terms of actual factors for PCL/PMMA coating thickness at 6 passes:

$1/\sqrt{(\text{Thickness})}(1/\sqrt{\mu m}) =$ + 0.51208
- 0.032363 * Traverse Speed(ips)
- 0.013027 * Spraying Distance(cm)
+ 4.55038E-004 * Traverse Speed(ips)*Spraying Distance(cm)
+ 7.58315E-004 * Traverse Speed(ips)^2
+ 1.00116E-004 * Spraying Distance(cm)^2 **(Eqn. 6)**

Final equation in terms of actual factors for PCL/PMMA coating thickness at 8 passes:

$1/\sqrt{(\text{Thickness})}(1/\sqrt{\mu m}) =$ + 0.34750
- 0.013904 * Traverse Speed(ips)
- 0.010335 * Spraying Distance(cm)
+ 2.62274E-004 * Traverse Speed(ips)*Spraying Distance(cm)
+2.45559E-004 * Traverse Speed(ips)^2
+ 1.00116E-004 * Spraying Distance(cm)^2 **(Eqn. 7)**

Final equation in terms of actual factors for PCL/PMMA coating thickness at 10 passes:

$$
\begin{aligned}
1/\sqrt{(\text{Thickness})}(1/\sqrt{\mu m}) = {} & + 0.20264 \\
& + 3.96702E\text{-}003 \quad * \text{Traverse Speed(ips)} \\
& - 6.97648E\text{-}003 \quad * \text{Spraying Distance(cm)} \\
& -1.05750E\text{-}004 \quad * \text{Traverse Speed(ips)} * \text{Spraying Distance(cm)} \\
& + 4.29157E\text{-}005 \quad * \text{Traverse Speed(ips)}^2 \\
& + 1.00116E\text{-}004 \quad * \text{Spraying Distance(cm)}^2 \qquad \textbf{(Eqn. 8)}
\end{aligned}
$$

The Predicted versus Actual graph in Figure 62, shows the predicted values plotted against the values experimentally obtained. Figure 62, shows a good fit between the model and the experimental data, where all the measured values lie close to the best-fit line representing the case of the actual values being equal to the predicted values. This means that this model accurately predicts the coating thickness.

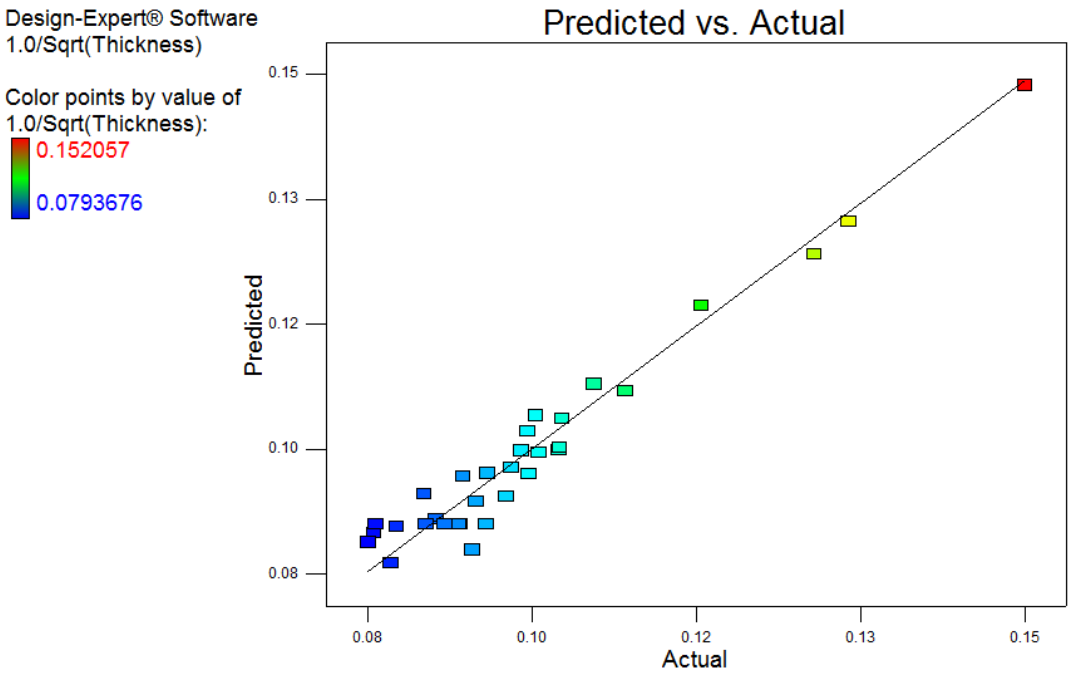

Figure 62: Predicted versus Actual values for PCL/PMMA coating thickness (1/√µm)

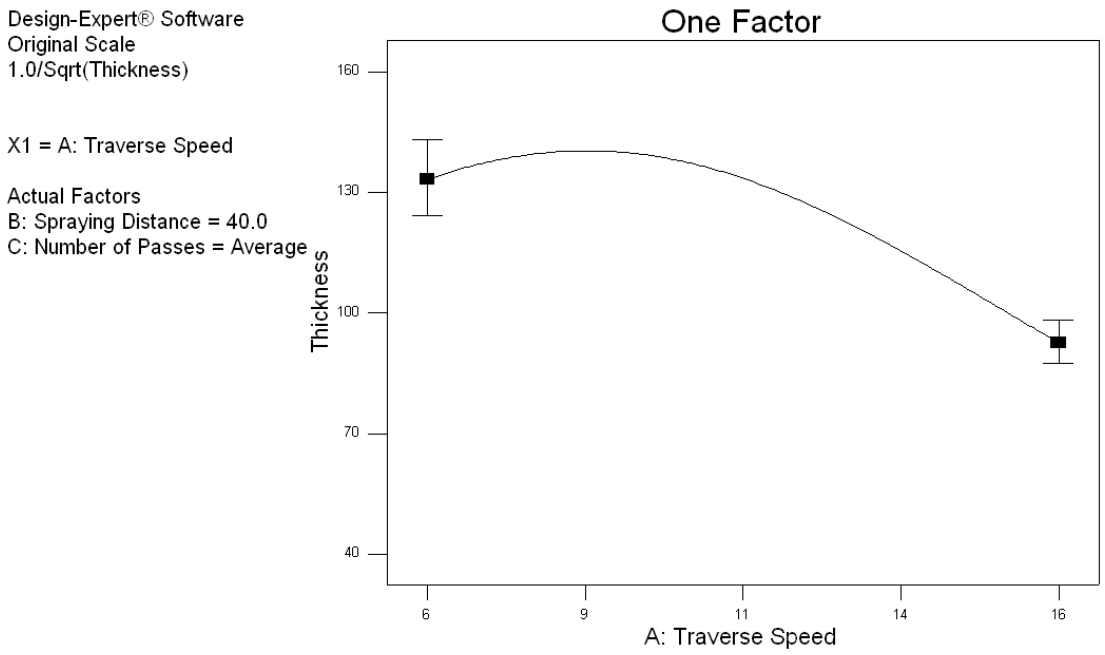

Figure 63: Average effect of traverse speed (A) (ips) on the thickness (1/√µm) of PCL/PMMA coatings

The traverse speed as a single factor as well as all the interactions involving it were found to have the strongest effect on the thickness of the PCL/PMMA coatings. The effects of factor A at mid-range spraying distance and average factor C are shown in Figure 63. The influence of the traverse speed on the coating thickness was not straightforward. Instead, the thickness started at a higher range when the traverse speed was at its lowest (0.152 m/s, 6ips). Following a slight increase in thickness to reach a peak at ~ (0.228 m/s, 9ips), the trend was inversed and the increase in traverse speed led to a decrease in coating thickness. The traverse speed directly affects the exposure time of the substrate to the spray plume, whereby the higher the build-up time, the thicker the coating. This trend is the opposite of the one observed with the PHBV/PMMA matrix (as will be demonstrated later) and is an indicator of the good thermal stability of the PCL material (as thick coatings were obtained despite high exposure time), even though it had the lowest melting temperature. This stability was probably due to the narrow and adequate range of particle size used in this case which resulted in homogenous coatings, as opposed to the large and multimodal distribution of PHBV particles, which results in different degrees of melting.

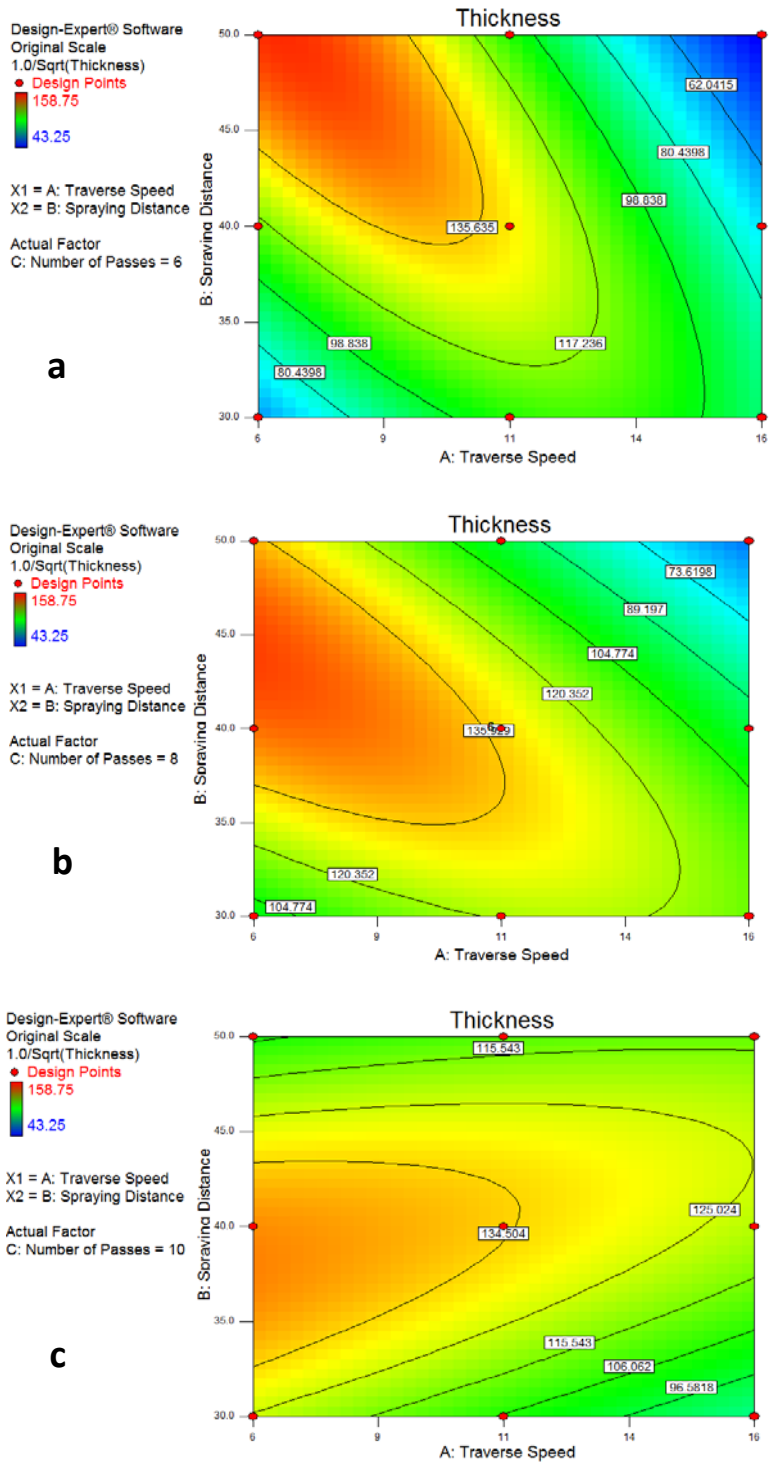

Figure 64: Interaction effects of traverse speed (ips) and spraying distance (cm) on thickness (µm) at a)6 passes, b)8 passes and c)10 passes

Figure64 shows the interaction effects of traverse speed and spraying distance, the second most influential element, on the coating thickness. These figures are consistent with the fact that longer exposure time, made possible by low traverse speed, results in more coating material built up and therefore in higher coating thickness. After 6 passes, the highest thickness occurs at low traverse speed and high spraying distance. Seeing that the coating build-up time was at its lowest (lowest number of passes), a high spraying distance was required in order to limit the destructive effect of the tail-end of the flame on the coating already built-up. As the number of passes (and therefore build-up time) increased, the effect of the spraying distance attenuates and higher coating thickness occurs at mid-range spraying distance. Table 44 shows the process parameters corresponding to the highest and lowest coating thickness.

Table 44: Spraying parameters for samples with the highest and lowest thickness

Run	Traverse Speed(ips)	Spraying Distance(cm)	Number of Passes	Thickness(µm)
R32	6	40	10	158.75
R1	16	50	6	43.25

Unsurprisingly, the highest coating thickness (158.75µm) occurred when the build-up time was at its highest (highest number of passes and lowest traverse speed) and a mid-range spraying distance so as to limit the destructive effect of the flame. On the other hand, the lowest coating thickness (43.25µm) occurred when the build-up time was at its lowest (lowest number of passes and highest traverse speed) and the highest spraying distance. The thickness model for PCL/PMMA showed a straightforward relationship between build-up time and layer thickness and will allow greater control on polymer coating thickness for drug release applications, where the latter coating property plays a regulating factor in the release kinetic.

4.5.4 PCL/PMMA Roughness Model Validation

Table 45: Roughness measurements for the PCL/PMMA DoE

Std	Run	R1(µm)	R2(µm)	R3(µm)	Average(µm)	SD(µm)
9	**R1**	1.9	2.4	3.2	2.50	0.66
12	**R2**	1.9	1.8	1.1	1.60	0.44
4	**R3**	1.5	1.2	2	1.57	0.40
24	**R4**	1.4	1.5	1.4	1.43	0.06
5	**R5**	2.2	1.7	2.4	2.10	0.36
17	**R6**	1.9	2	2.2	2.03	0.15
3	**R7**	2.2	2	2.7	2.30	0.36
26	**R8**	1.1	1.2	1	1.10	0.10
1	**R9**	1.6	1.3	1.5	1.47	0.15
14	**R10**	1.7	1.5	1.9	1.70	0.20
7	**R11**	1.8	1.6	2.7	2.03	0.59
28	**R12**	2.4	1.9	1.2	1.83	0.60
23	**R13**	1.5	1.6	1.8	1.63	0.15
18	**R14**	2.8	3.1	3	2.97	0.15
16	**R15**	1.9	1.1	2.5	1.83	0.70
6	**R16**	2.7	2	2.9	2.53	0.47
10	**R17**	1.3	1.4	1.5	1.40	0.10
31	**R18**	2.3	2.1	1.7	2.03	0.31
2	**R19**	1.4	2.4	2.5	2.10	0.61
20	**R20**	1.7	2.5	1.7	1.97	0.46
11	**R21**	2.1	1.7	1.8	1.87	0.21
30	**R22**	2.1	2.2	2.1	2.13	0.06
25	**R23**	0.7	0.9	0.8	0.80	0.10
13	**R24**	1.5	1.5	1.4	1.47	0.06
27	**R25**	1.4	1.9	1.3	1.53	0.32
19	**R26**	1.4	1.5	1.2	1.37	0.15
32	**R27**	2.3	2.1	2	2.13	0.15
29	**R28**	1.6	1.6	1.7	1.63	0.06
8	**R29**	1.7	1.8	1.6	1.70	0.10
15	**R30**	1.9	2	1.8	1.90	0.10
21	**R31**	1.8	1.5	1.8	1.70	0.17
22	**R32**	1.4	1.2	1.6	1.40	0.20

The backward selection method was used to automatically eliminate insignificant model terms in order to study the main effects on roughness (roughness measurements in Table 45). A natural log transformation was required in order to obtain the adequate model. Factors/interactions with p-values of less than 0.1 (90% confidence interval) were included in the model. The ANOVA table and model statistics are shown in Table 46.

Table 46: ANOVA table for the PCL/PMMA roughness model

Source	*Sum of Squares*	*Mean Square*	*F Value*	*p-value Prob>F*	*Significance*
Model	1.55	0.26	14.52	<0.0001	Significant
Significance					
A-Traverse Speed	0.46	0.46	26.11	<0.0001	
B-Spraying Distance	2.184E-004	2.184E-004	0.012	0.9127	
C-Number of Passes	0.67	0.34	18.90	<0.0001	
BC	0.41	0.21	11.60	0.0003	
Residual	0.45	0.018			
Lack of Fit	*0.38*	*0.019*	*1.39*	*0.3827*	*Not significant*
Pure Error	*0.068*	*0.014*			
Cor Total	2.00				
R^2	0.7770				
Adjusted R^2	0.7235				
Predicted R^2	0.6100				
Adeq Precision	15.625				

The ANOVA table for the roughness model shows a p-value of <0.0001. This indicates that the model was significant at more than a 99.99% confidence level. The lack of fit was also not significant, indicating that the model adequately fit the data.

The R^2 value was equal to 0.7770. The Adjusted R^2 and Predicted R^2 values were 0.7235 and 0.6100 respectively, with a difference of 0.1135. The Adequate Precision value was equal to 15.625. Therefore, it is possible to conclude that an adequate and relatively precise model has been developed.

The ANOVA table suggests that the polymer coating roughness was affected by all the process parameters (factors) tested: traverse speed (A), spraying distance (B), number of passes (C) as well as by the interaction BC. The ANOVA table also showed values of "Prob>F" less than 0.0500 for all models terms, except factor B (spraying distance) and BC, which furthermore confirmed the significance of these factors and the interaction between them. Factor B had a "Prob>F" value of 0.9127, which indicated that the influence of this factor on the coating roughness was very limited in comparison to other factors/interactions. Analysis of the F-values indicates that the effects of the factors/interactions can be classified by order of amplitude starting with the largest effect as follows: A-traverse speed > C-number of passes > BC > B-spraying distance.

The mathematical model for coating roughness was given in terms of coded factors (Eqn. 9) or actual factors (Eqn. 10-12).

Final equation on terms of coded factors for PCL/PMMA coating roughness:

$$\begin{aligned} \text{Ln(Roughness)(Ln(}\mu\text{m))} = {} & + 0.55 \\ & + 0.16 \quad * A \\ & - 3.483E\text{-}003 \quad * B \\ & + 0.14 \quad * C[1] \\ & + 0.072 \quad * C\,[2] \\ & + 0.036 \quad * BC\,[1] \\ & + 0.16 \quad * BC\,[2] \end{aligned} \qquad \textbf{(Eqn. 9)}$$

Final equation in terms of actual factors for PCL/PMMA coating roughness at 6 passes:

$$\begin{aligned} \text{Ln(Roughness)(Ln(}\mu\text{m))} = {} & + 0.20945 \\ & + 0.032143 \quad * \text{Traverse Speed(ips)} \\ & + 3.24743E\text{-}003 \quad * \text{Spraying Distance(cm)} \end{aligned} \qquad \textbf{(Eqn. 10)}$$

Final equation in terms of actual factors for PCL/PMMA coating roughness at 8 passes:

$$\begin{aligned} \text{Ln(Roughness)(Ln(}\mu\text{m))} = {} & - 0.37750 \\ & + 0.032143 \quad * \text{Traverse Speed(ips)} \\ & + 0.016142 \quad * \text{Spraying Distance(cm)} \end{aligned} \qquad \textbf{(Eqn. 11)}$$

Final equation in terms of actual factors for PCL/PMMA coating roughness at 10 passes:

Ln(Roughness)(Ln(µm))= + 0.79753
+ 0.032143 * Traverse Speed(ips)
- 0.020434 * Spraying Distance(cm) **(Eqn. 12)**

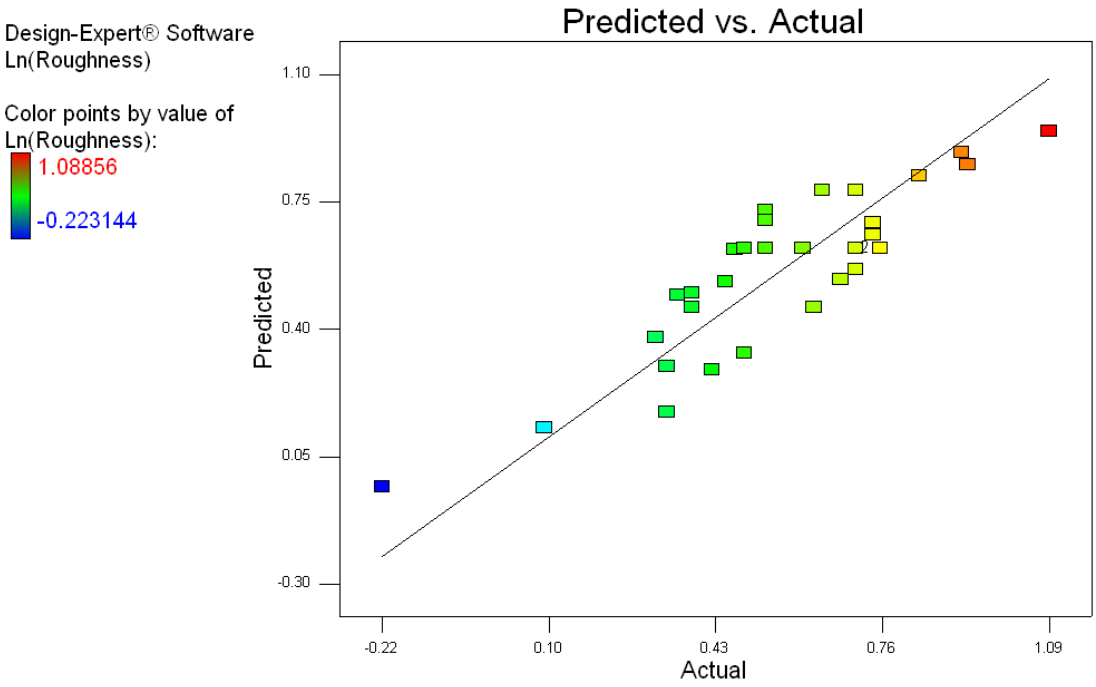

Figure 65: Predicted versus Actual values for PCL/PMMA coating roughness (Ln (µm))

The Predicted versus Actual graph in Figure 65, shows the predicted values plotted against the values experimentally obtained. Figure 65, shows a good fit between the model and the experimental data, meaning that this model accurately predicts the coating roughness.

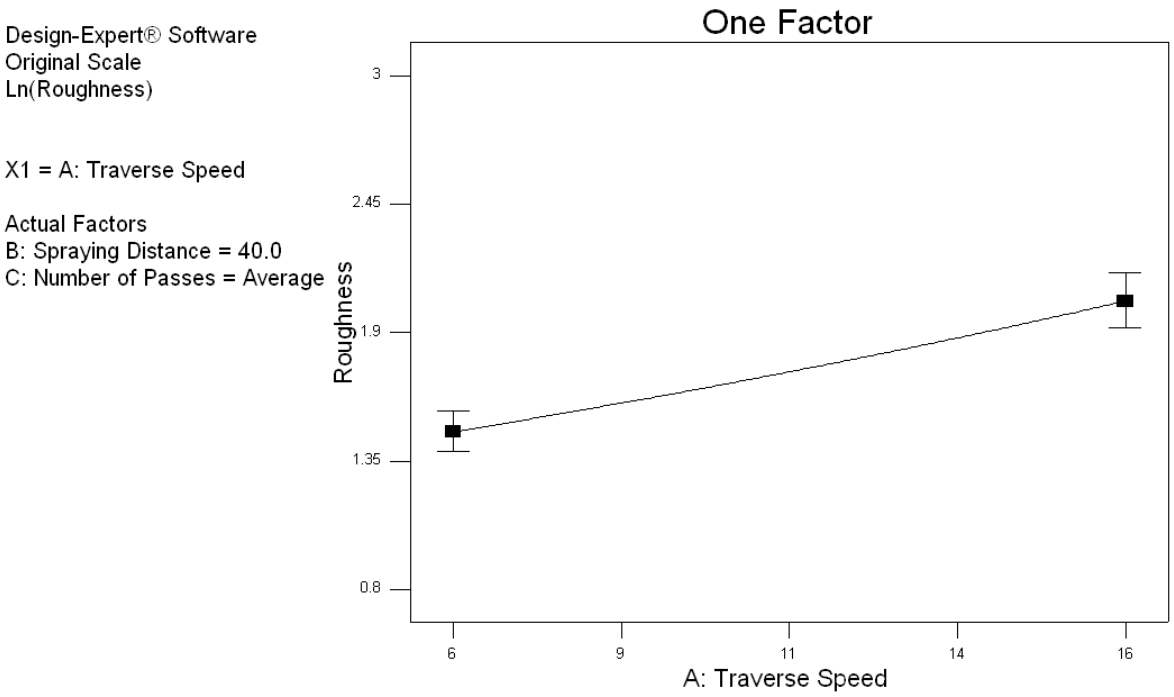

Figure 66: Average effect of Traverse Speed (ips) (A) on the roughness (μm) of PCL/PMMA coatings

As for the thickness model of PCL/PMMA, factor A-traverse speed had the largest influence on the coating roughness. Figure 66, shows that the latter factor affects the surface roughness when the average number of passes is considered and the spraying distance is at a mid-range value (40cm). The trend shown in Figure 66 is straightforward, whereby the traverse speed is directly proportional to the surface roughness of PCL/PMMA. At low traverse speeds, the tail-end of the flame flattens partially melted particles and fills the surface corrugations of the titanium substrates, which in turn reduces the coating roughness, similar to the coating types PC3 and PC4 show in Figure 55. As the traverse speed increases, the effect of the flame on built-up material reduces and the coating surface increases in roughness either due to the effect of the underlying substrate roughness or to the dynamic effect of the heat waves produced by the tail-end of the flame, similar to coating type PC1 and PC2 in Figure 55.

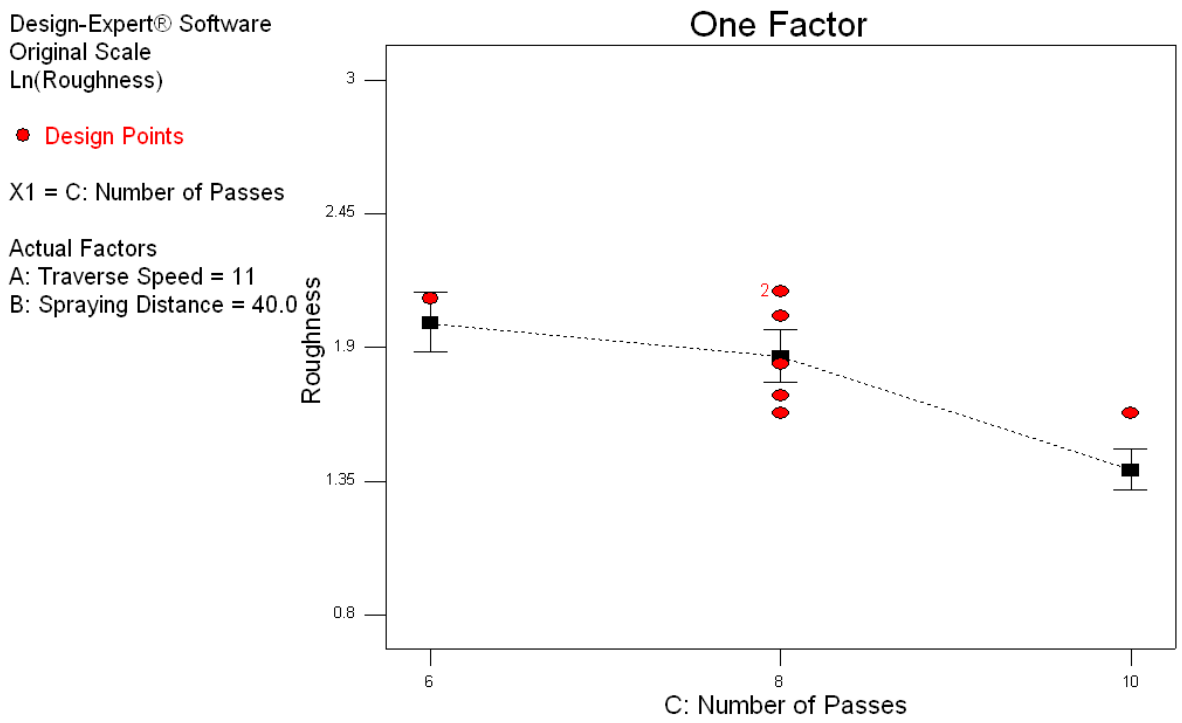

Figure 67: Average effect of number of passes(C) on the roughness (µm) of PCL/PMMA coatings

Figure 67, shows the effect of varying the number of passes on the coating roughness. Increasing the number of passes led to more material build up and therefore reduced the roughness caused by the underlying substrate topography, which was consistent with the observation drawn from Figure 66, where a higher build-up time causes a decrease in surface roughness. Table 47shows the process parameters corresponding to the highest and lowest coating thickness.

Table 47: Spraying parameters for samples with the highest and lowest roughness

Run	Traverse Speed(ips)	Spraying Distance(cm)	Number of Passes	Roughness(µm)
R14	16	50	8	2.97
R23	6	50	10	0.8

The highest coating roughness (2.97µm) was obtained when the build-up time is at a low level (highest traverse speed and mid-range number of passes) and the highest spraying distance. On the other hand, the lowest coating roughness (0.8µm) occurred when the build-up time was at its highest (highest number of passes and lowest traverse speed) and

the highest spraying distance. The same spraying distance in both cases confirms the limited effect of this factor on this coating roughness.

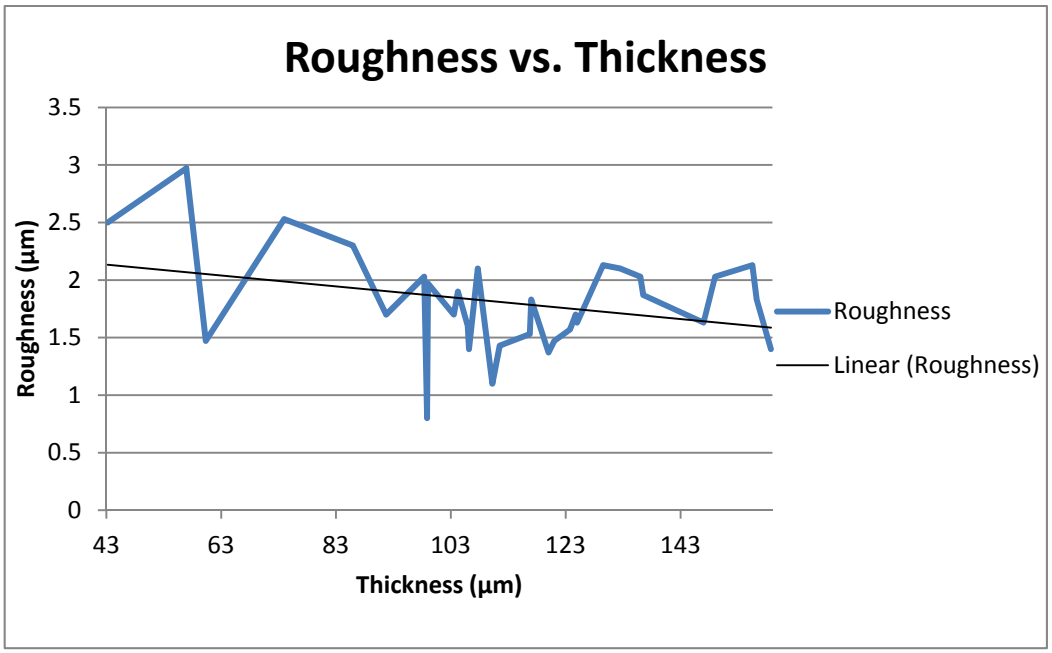

Figure 68: Roughness versus Thickness for PCL/PMMA coatings

The best-fit line in Figure 68 indicates that the coating thickness was inversely proportional to the coating roughness; which confirms the visual inspections of the sprayed samples, where the thinnest coating had an enhanced roughness due to the underlying substrate topography, whereas thicker coatings were not affected by the substrate roughness. The same phenomenon was observed with PHBV/PMMA coatings. The fact that the coatings with the highest thickness and lowest roughness were obtained using the same traverse speed and number of passes only confirms the latter observations.

4.5.5 PCL/PMMA Adhesion Model Validation

Table 48: Pull-off force measurements for the PCL/PMMA DoE

PCL/PMMA		
Std	**Run**	**Pull-off force (kg/cm^2)**
9	**R1**	30
12	**R2**	55
4	**R3**	59.6
24	**R4**	32
5	**R5**	32.1
17	**R6**	25
3	**R7**	35
26	**R8**	34
1	**R9**	40.5
14	**R10**	28.2
7	**R11**	58.7
28	**R12**	24.3
23	**R13**	41
18	**R14**	38.2
16	**R15**	57.9
6	**R16**	28.8
10	**R17**	33.8
31	**R18**	21.5
2	**R19**	30
20	**R20**	40.4
11	**R21**	19.8
30	**R22**	25.3
25	**R23**	80
13	**R24**	43.5
27	**R25**	27.8
19	**R26**	57
32	**R27**	26.5
29	**R28**	27.2
8	**R29**	23.8
15	**R30**	36.9
21	**R31**	46.5
22	**R32**	63

The backward selection method was used to automatically eliminate insignificant model terms in order to study the main effects on adhesion (adhesion measurements in Table 48). No transformation was required in order to obtain the adequate model. Factors/interactions with p-values of less than 0.1 (90% confidence interval) were included in the model. The ANOVA table and model statistics are shown in Table 49.

Table 49: ANOVA table for the PCL/PMMA adhesion model

Source	*Sum of Squares*	*Mean Square*	*F Value*	*p-value Prob>F*	*Significance*
Model	6069.98	758.75	36.25	<0.0001	Significant
Significance					
A-Traverse Speed	1490.58	1490.58	71.22	<0.0001	
B-Spraying Distance	16.82	16.82	0.80	0.3793	
C-Number of Passes	596.63	298.32	14.25	<0.0001	
AB	932.80	932.80	44.57	<0.0001	
AC	681.20	340.60	16.27	<0.0001	
A^2	1904.00	1904.00	90.98	<0.0001	
Residual	481.35	20.93			
Lack of Fit	*452.69*	*25.15*	*4.39*	*0.0545*	*Not significant*
Pure Error	*28.66*	*5.73*			
Cor Total	6551.32				
R^2	0.9265				
Adjusted R^2	0.9010				
Predicted R^2	0.8381				
Adeq Precision	21.981				

Based on the ANOVA table for the adhesion model, the model was significant at more than a 99.99% confidence level, with a p-value of <0.0001. The lack of fit is also not significant, indicating that the model adequately fits the data.

Based on Table 49 as well, it is possible to conclude that an adequate and relatively precise model has been developed. This is because the R^2 value was equal to 0.9265, the Adjusted R^2 and Predicted R^2 values in this model were 0.9010 and 0.8381 respectively, with a difference of 0.0629, and the Adequate Precision value was equal to 21.981.

The adequacy of the model being established, it is safe to say from the ANOVA table that the polymer coating adhesion is affected by all the process parameters (factors) tested: traverse speed (A), spraying distance (B), number of passes (C) as well as by the interactions of AB and AC. The ANOVA table also showed values of "Prob>F" less than 0.0500 for all model terms except factor B (spraying distance), which furthermore confirmed the significance of these factors and the interaction between them. Factor B had a "Prob>F" value of 0.9127, which indicated that the influence of this factor on the coating roughness is very limited in comparison to other factors/interactions. Analysis of the F-values indicated that the effects of the factors/interactions can be classified by order of amplitude starting with the largest effect as follows: A^2> A-traverse speed > AB > AC > C-number of passes > B-spraying distance.

The mathematical model for coating adhesion was given in terms of coded factors (Eqn. 13) or actual factors (Eqn. 14-16).

Final equation on terms of coded factors for PCL/PMMA coating adhesion:

$$\begin{aligned}\text{Adhesion}(kg/cm^2) = {} & + 29.78 \\ & - 9.10 \ * A \\ & + 0.97 \ *B \\ & - 2.84 \ * C[1] \\ & - 3.56 \ * C[2] \\ & - 8.82 \ * AB \\ & - 1.73 \ * AC[1] \\ & + 8.25 \ * AC[2] \\ & + 16.01 \ * A^2 \end{aligned} \quad \textbf{(Eqn. 13)}$$

Final equation in terms of actual factors for PCL/PMMA coating adhesion at 6 passes:

$$\begin{aligned}\text{Adhesion}(kg/cm^2) = {} & + 46.80457 \\ & - 9.20179 \quad * \text{Traverse Speed(ips)} \\ & + 2.03633 \quad * \text{Spraying Distance(cm)} \\ & - 0.17633 \quad * \text{Traverse Speed(ips)*Spraying Distance(cm)} \\ & + 0.64038 \quad * \text{Traverse Speed(ips)}^2 \end{aligned} \qquad \textbf{(Eqn. 14)}$$

Final equation in terms of actual factors for PCL/PMMA coating adhesion at 8 passes:

$$\begin{aligned}\text{Adhesion}(kg/cm^2) = {} & + 24.1251 \\ & - 7.20513 \quad * \text{Traverse Speed(ips)} \\ & + 2.03633 \quad * \text{Spraying Distance(cm)} \\ & - 0.17633 \quad * \text{Traverse Speed(ips)*Spraying Distance(cm)} \\ & + 0.64038 \quad * \text{Traverse Speed(ips)}^2 \end{aligned} \qquad \textbf{(Eqn. 15)}$$

Final equation in terms of actual factors for PCL/PMMA coating adhesion at 10 passes:

$$\begin{aligned}\text{Adhesion}(kg/cm^2) = {} & + 66.57235 \\ & - 10.15846 \quad * \text{Traverse Speed(ips)} \\ & + 2.03633 \quad * \text{Spraying Distance(cm)} \\ & - 0.17633 \quad * \text{Traverse Speed(ips)*Spraying Distance(cm)} \\ & + 0.64038 \quad * \text{Traverse Speed(ips)}^2 \end{aligned} \qquad \textbf{(Eqn. 16)}$$

Figure 69 of Predicted versus Actual showed a good fit between the model and the experimental data, where all the measured values lie close to the best-fit line, suggesting that this model accurately predicts the coating adhesion.

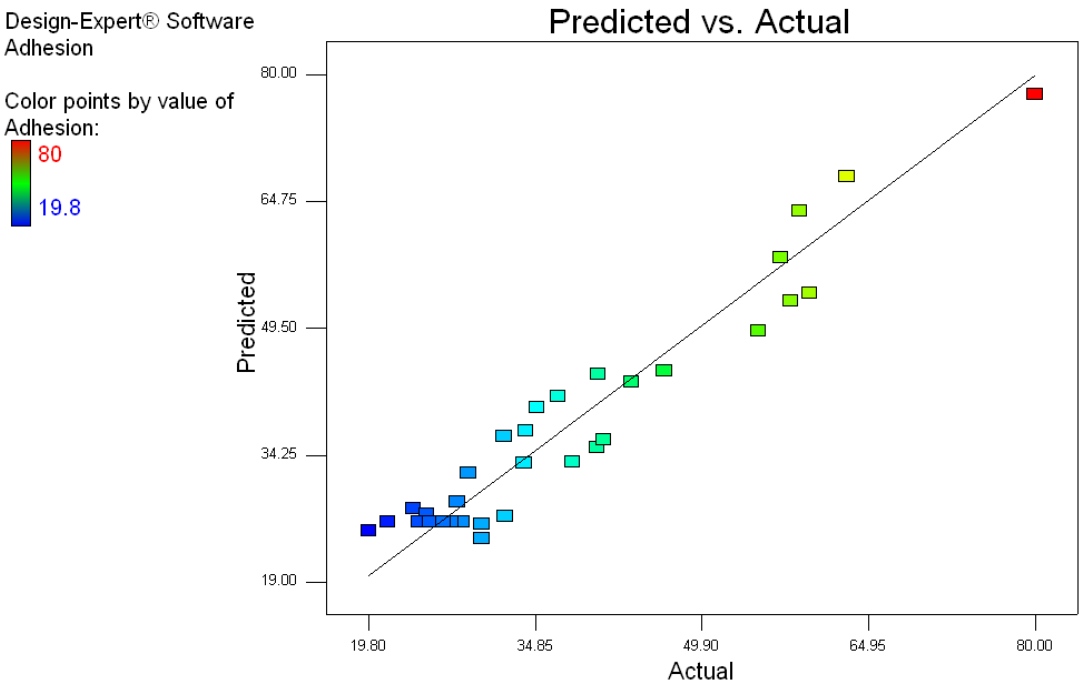

Figure 69: Predicted versus Actual values for PCL/PMMA coating adhesion (kg/cm^2)

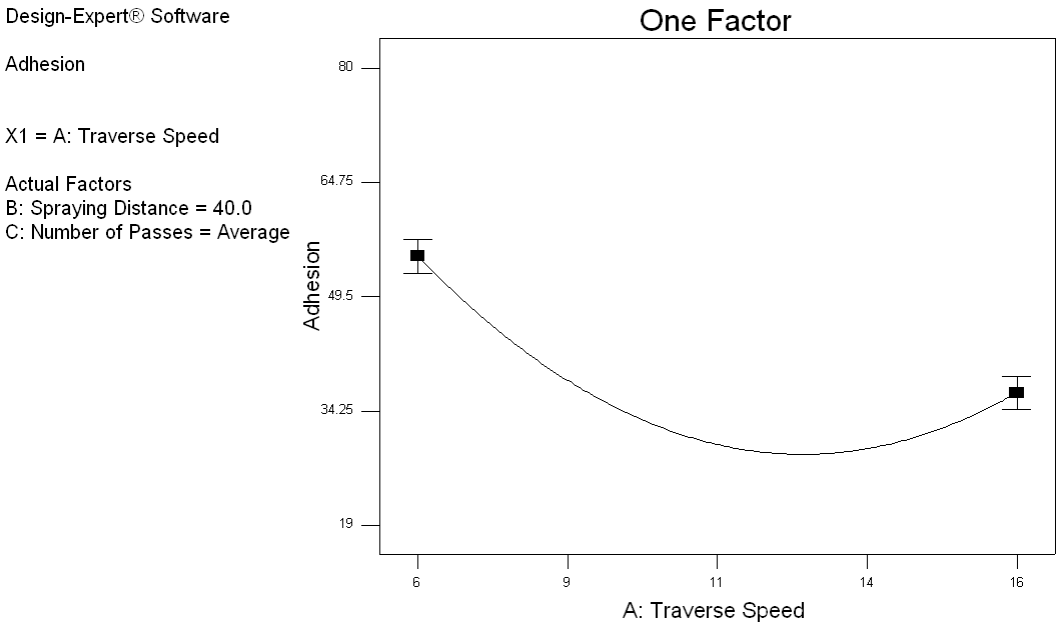

Figure 70: Average effect of traverse speed (ips) (A) and A^2(ips^2) on the adhesion (kg/cm^2) of PCL/PMMA coatings

Figure 70 shows the effect of varying the most influent factor in this model, the traverse speed, on the adhesion strength of PCL/PMMA coatings. The coating adhesion started at a higher range (50-55kg/cm^2) when the traverse speed was at its lowest value (0.154m/s, 6ips). From that point onwards the adhesion kept decreasing until a traverse speed of ~ 0.317 m/s, 12.5ips was reached. Higher traverse speed led to an inversed trend, where the coating adhesion increased again to an average of ~35kg/cm^2. Similar to the adhesion model of PHBV/PMMA coatings, the relationship between the process factor and the response was not straight forward. This was expected since the inter-locking mechanism between polymer coatings and metallic substrates dependent on many factors such as the degree of substrate pre-heat, the level of surface roughness, the degree of melting of polymer splats and the cooling rate of the substrate.

Figure 71 shows the effects of the interaction AB on the adhesion of PCL/PMMA coatings. This interaction involves factor A again, which confirms the importance of this factor in designing adequate thermal spraying processes.

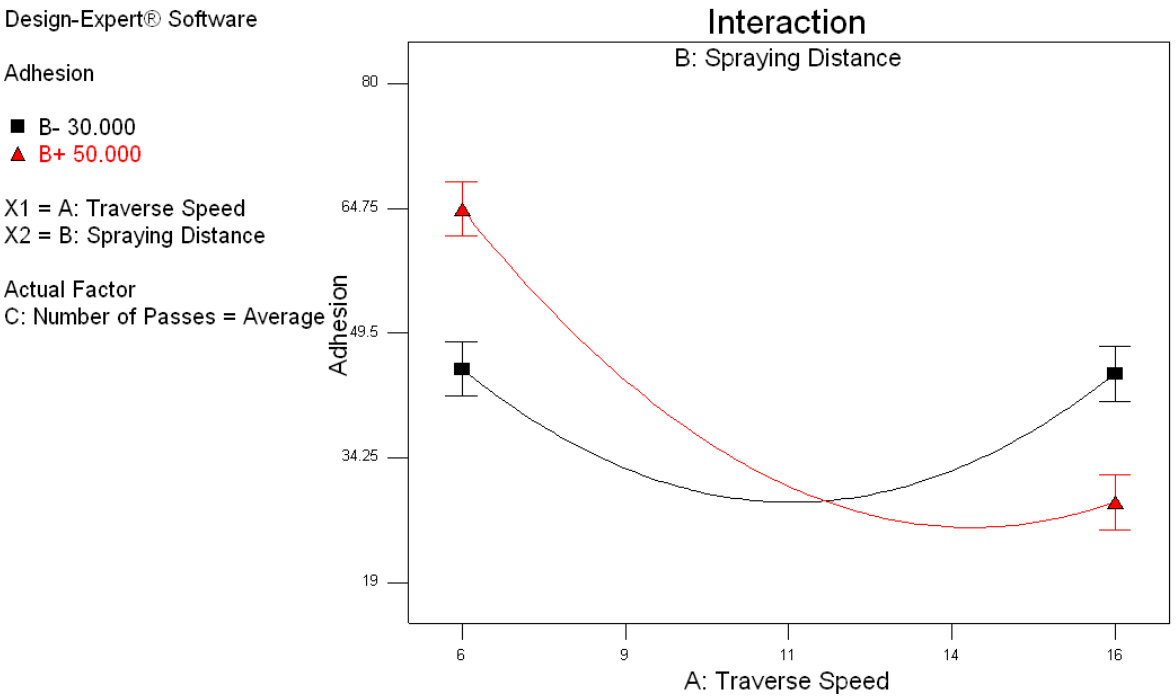

Figure 71: Average effect of interaction AB on the adhesion (kg/cm^2) of PCL/PMMA coatings

Figure 71 shows a very similar trend to the one observed in Figure 70, where the effect of varying the interaction AB was characterised by a concave parabolic curve. However, at higher spraying distance and traverse speed, the shape of the curve appears to straighten-out with a clearer direct proportionally existing between interaction AB and the coating adhesion. At the highest spraying distance, lower traverse speed lead to high coating adhesion. At the intersection point of ~12 ips, the spraying distance has no effect on the coating adhesion.

The highest coating adhesion (80 kg/cm^2) was obtained when the deposition time was at its highest level (lowest traverse speed and highest number of passes) and at the largest spraying distance. The lowest coating adhesion (19.08 kg/cm^2) occurred at a mid-range number of passes and traverse speed, and at the lowest spraying distance (Table 50).

Table 50: Spraying parameters for samples with the highest and lowest adhesion

Run	Traverse Speed(ips)	Spraying Distance(cm)	Number of Passes	Adhesion(kg/cm^2)
R23	6	50	10	80
R21	11	30	8	19.08

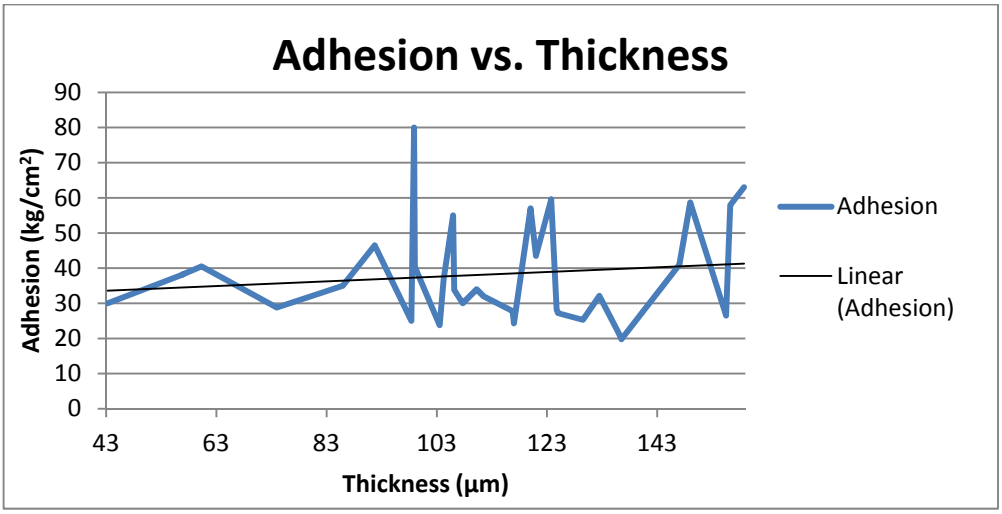

Figure 72: Adhesion versus Thickness for PCL/PMMA coatings

Figure 72 shows that a certain correlation between the thickness and the adhesion of PCL/PMMA coatings exists. The adhesion appeared to slightly increase with an increase in coating thickness. The trend observed in Figure 72 also confirmed the observations made from Figure 64 and Figure 70 and the influence of factor A on these two responses, where

an increase in traverse speed led to a decrease in thickness and in adhesion strength; confirming that to some extent, the latter responses are proportional to each other. Finally, the coatings with the highest adhesion and thickness were both obtained using the same process parameters (traverse speed = 6ips and 10 passes).

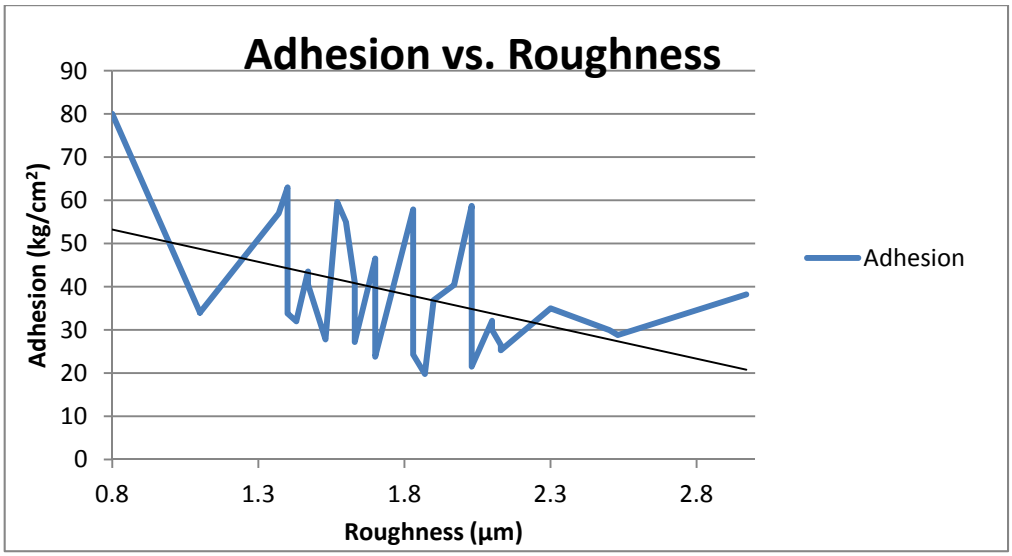

Figure 73: Adhesion versus Roughness for PCL/PMMA coatings

Figure 73 shows that the surface roughness and the adhesion strength of the PCL/PMMA coatings were inversely proportional to each other. Rougher coatings are generally characterised by less coating layers on the substrate, which is thought to reduce the adhesive strength of the coating material to the underlying titanium. This is substantiated by the fact that the coatings with the highest adhesion and the lowest roughness were obtained in the same run (R23). Additionally, another cause for the observed trend could be explained by the fact that coatings with higher roughness provided more topographic features which tend to reduce the contact area between the coating and the pull-off stud, whereas a lower roughness provides more "welding" points with the pull-off stud and therefore increases the coating adhesion value measured.

4.5.6 PCL/PMMA Wettability Model Validation

Table 51: Contact angle measurements for the PCL/PMMA DoE

Std	Run	CA1(°)	CA2(°)	CA3(°)	Average(°)	SD (°)
9	**R1**	59.34	57.89	59.95	59.06	1.06
12	**R2**	59.98	58.94	66.45	61.79	4.07
4	**R3**	59.99	60	57.76	59.25	1.29
24	**R4**	64.1	65.77	66.76	65.54	1.34
5	**R5**	58.53	53.85	57.94	56.77	2.55
17	**R6**	62.66	61.81	62.91	62.46	0.58
3	**R7**	57.76	57.57	56.12	57.15	0.90
26	**R8**	59.9	60.32	59.94	60.05	0.23
1	**R9**	58.27	57.92	62.57	59.59	2.59
14	**R10**	64.3	67.77	67.15	66.41	1.85
7	**R11**	59.96	58.45	58.7	59.04	0.81
28	**R12**	58.49	56.99	56.42	57.30	1.07
23	**R13**	59.19	60.99	64.63	61.60	2.77
18	**R14**	60.5	60.8	58.82	60.04	1.07
16	**R15**	58.22	55.29	56.9	56.80	1.47
6	**R16**	59.95	56.12	58.12	58.06	1.92
10	**R17**	59.87	56.71	58.07	58.22	1.59
31	**R18**	59.29	61.63	65.59	62.17	3.18
2	**R19**	59.25	57.48	59.06	58.60	0.97
20	**R20**	61.31	62.25	62.06	61.87	0.50
11	**R21**	60.15	57.65	58.64	58.81	1.26
30	**R22**	60.53	58.5	59.12	59.38	1.04
25	**R23**	57.96	58.72	58.31	58.33	0.38
13	**R24**	61.61	59.57	60.77	60.65	1.03
27	**R25**	59.84	57.99	58.12	58.65	1.03
19	**R26**	61.11	60.21	60.08	60.47	0.56
32	**R27**	64.24	65.89	62.15	64.09	1.87
29	**R28**	58.37	58.22	57.67	58.09	0.37
8	**R29**	62.42	60.88	62.12	61.81	0.82
15	**R30**	59.44	58.89	57.43	58.59	1.04
21	**R31**	59.66	59.76	58.31	59.24	0.81
22	**R32**	67.64	66.23	68.29	67.39	1.05
Average					60.23	1.35

The backward selection method was used to automatically eliminate insignificant model terms in order to study the main effects on contact angle/wettability (contact angle measurements in Table 51). None of the transformations available were used. It was found that the range of contact angle measurements was too narrow to yield any factors interactions and therefore a statistical analysis could not be performed on the present model. In fact, the best way to represent the relation between the set of responses is through the mean value. The ANOVA table and model statistics are shown in Table 52.

Table 52: ANOVA table for the PCL/PMMA wettability model

Source	*Sum of Squares*	*Mean Square*	*F Value*	*p-value Prob>F*	*Significance*
Model	50.34	12.59	1.94	0.1326	not significant
Significance					
B-Spraying Distance	0.014	0.014	2.140E-003	0.9634	
C-Number of Passes	31.71	15.86	2.44	0.1058	
B^2	18.50	18.50	2.85	0.1028	
Residual	175.21	6.49			
Lack of Fit	*110.59*	*5.03*	*0.39*	*0.9439*	*not significant*
Pure Error	*64.62*	*12.92*			
Cor Total	225.55				
R^2	0.2232				
Adjusted R^2	0.1081				
Predicted R^2	-0.0632				
Adeq Precision	4.222				

From the ANOVA table of the wettability model, it is clear that all factors/interactions had a negligible effect on the wettability of the polymer coatings. The average contact angle for PCL/PMMA coatings was 60.22^o. Angles less than 90^o are considered hydrophilic, and as previously mentioned, more hydrophilic surfaces increase the rate of cell adhesion and proliferation. Good wettability is also an indicator of the chemical integrity of the compound; PCL appears to withstand the heating effect of the flame spraying process very well.

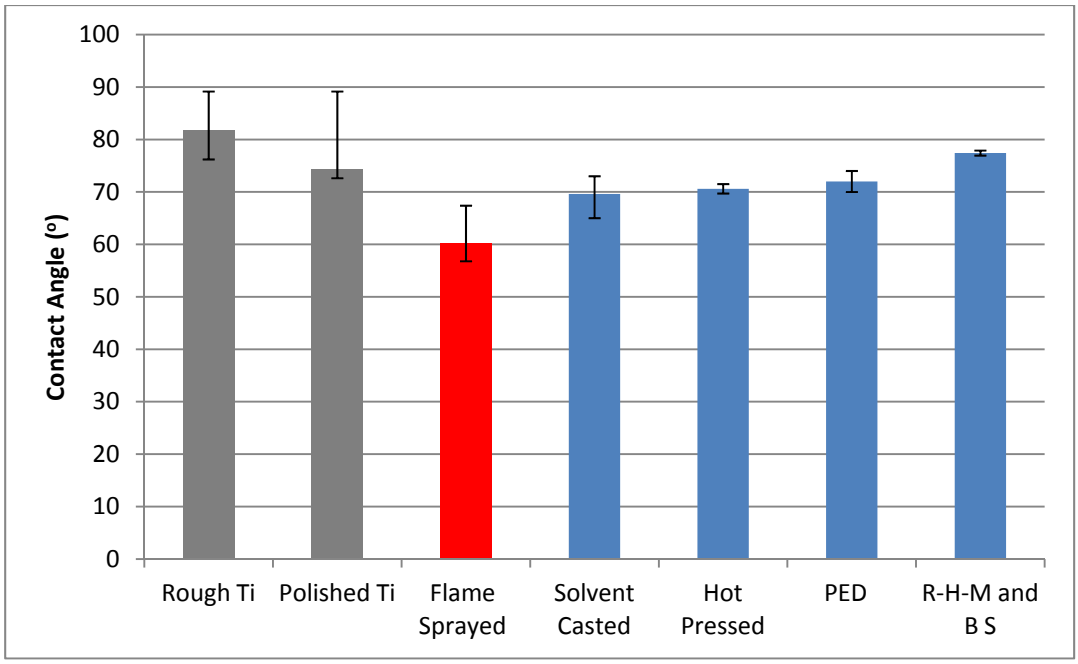

Figure 74: Contact angle comparison between different processes for PCL coating deposition

Figure 74 shows that the wettability of flame sprayed PCL coatings was better than that of PCL films/coatings obtained by using other processes. PCL produced using solvent evaporation resulted in an average contact angle of 69.6°[216],using a hot pressing technique (up to 90°C maximum temperature)the contact angle of the PCL films was 70.6°[230]. The average contact angle of Precision Extrusion Deposited (PED)PCL for bone scaffold applications was equal to 72°[231]. Finally, PCL films fabricated using a 2-roll-heated-mill and biaxial stretching produced an average contact angle of 77.42°[232]. Therefore, the flame spraying technique, with a much higher processing temperature, yielded a superior coating wettability compared to many well established cold and hot processing coating techniques. Figure 74 also shows that un-coated substrates (polished or sand-blasted) resulted in much hydrophobic surfaces, which confirms that the application of a biodegradable polymer matrix as a coating could make the implant surface more hydrophilic and therefore lead to a better osteoblast attachment and proliferation. Table 53 shows the parameters corresponding to the sample with the highest (R32) and lowest (R5) contact angles values.

Table 53: Spraying parameters for samples with the highest and lowest contact angle

Run	Traverse Speed(ips)	Spraying Distance(cm)	Number of Passes	Contact Angle (°)
R32	6	40	10	67.39
R5	11	40	6	56.77

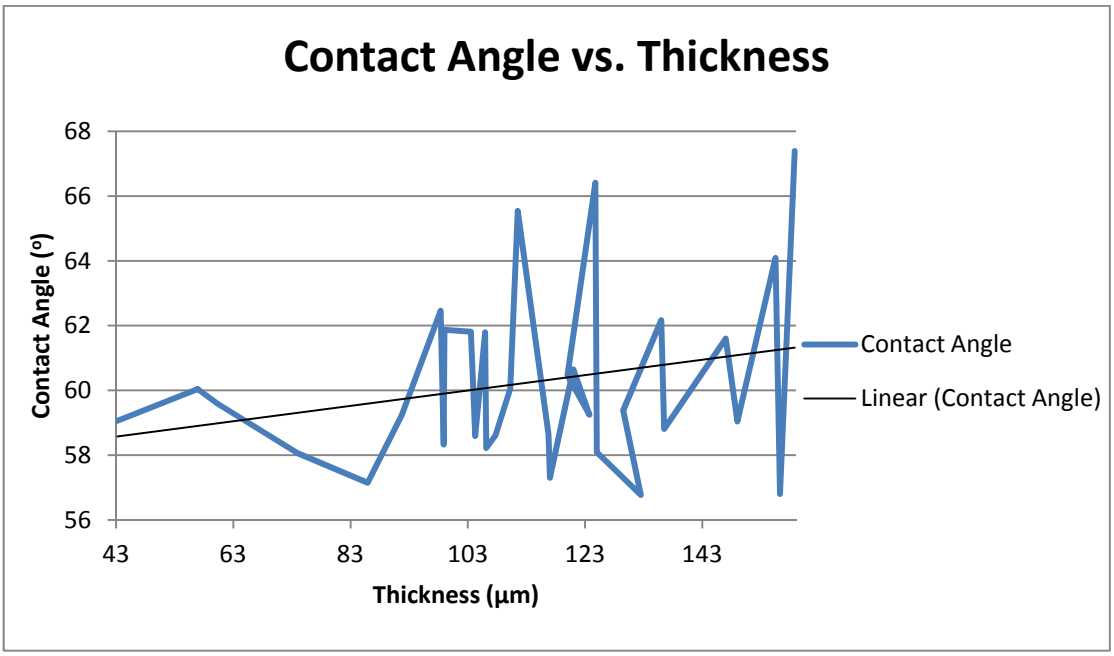

Figure 75: Contact Angle versus Thickness for PCL/PMMA coatings

Figure 75 shows that a relationship between the contact angle and the thickness of the PCL coating may exist. This observation confirms the trend observed with the PHBV coatings, where a potential cause was the effect of the long range van der Waals forces with the underlying substrate that became strongly thickness-dependent as the thickness of the polymer coating decreased[233]. This in turn is thought to affect the contact angle. This is substantiated by the fact that Run 32 yielded both, the highest thickness and the highest contact angle.

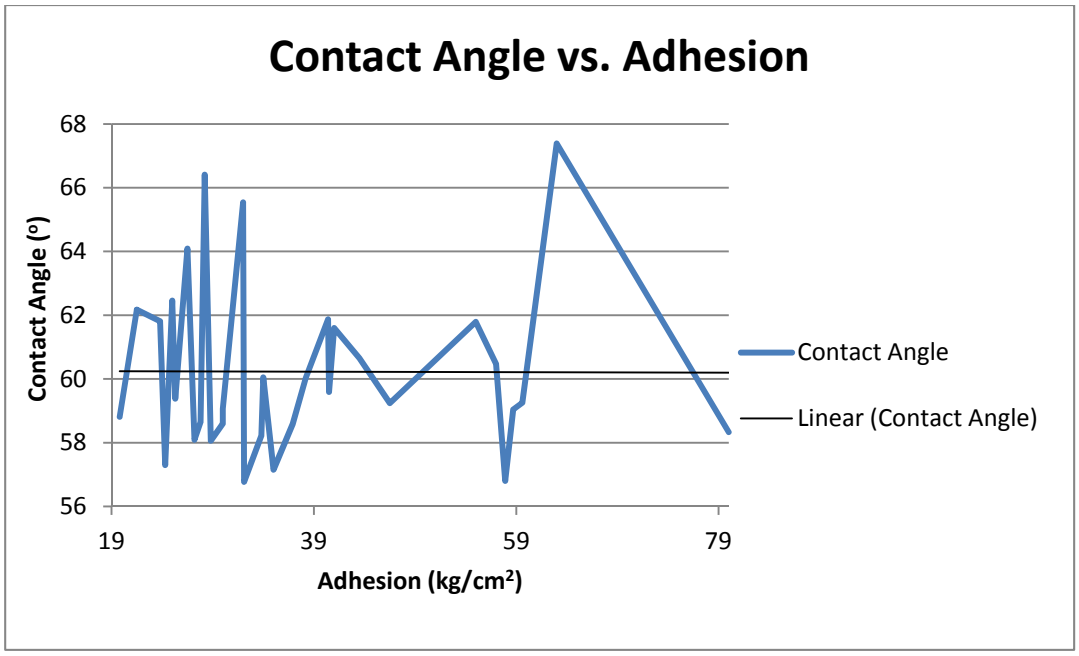

Figure 76: Contact Angle versus Adhesion for PCL/PMMA coatings

Figure 76 shows that the contact angle was not affected by the adhesion strength of the polymer coating to the titanium substrate.

4.5.7 DoE Layout for PHBV/PMMA

Based on the results of the screening stage and the parameters space investigation, it is now possible to use the DoE technique in order to optimise the PHBV/PMMA coatings with respect to the chosen coating characteristics. Table 54 summarises the experiments (Runs) to be carried out during this PHBV/PMMA DoE study. The coatings obtained from each run were then characterised with regards to thickness, roughness, adhesion and contact angle, respectively.

Table 54: PHBV/PMMA DoE layout

Std	Run	A:Traverse speed(ips(m/s))	B:Spraying Distance(cm)	C: Number of Passes
1	**R5**	9(0.228)	42.5	10
2	**R22**	11(0.279)	42.5	10
3	**R17**	13(0.330)	42.5	10
4	**R4**	9(0.228)	45	10
5	**R21**	11(0.279)	45	10
6	**R1**	13(0.330)	45	10
7	**R14**	9(0.228)	47.5	10
8	**R8**	11(0.279)	47.5	10
9	**R9**	13(0.330)	47.5	10
10	**R26**	9(0.228)	42.5	12
11	**R19**	11(0.279)	42.5	12
12	**R29**	13(0.330)	42.5	12
13	**R6**	9(0.228)	45	12
14	**R20**	11(0.279)	45	12
15	**R16**	13(0.330)	45	12
16	**R32**	9(0.228)	47.5	12
17	**R3**	11(0.279)	47.5	12
18	**R12**	13(0.330)	47.5	12
19	**R31**	9(0.228)	42.5	14
20	**R23**	11(0.279)	42.5	14
21	**R10**	13(0.330)	42.5	14
22	**R11**	9(0.228)	45	14
23	**R27**	11(0.279)	45	14
24	**R25**	13(0.330)	45	14
25	**R13**	9(0.228)	47.5	14
26	**R30**	11(0.279)	47.5	14
27	**R18**	13(0.330)	47.5	14
28	**R28**	11(0.279)	45	12
29	**R2**	11(0.279)	45	12
30	**R7**	11(0.279)	45	12
31	**R15**	11(0.279)	45	12
32	**R24**	11(0.279)	45	12

4.5.8 PHBV/PMMA Thickness Model Validation

Table 55: Thickness measurements for the PHBV/PMMA RSM study

Std	Run	T1(µm)	T2(µm)	T3(µm)	T4(µm)	Average(µm)	SD(µm)
6	**R1**	110	85	73	84	88	15.64
29	**R2**	80	65	73	82	75	7.70
17	**R3**	94	68	68.9	70.9	75.45	12.43
4	**R4**	72	64.7	66.2	68.4	67.82	3.17
1	**R5**	86	74	68	77	76.25	7.50
13	**R6**	68	59	65.3	62.3	63.65	3.88
30	**R7**	81	71	78	74.4	76.1	4.34
8	**R8**	59	73	74	58.5	66.12	8.53
9	**R9**	67	66.2	62.2	75.8	67.8	5.73
21	**R10**	54	53.7	47.5	49.2	51.1	3.25
22	**R11**	51.7	56.8	52	52	53.12	2.45
18	**R12**	109	81	69.9	74.4	83.57	17.55
25	**R13**	69	84	77.4	50	70.1	14.74
7	**R14**	74.4	67.5	61.6	80.7	71.05	8.29
31	**R15**	68	78	79.6	62.8	72.1	8.05
15	**R16**	94.1	93.8	75.2	74	84.27	11.18
3	**R17**	93	99.2	88	82.2	90.6	7.24
27	**R18**	69.4	75	72	70	71.6	2.52
11	**R19**	81.5	71.9	69	67.5	72.47	6.29
14	**R20**	65.8	86	85	60	74.2	13.27
5	**R21**	81.9	54	66	78	69.97	12.62
2	**R22**	90	88	85	84	86.75	2.75
20	**R23**	43.3	49	43.1	50.3	46.42	3.76
32	**R24**	62.9	79	82.6	61.5	71.5	10.85
24	**R25**	62.4	57	68	71	64.6	6.19
10	**R26**	51.8	58	55.7	54.5	55	2.58
23	**R27**	65	51	49	62.2	56.8	7.98
28	**R28**	75	69	73	67	71	3.65
12	**R29**	85	62	56	92	73.75	17.44
26	**R30**	63	61	63	74	65.25	5.91
19	**R31**	48	46	33	33	40	8.12
16	**R32**	83	82	65	71	75.25	8.73

The backward selection method was used to automatically eliminate insignificant model terms in order to study the main effects on thickness (thickness measurements in Table 55). No transformation was required in order to obtain the adequate model. Factors/interactions with p-values of less than 0.1 (90% confidence interval) were included in the model. For the present model, all factors were found to affect the coating thickness. The ANOVA table and model statistics are shown in Table 56.

Table 56: ANOVA table for the PHBV/PMMA thickness model

Source	*Sum of Squares*	*Mean Square*	*F Value*	*p-value Prob>F*	*Significance*
Model	3913.58	559.08	42.02	<0.0001	Significant
Significance					
A-Traverse Speed	589.96	589.96	44.34	<0.0001	
B-Spraying Distance	161.10	161.10	12.11	0.0019	
C-Number of Passes	1826.00	913.00	68.62	<0.0001	
AB	118.00	118.00	8.87	0.0065	
BC	1218.52	609.26	45.79	<0.0001	
Residual	319.32	13.31			
Lack of Fit	*297.82*	*15.67*	*3.64*	*0.0785*	*Not significant*
Pure Error	*21.51*	*4.30*			
Cor Total	4232.91				
R^2	0.9246				
Adjusted R^2	0.9026				
Predicted R^2	0.8544				
Adeq Precision	30.580				

Based on previous data analysis, the PHBV/PMMA thickness model was significant at more than a 99.99% confidence level with the lack of fit indicating that the model adequately fits the data.

The R^2 was equal to 0.9246. Similarly, the Adjusted R^2 and Predicted R^2 values were 0.9026 and 0.8544 respectively, with a difference of 0.0482. Finally, the Adequate Precision value was equal to 30.580. Therefore, it was possible to conclude that an adequate and relatively precise model had been developed.

With the adequacy of the model being established, it is safe to say from the ANOVA table, that the polymer coating thickness was affected by all of the process parameters (factors) tested: traverse speed (A), spraying distance (B), number of passes (C) as well as by the following interactions: AB, BC. The ANOVA table also showed values of "Prob>F" less than 0.0500 for all models terms, which confirms furthermore the significance of all factors and the interaction between them. It is possible to compare between the extents of the effect that each factor/interaction had on the coating thickness by looking at the F-value, classified by order of amplitude starting with the largest effect as follows: C-number of passes > BC > A-traverse speed >B-spraying distance > AB.
The mathematical model for coating thickness was given in terms of coded factors (Eqn. 17) and actual factors (Eqn. 18-20).

Final equation in terms of coded factors for PHBV/PMMA coating thickness:

Thickness(μm)= + 68.93
+ 5.72 * A
+ 2.99 * B
+ 7.11 * C[1]
+ 4.16 * C[2]
- 3.14 * A * B
-11.10 * BC[1]
+ 2.52 * BC[2] **(Eqn. 17)**

Final equation in terms of actual factors for PHBV/PMMA coating thickness at 10 passes:

Thickness(μm)= -120.005000
+ 31.08500 * Traverse Speed(ips)
+ 3.65683 * Spraying Distance(cm)
- 0.62717 * Traverse Speed(ips)* Spraying Distance(cm) **(Eqn. 18)**

Final equation in terms of actual factors for PHBV/PMMA coating thickness at 12 passes:

Thickness(μm)= -367.99143
+ 31.08500 * Traverse Speed(ips)
+ 9.10217 * Spraying Distance(cm)
- 0.62717 * Traverse Speed(ips)* Spraying Distance(cm) **(Eqn. 19)**

Final equation in terms of actual factors for PHBV/PMMA coating thickness at 14 passes:

Thickness(μm)= - 492.55944
+ 31.08500 * Traverse Speed(ips)
+ 11.52570 * Spraying Distance(cm)
- 0.62717 * Traverse Speed(ips)*Spraying Distance(cm) **(Eqn. 20)**

The coded factors model (Eqn.17) used the coded low and high levels (-1 and 1) from the experimental design and can be a quick method to calculate the response value (thickness in this case) at one of the experimental points. Whereas the actual factors model took into account the differences between the levels of the factors and the difference in effects, which is generally used to determine the response value when using any set of process parameters within the range of the experiment, and therefore to obtain the optimised parameters for a desired response.

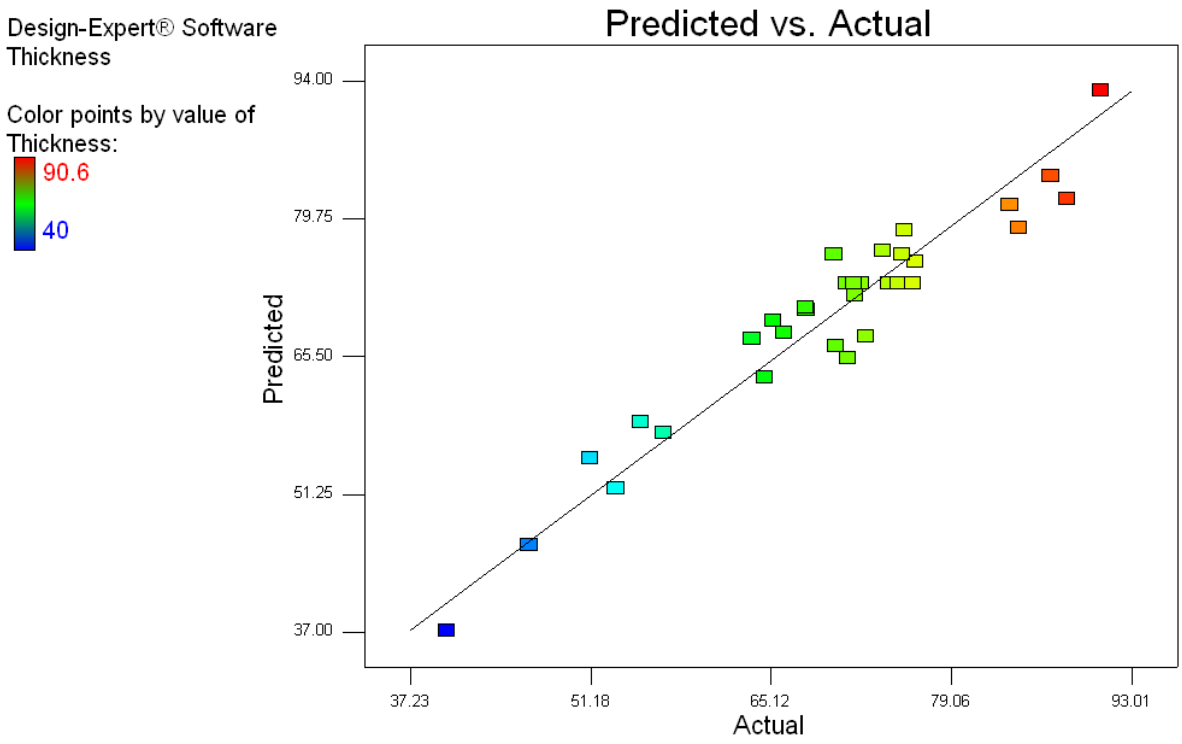

Figure 77: Predicted versus Actual values for PHBV/PMMA coating thickness (µm)

The Predicted versus Actual graph in Figure 77 shows the predicted values plotted against the values obtained experimentally. This graph is an indication of the accuracy of the model to predict actual values. Figure 77, shows a good fit between the model and the experimental data, where all the measured values are close to the best-fit line representing the case of the actual values being equal to the predicted values. The perturbation plot (Figure 78) was used to compare the effect of all the factors at a particular point in the design space on the coating thickness. The response was plotted by changing each factor over its range, while keeping the other factors constant. The steeper the slope the more sensitive is the response to that particular factor.

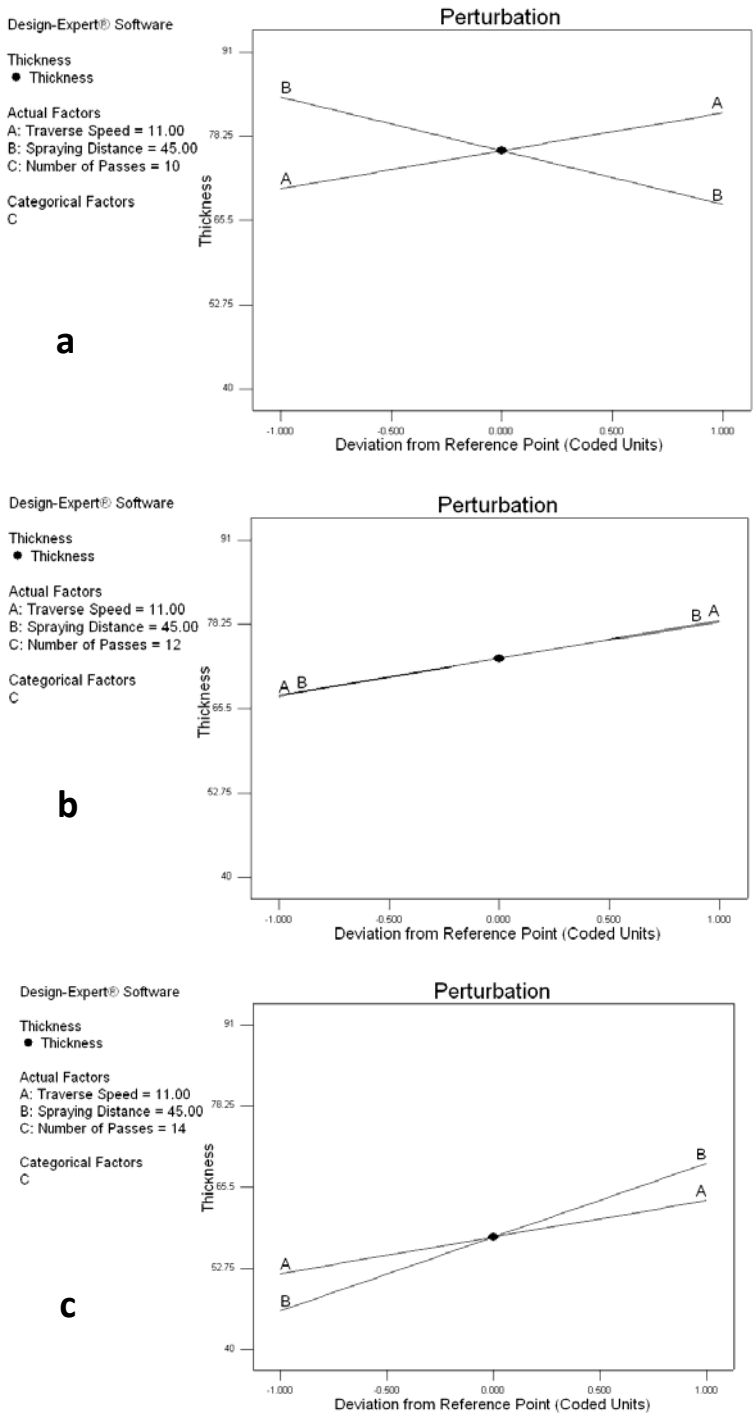

Figure 78: Perturbation plot of the PHBV/PMMA thickness (µm) model at a)10 passes, b)12 passes, c)14 passes

Figure 78shows that the variation of the number of passes (factor C), had a significant influence on how the remaining factors affect the thickness of the polymer coating.

However, it is interesting to note that the relationship between the number of passes and thickness was not the same (expected) relationship that is often observed with a ceramic or a metallic coating. In fact, in the case of flame sprayed PHBV/PMMA coatings, the perturbation plots showed that the range of coating thickness decreased as the number of passes was increased. This could be explained by the fact the low melting temperature of polymers causes the coating to be very sensitive to the exposure time to the flame as it traverses across the substrate. In fact, the exposure time is thought to have a greater heating effect on the deposited coating layers [43]. Figure 78a, showed that thickness was linearly related to factors A (traverse speed) and B (spraying distance). At 10 passes (C), factor A was directly proportional to the response while factor B was inversely proportional to the same response. Figure 78b shows a linear proportionality between the factors A and B and the thickness, whereby as the traverse speed and the spraying distance increased, the coating thickness increased at the same rate. In the latter case the slopes representing both factors were overlapping indicating a similar influence of these factors. Finally, Figure 78c shows the same relationship observed in Figure 78b, with different slopes for factors A and B. A higher traverse speed yielded shorter exposure time for the coating, thus, the relationship between the traverse speed and the thickness was consistent with the fact that the reduction in exposure time of the coating to the flame led to thicker coatings. The latter observation was also reported by Zhang et al. [43], where substantial thermal degradation of the polymer coating occurred at low traverse speeds. Zhang et al. [234], following the development of a computational model to predict the temperature profile over an organic coating on a metal surface as a result of the action of a moving flame, showed, that reducing the traverse speed can cause overheating of the coating under certain conditions, therefore leading to coating damage; which could be characterised by a reduction in thickness. This observation furthermore confirmed the effect of varying the traverse speed on the final coating thickness observed during this work. The relationship between the spraying distance and coating thickness observed in Figures78c and 78balso related to thermal degradation of the polymer, whereby the effect of the tail-end of the flame reduced, the further away the gun was placed from the substrate. In fact, the temperature at flame decreases from the core of the plume towards the outside (Figure 17), therefore shorter spraying distance exposes the polymer coatings to areas of the flame with higher

temperature. However, the latter observation does not apply to the relationship between factor B and thickness at 10 passes (Figure 78a), this can be explained by the fact that at a lower number of passes the degrading effect of the flame did not reach a destructive threshold intensity. Table 57 shows the spraying parameters corresponding to the samples with the highest (R17) and lowest (R31) thickness.

Table 57: Spraying parameters for samples with the highest and lowest thickness

Run	Traverse Speed(ips)	Spraying Distance(cm)	Number of Passes	Thickness(µm)
R17	13	42.5	10	90.6
R31	9	42.5	14	40

Table 57 confirms the observations made from the perturbation plot, where the thickest coatings were obtained with the maximum traverse speed (0.33m/s-13ips) and the minimum number of passes (10), whereas the thinnest coating was obtained with the minimum traverse speed (0.228m/s-9ips), the minimum spraying distance (42.5 cm) and the maximum number of passes (14).

This RSM model also showed that the interaction between the spraying distance and the number of passes (BC) as well as between the traverse speed and the spraying distance (AB) have an effect on the coating thickness. These interactions are shown in Figure 79, where the areas of highest thickness are shaded in red and the areas of lowest thickness are shaded in blue.

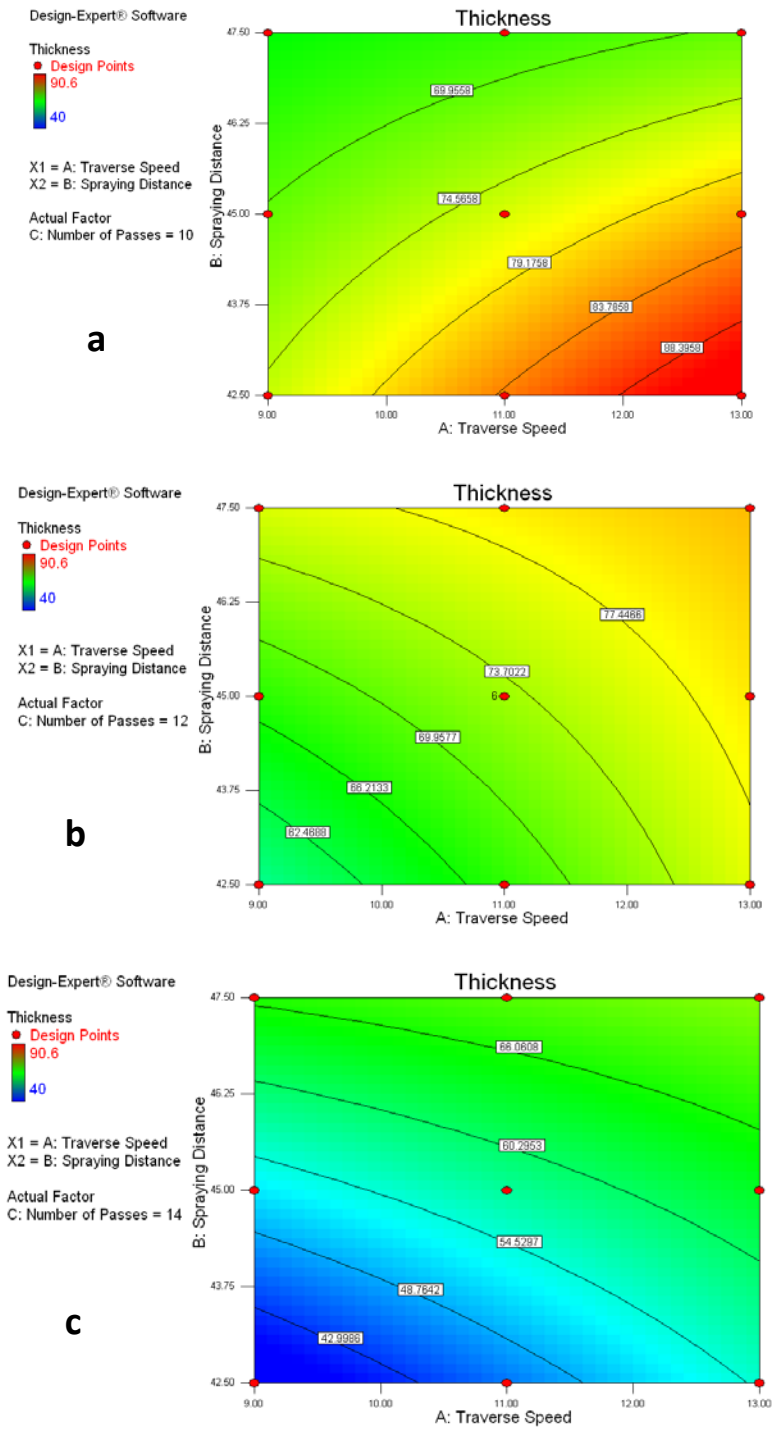

Figure 79: Interaction effects of traverse speed (ips) and spraying distance (cm) on thickness (µm)at a)10 passes, b)12 passes, c)14 passes

As mentioned previously, the traverse speed and spraying distance affect the exposure time and exposure temperature respectively, and both individually have an important impact on the resulting coating. Additionally, the fact that the type of relationship between those

factors and the coating thickness is the same (linear), the interaction (AB) between them unsurprisingly follows the same trend (inversed after 10 passes). Figure 79a shows that a higher coating thickness occurred at values of high traverse speed and low spraying distance. On the other hand, Figure 79band Figure 79cshowed that the coating thickness increased when the traverse speed and the spraying distance increased. A comparison between the above figures indicated that higher coating thicknesses were obtained at a lower number of passes. The latter observation along with the fact that higher coatings were obtained in all cases with a higher traverse speed, confirmed that higher exposure time led to a reduction of coating thickness. The final observation that could be made from the Figure 79 was, that the interaction between the spraying distance and the number of passes was linear in all cases but inversed in the situation where a decrease in spraying distance led to a decrease in coating thickness (at 10 passes), to a situation where an increase in spraying distance led to an increase in coating thickness (at 14 passes). This was confirmed by Figure 80showing the effect of the interaction of factors B and Chad on coating thickness.

The interaction (BC) between the spraying distance and the number of passes (Figure 80) was the most complex interaction of factors in this study. Nevertheless it has the most important impact on the final coating compared to any of the other factors/interactions. Figure 80 shows that the range of coating thickness increases in amplitude as the number of passes was reduced. It also confirmed that a relationship of linear proportionality existed between spraying distance(B) and thickness when the number of passes was set to 12 and 14 passes. Whereas spraying distance and thickness were inversely proportional to each other when the number of passes was set to 10 passes. The slope of the line representing the change in spraying distance was steeper at 14 passes than at 12 passes, indicating that the spraying distance has a greater influence on the final coating thickness at 14 passes. Finally, Figure 80 shows that the lowest coating thickness occurred at the lowest chosen spraying distance and highest number of passes, and that the thickest coating occurred at the lowest spraying distance and using the least number of passes. This confirms the individual factor results given in Table 57.

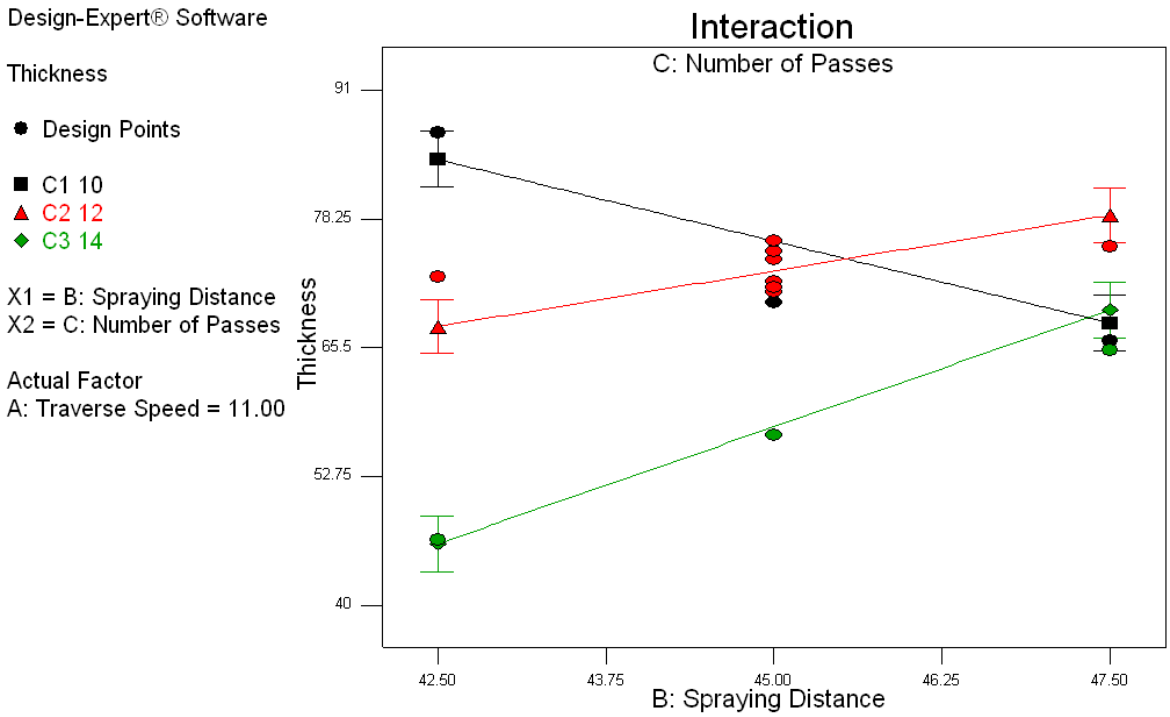

Figure 80: Interaction Effects of spraying distance (cm) and number of passes on thickness (µm) for PHBV/PMMA coatings

4.5.9 PHBV/PMMA Roughness Model Validation

Table 58: Roughness measurements for the PHBV/PMMA DoE

Std	Run	R1(µm)	R2(µm)	R3(µm)	Average(µm)	SD(µm)
6	**R1**	2.4	2.9	2.7	2.66	0.25
29	**R2**	2	1.3	2	1.76	0.4
17	**R3**	1.6	1.6	2.1	1.67	0.29
4	**R4**	3	3	2.4	2.8	0.35
1	**R5**	2.5	2.1	3.9	2.83	0.95
13	**R6**	5.2	2.9	3.1	3.73	1.27
30	**R7**	1.2	1.9	1.8	1.63	0.38
8	**R8**	1.5	1.9	2.1	1.83	0.31
9	**R9**	1.5	1.9	1.9	2.33	0.23
21	**R10**	2.9	3	2.3	2.73	0.38
22	**R11**	3.4	3.4	3.5	3.43	0.06
18	**R12**	1.8	1.9	2.6	2.1	0.44
25	**R13**	2.8	2.5	2.9	2.73	0.21
7	**R14**	3.5	2.8	3.1	3.13	0.35
31	**R15**	1.9	1.8	1.5	1.73	0.21
15	**R16**	2.3	2.4	1.9	2.2	0.26
3	**R17**	2	2.4	1.7	2.03	0.35
27	**R18**	1.9	2.1	2.4	2.13	0.25
11	**R19**	1.8	1.8	2	1.86	0.12
14	**R20**	1.9	1.7	1.4	1.66	0.25
5	**R21**	1.5	1.6	2.3	1.8	0.44
2	**R22**	1.6	2	1.4	1.66	0.31
20	**R23**	2.6	1.5	1.6	1.9	0.61
32	**R24**	2	1.5	1.6	1.7	0.26
24	**R25**	2	2.2	2.6	2.26	0.31
10	**R26**	3.9	5.3	4	4.4	0.78
23	**R27**	2	2	1.8	1.93	0.12
28	**R28**	1.2	1.6	2.3	1.7	0.56
12	**R29**	2	2.8	2	2.26	0.46
26	**R30**	1.2	1.9	1.5	1.53	0.35
19	**R31**	3.6	4.5	4.1	4.06	0.45
16	**R32**	2.6	2.6	3.3	2.83	0.4

The backward selection method was used to automatically eliminate insignificant model terms in order to study the main effects on roughness (roughness measurements in Table 58). The power transformation (lambda = -1.63) was required in order to obtain the adequate model. Factors/interactions with p-values of less than 0.1 (90% confidence interval) were included in the model. The ANOVA table and model statistics are shown in Table 59.

Table 59: ANOVA table for the PHBV/PMMA roughness model

Source	*Sum of Squares*	*Mean Square*	*F Value*	*p-value Prob>F*	*Significance*
Model	0.41	0.059	70.83	<0.0001	Significant
Significance					
A-Traverse Speed	0.057	0.057	68.79	<0.0001	
B-Spraying Distance	8.041E-003	8.041E-003	9.67	0.0048	
C-Number of Passes	1.204E-003	6.022-004	0.72	0.4949	
BC	0.022	0.011	12.98	0.0002	
A^2	0.30	0.30	361.08	<0.0001	
Residual	0.020	8.313E-004			
Lack of Fit	*0.018*	*9.541E-004*	*2.62*	*0.1453*	*Not significant*
Pure Error	*1.824E-003*	*3.647E-004*			
Cor Total	0.43				
R^2	0.9538				
Adjusted R^2	0.9404				
Predicted R^2	0.9207				
Adeq Precision	25.678				

The ANOVA table for the roughness model shows a p-value of <0.0001. This indicated that the model was significant at more than a 99.99% confidence level. An insignificant lack of fit indicated that the model adequately fits the data.

The R^2 value was equal to 0.9538, the Adjusted R^2 and Predicted R^2 values were 0.9404 and 0.9207 respectively, with a difference of 0.0197. Adequate Precision was equal to 25.678.Therefore, an adequate and relatively precise model has been developed.

With the adequacy of the model being established, the ANOVA table showed that the polymer coating roughness was affected by all the process parameters (factors) tested: traverse speed (A and A^2), spraying distance (B), number of passes (C) as well as the interaction BC between them. The ANOVA table also shows values of "Prob>F" less than 0.0500 for all models terms with the exception of factor C (number of passes), which furthermore confirms the significance of these factors and the interaction between them. Factor C had a "Prob>F" value of 0.4949, which indicated that the influence of this factor on the coating roughness was very limited in comparison to other factors/interactions. An analysis of the F-values indicated that the effects of the factors/interactions could be classified by order of amplitude starting with the largest effect as follows: A^2 > A-traverse speed > BC> B-spraying distance >C-number of passes.

The mathematical model for coating roughness was given in terms of coded factors (Eqn. 21) or actual factors (Eqn. 22-24):

Final equation in terms of coded factors for PHBV/PMMA coating roughness:

$$(\text{Roughness})^{-1.63}(\mu m^{-1.63}) = +0.41 + 0.056 * A + 0.021 * B + 3.813E\text{-}003 * C[1] + 5.242E\text{-}003 * C[2] - 0.047 * BC[1] + 0.012 * BC[2] - 0.20 * A^2 \quad \textbf{(Eqn. 21)}$$

Final equation in terms of actual factors for PHBV/PMMA coating roughness at 10 passes:

$$(\text{Roughness})^{-1.63}(\mu m^{-1.63}) = -5.51319 + 1.13375 * \text{Traverse Speed(ips)} - 0.010371 * \text{Spraying Distance(cm)} - 0.050253 * (\text{Traverse Speed(ips)})^2 \quad \textbf{(Eqn. 22)}$$

Final equation in terms of actual factors for PHBV/PMMA coating roughness at 12 passes:

$$(\text{Roughness})^{-1.63}(\mu m^{-1.63}) = -6.57124 + 1.13375 * \text{Traverse Speed(ips)} + 0.013173 * \text{Spraying Distance(cm)} - 0.050253 * \text{Traverse Speed(ips)}^2 \quad \textbf{(Eqn. 23)}$$

Final equation in terms of actual factors for PHBV/PMMA coating roughness at 14 passes:

$$(\text{Roughness})^{-1.63}(\mu m^{-1.63}) = -7.00795 + 1.13375 * \text{Traverse Speed(ips)} - 0.022560 * \text{Spraying Distance(cm)} - 0.050253 * \text{Traverse Speed(ips)}^2 \quad \textbf{(Eqn. 24)}$$

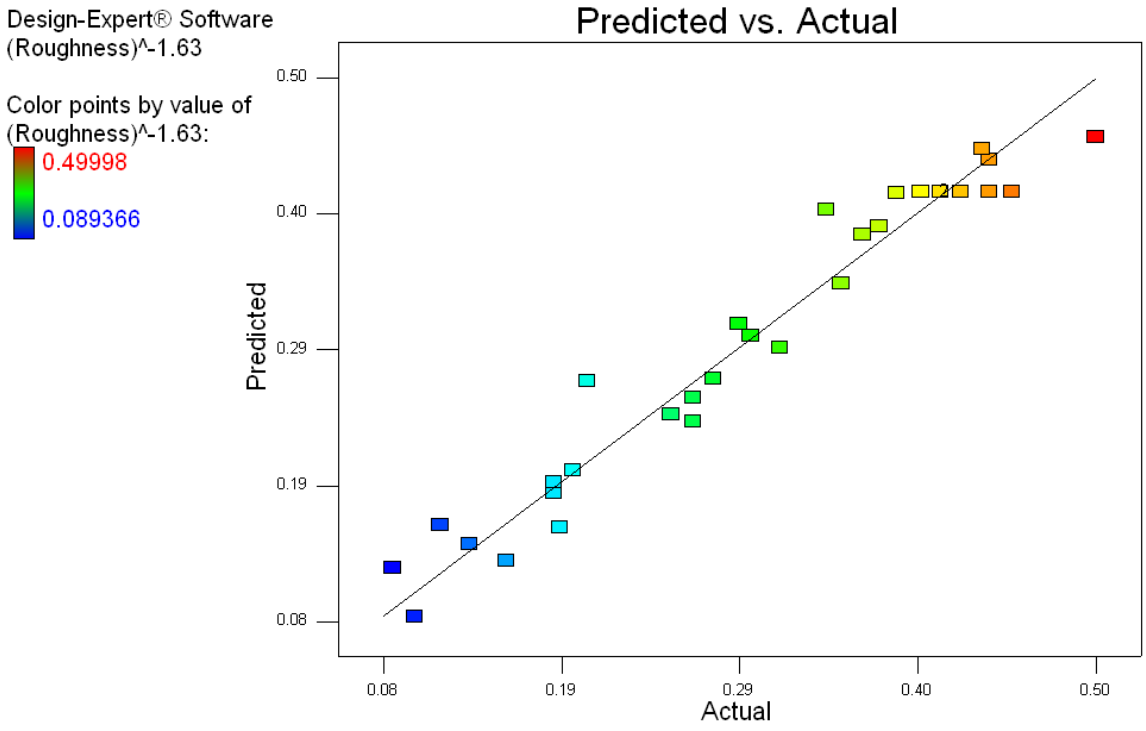

Figure 81: Predicted versus Actual values for PHBV/PMMA coating roughness ($\mu m^{-1.63}$)

The Predicted versus Actual graph in Figure 81 shows a good fit between the model and the experimental data, where all the measured values were close to the best-fit line representing the case of actual values aligned with predicted values, thus the model accurately predicts coating roughness. The perturbation plot (Figure 82) was used to compare the effect of all the factors at a particular point in the design space on the coating roughness.

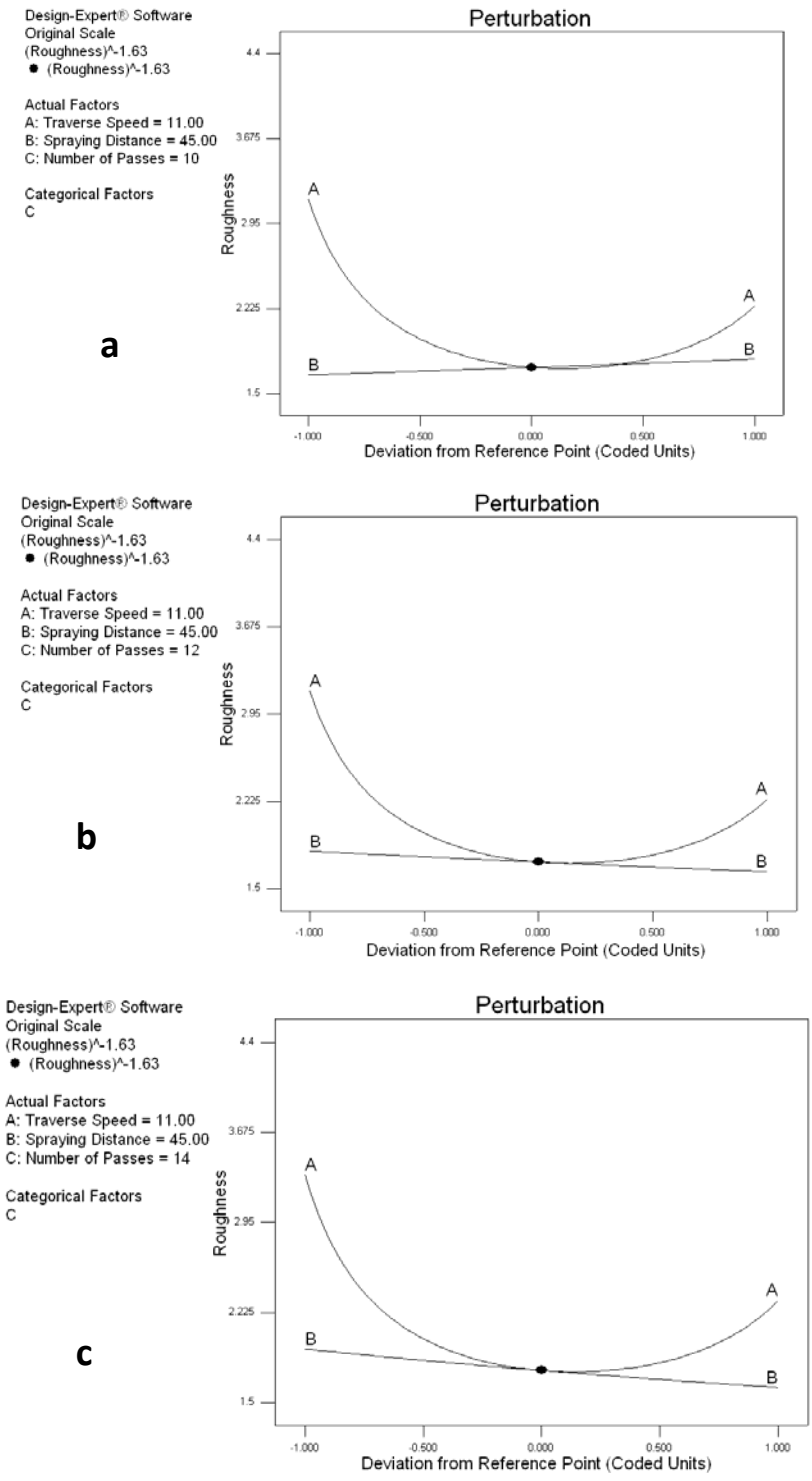

Figure 82: Perturbation plot for the PHBV/PMMA roughness (μm) model at a)10 passes, b)12 passes, c)14 passes

Figure 82 showed that the curve representing the relationship between the traverse speed (factor A) and the coating roughness had a concave parabolic shape, in contrast to the linear curve observed with the roughness model of PCL/PMMA. In fact, the increase in traverse speed starting from the lower limit of the range led to a decrease in roughness. At the mid-range value (around 11-11.5 ips, 0.279-0.292 m/s) the trend was reversed and the increase in traverse speed towards the upper limit led to an increase in coating roughness. In order to analyse the latter trend, the increase and decrease in roughness will be explained separately. Looking at the first half of the parabola where the increase in traverse speed led to a reduction in coating roughness, this higher roughness at low traverse speed could be caused by the fact that a higher exposure time led to more coating physical degradation, which through the burning-off of more polymer layers, further exposes the underlying rough titanium surface, thus, leading to a rougher polymer coating. In the second half of the parabola, the increase in traverse speed led to a higher coating roughness. This could be explained by the fact that the reduction in exposure time reduced the heating effect of the tail-end of the flame on the coating, which in turns did not contribute anymore to flattening partially melted particles. This type of particles is characterised by a harder core and an egg-shaped form, which contribute to the increase in surface roughness. Visual observations (similar to PC2 and PC5 in Figure 56) confirm this theory, whereby coatings with a high roughness from both ends of the traverse speed range did not look similar in structure. In fact, high surface roughness (R31=4.06 μm and R26=4.4 μm) corresponded to thin coating (R31=40 μm and R26=55 μm) similar to PC2 type coatings in Figure 56, which implied that the roughness of the underlying substrates had an effect on the roughness of the coating surface. On the other end of the traverse speed range (0.33 m/s, 13ips), the roughest coating (R10=2.73 μm) did not allow the titanium roughness to become visible, however, its surface topography was similar to that of PC5 type coatings in Figure 56. Figure 82 also showed that even though the spraying distance (factor B) had a lower influence on the roughness of the polymer coating compared to factor A, a linear relationship with the coating roughness did exist. After 10 passes (Figure 82a), an increase in the spraying distance led to a small increase in roughness. This trend was reversed after 12 and 14 passes, where an increase in spraying distance led to a limited decrease in coating roughness.

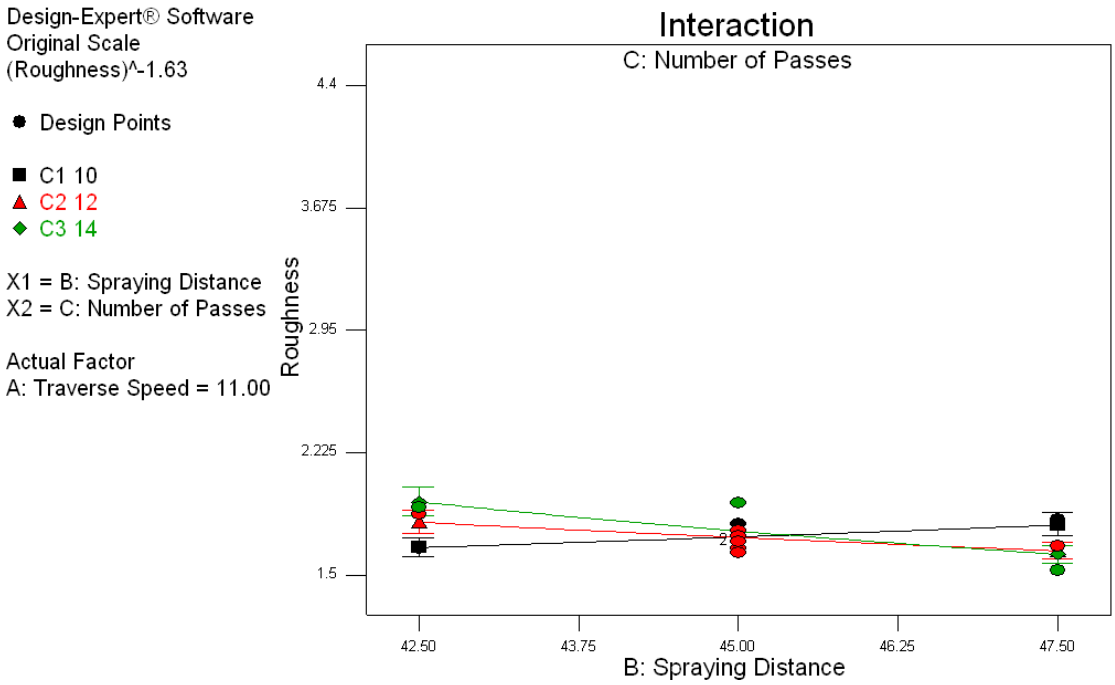

Figure 83: Interaction effect of spraying distance (cm) and number of passes on roughness (µm) for PHBV/PMMA coatings

The interaction between the spraying distance and the number of passes (Figure 83) confirmed the observations made from the perturbation plots where the increase in number of passes inversed the linear relationship between the spraying distance (B) and the coating roughness. At a spraying distance of 47.5 cm (B) and 10 passes (C), the roughness was higher than that at 12 and 14 passes, which could be explained by the fact that an increase in exposure time led to more particle melting (flattening of the surface particles) and therefore to a reduction in roughness. The increase in roughness at a higher spraying distance (10 passes) could also be explained by the fact that the large spraying distances resulted in larger in-flight travelling distances for the particles, which would lead to the partial re-solidification of some of the polymer particles (especially those furthest away from the centre of the plume).The trend was reversed at 42.5 cm, where a higher exposure time (12 and 14 passes)possibly led to evaporation of upper coating layers and therefore to exposing the underlying topography of the sand-blasted titanium substrate, therefore leading to an increase in coating roughness. It is important to note that the latter variation

occurred within a very narrow roughness range 1.6-2 µm, which underscores the sensitivity of the process used to obtain polymer coatings.

Table 60 shows the parameters corresponding to the sample with the highest (R31) and lowest (R30) roughness values.

Table 60: Spraying parameters for samples with the highest and lowest roughness

Run	Traverse Speed(ips)	Spraying Distance(cm)	Number of Passes	Roughness(µm)
R26	9	42.5	12	4.4
R30	11	47.5	14	1.53

Visual observations of all samples indicated that with thinner coatings it was possible to distinguish the rough sand-blasted surface of the titanium substrate, and that the roughness of titanium affected, to some extent, the roughness of the polymer coating. Therefore, in order to investigate the relationship between roughness and thickness, both responses were plotted against each other as shown in Figure 84.

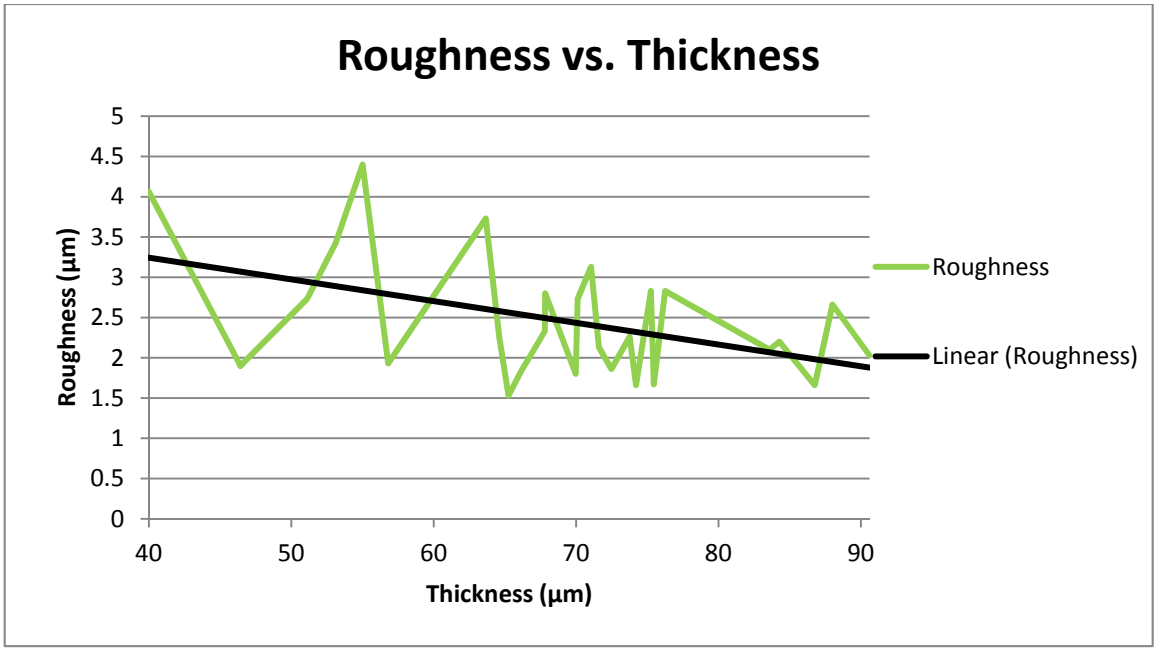

Figure 84: Roughness versus Thickness for PHBV/PMMA coatings

The best-fit line in Figure 84 indicates that a relationship between coating roughness and thickness does exist, where surface roughness decreases with increasing coating thickness; which confirms the visual inspections of the sprayed samples. It is thought that the thickness of the coating is expected to have an influence on the temperature profile of the coating surface, mainly due to the low thermal conductivity of polymers [234]. As a result, thicker coatings will display a substantially higher temperature gradient between the coating surface and the substrate, which leads to the melting/flattening of partially melted particles on thicker coatings and therefore reducing surface asperities. The understanding of which factors influence coating thickness is required when the rate of drug release needs to be controlled at a later stage. As the rate of drug release will be influenced by the polymeric deposit thickness, predicting deposit thickness and its associated roughness for cell attachment is of major importance in the upcoming research presented in this thesis.

4.5.10 PHBV/PMMA Adhesion Model Validation

Table 61: Pull-off force measurements for the PHBV/PMMA DoE

PHBV/PMMA		
Std	**Run**	**Pull-off force (kg/cm^2)**
6	**R1**	12.2
29	**R2**	9.1
17	**R3**	11.5
4	**R4**	35
1	**R5**	21.2
13	**R6**	10.7
30	**R7**	10.2
8	**R8**	38.5
9	**R9**	39.3
21	**R10**	62.8
22	**R11**	12.3
18	**R12**	18.2
25	**R13**	26.1
7	**R14**	20.7
31	**R15**	9.6
15	**R16**	15.3
3	**R17**	54.2
27	**R18**	12
11	**R19**	7.6
14	**R20**	49.3
5	**R21**	31.1
2	**R22**	80.6
20	**R23**	8.9
32	**R24**	14
24	**R25**	13.1
10	**R26**	26.7
23	**R27**	8.5
28	**R28**	21.4
12	**R29**	29.2
26	**R30**	29.2
19	**R31**	18.3
16	**R32**	18.8

The backward selection method was used to automatically eliminate insignificant model terms in order to study the main effects on adhesion (adhesion measurements in Table 61). The inverse transformation (lambda = -1) was required in order to obtain the adequate model. Factors/interactions with p-values of less than 0.1 (90% confidence interval) were included in the model. The ANOVA table and model statistics are shown in Table 62.

Table 62: ANOVA table for the PHBV/PMMA adhesion model

Source	*Sum of Squares*	*Mean Square*	*F Value*	*p-value Prob>F*	*Significance*
Model	0.032	2.699E-003	12.78	<0.0001	Significant
Significance					
A-Traverse Speed	8.350E-004	8.350E-004	3.95	0.0613	
B-Spraying Distance	9.612E-008	9.612E-008	4.552E-004	0.9832	
C-Number of Passes	0.013	6.323E-003	29.95	<0.0001	
AB	2.620E-004	2.620E-004	1.24	0.2792	
AC	4.684E-004	2.342E-004	1.11	0.3503	
A^2	1.150E-004	1.150E-004	0.54	0.4694	
B^2	3.732E-003	3.732E-003	17.67	0.0005	
A^2C	4.045E-003	2.022E-004	9.58	0.0013	
AB^2	7.922E-004	7.922E-004	3.75	0.0678	
Residual	4.012E-003	2.111E-004			
Lack of Fit	*3.336E-003*	*2.383E-004*	*1.76*	*0.2759*	*Not significant*
Pure Error	*7.922E-004*	*1.351E-004*			
Cor Total	0.036				
R^2	0.8898				
Adjusted R^2	0.8202				
Predicted R^2	0.6309				
Adeq Precision	10.058				

Based on previous data analysis, the PHBV/PMMA adhesion model was significant at more than a 99.99% confidence level with the lack of fit indicating that the model adequately fit the data.

The R^2 value was equal to 0.8898, hence indicating a good model adequacy. The Adjusted R^2 and Predicted R^2 values were 0.8202 and 0.6309 respectively, with a difference of 0.1893. Finally, the Adequate Precision was equal to 10.058.Therefore, having the R^2, Adequate Precision, Adjusted R^2 and Predicted R^2 values all exceeding the required thresholds; it is possible to conclude that an adequate and relatively precise model has been developed.

The ANOVA table showed that the polymer coating adhesion was affected by all the process parameters (factors) tested: traverse speed (A and A^2), spraying distance (B, B^2), number of passes (C) as well as the interaction; AB, AC, A^2C, AB^2 between them. An analysis of the F-values indicated that the effects of the factors/interactions can be classified by order of amplitude starting with the largest effect as follows: C-number of passes>B^2> A^2C > A-traverse speed>AB^2>AB>AC>A^2> B-spraying distance. The mathematical model for coating adhesion was given in terms of coded factor (Eqn. 25) or actual factors (Eqn. 26-28):

Final equation in terms of coded factors for PHBV/PMMA coating adhesion:

$$
\begin{aligned}
1/(\text{Adhesion})(1/(\text{kg/cm}^2)) = {} & +0.066 \\
& +2.571\text{E-}003 \quad * A \\
& -7.307\text{E-}005 \quad * B \\
& -0.024 \quad * C[1] \\
& +0.046 \quad * C[2] \\
& +4.673\text{E-}003 \quad * AB \\
& +7.11\text{E-}003 \quad * AC[1] \\
& -2.514\text{E-}003 \quad * AC[2] \\
& +1.133\text{E-}003 \quad * A^2 \\
& -0.023 \quad * B^2 \\
& +0.014 \quad * A^2C[1] \\
& -0.032 \quad * A^2C[2] \\
& -0.014 \quad * AB^2
\end{aligned}
\qquad \textbf{(Eqn. 25)}
$$

Final equation in terms of actual factors for PHBV/PMMA coating adhesion at 10 passes:

$1/(\text{Adhesion})(1/(kg/cm^2))=$ +18.42768

-2.40232 * Traverse Speed(ips)

-0.78835 * Spraying Distance(cm)

+0.10226 * Traverse Speed(ips)*Spraying Distance(cm)

+3.87868E-003 * Traverse Speed(ips)^2

+8.64493E-003 * Spraying Distance(cm)^2

-1.12581E-003 * Traverse Speed(ips)* Spraying Distance(cm)^2 **(Eqn. 26)**

Final equation in terms of actual factors for PHBV/PMMA coating adhesion at 12 passes:

$1/(\text{Adhesion})(1/(kg/cm^2))=$ +17.15056

-2.15264 * Traverse Speed(ips)

-0.78835 * Spraying Distance(cm)

+0.10026 * Traverse Speed(ips)*Spraying Distance(cm)

-7.68906E-003 * Traverse Speed(ips)^2

+8.64493E-003 * Spraying Distance(cm)^2

-1.12581E-003 * Traverse Speed(ips)* Spraying Distance(cm)^2 **(Eqn. 27)**

Final equation in terms of actual factors for PHBV/PMMA coating adhesion at 14 passes:

$1/(\text{Adhesion})(1/(kg/cm^2))=$ +18.58858

-2.42537 * Traverse Speed(ips)

-0.78835 * Spraying Distance(cm)

+0.10226 * Traverse Speed(ips)*Spraying Distance(cm)

+4.66036E-003 * Traverse Speed(ips)^2

+8.64493E-003 * Spraying Distance(cm)^2

-1.12581E-003 * Traverse Speed(ips)* Spraying Distance(cm)^2 **(Eqn. 28)**

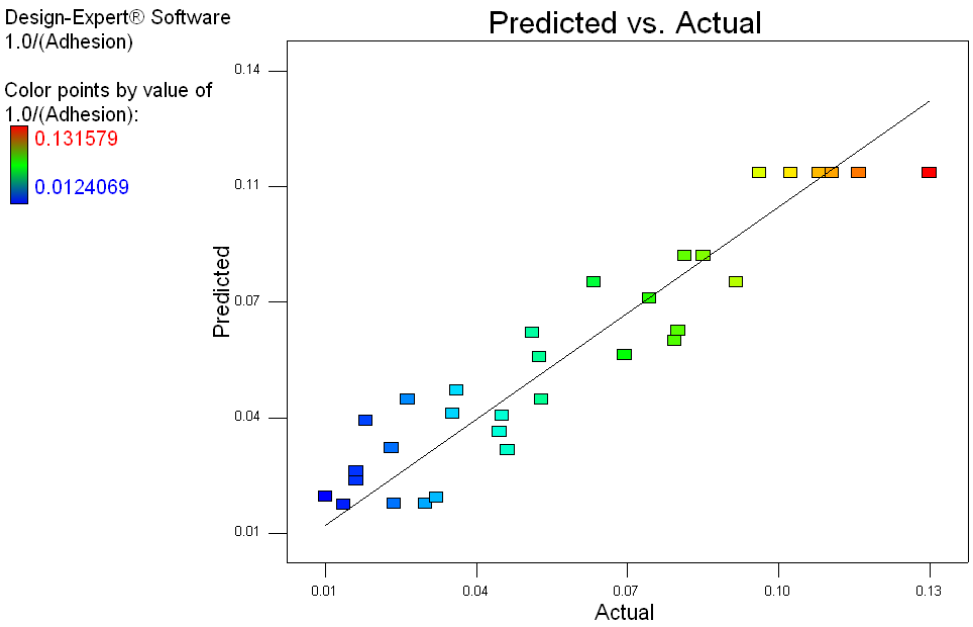

Figure 85: Predicted versus Actual values for PHBV/PMMA coating adhesion (1/(kg/cm^2))

The Predicted versus Actual graph in Figure 85 shows a good fit between the model and the experimental data, where all the measured values lie close to the best-fit line meaning that this model accurately predicts the coating adhesion.

Figure 86 shows the effect of varying the most influential factor in this model, the number of passes on coating adhesion. Coating adhesion was reduced at 12 passes compared to 10 and 14 passes. The latter two settings appear to have a similar range of adhesion values. It is obvious that in this case, the relationship between the process factor and the response was not straight forward. This was expected since the inter-locking mechanism between polymer coatings and metallic substrates could be dependent on many factors such as the degree of substrate pre-heat, the level of surface roughness, the degree of melting of polymer splats and the cooling rate of the substrate post-spray.

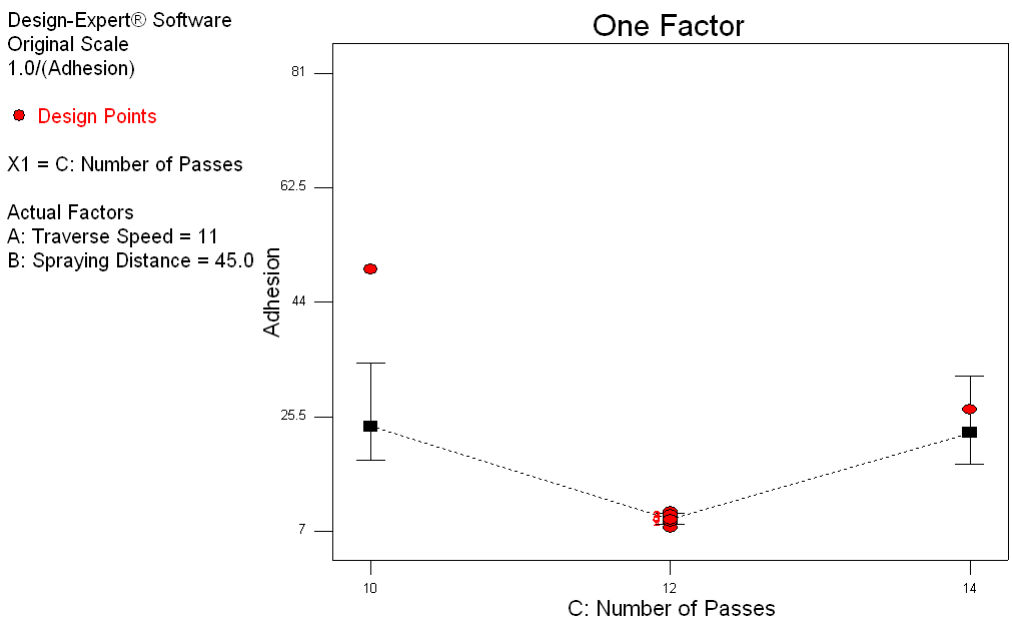

Figure 86: Variation effects of the number of passes on the coating adhesion (kg/cm^2) for PHBV/PMMA coatings

Table 63 shows the parameters corresponding to the sample with the highest (R31) and lowest (R30) roughness values.

Table 63: Spraying parameters for samples with the highest and lowest adhesion

Run	Traverse Speed(ips)	Spraying Distance(cm)	Number of Passes	Adhesion (kg/cm^2)
R23	11	42.5	14	80.6
R20	11	45	12	7.6

Comparison of the adhesion versus roughness values for the entire set of samples (Figure 87) shows that adhesion tends to decrease with the increase in roughness. This correlation could be explained by the fact that for a certain category of rough coatings, the surface roughness was caused by partially solidified polymer particles, which can have a negative impact on the mechanical interlocking between particles within the substrate and the overlapping lamellae, therefore increasing the likelihood of cohesive failure. This is substantiated by the fact that to a certain extent failure at stud/coating bonds was caused by cohesive failure. Knowing that the particles spreading upon impact is critical to obtain good coating adhesion, the inadequate spreading that partially solidified particle undergo, leads to interfacial voidage and as a result, a loss in the structural integrity of the coating.

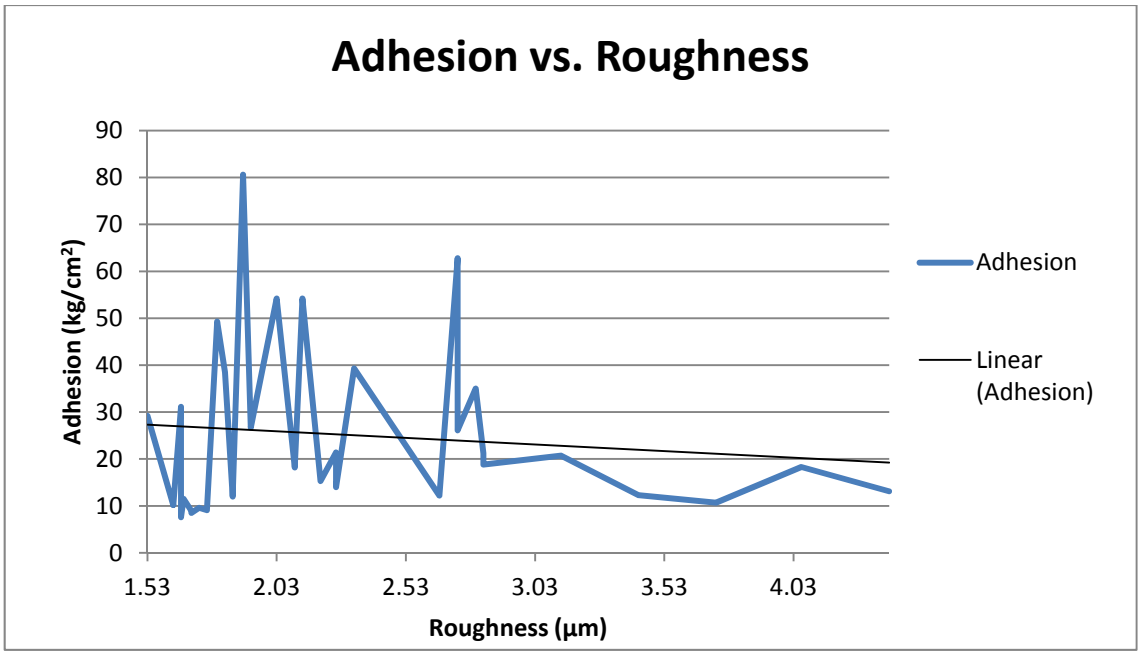

Figure 87: Adhesion versus Roughness for PHBV/PMMA coatings

Figure 88confirms the trend observed in Figure 72, whereby the coating adhesion is affected by the coating thickness. The bond strength of PHBV/PMMA flame sprayed coatings tends to decrease with an increase in layer thickness. A similar observation was made by Hadad et al. [235], were the bond strength of thermal spray coatings decreased with increasing coating thickness. Such a trend was the opposite of the trend observed with PCL/PMMA coatings, which suggests that the adhesion mechanism differs from one polymer to the other, depending on the melting temperature, the molecular weight and the density of each polymer. This correlation was related to the fact that residual stresses in the coating produce more driving force for interface crack propagation in thicker coatings [236]. Such residual stresses can potentially be caused by a number of factors, where the most likely ones are the shrinkage effects during the cooling of the substrate post-spraying, the thermal coefficient mismatch between coating and substrate materials, and the degree of rigidity of the polymers used.

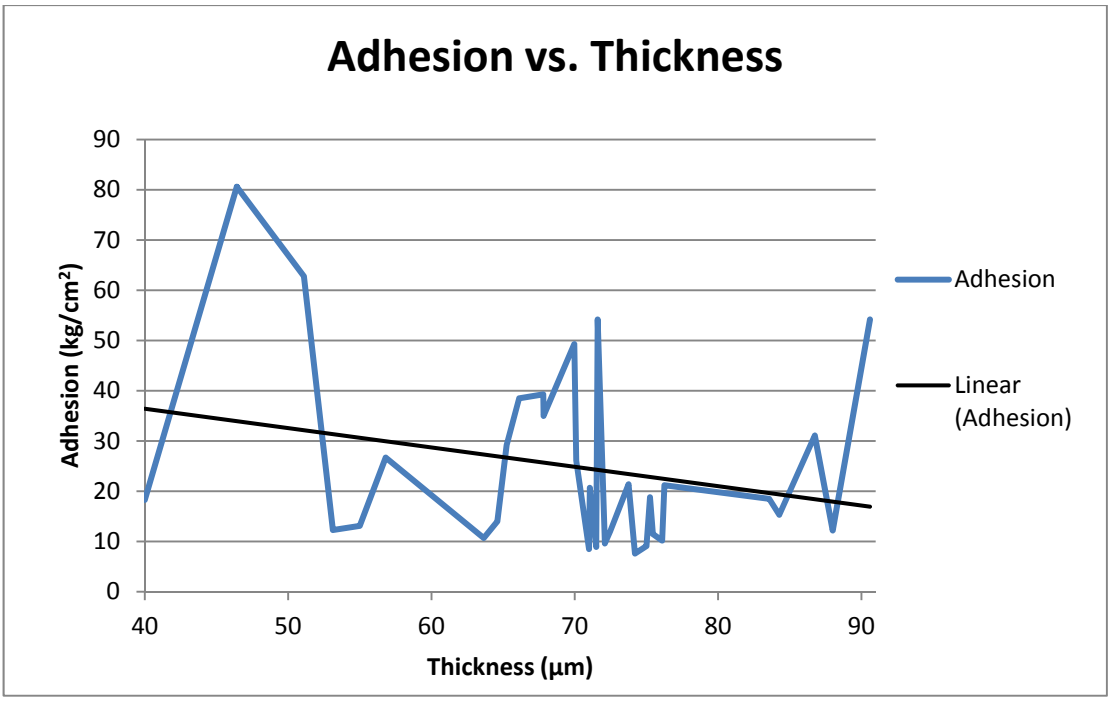

Figure 88: Adhesion versus Thickness for PHBV/PMMA coatings

Following visual inspections, the type of failure observed on most of the samples was caused by a mix of adhesive and cohesive failures. One of the obvious factors that might have contributed to such a failure type is the adhesive used. In fact, the cyanoacrylate used is not adapted to the particular specifications of this work and might have increased the likelihood of cohesive failure rather than fully adhesive failure. Figure 89 shows an SEM image of the failing interface. The sample was not gold coated which led to the polymer electrically charging. The area within the circle represents the stud/coating interface.

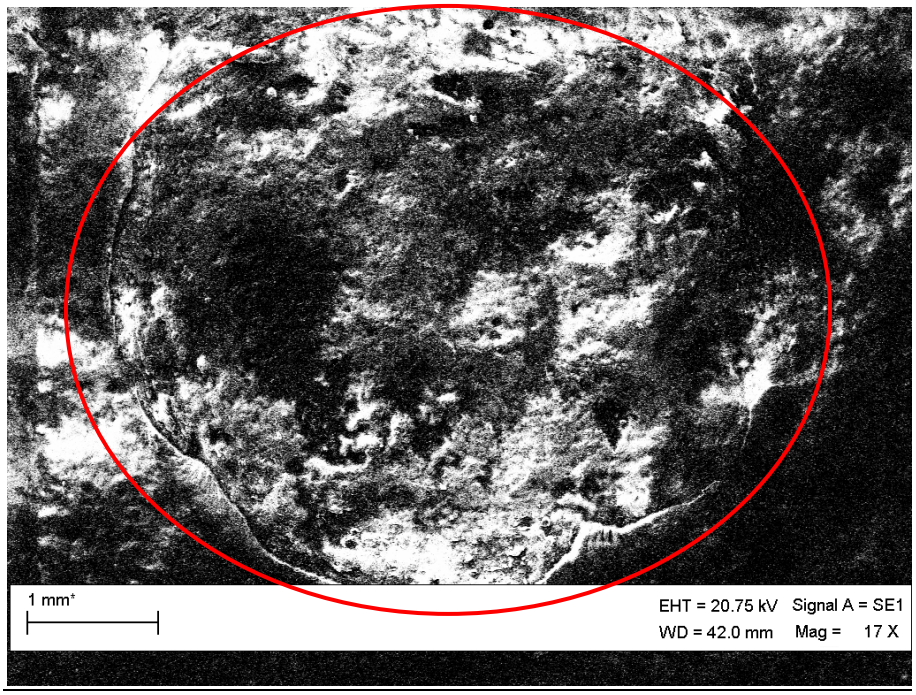

Figure 89: Surface morphology following adhesion testing

A mixture of dark (titanium) and clear (polymer) shades inside the test area (red circle) confirmed the occurrence of cohesive and adhesive failure simultaneously. The very irregular topography of the pull-off area compared to the smooth coating surface prior to the test, also confirmed that the failure was caused by the two mechanisms mentioned above.

4.5.11 PHBV/PMMA Wettabilitty Model Validation

Table 64: Contact angle measurements for the PHBV/PMMA DoE

Std	Run	CA1(°)	CA2(°)	CA3(°)	Average(°)	SD (°)
6	**R1**	56.36	60.35	56.56	57.75	2.24
29	**R2**	58.71	55.98	53.70	56.13	2.50
17	**R3**	67.13	66.77	64.43	66.11	1.46
4	**R4**	58.33	59.93	58.22	58.82	0.95
1	**R5**	57.53	56.02	57.10	56.88	0.77
13	**R6**	60.48	59.52	58.31	59.43	1.08
30	**R7**	56.24	55.78	58.65	56.89	1.54
8	**R8**	55.03	58.59	60.44	58.02	2.74
9	**R9**	61.20	58.78	60.30	60.09	1.22
21	**R10**	59.35	60.36	56.24	58.65	2.14
22	**R11**	54.72	55.07	59.65	56.48	2.75
18	**R12**	60.30	58.54	59.65	59.49	0.88
25	**R13**	58.18	58.77	59.18	58.71	0.50
7	**R14**	61.92	58.18	58.82	59.64	2.00
31	**R15**	58.59	54.02	55.42	56.01	2.34
15	**R16**	60.60	60.32	63.60	61.50	1.81
3	**R17**	60.83	60.43	61.16	60.80	0.36
27	**R18**	60.90	62.67	62.11	61.89	0.90
11	**R19**	61.11	61.24	61.83	61.39	0.38
14	**R20**	54.66	56.29	58.61	56.52	1.98
5	**R21**	63.63	60.33	59.30	61.08	2.26
2	**R22**	56.79	55.19	59.27	57.08	2.05
20	**R23**	54.64	57.56	58.56	56.92	2.03
32	**R24**	58.73	56.20	54.03	56.32	2.35
24	**R25**	61.76	56.66	60.30	59.57	2.62
10	**R26**	57.88	58.46	56.06	57.46	1.25
23	**R27**	54.61	55.43	57.41	55.81	1.43
28	**R28**	57.02	58.53	55.36	56.97	1.58
12	**R29**	56.40	54.84	55.55	55.59	0.78
26	**R30**	60.08	59.44	59.84	59.78	0.32
19	**R31**	60.25	59.13	59.11	59.49	0.65
16	**R32**	58.46	61.22	61.83	60.50	1.79
Average					58.68	1.55

The backward selection method was used to automatically eliminate insignificant model terms in order to study the main effects on contact angle/wettability (contact angle measurements in Table 64). None of the transformations available were used. It was found that the range of contact angle measurements was too narrow to yield any factor interaction and therefore a statistical analysis could not be performed on the present model. In fact, the best method to represent the relation between the different responses was through the mean value. The ANOVA table and model statistics are shown in Table 65.

Table 65: ANOVA table for the PHBV/PMMA wettability model

Source	*Sum of Squares*	*Mean Square*	*F Value*	*p-value Prob>F*	*Significance*
Model	40.15	4.46	1.59	0.1785	not significant
Significance					
A-Traverse Speed	4.31	4.31	1.54	0.2277	
B-Spraying Distance	0.18	0.18	0.063	0.8039	
C-Number of Passes	5.339E-003	5.339E-003	1.907E-003	0.9656	
AB	0.25	0.25	0.089	0.7681	
AC	0.46	0.46	0.16	0.6891	
BC	0.40	0.40	0.14	0.7092	
A^2	0.29	0.29	0.10	0.7512	
ABC	*14.36*	*14.36*	*5.13*	*0.0337*	
A^2B	*8.52*	*8.52*	*3.04*	*0.0951*	
Residual	61.59	2.80			
Lack of Fit	*61.22*	*3.60*	*49.05*	*0.0002*	*significant*
Pure Error	*0.37*	*0.073*			
Cor Total	101.74				
R^2	0.3946				
Adjusted R^2	0.1470				
Predicted R^2	-0.2980				
Adeq Precision	6.628				

From the ANOVA table of the wettability model, it was clear that all factors/interactions, had a negligible effect on the wettability of the polymer coatings. The wettability of coating surfaces partially reflects their surface chemistries; and although the exact mechanisms of the effect that surface chemistry have on cell responses is not fully understood, previous studies have demonstrated that an increase in surface wettability results in an increase of cell spreading and adhesion [237, 238].

The average contact angle for PHBV/PMMA coatings was 58.68^{o}. Angles less than 90^{o} are considered hydrophilic and therefore adequate for good cellular adhesion. Additionally, smaller contact angles characterising more wettable surfaces, are thought to lower friction and to increase the adhesive wear performance for orthopaedic implants [239]. The coating surface chemistry can influence the wettability, which in turn alters the adherence ability of proteins and bone cells to a bone implant [240]. Specifically, more hydrophilic surfaces increase the rate of cell adhesion and proliferation. Due to the fact that good hydrophilicity is an indicator of the chemical integrity of the compound, it can be assumed that the flame spraying technique did not chemically degrade the polymer powders being sprayed, especially the PHBV powder. To support the latter statement, Figure 90was used to compare the contact angle measured for the flame sprayed PHBV/PMMA for both PHB and PHBV coatings, obtained by using other techniques known for their less destructive nature.

Figure 90 shows that the contact angle of flame sprayed PHBV/PMMA coatings was smaller than that of PHBV coatings obtained by solvent casting (84^{o}) [241], which is a cold processing technique. Using hot pressing (process temperature up to 190^{o}C), contact angles of PHB films grafted with different monomers and degrees of grafting varied from 61^{o} to 74^{o}[242].Using spin-coating (cold processing), the contact angle of PHBV films was found to be 82^{o} ±2^{o}[243], and PHBV coatings yielded an average contact angle of 86.25^{o} [216]using electro-spinning. Therefore, the flame spraying technique, with its high processing temperatures, yielded superior coating wettability compared to many well established cold processing coating techniques. The difference in contact angles between the flame sprayed coating and the coatings obtained using different techniques may also be the result of the addition of PMMA to the PHBV compound. Nonetheless, the small contact

angles obtained are an encouraging factor in light of the use of flame spraying for building high quality drug delivering polymer coatings.

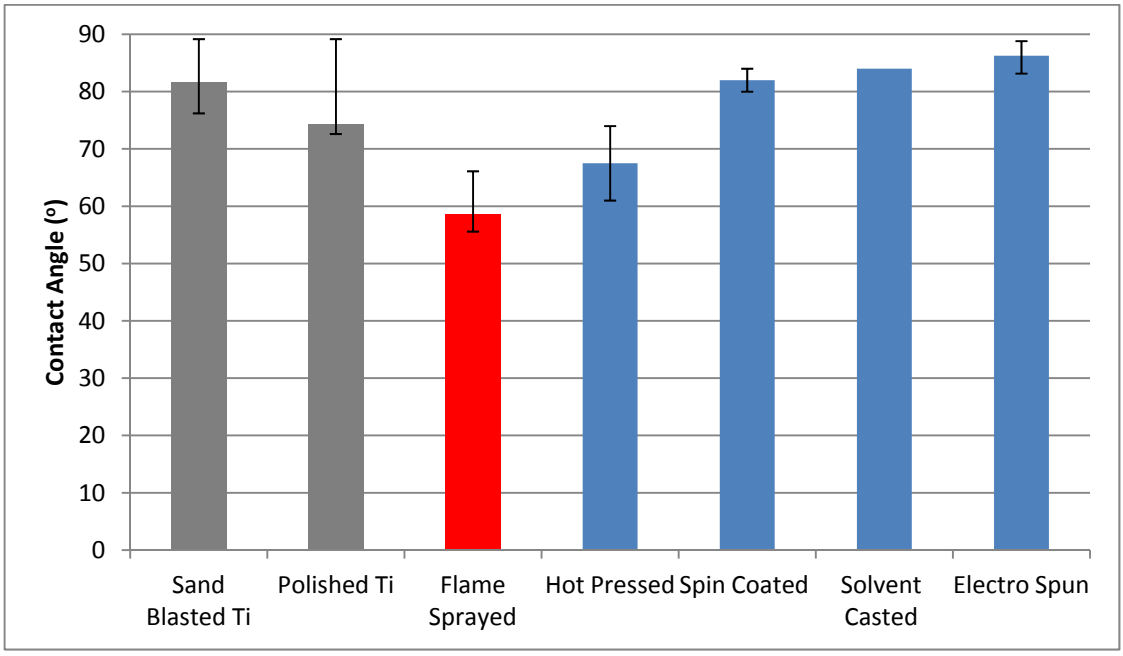

Figure 90: Contact angle comparison between different processes for PHBV/PHB coating deposition

Figure 90also shows that coating titanium implants (either polished or sand-blasted) with a biodegradable polymer matrix can cause the implant surface to be more hydrophilic and therefore leads to enhanced osteoblast attachment and proliferation. It is interesting to note that polished titanium surfaces had a smaller contact angle compared to sand-blasted surfaces; indicating that increased roughness does not necessarily improve the wettability of the implant. The same observation was made by Jaeger et al. [240] and is confirmed in Figure 90.

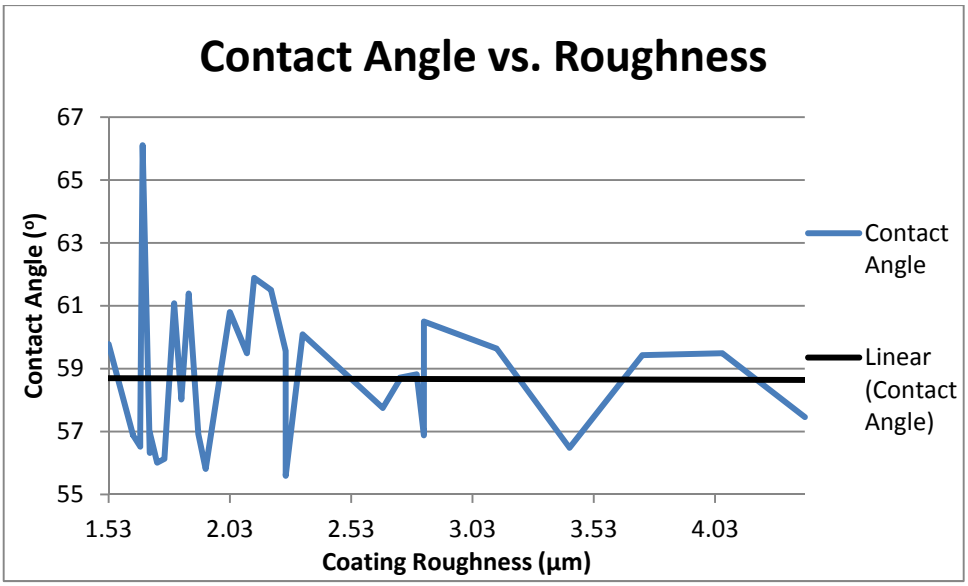

Figure 91: Contact angle versus Roughness for PHBV/PMMA coatings

Figure 91 clearly shows that the contact angle was not affected by the degree of coating roughness. A similar trend was observed during a study of polystyrene surfaces, where following an initial increase in water contact angle after grinding of the polymer surface (roughness change: 18.7nm to 542nm), it was noted that further roughening did not cause significant change in water contact angle [244]. This observation indicates that the wettability of PHBV coatings is not dependent on physical surface factors but rather on the chemical state of the polymer following processing.

Table 66 shows the parameters corresponding to the sample with the highest (R3) and lowest (R29) contact angle values.

Table 66: Spraying parameters for samples with the highest and lowest contact angle

Run	Traverse Speed(ips)	Spraying Distance(cm)	Number of Passes	Contact Angle(°)
R3	11	47.5	12	66.11
R29	13	42.5	12	55.59

According to Figure 92 the contact angle was found to depend, slightly, on the thickness of the coating. Specifically, as contact angle increased (hydrophilicity decreased) with increased coating thickness. This was confirmed by the findings by Li et al. [233]in regards to the effect of polystyrene film thickness on contact angle; where the long-range van der

Waals forces with the underlying substrate became strongly thickness dependent, and therefore affecting the observed contact angle.

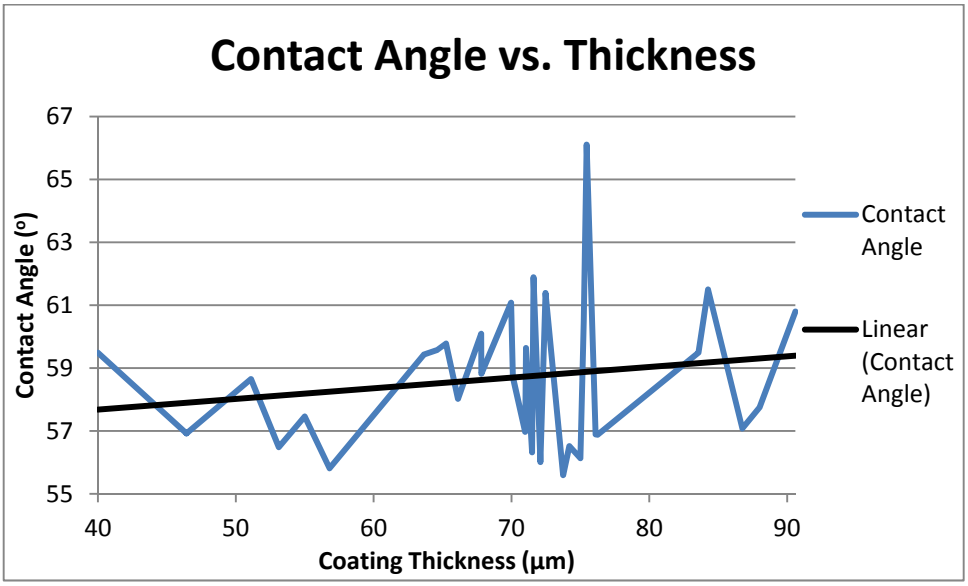

Figure 92: Contact angle versus Thickness for PHBV/PMMA coatings

4.5.12 RSM Experiment Summary

The response surface methodology study confirmed the complex and challenging nature of the task that obtaining biodegradable polymer coatings represent. This study showed a number of similarities between the behaviour of PCL/PMMA and PHBV/PMMA polymers. It also showed some differences, which could be attributed to the feedstock powder characteristics (melting temperature, molecular weight, powder density etc.). The higher quality PCL coatings were obtained with fewer complications compared to the PHBV matrix. The flame spraying process appeared to be more stable and the coatings more homogenous. The main reason for this is thought to be the narrower range of particle size (for PCL powder), which provides a more uniform melting of the feedstock powder in the flame. A narrow particle size distribution also offers a more repeatable process. Finally, this DoE study allowed a deeper understanding of how important process parameters can affect the coating characteristics and provided a very useful tool to control those characteristics in light of the production of optimised coatings.

4.6 Optimisation Process for Polymer Coatings

According to literature research, polymer coated Ti implants were not investigated in the past, thus it was not clear what level of thickness, roughness or adhesion would be optimal for either a drug delivery or a structural application, and which coating response should be optimised to the detriment of the remaining two responses (if need be). This section reviews coating requirements for each response (thickness, roughness, adhesion) and concludes with the optimisation protocol. The coatings obtained from this mechanically driven optimisation process were characterised and compared to a biological, chemical and physical prospective using the characterisation techniques described in chapter 3.

4.6.1 Thickness Requirements

It is important to note that the coatings obtained during this research were relatively low in comparison to the coating thickness generated by the thermal spraying of other materials such as ceramics and metals. The low melting and degradation properties of polymers (PCL and PHBV in this case) made it very difficult to build high coating thickness.

In order to predict optimal values of thickness, it was important to look at the effect of thickness from two points-of-view; physically and biologically (drug release kinetics). From a physical point of view, little research was done in investigating the correlation between the thickness of polymer coatings and residual stresses; therefore, an optimal thickness range for high mechanical performance was not clear. A study investigating HA/PCL composite coatings by a dip-drying process on an HA scaffold as a drug delivery system [94]concluded, that weight loss data showed that thicker coatings resulted in a reduced dissolution.

From a biological prospective, a number of thickness references are available in literature for drug eluting polymer coatings for specific bone applications (such as fixation plates and screws). Schmidmaier et al. [245] used a dipping technique to apply PDLLA coatings on titanium substrates and obtained an average thickness of 14.8 μm. These coatings were designed to possibly deliver growth factors locally. Fast initial release of incorporated growth factors was observed (around 50% in the initial 48 hours) and it is thought that the coating modification (thickness included) could alter the release kinetics. This observation was confirmed by a study investigating PDLLA drug eluting coatings on plaster of Paris

implants [246], where thicker coatings made the diffusion of the antibiotic through defects in the matrix less likely, thus, reducing the daily release of antibiotics. Thickness in the latter study varied from 69 μm to 162 μm. It is important to consider the thickness values observed in drug-delivery studies with care, as the majority of them were not designed for a load-bearing application (in contrast to the proposed application of the present work) and their main concern was the drug release kinetics.

It is clear from literature that the thickness of drug-eluting coatings is mainly dictated by the need to control the release rate (i.e. the biological action) rather than by mechanical concerns, thus the thinner the coating the faster the release. Therefore, coating thickness can be tailored to specific applications and biological conditions. Seeing that the dissolution rate was not a primary concern at this stage of the research and that maximising or minimising thickness could compromise more important responses (adhesion and roughness), it was decided that the response requirement for the optimisation should be to keep the thickness within the range of the values that were already obtained.

4.6.2 Roughness Requirements

The surface roughness of orthopaedic coatings/implants highly affects osteoblast cell attachment and resulting bone growth following implantation. Increasing surface roughness for implant coatings improves surface bioactive properties. These properties directly affect cell attachment via enhanced formation of focal contacts, or indirectly through selective adsorption of serum proteins required for cell attachment. Therefore, coating roughness should be maximised.

4.6.3 Adhesion Requirements

Across industries and specifically in implant technology, coating adhesion is recognised as being one of the most important factors influencing the performance of coated implants, the load-bearing ones in particular. Therefore, coating adhesion should be maximised.

4.6.4 Optimisation Summary

Therefore, the aim of coating optimisation was to produce polymer coatings with high adhesion and roughness as shown in Table 67.

Table 67: Polymer coating optimisation parameters

	Importance	Goal
Roughness (µm)	++++	Maximise
Adhesion (kg/cm^2)	+++++	Maximise
Thickness (µm)	n/a	Within range
Contact angle (^{o})	model inconclusive	Within range

The top five solutions, based on their desirability, are presented in the Table 68 and 69.

Table 68: PCL/PMMA optimisation results

	Solution Number				
	1	2	3	4	5
Factors					
Traverse Speed (ips)	**6**	6	6	6	6
Spraying Distance (cm)	**50**	48.7	50	49.9	50
Number of Passes	**6**	6	8	8	8
Response					
Thickness (µm)	**153.72**	151.65	137.95	138.27	137.68
Adhesion (kg/cm^2)	**65.56**	62.27	52.86	52.78	52.544
Roughness (µm)	**1.75**	1.75	1.86	1.86	1.86
Contact Angle (^{o})	**60.22**	60.22	60.22	60.22	60.22
Desirability	**0.668**	0.655	0.590	0.589	0.587

Table 69: PHBV/PMMA optimisation results

	Solution Number				
	1	2	**3**	4	5
Factors					
Traverse Speed (ips)	9	9	**13**	13	13
Spraying Distance (cm)	47.5	47.4	**42.5**	42.6	42.5
Number of Passes	10	10	**14**	14	14
Response					
Thickness (µm)	65.85	66.15	**53.24**	53.47	52.77
Adhesion (kg/cm^2)	29.84	28.67	**54.98**	49.10	58.17
Roughness (µm)	3.53	3.51	**2.71**	2.69	2.54
Contact Angle (^{o})	59.12	59.12	**59.12**	59.12	59.12
Desirability	0.859	0.851	**0.850**	0.839	0.826

The software used, generates a number of possible solutions depending on the importance of each factor and uses complex mathematical functions to balance the optimised values for the coating properties being optimised. It is then at the user's discretion to choose the optimal set of parameters that can yield the preferable balance of optimal coating characteristics, based on literature and previous experimentation.

Solution 1 was chosen for optimal PCL/PMMA coatings, because of its higher adhesion and desirability values over other solutions (Table 68).

Solution 3 was chosen for optimal PHBV/PMMA coatings because of its high adhesion prediction (almost double the value of solutions 1 and 2) and to the similarity with higher desirability values (0.009 and 0.001 differences with solution 1 and 2 respectively). Even though, solution 5 showed a higher adhesion value (58.17 kg/cm^2), the roughness level was relatively larger for solution 3, which balanced with the 54.98 kg/cm^2 adhesion value, suggesting that solution 3 would be more suitable.

4.6.5 Optimisation Validation

The mono-layer PCL/PMMA and PHBV/PMMA coatings were obtained after flame spraying the powders using the optimised process parameters (solutions 1 and 3 respectively). In order to confirm that the coatings obtained were in fact optimal, the same characterisation techniques were used; that is: thickness, roughness, adhesion, and contact angle measurements. Three different coatings were produced for each matrix and the average was calculated. The results of this validation study are shown in Table 70.

Table 70: Predicted versus actual responses for optimal polymer coatings

	PCL/PMMA (solution1)			PHBV/PMMA (solution3)		
	Predicted	**Actual**	**%Error**	**Predicted**	**Actual**	**%Error**
Thickness (µm)	153.72	123	19.98	53.24	60.9	14.38
Roughness (µm)	1.75	1.83	4.57	2.71	2.63	2.95
Adhesion (kg/cm^2)	65.56	63.2	3.59	54.98	57.8	5.19
Contact Angle (^{0})	60.22	61.89	2.77	59.12	59.82	1.18

The coatings characteristics obtained for the optimised settings were very similar to the predicted ones. The thickness error was higher than the other three responses, which is not

a primary concern, seeing that this coating response was not optimised and that the actual value was still within range. The lower thickness obtained for both polymers could actually be advantageous as lower thicknesses had been associated to faster drug release, as discussed previously. The errors for the other three responses varied between 1.18 and 5.19%, and were deemed acceptable.

4.6.6 Polymer Coatings Composition

It is essential to monitor the chemical state of the biodegradable polymers throughout a study based on thermal spraying. In fact, due to the high process temperatures reached during flame spraying, such a process could have a destructive effect on feedstock materials and may lead to material degradation. FTIR was used for this project to compare the polymer powders to the corresponding optimised coatings obtained. The challenge with this approach was, that polymers having the same basic elements results in FTIR spectra showing an overlap of characteristic bands, which makes it difficult to distinguish between bands when dealing with a matrix of two or more polymers.

a) PCL/PMMA

PCL characteristic bands were investigated and compiled by Elzein et al.[41]. These peaks were present in the FTIR spectrum performed during this project (Figure 93) and are as follows: two absorption bands at 2945 cm^{-1} and 2895 cm^{-1} representing asymmetric and symmetric CH_2 stretching respectively. The peak appearing at 1733 cm^{-1} corresponds to carbonyl stretching. C-O and C-C stretching in the crystalline phase appear at 1297 cm^{-1}; whereas the stretching of C-O and C-C in the amorphous phase appears at 1166 cm^{-1}. As for the PHBV matrix, the spectrum of the PCL/PMMA coating fit perfectly with the PCL and PCL/PMMA spectra. In fact, comparing the latter spectra (powder and coating) shows that the PCL characteristic peaks were still present in the compound after thermal spraying. This confirms that little or no degradation affects the biodegradable polymer following flame spraying of the powder.

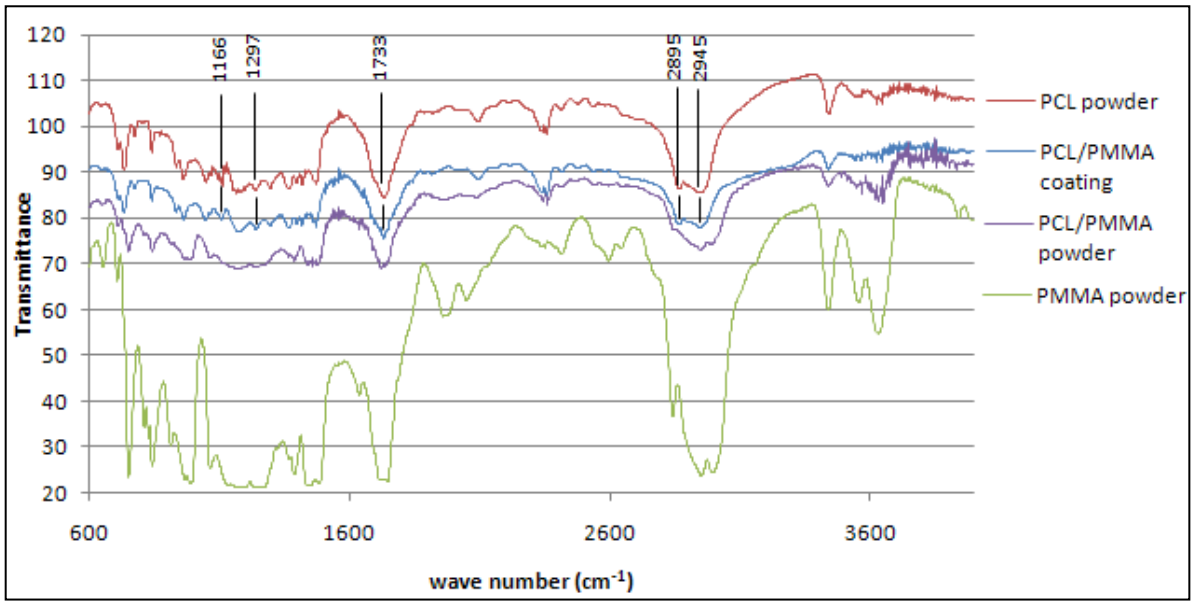

Figure 93: FTIR spectrum for PCL/PMMA coatings

Based on the powder characterisation analysis, a number of factors suggest that during the spraying of PCL/PMMA compound, PMMA particles have disintegrated in-flight. The first factor is the fact the small size of PMMA particles and their spherical morphology, which leads to an easier and faster heat diffusion, in contrast to the much higher average particle size for the PCL feedstock. The second factor is the fact that no coating was obtained when PMMA was sprayed separately, instead, very small patches of melted polymer were found on the substrate, covering negligible areas.

Disintegration of PMMA particles could also be explained by the fact that at relatively high temperatures PMMA has the specificity of undergoing an unzipping of the polymer chain [247], which simply means a reverse of its polymerisation. This phenomenon directly results in the formation of the monomer and consequently the volatilisation of the polymer at temperatures greater than the ceiling temperature of 155^{o}C [224].

The presence/absence of PMMA in the final coating does not present a concern in itself for the future viability of the project. In fact, PMMA was only used as an additive to improve the powder flowability and the use of flame spray-specific biodegradable powder in the next stage of the project should resolve the flowability issue.

b) PHBV/PMMA

Figure 94 shows the FTIR spectra of feedstock powders (PHBV, PMMA and PHBV/PMMA) as well as the spectrum of the coating obtained. It was noticeable that the latter spectrum almost resembles more of the PHBV rather than the PMMA or the PHBV/PMMA powders, which suggests that the PMMA powder may not be present in the coating. DTA analysis of the coating was not conclusive in confirming the absence of PMMA from the coating. PHBV is characterised by hydroxyl, alkyl, and carboxyl groups appearing as absorption bands respectively at 3442 cm^{-1}, 2976 cm^{-1} /2934 cm^{-1} and 1724 cm^{-1} [248]. It is clear from the coating spectra that no change occurred in the characteristic peaks of PHBV before and after coating, which confirms that little or no degradation resulted from flame spraying of this biodegradable polymer. Additionally, the band appearing at 1455 cm^{-1} corresponds to the asymmetrical deformation of C-H bond in CH_2 groups. The absorptions appearing at 1291 $cm^{-1}$are attributed to the ester group in PHBV and correspond to the stretching of the C=O bond. The series of intense bands located between 980 and 1290 cm^{-1} correspond to the stretching of the C-O bond of the ester group [249]. The decrease in band intensities relates to the loss of the polymer in the case of PMMA.

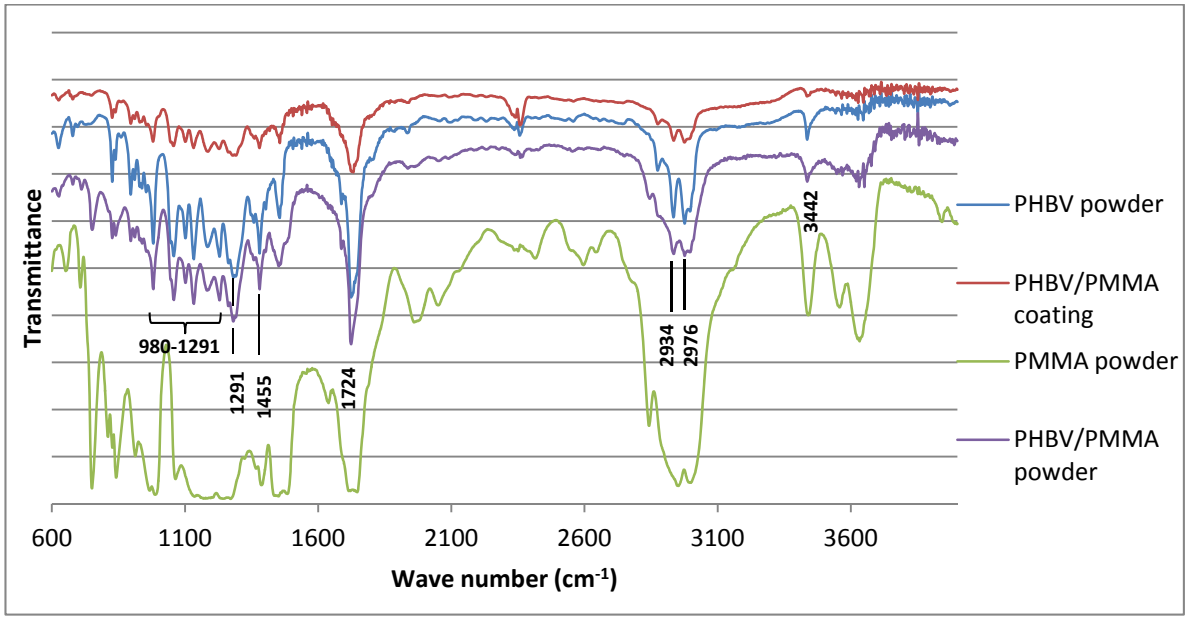

Figure 94: FTIR spectrum for PHBV/PMMA coatings

The same observations made for the PCL FTIR are applicable to the PHBV spectrum with regards to the presence/absence of PMMA powder in the final coating. Additionally, the thermal conductivity of PMMA (0.193 W/mK) was higher than that of PHBV (0.15 W/mK), which would result in heating of PMMA particles at a higher rate.

4.7 Hydroxyapatite Coating Production

After the production of optimised polymer coatings, it was essential to test the performance of a bi-layer coating (HA/polymer) from certain aspects, as a first step towards a ceramic-polymer combined drug delivery system. This project followed previous work on the development of bioactive HA thermally sprayed orthopaedic coatings [89]. Therefore, the plasma spraying parameters for the production of stable HA coatings with a dense, long lasting coating that is able to maintain its integrity for a long period following implantation were compared to HA with added polymeric DDS. In order to obtain such coatings, four responses were maximised (roughness, crystallinity, purity, thickness).

Following a DoE optimisation stage [89], the spraying parameter selected for producing stable HA coatings were as shown in chapter 2.After the production of plasma sprayed stable HA layers, three coatings were characterised for different responses (roughness, thickness, crystallinity, purity). Three measurements were taken for each characterisation technique and the average results are shown in Table 71.

Table 71: Characterisation of HA stable coatings

	Coating 1				Coating 2				Coating 3			
Roughness(µm)	8	7.5	8.5	**8**	8.7	9.5	7.5	**8.5**	8.5	7.5	8.2	**8**
Thickness(µm)	337	338	349	**341**	358	329	359	**348**	326	375	351	**350**
Crytallinity(%)	**84.5**				**84.5**				**83.3**			
Purity(%)	**98.2**				**97.55**				**98.1**			

Table 72shows the measured responses versus the predicted responses. A certain percentage of error exists. However, this level of errors was deemed acceptable as the values obtained fall within the range of optimised stable HA coatings.

Optimised PCL/PMMA and PHBV/PMMA coatings were then flame sprayed onto the previously sprayed HA coatings to form a bi-layer orthopaedic coating.

Table 72: Predicted versus actual response values for HA stable layer

Stable HA Layer			
	Predicted (from [89])	**Actual (from this research)**	**% Error**
Roughness (µm)	8.6	8.21	**4.53**
Thickness (µm)	413	346	**16**
Crytallinity (%)	84.69	84.1	**0.69**
Purity (%)	98.53	97.95	**0.58**

4.8 Mono-layer and Bi-layer Coatings as DDS

Following the flame spray of the PHBV/PMMA matrix using the optimised parameters (Traverse speed = 13ips, Spraying distance =42.5cm, Number of Passes =14passes) for the final biological and physical studies, coatings with a very different a morphology and appearance were obtained. In fact, the size and shape of the flame was different and the coatings were burnt off. After a few runs, the same observations persisted and no viable coatings obtained. After narrowing downs the potential causes of such a problem, it was concluded that the only difference between the spraying of the optimised parameters and the DoE samples was the fact that a new batch of PHBV powder was used. After contacting the supplier, it was confirmed that due to the biological nature of the manufacturing process of the PHBV powder (biological fermentation) inconsistencies can occur with regards to some powder properties. Amongst the feedstock material properties that can affect the morphology and the microstructure of thermally sprayed polymer coatings are the particle size and the molecular weight ranges. In fact, a large particle size or molecular weight distribution tended to facilitate the formation of numerous heterogeneities within the coating microstructure, creating voids, a range of splat aspect ratios, and degraded material [111]. It is generally agreed that a narrow range for particle size distribution is required to take advantage of the optimum particle trajectories through the heat source in order for a dense coating to be formed [111]. This confirmed the visual observation whereby PCL coatings looked more dense and compact in comparison to the PHBV coatings. The characterisations of the PHBV particles have already shown the large and non-Gaussian distribution of the particles; nonetheless, after thorough screening and experimentation a narrow window of spraying was achieved. Seeing that the particle size distribution of the first and the second batch were very similar and equally un-adapted for such an application,

the remaining factor that could have affected the final coatings was the molecular weight. Asenjo et al. [250] suggested that some PHB-producing organisms can yield a wide molecular weight distribution at the end of a batch growth. The difficulty in obtaining a sufficiently narrow and consistent molecular weight distribution hinged the wider use of PHB polymers in some areas. The widening of this distribution is thought to occur mainly at the end of batch and fed-batch fermentation and to a lesser extent during the extraction process. A variation in molecular weight can also affect the melting and decomposition temperature of polymer particle in-flight and therefore affect the resulting coating structure.

At this stage of the project, it was impossible to carry out another full process investigation (screening + DoE), hence the optimised parameters had to be re-adjusted in order to obtain viable coatings. Following a thorough parameter range investigation, viable coatings were produced with a traverse speed of 11ips, a spraying distance of 50cm and 8 passes (compared to 13ips, 42.5cm and 14 passes respectively). The same parameters were used to spray PHBV/PMMA on HA coated discs and the resulting coatings are shown in Figure 95. Table 73 shows the change in coating characteristics between the optimised PHBV/PMMA settings and the re-adjusted settings.

Table 73: Optimised versus Adjusted PHBV/PMMA coatings

	PHBV/PMMA		
	Optimised	**Adjusted**	**%Error**
Thickness (µm)	53.24	37.7	29.18
Roughness (µm)	2.71	2.23	17.71
Adhesion (kg/cm^2)	54.98	45.7	16.87
Contact Angle (^{o})	59.12	59.28	0.27

The errors for the two most important responses, roughness and adhesion, were respectively at 17.71% and 16.87%. These errors are deemed acceptable, taking into account the actual circumstances and the fact that the adjusted values were still present within the higher end of the response range that was obtained during the DoE investigation of the PHBV/PMMA matrix. The contact angle value (59.28^o) confirmed the ability of this process to consistently produce coatings with superior wetting properties.

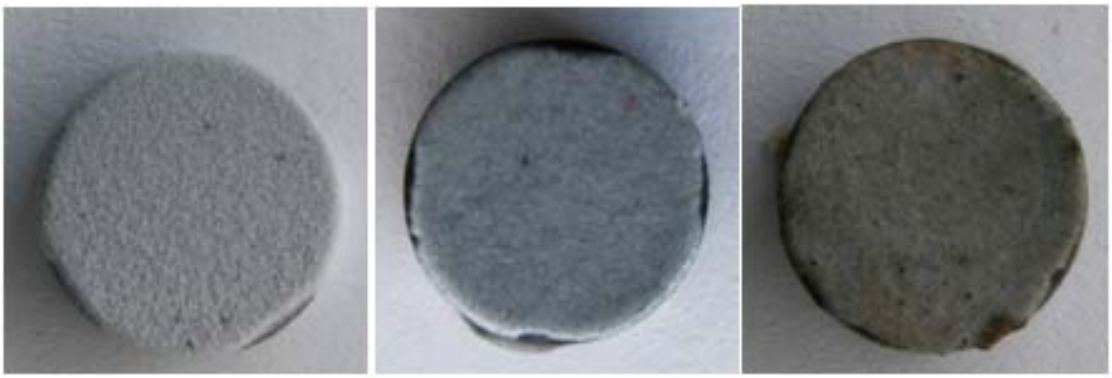

Figure 95: From left to right: mono-layer HA coating, bi-layer PCL/HA coating, bi-layer PHBV/HA coating

Figure 95 shows the appearance of the HA coating prior and following the flame spray of polymer layers. The PCL/HA compound had a clear transparent appearance, which was expected, seeing the clean surface finishing obtained with PCL coated Ti. On the other hand the PHBV coated HA appeared darker, which is undoubtedly due to the inconsistent nature of the spraying process caused by the multimodal powder size distribution. It is thought that the use of powders containing sizeable quantities of fine particles (dust) would lead to excessive coating oxidation and voids [112]. From the characterisation of the PHBV powder, it was found that half of the particles were below 15.92 μm in size with a peak occurring between 0.1 and 1 μm, which explained the difficulty in obtaining coatings with this powder and the oxidation occurring when coatings are finally obtained.

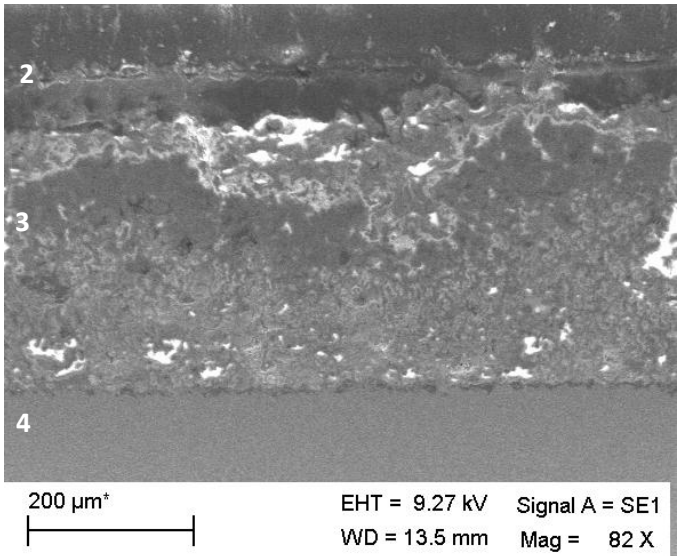

Figure 96: Cross-sectional view of an PCL/HA bi-layer coating

Figure 96 shows a cross-sectional view of the bi-layer coating (PCL/HA). The four material layers numbered from 1 to 4 correspond to: resin, polymer (PCL/PMMA), ceramic (HA), metal (titanium) respectively. The presence of more pores on the HA layer suggested that the polymer coating was more dense than the HA coating.

The adhesive strength of PCL-based coatings appeared to be reduced when sprayed onto HA, where PHBV increased, when applied on the bioceramic material (Table 74).The adhesive strength went from 63.2 kg/cm^2 on bare titanium substrate to 40.5 kg/cm^2 on HA. Poor interfacial adhesion between HA and PCL has been observed with PCL/HA blends on some occasions [251]. The reason behind that was simply attributed to the difference in the chemical nature of the two components and their different surface energy, which could cause decay in the mechanical properties of the composite [251]. Additionally, such a trend confirmed observations from Figure 73 (adhesion versus roughness), in which the adhesion of PCL/PMMA coatings on Ti substrates was inversely proportional to roughness. In fact, the loss of adhesion of the PCL/PMMA coating on the HA coating coincided with an increase in surface roughness.

Table 74: Bi-layer coatings mechanical characterisation

	Samples	Roughness (µm)	Adhesion (kg/cm^2)	Contact Angle (^{o})
HA/ PCL/PMMA	S1	3.5	42.1	61.04
	S2	3.3	34.3	58.99
	S3	2.7	45.1	57.53
	Average	**3.16**	**40.5**	**59.18**
PCL/PMMA		**1.83**	**63.2**	**61.89**
HA/ PHBV/PMMA	S1	11	73.1	34.91
	S2	7.5	107.5	28.26
	S3	8.5	90	45.8
	Average	**9**	**90.2**	**36.32**
PHBV/PMMA		**2.23**	**45.7**	**59.28**

On the other hand, pull-off testing of the polymer on ceramic bi-layers showed that the adhesive strength of PHBV/PMMA coatings increased when applied on a bioceramic material rather than on titanium. In fact the adhesive strength doubled from 45.7kg/cm^2 for the adjusted PHBV coatings on bare titanium to an average of 90.2 kg/cm^2 when applied on HA. In a study investigating the mechanical properties of HA/PHBV nanocomposites

[252], it was reported that the presence of HA with a polymer matrix may lead to the formation of transcrystalline layers at the HA-polymer interface. The formation of these layers results in enhancing the mechanical properties of the compound and as a result a stronger bonding between the ceramic material and the polymer matrix [253], which explains the increase in the PHBV coating adhesion.

PCL coatings with a much higher thickness than PHBV coatings (123 μm for PCL, 37.7 μm for PHBV) showed an increase in roughness from 1.83 μm to 3.16 μm, which confirms two points: firstly that the roughness of the polymer coatings is affected by roughness of the underlying HA topography, and secondly that the increase in thickness of polymer coatings attenuates the effect of the latter point. Similarly, the roughness of PHBV coatings dramatically increased from an average of 2.23μm to 9 μm. This could be explained again by the fact that, due to the relatively low thickness of PHBV coatings, the roughness at the top surface was affected by the topography of the underlying HA coating. This was substantiated by the fact that, the same phenomena was observed during the DoE study of the PHBV/PMMA matrix.

Finally, Table 74 shows that the contact angle of PCL coatings was not affected by the presence of a stable HA layer beneath, with a slight decrease from 61.89^{o} to 59.18^{o}. On the other hand, the contact angle for the PHBV was considerably affected by the presence of the underlying HA coating, with a decrease from 59.28^{o} to 36.32^{o}, thus improving the wetting properties of the top polymer layer, which in turn would lead to better bone regeneration.

4.9 Physio-Chemical Analysis

4.9.1 Coating pH

Previous studies have suggested that the release of acidic degradation by-products of degradable polymers may lead to a decrease in the level of pH in the direct vicinity of the implanted material [254, 255], which resulted in inflammatory responses and failure to provide an adequate environment for a successful bone-implant integration. It is therefore crucial that the flame sprayed polymer coatings produced in this work displays neutral levels of pH (~7) in order to guarantee the physio-chemical integrity of potentially polymer coated orthopaedic implants.

In the case of pure HA coatings, pH level initially decrease from7.8 to7.3 over the first week, before gradually increasing up to 8.1.This increase in pH value is caused by the formation of the OH^- that is caused by the following reaction: $CaO+H_2O \leftrightarrow Ca^{2+} + 2OH^-$ [256].On the other hand, pH levels for coatings made of pure polymer or of an HA/polymer compound started at a slightly lower levels7.4-7.6 and gradually decreased to settle at levels ranging from 6.7-7.1 (Figure 97).

Table 75 shows all pH measurements performed over a period of 31 days for different coatings. The degradation by-products of PCL are non-toxic and resorbable by nature [257], therefore the flame spraying techniques did not affect this material property and the pH of the solution did not show any acidity.

The change in pH of polymer-based coating was more stable than the trend observed with pure HA coatings. It is also important to note that the decrease in pH of polymer-based coatings coincided with a decrease in pH of the deionised water sample to similar levels (6.8-7). Such pH levels are still considered within the neutral range and do not represent a degrading factor in light of the use of such coatings as a load-bearing orthopaedic coatings. Comparison of pH for polymer-based coatings and deionised water suggests that the degradation by-products of the flame sprayed coating did not cause any increase in acidity in addition to the change naturally observed with the water sample. Therefore the coatings obtained are expected to display neutral pH levels *in vivo*.

The bi-layer coatings have the advantage of including HA in the compound, which was observed to increase the pH towards the basic-end of the spectrum (7.9-8.1). This could represent an advantage as higher pH values were found to enhance the rate of apatite formation on an HA/polymer bone scaffold [258]. In fact, many more apatite particles formed on the outer surface of the composite scaffold after 30 days of incubation at a higher pH value of 7.7 than at lower pH values of 7.1 and 7.4. The average particle density was also found to be larger at higher pH values. The presence of such an apatite layer on the surface of orthopaedic implants is generally considered as a positive biological response from host tissue. Additionally, the formation of a collagen-free apatite layer is an essential requirement for ossetointergration of bone implants [259].

Table 75: pH levels over 31 days

Day	Di-Water	Titanium	HA1	HA2	HA3	HA	PCL1	PCL2	PCL3	PCL	PHBV1	PHBV2	PHBV3	PHBV	PCL/HA1	PCL/HA2	PCL/HA3	PCL/HA	PHBV/HA1	PHBV/HA2	PHBV/HA3	PHBV/HA
1	7	7.8	8.1	7.8	7.5	7.8	7.6	7.5	7.7	7.6	7.4	7.5	7.4	7.4	7.4	7.6	7.8	7.6	7.5	7.5	7.4	7.4
2	7	7.1	7.7	8.3	8.2	8.1	7.2	7.3	7.4	7.3	7.2	7.3	7.3	7.2	7.6	6.9	7.5	7.3	7.2	7.1	7.2	7.1
3	6.8	6.9	7.6	7.8	7.5	7.6	7.0	7.3	7.1	7.1	6.9	7.0	7.2	7.0	6.8	6.9	6.9	6.8	7.4	7.0	7.2	7.2
4	6.8	6.8	7.3	7.5	7.6	7.5	6.9	6.9	7.1	6.9	6.7	7.0	7.2	6.9	6.7	6.5	7.0	6.7	6.8	7.0	7.2	7.0
5	6.7	7.0	7.5	7.5	7.3	7.4	7.0	7.0	6.7	6.9	7.1	6.7	7.0	6.9	6.6	6.6	6.8	6.6	6.7	7.0	7.1	6.9
6	6.7	6.9	7.4	7.2	7.3	7.3	6.8	6.9	6.6	6.7	6.8	6.9	7.1	6.9	6.6	6.6	6.9	6.7	6.7	6.8	7.1	6.8
7	6.7	6.8	7.2	7.3	7.3	7.3	6.6	7.0	6.7	6.7	6.7	6.9	7.0	6.8	6.8	6.7	6.8	6.7	6.7	6.9	7.0	6.8
8	6.6	6.8	7.2	7.3	7.3	7.3	6.6	7.0	6.7	6.7	6.8	6.9	7.0	6.9	6.7	6.7	6.8	6.7	6.8	6.8	7.0	6.8
9	6.6	6.8	7.2	7.3	7.4	7.3	6.8	6.9	6.8	6.8	6.9	7.0	7.0	6.9	6.7	6.8	6.9	6.8	6.9	7.0	7.1	7.0
10	6.6	6.9	7.3	7.3	7.4	7.3	6.7	6.8	6.7	6.7	7.0	6.9	6.9	6.9	6.7	6.8	6.9	6.8	6.9	6.6	7.2	6.9
11	6.6	7.0	7.3	7.4	7.5	7.4	7.0	6.7	6.9	6.8	7.0	7.0	7.0	7.0	6.8	6.9	7.0	6.9	7.0	6.8	7.2	7.0
12	6.6	7.0	7.4	7.5	7.5	7.5	6.8	6.8	6.8	6.8	7.0	6.9	6.9	6.9	6.7	7.0	6.9	6.8	7.0	6.9	7.1	7.0
13	6.7	7.1	7.5	7.4	7.5	7.5	7.1	6.9	6.9	6.9	7.0	6.9	7.0	6.9	7.0	6.9	7.0	6.9	7.1	7.0	7.0	7.0
14	6.7	7.1	7.5	7.5	7.6	7.5	7.1	7.0	7.0	7.0	7.1	7.0	6.9	7.0	6.9	7.0	7.1	7.0	7.0	7.1	7.0	7.0
15	6.7	7.1	7.5	7.6	7.6	7.5	7.0	6.9	7.0	6.9	7.1	6.9	7.1	7.0	6.9	6.9	6.9	6.9	6.9	7.0	7.1	7.0
16	6.8	7.2	7.7	7.8	7.7	7.7	7.1	7.0	6.9	7.0	7.2	7.0	7.1	7.1	7.0	6.9	6.8	6.9	6.9	7.1	7.1	7.0
17	6.8	7.2	7.9	7.8	7.8	7.8	7.0	7.0	6.9	6.9	7.1	7.0	7.2	7.1	7.0	7.0	6.9	6.9	7.0	7.3	7.0	7.1
18	6.8	7.1	7.6	8.0	7.9	7.8	7.1	7.1	7.1	7.1	7.1	6.8	7.0	6.9	6.9	7.0	7.1	7.0	7.2	7.0	6.9	7.0
19	6.8	7.1	7.9	8.0	7.9	7.9	7.2	7.0	7.1	7.1	7.1	6.8	7.1	7.0	7.1	7.1	7.1	7.1	7.2	7.1	6.9	7.0
20	6.8	7.2	7.9	7.9	7.9	7.9	7.0	7.3	7.2	7.1	7.2	7.0	7.0	7.0	7.0	7.1	7.1	7.0	7.2	7.3	6.9	7.1
21	6.7	7.2	7.9	7.9	7.9	7.9	7.2	7.2	7.2	7.2	7.2	6.9	6.9	7.0	7.1	6.9	7.2	7.0	7.1	7.2	6.8	7.0
22	6.8	7.2	7.9	8.0	7.9	7.9	7.1	7.3	7.2	7.2	7.1	6.9	6.8	6.9	7.2	6.9	7.2	7.1	7.1	7.3	6.8	7.0
23	6.8	7.1	7.8	7.9	7.8	7.8	7.2	7.0	7.0	7.0	7.3	6.8	6.9	7.0	7.1	7.0	7.3	7.1	7.0	7.1	7.0	7.0
24	6.9	7.2	7.9	8.0	7.9	7.9	7.3	6.9	7.0	7.0	7.1	7.0	7.0	7.0	7.1	7.0	7.1	7.0	6.8	7.2	6.9	6.9
25	6.8	7.1	7.9	8.0	8.0	8.0	7.1	7.1	6.9	7.0	7.2	7.1	7.0	7.1	7.2	7.1	7.0	7.1	6.9	7.1	6.8	6.9
26	6.9	7.2	8.0	8.0	8.0	8.0	7.0	6.9	6.9	6.9	7.1	7.0	6.9	7.0	7.1	7	7.2	7.1	6.9	7.0	6.7	6.8
27	6.8	7.1	8.0	8.1	8.0	8.0	7.1	7.0	6.9	7.0	7.0	7.0	6.8	6.9	7.0	6.8	7.3	7.0	7.0	7.2	6.7	6.9
28	6.9	7.0	8.0	8.1	8.0	8.0	7.2	7.2	7.0	7.1	7.0	7.1	6.9	7.0	7.0	6.9	7.1	7.0	7.1	7.0	6.8	6.9
29	6.9	7.1	8.0	8.1	8.0	8.0	7.1	7.0	7.2	7.1	7.1	7.2	7.0	7.1	6.9	7.1	6.9	6.9	6.9	6.9	7.0	6.9
30	6.8	7.0	8.0	8.1	8.1	8.1	7.0	7.3	7.1	7.1	6.9	7.3	7.0	7.0	6.9	7.2	6.9	7.0	7.0	6.9	7.1	7.0
31	6.9	7.0	8.0	8.1	8.1	8.1	7.2	7.0	7.3	7.1	7.0	7.2	7.2	7.1	7.1	7.2	7.0	7.1	7.2	6.9	7.1	7.0

Looking at the pH levels for specific polymers (PCL and PHBV), it was interesting to compare the evolution of the pH over time and the range of values reached for the flame sprayed coatings with the same polymers processed via other methods. In the case of PCL, hot pressed samples of this polymer were studied *in vitro* with the aim of monitoring the pH changes of PCL while it degraded and the effects of its by-products [260]. It was found that pH increased over 28 days from 6.8 to 9.6, which contrasted with the stable and neutral pH levels obtained with the flame sprayed PCL coatings produced in this project. Another study that included monitoring pH levels for solvent casted PCL over a 56 days degradation period [261] revealed that pH level oscillated between 5 and 5.5. Although stable over time, such acidic levels of pH may be caused by the release of by-products and could negatively affect the bone regeneration process on the surface of the implant coating. As for the PHBV material, it was found that pH levels decreased from 7.4 to 7.2 after 4 weeks and to 5.8 over a period of 9 weeks with PHBV scaffolds obtained via compression moulding, thermal processing, and salt particulate leaching [262].

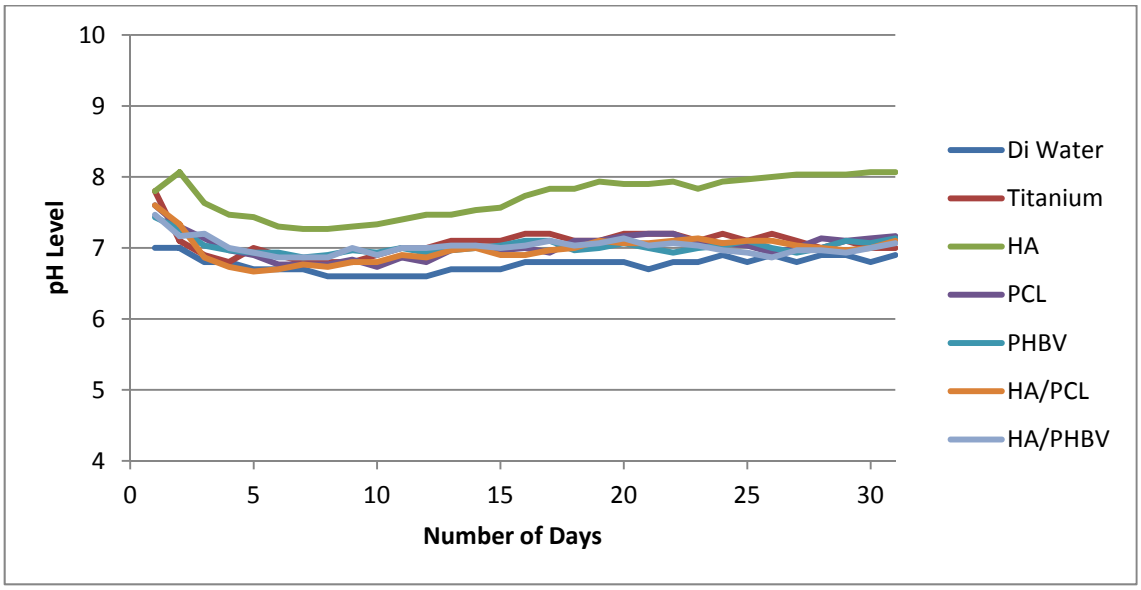

Figure 97: pH change over 31 days

From the comparison of the pH levels and the change in pH of PCL and PHBV compounds obtained using different production techniques, flame sprayed materials displayed excellent behaviour with regards to the latter characteristic whereby the pH values remained in a physiologically acceptable level of7.2 to 6.7, and therefore, it is safe to assume that the pH

levels displayed by all coatings are suitable for application requiring rapid implant ossteoingration.

4.9.2 Coating Conductivity

Conductivity relates to the ionic concentration and the strength of the solution. The conductivity of biomaterials used for a bone implant application partly reflects its oestrogenic potential (suitability for bone repair); the higher the conductivity of the material the better is the implant integration. The increase in material conductivity induced by physical or chemical surface treatments [263] is thought to result in the increased pull-out forces seen in an *in vivo* study.

Pure hydroxyapatite has osteoconductive properties similar to bone, which is thought to allow a better bonding to the bone [264], however, its poor biodegradability represents a drawback as it prevents the natural bone regrowth for an extended period. Additionally, findings by Petersson et al. [263] indicated that alteration (by increasing) of the semi-conducting properties of titanium implant surfaces could be a tool for inducing a wanted biological response.

A part from a specific class (Conducting Polymers, CP), polymers are known to have very poor conductivity, PCL, PMMA and PHBV, do not belong to this class of polymers (CP).Surface eroding polymers do not allow the solution to penetrate into the material, thus eroding gradually layer by layer. Whereas bulk eroding polymers absorb the immersion solution much more, allowing degradation to occur both inside and outside the coatings. Therefore, the latter erosion mechanism would generate a larger rate of ion release, which explains the much higher conductivity levels observed with PCL-based coatings in comparison to PHBV-based coatings (Figure 98).

All conductivity measurements started at 0 μS/cm. The conductivities of the titanium and the deionised water remained very low in comparison to all other samples. From the first days, it was obvious that samples with HA present in the coatings were showing higher conductivities that pure polymeric materials.

Good conductivity performances for PCL were previously observed by Micusik et al. [265] where the highest electrical conductivity achieved for a set of different polymer matrices was obtained with composites based on the PCL matrix. A similar observation was made

by Basavaraja et al.[266] where the conductivity of polymer films was increased with the increase of PCL below a critical level.

The conductivity observed with pure polymer coatings suggested that PCL-based coatings were slightly more conductive than PHBV-based coatings. A similar trend was observed by Sanchez-Garcia et al. [267] where the conductivity of PHBV-based matrices increased at a lower rate and was smaller than the conductivity of PCL-based matrices, were the additives in each case was the same material (carbon nanotubes) at an increasing proportion.

The conductivity levels for PCL/HA and PHBV/HA compounds confirmed the slightly superior conductivity potential of PCL over PHBV. The fact that the latter compounds had higher conductivity than pure polymer coatings was a result of the presence of HA in the compound, which was seen to display the largest conductivity of all.

The minor variations in conductivity for the deionised water are probably due to the fact that conductivity is slightly affected by temperature. Therefore, minor temperature fluctuations inside the water bath could explain the latter observation. The poor conductivity of titanium alloys [268] was confirmed in this study, where the conductivity of the Ti solution was similar to that of deionized water.

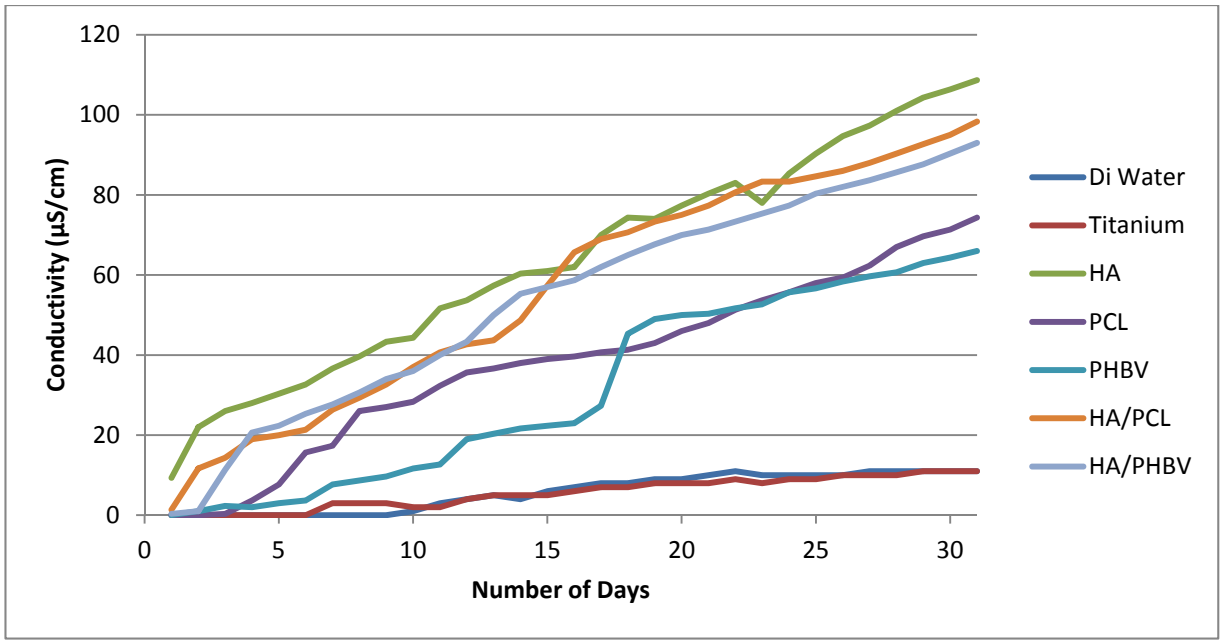

Figure 98: Conductivity change over 31 days

Table 76 shows all conductivity measurements performed over a period of 31 days for different coatings.

Table 76: Conductivity levels over 31 days in µS/cm

Day	Di-Water	Titanium	HA1	HA2	HA3	HA	PCL1	PCL2	PCL3	PCL	PHBV1	PHBV2	PHBV3	PHBV	PCL/HA1	PCL/HA2	PCL/HA3	PCL/HA	PHBV/HA1	PHBV/HA2	PHBV/HA3	PHBV/HA
1	0	**0**	5	11	12	**9**	0	0	0	**0**	0	0	0	**0**	0	4	0	**1**	0	0	1	**0**
2	0	**0**	18	23	25	**22**	0	0	0	**0**	2	0	1	**1**	9	25	1	**12**	1	0	2	**1**
3	0	**0**	22	24	32	**26**	1	0	0	**0**	2	3	2	**2**	12	29	2	**14**	10	11	13	**11**
4	0	**0**	25	26	33	**28**	1	1	9	**4**	2	2	2	**2**	21	31	5	**19**	20	23	19	**21**
5	0	**0**	27	29	35	**30**	8	1	14	**8**	3	3	3	**3**	19	33	8	**20**	21	24	22	**22**
6	0	**0**	30	30	38	**33**	27	1	19	**16**	4	3	4	**4**	21	33	10	**21**	24	27	25	**25**
7	0	**3**	33	35	42	**37**	30	1	21	**17**	5	12	6	**8**	34	35	10	**26**	26	29	28	**28**
8	0	**3**	37	38	44	**40**	32	21	25	**26**	8	11	7	**9**	38	38	12	**29**	29	31	32	**31**
9	0	**3**	41	42	47	**43**	34	22	25	**27**	8	12	9	**10**	41	39	18	**33**	33	34	35	**34**
10	1	**2**	47	45	41	**44**	37	23	25	**28**	9	15	11	**12**	50	42	19	**37**	36	37	35	**36**
11	3	**2**	52	49	54	**52**	36	35	26	**32**	9	17	12	**13**	58	43	21	**41**	39	41	40	**40**
12	4	**4**	53	51	57	**54**	38	42	27	**36**	10	32	15	**19**	61	44	23	**43**	41	44	45	**43**
13	5	**5**	56	56	60	**57**	39	42	29	**37**	10	37	14	**20**	63	45	23	**44**	55	49	46	**50**
14	4	**5**	62	60	59	**60**	41	44	29	**38**	11	38	16	**22**	65	46	35	**49**	63	53	50	**55**
15	6	**5**	63	62	58	**61**	44	44	29	**39**	11	48	16	**22**	65	59	48	**57**	65	54	52	**57**
16	7	**6**	66	65	55	**62**	43	46	30	**40**	12	41	16	**23**	67	68	62	**66**	67	55	54	**59**
17	8	**7**	68	70	72	**70**	45	45	32	**41**	24	41	17	**27**	68	69	70	**69**	70	60	56	**62**
18	8	**7**	72	75	76	**74**	44	46	34	**41**	31	88	17	**45**	70	71	71	**71**	73	65	57	**65**
19	9	**8**	72	75	75	**74**	46	48	35	**43**	32	97	18	**49**	71	75	74	**73**	75	68	60	**68**
20	9	**8**	74	77	81	**77**	49	49	40	**46**	34	98	18	**50**	73	76	76	**75**	75	73	62	**70**
21	10	**8**	77	80	84	**80**	50	52	42	**48**	33	99	19	**50**	73	80	79	**77**	76	75	63	**71**
22	11	**9**	79	82	88	**83**	55	53	46	**51**	34	100	21	**52**	75	84	83	**81**	77	78	65	**73**
23	10	**8**	81	80	73	**78**	56	55	50	**54**	36	100	22	**53**	76	85	89	**83**	79	80	67	**75**
24	10	**9**	83	82	91	**85**	57	55	55	**56**	37	105	25	**56**	75	85	90	**83**	82	81	69	**77**
25	10	**9**	86	86	99	**90**	59	56	59	**58**	38	106	26	**57**	76	86	92	**85**	82	86	73	**80**
26	10	**10**	89	89	106	**95**	60	58	60	**59**	40	107	28	**58**	78	88	92	**86**	86	88	72	**82**
27	11	**10**	92	93	107	**97**	61	60	66	**62**	41	109	29	**60**	82	89	93	**88**	88	89	74	**84**
28	11	**10**	93	95	115	**101**	68	63	70	**67**	42	110	30	**61**	85	91	95	**90**	89	92	76	**86**
29	11	**11**	96	97	120	**104**	69	65	75	**70**	45	112	32	**63**	88	94	96	**93**	91	94	78	**88**
30	11	**11**	96	101	122	**106**	68	68	78	**71**	47	113	33	**64**	92	96	97	**95**	94	95	82	**90**
31	11	**11**	97	103	126	**109**	70	70	83	**74**	48	115	35	**66**	96	99	100	**98**	95	99	85	**93**

4.9.3 Coating Weight Loss

Coating degradation for biodegradable materials should be sustained over a long period of time in order not to compromise the load transfer from the upper implant layer to the new bone tissue.

The percentage weight loss for coatings was investigated over a period of 4 weeks, which correspond to the post-operative time period, where implant failure is more likely to occur. Degradation studies by Lu et al. [215] suggested that the degradation rate of polymer films can be engineered by varying film thicknesses.

In the context of drug release and using DSC data, Maia et al. [179] observed that the glass transition temperature was reduced by the incorporation of hydroxyvalerate (HV) into the polymer chain (PHB). This indicates that PHBV loses some crytallinity in comparison to PHB. Lower crystallinity is thought to result in a larger increase in the release rates for drug delivering polymers. Therefore, the use of PHBV for drug delivery purposes offers an alternative means of controlling the drug release rate, in addition to mechanical features such as the coating thickness.

Figure 99 shows the percentage weight loss over 28 days, with weight measurements every 7 days. It is important to note that samples taken out for measurement were not immersed back for further reading, therefore for every time period (7days), different samples were considered.

At week 1, the PCL-based coatings showed a weight loss of less than 1%, while PHBV-based coatings showed a weight loss between 1.5-2%. From that point on, PHBV/HA coatings resulted in a stable and almost unchanged weight loss varying between 1.79% and 1.94%. PHBV coatings on the other hand resulted in a steady increase in weight loss going from 1.63% to 2.54%. It can be seen for both PHBV-based coatings that the initial burst in weight loss (week 1) was larger than the weight loss observed over the following three weeks. This could be interpreted as a positive feature when an initial higher burst of drug/growth factor is desired directly post-implantation, followed by a steadier drug release and polymer degradation.

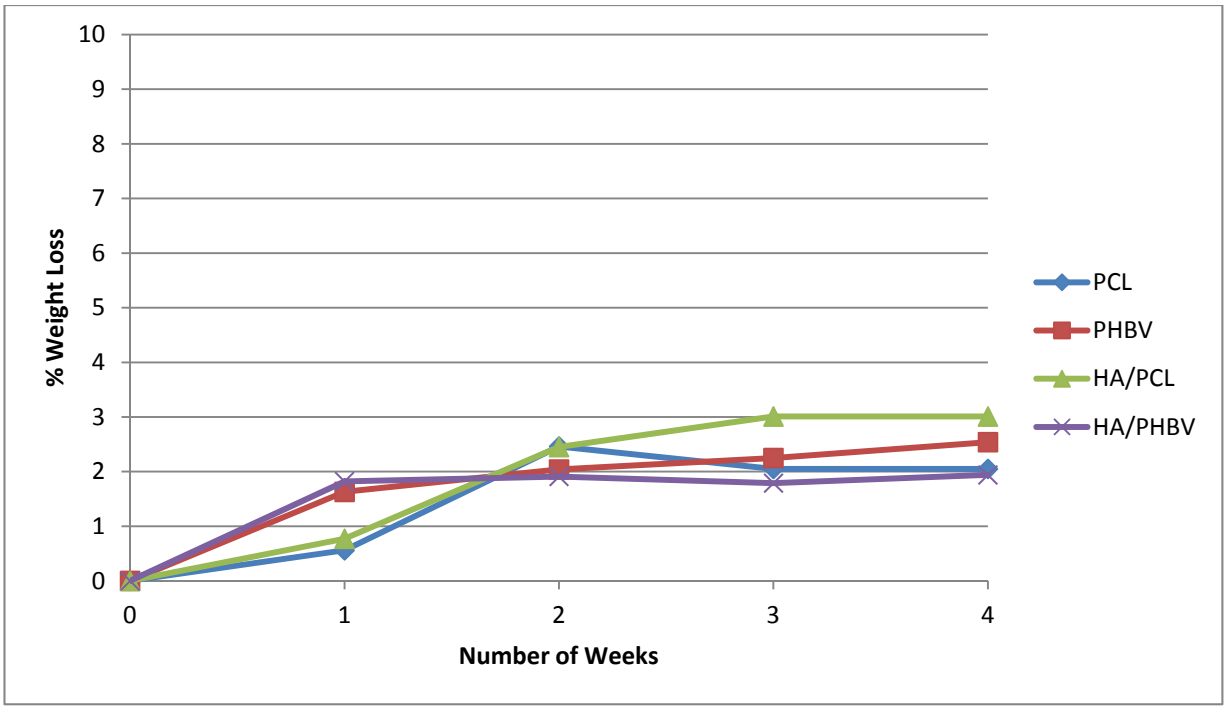

Figure 99: Mono-layer and bi-layer coatings degradation over 28 days

On the other hand, the largest burst in weight loss for PCL-based coatings occurred between week 1 and week 2. In fact for both pure polymeric coatings and bi-layer coatings, the percentage weight loss went from 0.56% and 0.77% to 2.46% and 2.45% respectively. From week 2, the weight loss for both PCL-based coatings diverged. Pure polymeric coatings remained below the threshold observed in week 2 (2.46%), with a stable weight loss value of 2.05% in week 3 and week 4. This contrasts with PCL/HA coatings, which showed an increase from 2.45% to a stable value of 3.01% in week 3 and week 4, similar to what was observed for pure polymeric coatings. Similar levels of PCL weight loss were observed by Malberg et al.[269], where the total mass loss for pure PCL films following a 30 days period immersion in PBS resulted in a decrease of the weight of films from 100% to ~98.5%.

Regeneration of the bone tissue that is contact with the bioactive implant while it is resorbing is a complex process, which still requires further research. Form the degradation curves in Figure99, it is difficult to be conclusive about the behaviour of different polymers compared to each other, and similarly about the behaviour of pure polymeric coatings and

bi-layer coatings compared to each other. However, it is clear that the initial trend of weight loss for all coating types is consistent with requirements of potentially load-bearing orthopaedic coatings, in terms of keeping weight loss minimal during the first couple of weeks following implantation.

The minimal initial weight loss could also be an indicator that no fragmentation or delamination occurred, which would indicate high coating cohesion. This feature was the result of the process used in this project, where the interlocking of melted particles upon impact on the substrate promoted the inter-lamellar cohesion within the polymer coatings. In addition to the inter-lamellar cohesion, slow degradation of both PCL and PHBV based polymers was expected (as previously mentioned for both polymers) and is thought to be due to high inter-molecular cohesion. Such a feature is usually an indicator that the chemical state of the polymer was not altered [270], and could considered as a confirmation of the chemical integrity of the flame sprayed mono-layer and bi-layers polymer coatings.

Table 77 and 78 show all weight data collected throughout this *in vitro* degradation study, where SW: weight of the uncoated Ti disc (Ti+HA for bi-layer coatings), Wo: weight of coated samples pre-immersion, CW: coating weight (=Wo-SW), Wf: weight of coated samples post-immersion, Actual WL: actual weight loss (=Wf-Wo), %WL: percentage weight loss. The unit for all weight measurements is gram.

Table 77: Weight loss data for PCL-based coating over 28 days

Week	Measures	PCL1	PCL2	PCL3	PCL	PCL/HA1	PCL/HA2	PCL/HA3	PCL/HA
1	SW	0.6792	0.686	0.6916		0.7502	0.7465	0.7751	
	Wo	0.6889	0.6902	0.7069		0.7643	0.7569	0.7905	
	CW	0.0097	0.0042	0.0153		0.0141	0.0104	0.0154	
	Wf	0.6888	06902	0.7068		0.7642	0.7568	0.7904	
	Actual WL	1E-04	0	1E-04		1E-04	1E-04	1E-04	
	% WL	1.03	0	0.65	**0.56**	0.70	0.96	0.64	**0.77**
2	Substrate weight	0.678	0.693	0.6945		0.7167	0.7419	0.7278	
	Wo	0.6886	0.704	0.7081		0.7325	0.7517	0.7402	
	Coating weight	0.0106	0.011	0.0136		0.0158	0.0098	0.0124	
	Wf	0.6884	0.7038	0.7076		0.7322	0.7514	0.7399	
	Actual WL	0.0002	0.0002	0.0005		0.0003	0.0003	0.0003	
	% WL	1.88	1.81	3.67	**2.46**	1.89	3.06	2.41	**2.45**
3	Substrate weight	0.6886	0.6831	0.6838		0.7499	0.7175	0.7152	
	Wo	0.699	0.695	0.6956		0.765	0.7318	0.7269	
	Coating weight	0.0104	0.0119	0.0118		0.0151	0.0143	0.0117	
	Wf	0.6988	0.6949	0.6952		0.7647	0.7314	0.7264	
	Actual WL	0.0002	1E-04	0.0004		0.0003	0.0004	0.0005	
	% WL	1.92	0.84	3.38	**2.05**	1.98	2.79	4.27	**3.01**
4	Substrate weight	0.6886	0.6831	0.6838		0.7499	0.7175	0.7152	
	Wo	0.699	0.695	0.6956		0.765	0.7318	0.7269	
	Coating weight	0.0104	0.0119	0.0118		0.0151	0.0143	0.0117	
	Wf	0.6988	0.6949	0.6952		0.7647	0.7314	0.7264	
	Actual WL	0.0002	1E-04	0.0004		0.0003	0.0004	0.0005	
	% WL	1.92	0.84	3.38	**2.05**	1.98	2.79	4.27	**3.01**

Table 78: Weight loss data for PHBV-based coating over 28 days

Week	Measures	PHBV1	PHBV2	PHBV3	PHBV	PHBV/HA1	PHBV/HA2	PHBV/HA3	PHBV/HA
1	Substrate weight	0.7118	0.6971	0.7018		0.7715	0.6985	0.7123	
	Wo	0.7159	0.7052	0.7073		0.779	0.7058	0.7194	
	Coating weight	0.0041	0.0081	0.0055		0.0075	0.0073	0.0071	
	Wf	0.7158	0.705	0.7073		0.779	0.7054	0.7194	
	Actual WL	1E-04	0.0002	0		0	0.0004	0	
	% WL	2.43	2.46	0	**1.63**	0	5.47	0	**1.82**
2	Substrate weight	0.6982	0.6783	0.6835		0.7114	0.6941	0.7264	
	Wo	0.7017	0.6859	0.6892		0.7186	0.7025	0.7333	
	Coating weight	0.0035	0.0076	0.0057		0.0072	0.0084	0.0069	
	Wf	0.7017	0.6857	0.689		0.7185	0.7025	0.733	
	Actual WL	0	0.0002	0.0002		1E-04	0	0.0003	
	% WL	0	2.63	3.50	**2.04**	1.38	0	4.34	**1.91**
3	Substrate weight	0.6962	0.677	0.6895		0.7611	0.7116	0.7468	
	Wo	0.7021	0.6843	0.6945		0.7685	0.7195	0.7531	
	Coating weight	0.0059	0.0073	0.005		0.0074	0.0079	0.0063	
	Wf	0.7019	0.6842	0.6944		0.7685	0.7192	0.753	
	Actual WL	0.0002	1E-04	1E-04		0	0.0003	1E-04	
	% WL	3.38	1.36	2	**2.25**	0	3.79	1.58	**1.79**
4	Substrate weight	0.6962	0.677	0.6897		0.7563	0.7357	0.7246	
	Wo	0.702	0.6843	0.6963		0.7638	0.7438	0.7298	
	Coating weight	0.0058	0.0073	0.0066		0.0075	0.0081	0.0052	
	Wf	0.7019	0.6842	0.696		0.7636	0.7437	0.7297	
	Actual WL	1E-04	1E-04	0.0003		0.0002	1E-04	1E-04	
	% WL	1.72	1.36	4.54	**2.54**	2.66	1.23	1.92	**1.94**

4.10 Biological Analysis

The results of the biological analysis can be found in appendix D, as the post-DOE biological assessment with regards to the XTT viability assay was inconclusive. On the other hand, the ALP assay showed that the expression level of alkaline phosphatase was much higher for PHBV coatings than for PCL coatings and pure HA coatings. The ALP assay showed that the expression level of alkaline phosphatase was much higher for PHBV/HA coatings than for PCL/HA coatings compared to pure HA coatings, thus demonstrating the benefit of using bi-layer polymer/ceramic coatings for orthopaedic applications.

5 Conclusions and Recommendations for Future Work

5.1 Conclusions

The outcomes of this project have largely contributed to the field of polymer thermal spraying and of drug-delivery coatings for implant application. In fact, the main challenges identified at the start of this project were successfully overcome.

- Viable biodegradable PCL-based and PHBV-based polymer coatings were obtained (for both polymeric mono-layer coatings and for bi-layer HA integrated coatings); these coatings are very promising candidates to act as a drug delivery vehicles post implant surgery for the following reasons:
  - The chemical functionality of PCL-based and PHBV-based polymers was retained following the flame spraying process, with polymer-characteristic peaks remaining visible throughout the spectra. Even though, the exact mechanism of interaction between surface properties and cells is not fully understood; it is broadly recognised that the chemistry and topography of implant surfaces determine to a large extent the biological performance of the implanted devices. This furthermore confirms that the rough, hydrophilic and chemically stable coatings obtained, are ideal candidates for orthopaedic implants applications
  - The degradation by-products of the mono-layer polymer coatings and of the bi-layer HA integrated coatings were not acidic in nature and did not generate a hostile implantation environment *in vitro* with regards to pH levels.
  - The conductivity measurements of PCL-based PHBV-based coatings showed that pure polymer coatings had a much larger conductivity potential than bare titanium substrates. The conductivity of the coatings was enhanced further by the addition of an HA base layer.
  - The degradation of pure polymeric matrices and of the bi-layer HA integrated coatings was minimal during the first month of the *in vitro* analysis, which guarantees the mechanical integrity of the implant coatings post-implantation, when the desired application is load-bearing orthopaedic (femoral) implants, and provides a drug delivery system with a long-lasting release rate.

- The preliminary biological assessment showed that the performance of pure polymeric coatings after 3 days and 5 days was superior to Ti-only compounds, suggesting a faster osteointegration post-implantation. In fact, the integration of titanium implants in orthopaedic applications is a passive process that results in mechanical fixation only, which may lead to implant loosening and anchorage failure. Bioactive polymers (PCL and PHBV) will therefore increase the biointegration of the implant and the bone tissue.

➢ The statistical models developed during this project provide an invaluable insight into the relationship between flame sprayed polymer coatings and thermal spray processing parameters. These statistical models, through mathematical equations, will also allow future researchers in the area to predict the characteristics of the coatings for given process parameters in order to obtain the desired values of coating properties. This is evidential by the following:

- The Design of Experiments analysis of PCL-based PHBV-based matrices provided a thorough understanding of the relationship between three process factors on one hand: spraying distance, traverse speed, number of passes; and four important coatings characteristics on the other hand: coating thickness, coating roughness, coating adhesion, coating wettability.
- The coating thickness can be modelled for both polymeric matrices, which will allow a better control over the coating degradation rate and as a direct result, of the drug release kinetic, where the desired application is drug transport and release.
- The coating roughness can be controlled for both polymeric matrices, which will allow the operator to maximise or minimise the surface roughness of the implants based on a number of considerations.
- The coating adhesion can be modelled and maximised for both polymeric matrices, which will reduce the likelihood of coating delamination under shear stress, where the desired application is load-bearing orthopaedic (femoral) implants.
- The coating wettability could not be predicted, however, all values for both polymeric matrices fall within a hydrophilic range that would improve cellular activity on the surface of the coatings and guarantee superior wetting properties than

bare titanium implants or polymer coatings obtained using different processing methods.

- Optimised and viable polymer coatings with a maximised adhesion and roughness, as well as thickness and wettability within range (for both polymeric matrices), were successfully deposited using the flame spraying technique, on bare Ti and on plasma sprayed stable HA coatings.
- The optimal PCL-based coatings were obtained using the following process parameters: traverse speed of 0.152 m/s, spraying distance of 50 cm, and 6 passes.
- The optimal PHBV-based coatings were obtained using the following process parameters: traverse speed of 0.33 m/s, spraying distance of 42.5 cm, and 14 passes.

5.2 Recommendations for Future Work

The findings in this work have contributed greatly to the knowledge regarding flame spraying of polymers in general and of biodegradable PCL and PHBV polymers in particular. Future researchers in the field should find the statistical models developed during this project and the knowledge gained extremely valuable. By the completion of this work, further research and development steps that would contribute to this subject have been identified. These recommendations are as follows:

- The development of polymer powder with a specifically tailored morphology and particle size distribution will dramatically improve the quality of the coatings obtained and the controllability over the final coating characteristics.
- Spray drying of polymer materials could be used in order to obtain powder with spherical morphology which would improve the powder flowability and allow fully degradable drug delivery coatings to be produced.
- Alternatively to spray drying and preferably, if the particle size range is suitable and the powder morphology is still irregular, an external powder feeding system could be used, where a carrier gas (e.g. Argon) would lead to continuous and controllable powder feeding rate.
- More developed oxy-acetylene spraying systems (commercially available) could be used, which would allow control over more process parameters, especially oxygen and acetylene flow rates. This improved control over the process leads in turn to

more stable spraying, better coatings repeatability and more precise control over final coating responses. It could also provide a control over the temperature of the flame and a certain level of control over the melting degree of in-flight particles, which in turns allows more responses to be controlled such as the coating porosity. The latter property is thought to have an effect on the degradation rate of polymers and the drug release rate for drug delivery systems.

- Thermal characterisation of the flame could be very useful in understanding the thermal cycle that in-flight particles go through. Such a study would require the use of thermal vision equipment for temperature profiling as well as high speed camera for velocity profiling.
- Depending on the dissolution rate suggested by physicians, the HV fraction in the PHBV co-polymer could be manipulated in order to customise the polymer for the proposed application (DDS) and optimised for bone regeneration.
- More thorough degradation tests would need to be performed for drug-loaded polymer coatings with the constant monitoring of the mechanical properties of the coatings.
- The post-DOE biological assessment was not conclusive overall, thus an optimised study in terms of adequate cell line and assay protocols would be required.

Publications Arising From This Work

1. *'Thermal Spraying of Biopolymers for Orthopaedic Applications'* (Oral presentation)
   A., Chebbi, J., Podporska, J., Stokes,
   Bioengineering in Ireland 2011, Galway, Ireland
2. *'Plasma Spraying of Therapeutic Drug Delivery System onto Femoral orthopaedic Implant'* (Poster)
   A., Chebbi, J., Stokes,
   IRCSET/SEI Symposium 2009, Dublin, Ireland
3. *'Design of Experiments Analysis of Thermally Sprayed Biopolymer Matrix for Orthopaedic Applications'* (Oral presentation)
   A., Chebbi, J., Stokes
   Faculty Research Day 2011, DCU, Dublin, Ireland
4. *'Design of Experiments Analysis of Thermally Sprayed PCL/PMMA Coatings'* (Poster)
   A., Chebbi, J., Stokes,
   European Conference on Biomaterials 2011, Dublin, Ireland
5. *'Thermal Spraying of Bioactive Polymer Coatings for Orthopaedic Applications'* (Oral Presentation),
   A., Chebbi, J., Stokes,
   International Thermal Spray Conference 2011, Hamburg, Germany
6. '*Thermal Spraying of Bioactive Polymers for Orthopaedic Applications*' (Journal Article),
   A., Chebbi, J., Stokes,
   International Journal of Nano and Biomaterials 2011 (in review)

References

[1] Itasaka, T., Kawai, A., Sato, T., 2001, "Diagnosis of Infection After Total Hip Arthroplasty," Journal of Orthopaedic Science, 6(4) pp. 320-326.

[2] Ostermann, P. A. W., Henry, S. L., and Seligson, D., 1993, "The Role of Local Antibiotic-Therapy in the Management of Compound Fractures," Clinical Orthopaedics and Related Research, (295) pp. 102-111.

[3] Lew, D. P., and Waldvogel, F. A., 1997, "Osteomyelitis," New England Journal of Medicine, 336(14) pp. 999-1007.

[4] Gursel, I., Yagmurlu, F., Korkusuz, F., 2002, "In Vitro Antibiotic Release from Poly(3-Hydroxybutyrate-Co-3-Hydroxyvalerate) Rods," Journal of Microencapsulation, 19(2) pp. 153-164.

[5] Türesin, F., Gürsel, İ., and Hasirci, V., 2001, "Biodegradable Polyhydroxyalkanoate Implants for Osteomyelitis Therapy: In Vitro Antibiotic Release," Journal of Biomaterials Science -- Polymer Edition, 12(2) pp. 195-207.

[6] Korkusuz, F., Korkusuz, P., Eksioglu, F., 2001, "In Vivo Response to Biodegradable Controlled Antibiotic Release Systems," Journal of Biomedical Materials Research Part A, 55(2) pp. 217-228.

[7] Neo, M., Nakamura, T., Yamamuro, T., 1993, "Transmission Electron Microscopic Study of Apatite Formation on Bioactive Ceramics in Vivo," Bone-Bonding Materials.Leiderdorp: Reed Healthcare Communications.p, pp. 111–20.

[8] Tortora, G.J., 2006, "Principles of anatomy and physiology," J. Wiley, Hoboken, NJ, .

[9] Hench, L.L., and Jones, J.R., 2005, "Biomaterials, artificial organs and tissue engineering," CRC Press; Woodhead, Boca Raton; Cambridge, pp. 284.

[10] Rho, J. Y., Kuhn-Spearing, L., and Zioupos, P., 1998, "Mechanical Properties and the Hierarchical Structure of Bone," Medical Engineering & Physics, 20(2) pp. 92-102.

[11] Garcia-Alonso, D., 2009, "Plasma Spray Deposition of Hydroxyapatite Based Composites as a Step Towards Bone Scaffolds," .

[12] Orlovskii, V. P., Komlev, V. S., and Barinov, S. M., 2002, "Hydroxyapatite and Hydroxyapatite-Based Ceramics," Inorganic Materials, 38(10) pp. 973-984.

[13] Lundon, K., 1999, "Orthopedic rehabilitation science : principles for clinical management of bone," Butterworth-Heinemann, Boston, pp. 204.

[14] National Center for Chronic Disease Prevention and Health Promotion, "Http://www.Cdc.gov/ARTHRITIS/data_statistics/arthritis_related_statistics.Htm," 2009(11/27) .

[15] Ghista, D.N., 1980, "Biomechanics of medical devices," M. Dekker, New York, .

[16] Scales, J. T., 1966-1967, "Arhtroplasty of the hip using foregein materials: a history," Lubrication and wear in living and artificial human joints, Anonymous Institution of Mechanical Engineers, London, pp. 63-84.

[17] Levingstone, T., and Hingston, J., 2008, "Guide to Hip Replacement for Engineers: Design, Materials and Stress Issues," Dublin City University, Dublin, .

[18] MEDCARE Hospital Dubai, "Http://www.Medcareorthopaedics.com/health-Library-Details.Aspx?hid=10," 2010(04/08) .

[19] Lohana, P., Woodnutt, D. J., and Boyce, D. E., 2010, "Sciatic Nerve Palsy – a Complication of Posterior Approach using Enhanced Soft Tissue Repair for Total Hip Arthroplasty," Journal of Plastic, Reconstructive & Aesthetic Surgery, 63(4) pp. e400-e401.

[20] Ooms, E. M., Wolke, J. G. C., van de Heuvel, M. T., 2003, "Histological Evaluation of the Bone Response to Calcium Phosphate Cement Implanted in Cortical Bone," Biomaterials, 24(6) pp. 989-1000.

[21] Maloney, W.J., 1998, "Hip Surgery: Materials and Developments,"Informa HealthCare, London, .

[22] Hench, L.L., and Wilson, J., 1993, "An Introduction to bioceramics," World Scientific, Singapore ; River Edge, N.J., pp. 386.

[23] Geesink, R. G. T., Degroot, K., and Klein, C. P. A. T., 1988, "Bonding of Bone to Apatite-Coated Implants," Journal of Bone and Joint Surgery-British Volume, 70(1) pp. 17-22.

[24] Oonishi, H., Yamamoto, M., Ishimaru, H., 1989, "The Effect of Hydroxyapatite Coating on Bone-Growth into Porous Titanium-Alloy Implants," Journal of Bone and Joint Surgery-British Volume, 71(2) pp. 213-216.

[25] Poulmaire, D., Ducos, M., Setti, Y., 1991, "Development of dental implants in titanium with HA coatings," Proceedings on 2nd Plasma-Technik-Symposium Plasma-Technik AG, Anonymous 3, pp. 191–202.

[26] Matejka, D., Palka, V., Brezovsky, M., 1991, "Plasma coated composite intraosseous implants," Proceedings on 2nd Plasma-Technik-Symposium Plasma-Technik AG, Anonymous 3, pp. 171–177.

[27] Stephenson, P. K., Freeman, M. A. R., Revell, P. A., 1991, "The Effect of Hydroxyapatite Coating on Ingrowth of Bone into Cavities in an Implant," The Journal of Arthroplasty, 6(1) pp. 51-58.

[28] Kettner, R., 1996, "The unique interface reaction of H.A.C." Hydroxyapatite Ceramic, a Decade of Experience in Hip Arthroplasty, the Proceedings of a Two Day Symposium : Held at the Royal College of Surgeons of England on Thursday 2nd & Friday 3rd November 1995, R. Furlong, ed. Furlong Research Foundation, London, pp. 41-55.

[29] Osborn, J. F., and Pfeifer, G., 1983, "Hydroxyapatite Ceramic for Bone-Replacement - Experimental and Clinical-Results," Langenbecks Archiv Fur Chirurgie, 361pp. 738-738.

[30] Furlong, R. J., and Osborn, J. F., 1991, "Fixation of Hip Prostheses by Hydroxyapatite Ceramic Coatings," Journal of Bone & Joint Surgery, British Volume, 73(5) pp. 741.

[31] Soballe, K., 1996, "The Role of H-A.C. in Ingrowth Prosthesis ," Hydroxyapatite Ceramic, a Decade of Experience in Hip Arthroplasty, the Proceedings of a Two Day Symposium : Held at the Royal College of Surgeons of England on Thursday 2nd & Friday 3rd November 1995, R. Furlong, ed. Furlong Research Foundation, London, pp. 57-67.

[32] Carlsson, L.V., Macdonald, W., Jacobsson, C.M., 2003, "Biomaterials in Orthopedics,"Marcel Dekker, New York, pp. 223-239.

[33] Valiathan, M. S., and Krishnan, V. K., 1999, "Biomaterials: An Overview," The National Medical Journal of India, 12(6) pp. 270-274.

[34] Basu, B., Katti, D.S., and Kumar, A., 2009, "Advanced biomaterials fundamentals, processing, and applications," John Wiley & Sons, Hoboken, N.J., pp. 746.

[35] Rey, C., 1998, "Calcium Phosphates in Biological and Industrial Systems,"Kluwer Academic, Boston, Mass. ; London, pp. 217-253.

[36] Giavaresi, G., Tschon, M., Borsari, V., 2004, "New Polymers for Drug Delivery Systems in Orthopaedics: In Vivo Biocompatibility Evaluation," Biomedicine & Pharmacotherapy, 58(8) pp. 411-417.

[37] Ramakrishna, S., Mayer, J., Wintermantel, E., 2001, "Biomedical Applications of Polymer-Composite Materials: A Review," Composites Science and Technology, 61(9) pp. 1189-1224.

[38] Dumitriu, S., 1994, "Polymeric biomaterials," Marcel Dekker, New York, .

[39] Sinha, V. R., Bansal, K., Kaushik, R., 2004, "Poly-ε-Caprolactone Microspheres and Nanospheres: An Overview," International Journal of Pharmaceutics, 278(1) pp. 1-23.

[40] Rezwan, K., Chen, Q. Z., Blaker, J. J., 2006, "Biodegradable and Bioactive Porous polymer/inorganic Composite Scaffolds for Bone Tissue Engineering," Biomaterials, 27(18) pp. 3413-3431.

[41] Elzein, T., Nasser-Eddine, M., Delaite, C., 2004, "FTIR Study of Polycaprolactone Chain Organization at Interfaces," Journal of Colloid and Interface Science, 273(2) pp. 381-387.

[42] Pitt, C. G., Gratzl, M. M., Kimmel, G. L., 1981, "Aliphatic Polyesters II. the Degradation of Poly(D,L-Lactide), Poly(ε-Caprolactone) and their Copolymers in Vivo," Biomaterials, 2(4) pp. 215-220.

[43] Zhang, T., Gawne, D. T., and Bao, Y., 1997, "The Influence of Process Parameters on the Degradation of Thermally Sprayed Polymer Coatings," Surface & Coatings Technology, 96(2-3) pp. 337-344.

[44] Abou-Aiad, T. H. M., 2007, "Morphology and Dielectric Properties of Polyhydroxybutyrate (PHB)/poly(Methylmethacrylate) (PMMA) Blends with some Antimicrobial Applications," Polymer-Plastics Technology and Engineering, 46(4) pp. 435-439.

[45] Hagan, C. P., Orr, J. F., Mitchell, C. A., 2009, "Real Time Monitoring of the Polymerisation of PMMA Bone Cement using Raman Spectroscopy," Journal of Materials Science-Materials in Medicine, 20(12) pp. 2427-2431.

[46] Tihan, T. G., Ionita, M. D., Popescu, R. G., 2009, "Effect of hydrophilic–hydrophobic Balance on Biocompatibility of Poly(Methyl Methacrylate) (PMMA)–hydroxyapatite (HA) Composites," Materials Chemistry and Physics, 118(2-3) pp. 265-269.

[47] Zinn, M., Witholt, B., and Egli, T., 2001, "Occurrence, Synthesis and Medical Application of Bacterial Polyhydroxyalkanoate," Advanced Drug Delivery Reviews, 53(1) pp. 5-21.

[48] Holmes, P. A., 1985, "Applications of Phb - a Microbially Produced Biodegradable Thermoplastic," Physics in Technology, 16(1) pp. 32-36.

[49] Otari, S. V., and Ghosh, J. S., 2009, "Production and Characterisation of the Polymer Polyhydroxy Butyrate-Co-Polyhydroxy Valerate by *Bacillus Megaterium* NCIM2475," Current Research Journal of Biological Science, 1(2) pp. 23-26.

[50] Nair, L. S., and Laurencin, C. T., 2007, "Biodegradable Polymers as Biomaterials," Progress in Polymer Science, 32(8-9) pp. 762-798.

[51] Sabir, M. I., Xu, X., and Li, L., 2009, "A Review on Biodegradable Polymeric Materials for Bone Tissue Engineering Applications," Journal of Materials Science, 44(21) pp. 5713-5724.

[52] Iwata, T., Doi, Y., Tanaka, T., 1997, "Enzymatic Degradation and Adsorption on Poly[(R)-3-Hydroxybutyrate] Single Crystals with Two Types of Extracellular PHB Depolymerases from Comamonas Acidovorans YM1609 and Alcaligenes Faecalis T1," Macromolecules, 30(18) pp. 5290-5296.

[53] Schneider, S.J., and American Society for Metals. Handbook Committee, 1991, "Ceramics and glasses," ASM International, Metals Park, Ohio, .

[54] Gross, K. A., and Berndt, C. C., 1998, "Thermal Processing of Hydroxyapatite for Coating Production," Journal of Biomedical Materials Research, 39(4) pp. 580-587.

[55] Kuriakose, T. A., Kalkura, S. N., Palanichamy, M., 2004, "Synthesis of Stoichiometric Nano Crystalline Hydroxyapatite by Ethanol-Based Sol-Gel Technique at Low Temperature," Journal of Crystal Growth, 263(1-4) pp. 517-523.

[56] Schmitz, J. P., Hollinger, J. O., and Milam, S. B., 1999, "Reconstruction of Bone using Calcium Phosphate Bone Cements: A Critical Review," Journal of Oral and Maxillofacial Surgery, 57(9) pp. 1122-1126.

[57] Takezawa, Y., Doi, Y., Shibata, S., 1987, "Self-Setting Apatite Cement II. Hydroxyapatite as Setting Accelerator," J Jpn Soc Dental Mater Devices, 6pp. 426-431.

[58] Blokhuis, T. J., Termaat, M. F., den Boer, F. C., 2000, "Properties of Calcium Phosphate Ceramics in Relation to their in Vivo Behavior," The Journal of Trauma, 48(1) pp. 179.

[59] Wise, D.L., 1995, "Encyclopedic handbook of biomaterials and bioengineering," Marcel Dekker, New York, .

[60] Nicholson, J.W., 2002, "The chemistry of medical and dental materials," Royal Soc. of Chemistry, Cambridge, .

[61] LeGeros, R. Z., 2002, "Properties of Osteoconductive Biomaterials: Calcium Phosphates," Clinical Orthopaedics and Related Research, (395) pp. 81-98.

[62] Osborn, J. F., and Newesely, H., 1980, "The Material Science of Calcium Phosphate Ceramics," Biomaterials, 1(2) pp. 108-111.

[63] LeGeros, R. Z., Orly, I., Gregoire, M., 1991, "Substrate Surface Dissolution and Interfacial Biological Mineralization," The Bone-Biomaterial Interface, pp. 76–88.

[64] Heughebaert, M., LeGeros, R. Z., Gineste, M., 2004, "Physicochemical Characterization of Deposits Associated with HA Ceramics Implanted in Nonosseous Sites," Journal of Biomedical Materials Research, 22(S14) pp. 257-268.

[65] Jarcho, M., Kay, J. F., Gumaer, K. I., 1977, "Tissue, Cellular and Subcellular Events at a Bone-Ceramic Hydroxylapatite Interface," Journal of Bioengineering, 1(2) pp. 79-92.

[66] Hotz, G., and Herr, G., 1994, "Bone Substitute with Osteoinductive Biomaterials — Current and Future Clinical Applications," International Journal of Oral and Maxillofacial Surgery, 23(6, Part 2) pp. 413-417.

[67] Tsiridis, E., Bhalla, A., Zubier, A., 2006, "Enhancing the Osteoinductive Properties of Hydroxyapatite by the Addition of Human Mesenchymal Stem Cells, and Recombinant Human Osteogenic Protein-1 (BMP-7) in Vitro," Injury-International Journal of the Care of the Injured, 37pp. S25-S32.

[68] Sun, L. M., Berndt, C. C., Gross, K. A., 2001, "Material Fundamentals and Clinical Performance of Plasma-Sprayed Hydroxyapatite Coatings: A Review," Journal of Biomedical Materials Research, 58(5) pp. 570-592.

[69] Morscher, E. W., 1991, "Hydroxyapatite Coating of Prostheses," Journal of Bone and Joint Surgery-British Volume, 73(5) pp. 705-706.

[70] Kehoe, S., 2008, "Optimisation of Hydroxyapatite (HAp) for Orthopaedic Application Via the Chemical Precipitation Technique," .

[71] Suchanek, W., and Yoshimura, M., 1998, "Processing and Properties of Hydroxyapatite-Based Biomaterials for use as Hard Tissue Replacement Implants," Journal of Materials Research, 13(1) pp. 94-117.

[72] Vallet-Regi, M., 2001, "Ceramics for Medical Applications," Journal of the Chemical Society-Dalton Transactions, (2) pp. 97-108.

[73] Kutz, M., 2003, "Standard handbook of biomedical engineering and design," McGraw-Hill, New York ; London, .

[74] Wachter, N. J., Krischak, G. D., Mentzel, M., 2002, "Correlation of Bone Mineral Density with Strength and Microstructural Parameters of Cortical Bone in Vitro," Bone, 31(1) pp. 90-95.

[75] LeGeros, R. Z., 1988, "Calcium Phosphate Materials in Restorative Dentistry: A Review," Advances in Dental Research, 2(1) pp. 164.

[76] Khor, K. A., Gu, Y. W., Quek, C. H., 2003, "Plasma Spraying of Functionally Graded hydroxyapatite/Ti-6Al-4V Coatings," Surface & Coatings Technology, 168(2-3) pp. 195-201.

[77] Yang, Y. C., Chang, E., Hwang, B. H., 2000, "Biaxial Residual Stress States of Plasma-Sprayed Hydroxyapatite Coatings on Titanium Alloy Substrate," Biomaterials, 21(13) pp. 1327-1337.

[78] Bronzino, J.D., 2000, "The biomedical engineering handbook," CRC Press; Springer, Boca Raton, FL; Heidelberg, .

[79] Tsui, Y. C., Doyle, C., and Clyne, T. W., 1998, "Plasma Sprayed Hydroxyapatite Coatings on Titanium Substrates Part 1: Mechanical Properties and Residual Stress Levels," Biomaterials, 19(22) pp. 2015-2029.

[80] Li, H., Khor, K. A., and Cheang, P., 2004, "Thermal Sprayed Hydroxyapatite Splats: Nanostructures, Pore Formation Mechanisms and TEM Characterization," Biomaterials, 25(17) pp. 3463-3471.

[81] Black, J., and Hastings, G., 1998, "Handbook of biomaterial properties," Chapman & Hall, London, .

[82] Gibbons, D.E., 1982, "Biocompatibility of Orthopedic Implants,"CRC Press, Boca Raton, Fla., .

[83] Rokkum, M., Brandt, M., Bye, K., 1999, "Polyethylene Wear, Osteolysis and Acetabular Loosening with an HA-Coated Hip Prosthesis - A Follow-Up of 94 Consecutive Arthroplasties," Journal of Bone and Joint Surgery-British Volume, 81B(4) pp. 582-589.

[84] Liao, C. J., Lin, F. H., Chen, K. S., 1999, "Thermal Decomposition and Reconstitution of Hydroxyapatite in Air Atmosphere," Biomaterials, 20(19) pp. 1807-1813.

[85] Skinner, H. C. W., Kittelberger, J. S., and Beebe, R. A., 1975, "Thermal Instability in Synthetic Hydroxyapatites," Journal of Physical Chemistry, 79(19) pp. 2017-2019.

[86] Kijima, T., and Tsutsumi, M., 1979, "Preparation and Thermal-Properties of Dense Polycrystalline Oxyhydroxyapatite," Journal of the American Ceramic Society, 62(9-10) pp. 455-460.

[87] Wang, P. E., and Chaki, T. K., 1993, "Sintering Behavior and Mechanical-Properties of Hydroxyapatite and Dicalcium Phosphate," Journal of Materials Science-Materials in Medicine, 4(2) pp. 150-158.

[88] Tampieri, A., Celotti, G., Sprio, S., 2000, "Characteristics of Synthetic Hydroxyapatites and Attempts to Improve their Thermal Stability," Materials Chemistry and Physics, 64(1) pp. 54-61.

[89] Levingstone, T., 2008, "Optimisation of Plasma Sprayed Hydroxyapatite Coatings," .

[90] Doyle, C., Tanner, E. T., and Bonfield, W., 1991, "Invitro and Invivo Evaluation of Polyhydroxybutyrate and of Polyhydroxybutyrate Reinforced with Hydroxyapatite," Biomaterials, 12(9) pp. 841-847.

[91] Bucholz, R. W., Carlton, A., and Holmes, R., 1989, "Interporous Hydroxyapatite as a Bone-Graft Substitute in Tibial Plateau Fractures," Clinical Orthopaedics and Related Research, (240) pp. 53-62.

[92] Kim, H. W., Lee, S. Y., Bae, C. J., 2003, "Porous ZrO2 Bone Scaffold Coated with Hydroxyapatite with Fluorapatite Intermediate Layer," Biomaterials, 24(19) pp. 3277-3284.

[93] Kim, H. W., Noh, Y. J., Koh, Y. H., 2002, "Effect of CaF2 on Densification and Properties of Hydroxyapatite-Zirconia Composites for Biomedical Applications," Biomaterials, 23(20) pp. 4113-4121.

[94] Kim, H. W., Knowles, J. C., and Kim, H. E., 2004, "Hydroxyapatite/poly(Epsilon-Caprolactone) Composite Coatings on Hydroxyapatite Porous Bone Scaffold for Drug Delivery," Biomaterials, 25(7-8) pp. 1279-1287.

[95] Luklinska, Z. B., and Bonfield, W., 1997, "Morphology and Ultrastructure of the Interface between Hydroxyapatite-Polyhydroxybutyrate Composite Implant and Bone," Journal of Materials Science-Materials in Medicine, 8(6) pp. 379-383.

[96] Shishatskaya, E. I., Khlusov, I. A., and Volova, T. G., 2006, "A Hybrid PHBhydroxyapatite Composite for Biomedical Application: Production, in Vitro and in Vivo Investigation," Journal of Biomaterials Science, Polymer Edition, 17(5) pp. 481-498.

[97] Knowles, J. C., and Hastings, G. W., 1992, "Invitro Degradation of a Polyhydroxybutyrate Polyhydroxyvalerate Copolymer," Journal of Materials Science-Materials in Medicine, 3(5) pp. 352-358.

[98] Boeree, N. R., Dove, J., Cooper, J. J., 1993, "Development of a Degradable Composite for Orthopedic use - Mechanical Evaluation of an Hydroxyapatite Polyhydroxybutyrate Composite-Material," Biomaterials, 14(10) pp. 793-796.

[99] Luklinska, Z. B., and Schluckwerder, H., 2003, "In Vivo Response to HA-polyhydroxybutyrate/polyhydroxyvalerate Composite," Journal of Microscopy-Oxford, 211pp. 121-129.

[100] Tsukeoka, T., Suzuki, M., Ohtsuki, C., 2006, "Mechanical and Histological Evaluation of a PMMA-Based Bone Cement Modified with Gamma-Methacryloxypropyltrimethoxysilane and Calcium Acetate," Biomaterials, 27(21) pp. 3897-3903.

[101] Sun, L., Berndt, C.C., and Gross, K.A., 2001, "Characterization and mechanical properties of flame sprayed hyoroxyapatite/polymer composite coatings," ASM INTERNATIONAL, MATERIALS PARK; 9503 KINSMAN RD, MATERIALS PARK, OH 44073 USA, pp. 326.

[102] Huiskes, R., Weinans, H., and Dalstra, M., 1989, "Adaptive Bone Remodeling and Biomechanical Design Considerations - for Noncemented Total Hip-Arthroplasty," Orthopedics, 12(9) pp. 1255-1267.

[103] Sun, L. M., Berndt, C. C., and Gross, K. A., 2002, "Hydroxyapatite/polymer Composite Flame-Sprayed Coatings for Orthopedic Applications," Journal of Biomaterials Science-Polymer Edition, 13(9) pp. 977-990.

[104] Ural, E., Kesenci, K., Fambri, L., 2000, "Poly(D,L-cactide/epsilon-Caprolactone)/hydroxyapatite Composites," Biomaterials, 21(21) pp. 2147-2154.

[105] American Society for Metals. Handbook Committee, and American Society for Metals, 1990, "ASM handbook," ASM International, Materials Park, OH, .

[106] Clark, R.J.H., 1968, "The chemistry of titanium and vanadium : an introduction to the chemistry of the early transition elements," Elsevier Pub. Co, Amsterdam, .

[107] Long, M., and Rack, H. J., 1998, "Titanium Alloys in Total Joint Replacement - a Materials Science Perspective," Biomaterials, 19(18) pp. 1621-1639.

[108] Steinemann, S. G., 1998, "Titanium - the Material of Choice?" Periodontology 2000, 17pp. 7-21.

[109] Steinemann, S.G., 1980, "Evaluation of Biomaterials,"Wiley, New York, USA, .

[110] Semlitsch, M. F., Weber, H., Streicher, R. M., 1992, "Joint Replacement Components made of Hot-Forged and Surface-Treated Ti-6al-7nb Alloy," Biomaterials, 13(11) pp. 781-788.

[111] J.R. Davis & Associates, and ASM International. Thermal Spray Society Training Committee, 2004, "Handbook of thermal spray technology," ASM International, Materials Park, OH, .

[112] AWS Committee on Thermal Spraying, 1985, "Thermal Spraying: Practice, Theory, and Application," American Welding Society, Miami, Florida, pp. 183.

[113] Rossnagel, S.M., Cuomo, J.J., and Westwood, W.D., 1990, "Handbook of plasma processing technology : fundamentals, etching, deposition, and surface interactions," Noyes Publications, Park Ridge, N.J, .

[114] Fantassi, S., Vardelle, M., Fauchais, P., 1992, "Investigation of the Splat Formation Vs. Different Particulate Temperatures and Velocities Prior to Impact," Thermal Spray: International Advances in Coatings Technology, pp. 755-760.

[115] Leung, K., Heberlein, J., and Pfender, E., 1995, "Particle trajectory control with the use of different carrier gases," 8th National Thermal Spray Conference, ASM International, Anonymous pp. 39.

[116] Li, T. T., Lee, J. H., Kobayashi, T., 1996, "Hydroxyapatite Coating by Dipping Method, and Bone Bonding Strength," Journal of Materials Science-Materials in Medicine, 7(6) pp. 355-357.

[117] Raemdonck, W., Ducheyne, P., and Meester, P., 2006, "Auger Electron Spectroscopic Analysis of Hydroxylapatite Coatings on Titanium," Journal of the American Ceramic Society, 67(6) pp. 381-384.

[118] Jaffe, W. L., and Scott, D. F., 1996, "Total Hip Arthroplasty with Hydroxyapatite-Coated Prostheses," Journal of Bone and Joint Surgery-American Volume, 78A(12) pp. 1918-1934.

[119] Locardi, B., Pazzaglia, U. E., Gabbi, C., 1993, "Thermal-Behavior of Hydroxyapatite Intended for Medical Applications," Biomaterials, 14(6) pp. 437-441.

[120] Ong, J. L., and Lucas, L. C., 1994, "Post-Deposition Heat Treatments for Ion Beam Sputter Deposited Calcium Phosphate Coatings," Biomaterials, 15(5) pp. 337-341.

[121] Silva, P. L., Santos, J. D., Monteiro, F. J., 1998, "Adhesion and Microstructural Characterization of Plasma-Sprayed hydroxyapatite/glass Ceramic Coatings Onto Ti-6A1-4V Substrates," Surface and Coatings Technology, 102(3) pp. 191-196.

[122] Park, E., Condrate, R. A., Lee, D., 2002, "Characterization of Hydroxyapatite: Before and After Plasma Spraying," Journal of Materials Science-Materials in Medicine, 13(2) pp. 211-218.

[123] Sun, L. M., Berndt, C. C., Khor, K. A., 2002, "Surface Characteristics and Dissolution Behavior of Plasma-Sprayed Hydroxyapatite Coating," Journal of Biomedical Materials Research, 62(2) pp. 228-236.

[124] Anonymous "Implants for Surgery- Hydroxyapatite. Part1: Ceramic Hydroxyapatite," BS ISO13779-1:2000, pp. International Organisation for Standards, 2000.

[125] Anonymous "Implants for Surgery- Hydroxyapatite. Part2: Coatings Hydroxyapatite," BS ISO13779-2:2000, pp. International Organisation for Standards, 2000.

[126] Soballe, K., and Overgaard, S., 1996, "The Current Status of Hydroxyapatite Coating of Prostheses," Journal of Bone and Joint Surgery-British Volume, 78B(5) pp. 689-691.

[127] Ducheyne, P., Radin, S., and King, L., 1993, "The Effect of Calcium-Phosphate Ceramic Composition and Structure on Invitro Behavior .1. Dissolution," Journal of Biomedical Materials Research, 27(1) pp. 25-34.

[128] Weng, J., Liu, Q., Wolke, J. G. C., 1997, "The Role of Amorphous Phase in Nucleating Bone-Like Apatite on Plasma-Sprayed Hydroxyapatite Coatings in Simulated Body Fluid," Journal of Materials Science Letters, 16(4) pp. 335-337.

[129] Taylor, M. P., 1995, "Assessment of Plasma-Sprayed Hydroxyapatite Coatings," .

[130] Rouahi, M., Champion, E., Hardouin, P., 2006, "Quantitative Kinetic Analysis of Gene Expression during Human Osteoblastic Adhesion on Orthopaedic Materials," Biomaterials, 27(14) pp. 2829-2844.

[131] Heimann, R. B., 2006, "Thermal Spraying of Biomaterials," Surface and Coatings Technology, 201(5) pp. 2012-2019.

[132] Berndt, C. C., and Gross, K., 1992, "Characteristics of Hydroxylapatite Bio-Coatings," Thermal Spray: International Advances in Coatings Technology; Orlando, Florida; USA, pp. 465-470.

[133] Gross, K. A., and Babovic, M., 2002, "Influence of Abrasion on the Surface Characteristics of Thermally Sprayed Hydroxyapatite Coatings," Biomaterials, 23(24) pp. 4731-4737.

[134] Niederauer, G. G., McGee, T. D., Keller, J. C., 1994, "Attachment of Epithelial Cells and Fibroblasts to Ceramic Materials," Biomaterials, 15(5) pp. 342-352.

[135] Deligianni, D. D., Katsala, N. D., Koutsoukos, P. G., 2001, "Effect of Surface Roughness of Hydroxyapatite on Human Bone Marrow Cell Adhesion, Proliferation, Differentiation and Detachment Strength," Biomaterials, 22(1) pp. 87-96.

[136] Geesink, R. G. T., Degroot, K., and Klein, C. P. A. T., 1987, "Chemical Implant Fixation using Hydroxyl-Apatite Coatings - the Development of a Human Total Hip-Prosthesis for Chemical Fixation to Bone using Hydroxyl-Apatite Coatings on Titanium Substrates," Clinical Orthopaedics and Related Research, (225) pp. 147-170.

[137] De Groot, K., 1987, "High Tech Ceramics,"Elsevier, Amsterdam, pp. 381-386.

[138] Brown, S. D., 1984, "The Medical-Physiological Potential of Plasma-Sprayed Ceramic Coatings," Thin Solid Films, 119(2) pp. 127-139.

[139] Matejka, D., and Benko, B., 1989, "Plasma spraying of metallic and ceramic materials," Wiley, New York, .

[140] Pawłowski, L., 1995, "The science and engineering of thermal spray coatings," Wiley, Chichester ; New York, pp. 414.

[141] Heimann, R.B., 1996, "Plasma-spray coating : principles and applications," Vch, Weinheim ; Cambridge, .

[142] Yang, Y. C., and Chang, E., 2001, "Influence of Residual Stress on Bonding Strength and Fracture of Plasma-Sprayed Hydroxyapatite Coatings on Ti–6Al–4V Substrate," Biomaterials, 22(13) pp. 1827-1836.

[143] Bennett, A., 1986, "Properties of Thermal Barrier Coatings," Materials Science and Technology, 2(3) pp. 257-261.

[144] Evans, A. G., Crumley, G. B., and Demaray, R. E., 1983, "On the Mechanical Behavior of Brittle Coatings and Layers," Oxidation of Metals, 20(5) pp. 193-216.

[145] Scardi, P., Leoni, M., and Bertamini, L., 1996, "Residual Stresses in Plasma Sprayed Partially Stabilised Zirconia TBCs: Influence of the Deposition Temperature," Thin Solid Films, 278(1-2) pp. 96-103.

[146] Eberhardt, A. W., Zhou, C., and Rigney, E. D., 1994, "Bending and thermal stresses in a fatigue experiment of hydroxyapatite coated titanium rods," Proc 7th National Thermal Spray Conf ASM Int, Anonymous pp. 165—9.

[147] Sergo, V., Sbaizero, O., and Clarke, D. R., 1997, "Mechanical and Chemical Consequences of the Residual Stresses in Plasma Sprayed Hydroxyapatite Coatings," Biomaterials, 18(6) pp. 477-482.

[148] Yang, Y. C., 2007, "Influence of Residual Stress on Bonding Strength of the Plasma-Sprayed Hydroxyapatite Coating After the Vacuum Heat Treatment," Surface and Coatings Technology, 201(16-17) pp. 7187-7193.

[149] Yang, Y. C., Chang, E., and Lee, S. Y., 2003, "Mechanical Properties and Young's Modulus of Plasmasprayed Hydroxyapatite Coating on Ti Substrate in Simulated Body Fluid," Journal of Biomedical Materials Research Part a, 67A(3) pp. 886-899.

[150] Yang, Y. C., and Chang, E., 2003, "The Bonding of Plasma-Sprayed Hydroxyapatite Coatings to Titanium: Effect of Processing, Porosity and Residual Stress," Thin Solid Films, 444(1-2) pp. 260-275.

[151] Standard specification for composition of ceramic hydroxylapatite for surgical implants, F1185-88:415-5, "ASTM 1988;" .

[152] Sobolev, V. V., and Guilemany, J. M., 1999, "Flattening of Droplets and Formation of Splats in Thermal Spraying: A Review of Recent Work - Part 1," Journal of Thermal Spray Technology, 8(1) pp. 87-101.

[153] Fauchais, P., Fukumoto, M., Vardelle, A., 2004, "Knowledge Concerning Splat Formation: An Invited Review," Journal of Thermal Spray Technology, 13(3) pp. 337-360.

[154] Zhang, T., Gawne, D. T., and Bao, Y., 1996, "The Effect of Deposition Parameters on the Degradation of Plasma Sprayed Polymer Coatings," Thermal Spray: Practical Solutions for Engineering Problems.Materials Park: ASM International, pp. 231-237.

[155] Ivosevic, M., Cairncross, R. A., and Knight, R., 2006, "3D Predictions of Thermally Sprayed Polymer Splats: Modeling Particle Acceleration, Heating and Deformation on Impact with a Flat Substrate," International Journal of Heat and Mass Transfer, 49(19-20) pp. 3285-3297.

[156] Allen, N.S., and Edge, M., 1992, "Fundamentals of polymer degradation and stabilisation," Elsevier Science Publishers, .

[157] Croft, D.R., and Lilley, D.G., 1977, "Heat transfer calculations using finite difference equations," Applied Science Publishers, London, .

[158] Liao, H., Beche, E., and Coddet, C., 1998, "On the microstructure of thermally sprayed “PEEK” polymer," Thermal Spray: Meeting the Challenges of the 21st Century, ASM International, Materials Park, OH, Anonymous pp. 25–301.

[159] Bao, Y., and Gawne, D. T., 1991, "Plasma Spray Deposition of Nylon-11 Coatings," Transactions of the Institute of Metal Finishing, 69pp. 80-85.

[160] Pitt, C.G., 1990, "Biodegradable Polymers as Drug Delivery Systems,"Dekker, New York, pp. 71-119.

[161] Brogan, J. A., and Berndt, C. C., 1997, "The Coalescence of Combustion-Sprayed Ethylene Methacrylic Acid Copolymer," Journal of Materials Science, 32(8) pp. 2099-2106.

[162] Brogan, J. A., 2000, "Thermal-Spraying of Polymers and Polymer Blends," MRS Bulletin, 25(7) pp. 48-53.

[163] Skorokhod, A. Z., Pisanova, E. V., Zhandarov, S. F., 1995, "Transformation of Polymers in a Stream of Low-Temperature Arc Discharge Plasma," Journal of Applied Polymer Science, 57(11) pp. 1263-1268.

[164] Petrovicova, E., and Schadler, L. S., 2002, "Thermal Spraying of Polymers," International Materials Reviews, 47(4) pp. 169-190.

[165] Bao, Y., Gawne, D. T., and Zhang, T., 1998, "Effect of thermal spray parameters on the adhesion of polymer-based coatings on steel," Thermal spray: A united forum for scientific and technological advances, Anonymous pp. 209-213.

[166] Petrovicova, E., 1999, "Structure and Properties of Polymer Nano-Composite Coating Applied by the HVOF Process," .

[167] Bao, Y., Gawne, D. T., Vesely, D., 1994, "Formation and Microstructure of Plasma Sprayed Polyamide Coatings," Surface Engineering, 10(4) pp. 307-313.

[168] Humphrey, J. S., Mehta, S., Seaber, A. V., 1998, "Pharmacokinetics of a Degradable Drug Delivery System in Bone," Clinical Orthopaedics and Related Research, (349) pp. 218-224.

[169] Garvin, K. L., and Hanssen, A. D., 1995, "Current Concepts Review Infection After Total Hip-Arthroplasty Past, Present, and Future," Journal of Bone and Joint Surgery-American Volume, 77(10) pp. 1576-1588.

[170] Garvin, K. L., Miyano, J. A., Robinson, D., 1994, "Polylactide/polyglycolide Antibiotic Implants in the Treatment of Osteomyelitis - a Canine Model," Journal of Bone and Joint Surgery-American Volume, 76A(10) pp. 1500-1506.

[171] Lloyd, A. W., 2002, "Interfacial Bioengineering to Enhance Surface Biocompatibility," Medical Device Technology, 13(1) pp. 18-21.

[172] Yagmurlu, M. F., Korkusuz, F., Gursel, I., 1999, "Sulbactam-Cefoperazone Polyhydroxybutyrate-Co-Hydroxyvalerate (PHBV) Local Antibiotic Delivery System: In Vivo Effectiveness and Biocompatibility in the Treatment of Implant-Related Experimental Osteomyelitis," Journal of Biomedical Materials Research, 46(4) pp. 494-503.

[173] Gursel, I., and Hasirci, V., 1995, "Properties and Drug Release Behaviour of Poly (3-Hydroxybutyric Acid) and various," J.MICROENCAPSULATION, 12(2) pp. 185-181.

[174] Khang, G., Kim, S. W., Cho, J. C., 2001, "Preparation and Characterization of Poly(3-Hydroxybutyrate-Co-3-Hydroxyvalerate) Microspheres for the Sustained Release of 5-Fluorouracil," Bio-Medical Materials and Engineering, 11(2) pp. 89-103.

[175] Sendil, D., Gursel, I., Wise, D. L., 1999, "Antibiotic Release from Biodegradable PHBV Microparticles," Journal of Controlled Release, 59(2) pp. 207-217.

[176] Coombes, A. G. A., Rizzi, S. C., Williamson, M., 2004, "Precipitation Casting of Polycaprolactone for Applications in Tissue Engineering and Drug Delivery," Biomaterials, 25(2) pp. 315-325.

[177] Nandi, S. K., Mukherjee, P., Roy, S., 2009, "Local Antibiotic Delivery Systems for the Treatment of Osteomyelitis – A Review," Materials Science and Engineering: C, 29(8) pp. 2478-2485.

[178] Jyothi, N. V. N., Prasanna, P. M., Sakarkar, S. N., 2010, "Microencapsulation Techniques, Factors Influencing Encapsulation Efficiency," Journal of Microencapsulation, 27(3) pp. 187-197.

[179] Maia, J. L., Santana, M. H. A., and Re, M. I., 2004, "The Effect of some Processing Conditions on the Characteristics of Biodegradable Microspheres obtained by an Emulsion Solvent Evaporation Process," Brazilian Journal of Chemical Engineering, 21(1) pp. 1-12.

[180] Blanco-Prieto, M. J., Lecaroz, C., Renedo, M. J., 2002, "In Vitro Evaluation of Gentamicin Released from Microparticles," International Journal of Pharmaceutics, 242(1-2) pp. 203-206.

[181] Simioni, A. R., Vaccari, C., Re, M. I., 2008, "PHBHV/PCL Microspheres as Biodegradable Drug Delivery Systems (DDS) for Photodynamic Therapy (PDT)," Journal of Materials Science, 43(2) pp. 580-584.

[182] Schnieders, J., Gbureck, U., Thull, R., 2006, "Controlled Release of Gentamicin from Calcium Phosphate - Poly(Lactic Acid-Co-Glycolic Acid) Composite Bone Cement," Biomaterials, 27(23) pp. 4239-4249.

[183] Prior, S., Gamazo, C., Irache, J. M., 2000, "Gentamicin Encapsulation in PLA/PLGA Microspheres in View of Treating Brucella Infections," International Journal of Pharmaceutics, 196(1) pp. 115-125.

[184] Patel, P., Mundargi, R. C., Babu, V. R., 2008, "Microencapsulation of Doxycycline into Poly(Lactide-Co-Glycolide) by Spray Drying Technique: Effect of Polymer Molecular Weight on Process Parameters," Journal of Applied Polymer Science, 108(6) pp. 4038-4046.

[185] Nijenhuis, A. J., Colstee, E., Grijpma, D. W., 1996, "High Molecular Weight Poly(-Lactide) and Poly(Ethylene Oxide) Blends: Thermal Characterization and Physical Properties," Polymer, 37(26) pp. 5849-5857.

[186] Ciapetti, G., Ambrosio, L., Savarino, L., 2003, "Osteoblast Growth and Function in Porous Poly Epsilon-Caprolactone Matrices for Bone Repair: A Preliminary Study," Biomaterials, 24(21) pp. 3815-3824.

[187] Iooss, P., Le Ray, A. M., Grimandi, G., 2001, "A New Injectable Bone Substitute Combining Poly(□-Caprolactone) Microparticles with Biphasic Calcium Phosphate Granules," Biomaterials, 22(20) pp. 2785-2794.

[188] Jameela, S. R., Suma, N., and Jayakrishnan, A., 1997, "Protein Release from Poly(Epsilon-Caprolactone) Microspheres Prepared by Melt Encapsulation and Solvent Evaporation Techniques: A Comparative Study," Journal of Biomaterials Science-Polymer Edition, 8(6) pp. 457-466.

[189] Rossi, S., Azghani, A. O., and Omri, A., 2004, "Antimicrobial Efficacy of a New Antibiotic-Loaded Poly(Hydroxybutyric-Co-Hydroxyvaleric Acid) Controlled Release System," Journal of Antimicrobial Chemotherapy, 54(6) pp. 1013-1018.

[190] Majid, S. A., Lindberg, L. T., Gunterberg, B., 1985, "Gentamicin-Pmma Beads in the Treatment of Chronic Osteomyelitis," Acta Orthopaedica Scandinavica, 56(3) pp. 265-268.

[191] Stabile, D. E., and Jacobs, A. M., 1990, "Development and Application of Antibiotic-Loaded Bone-Cement Beads," Journal of the American Podiatric Medical Association, 80(7) pp. 354-359.

[192] Henry, S. L., and Galloway, K. P., 1995, "Local Antibacterial Therapy for the Management of Orthopedic Infections - Pharmacokinetic Considerations," Clinical Pharmacokinetics, 29(1) pp. 36-45.

[193] Moroni, A., Hoang-Kim, A., Lio, V., 2006, "Current Augmentation Fixation Techniques for the Osteoporotic Patient," Scandinavian Journal of Surgery, 95(2) pp. 103-109.

[194] De Giglio, E., Cometa, S., Sabbatini, L., 2005, "Electrosynthesis and Analytical Characterization of PMMA Coatings on Titanium Substrates as Barriers Against Ion Release," Analytical and Bioanalytical Chemistry, 381(3) pp. 626-633.

[195] Zhang, X. C., Wyss, U. P., Pichora, D., 1994, "Biodegradable Controlled Antibiotic Release Devices for Osteomyelitis - Optimization of Release Properties," Journal of Pharmacy and Pharmacology, 46(9) pp. 718-724.

[196] Hendricks, K. J., Lane, D., Burd, T. A., 2001, "Elution Characteristics of Tobramycin from Polycaprolactone in a Rabbit Model," Clinical Orthopaedics and Related Research, (392) pp. 418-426.

[197] Dash, A. K., and Suryanarayanan, R., 1991, "Solid-State Properties of Tobramycin," Pharmaceutical Research, 8(9) pp. 1159-1165.

[198] Wang, G., Liu, S. J., Ueng, S. W. N., 2004, "The Release of Cefazolin and Gentamicin from Biodegradable PLA/PGA Beads," International Journal of Pharmaceutics, 273(1-2) pp. 203-212.

[199] Rosenkrantz, B.E., Greco, J.R., Hoogerheide, J.G., 1980, "Analytical Profiles of Drug Substances,"Academic Press, London, pp. 295.

[200] Fernandes, N. S., Carvalho, M. A. D., Mendes, R. A., 1999, "Thermal Decomposition of some Chemotherapic Substances," Journal of the Brazilian Chemical Society, 10(6) pp. 459-462.

[201] Montgomery, D.C., 2008, "Design and analysis of experiments," John Wiley & Sons Inc, .

[202] Anonymous "Sulzer Metco Product Data Sheet," (03/14) .

[203] Scott, K.T., and Kingswell, R., 1991, "Advanced Surface Coatings: A Handbook of Surface Engineering,"Chapman and Hall, New York, pp. 217-243.

[204] Griffiths, B. J., Gawne, D. T., and Dong, G., 1997, "The Role of Grit Blasting in the Production of High-Adhesion Plasma Sprayed Alumina Coatings," Proceedings of the Institution of Mechanical Engineers Part B-Journal of Engineering Manufacture, 211(1) pp. 1-9.

[205] Amada, S., and Hirose, T., 1998, "Influence of Grit Blasting Pre-Treatment on the Adhesion Strength of Plasma Sprayed Coatings: Fractal Analysis of Roughness," Surface and Coatings Technology, 102(1-2) pp. 132-137.

[206] Anonymous "ZEISS EVO LS15 SEM Instruction Manual," .

[207] British Standard Institution, ""Sample Preparation Dispersing Procedures for Powders in Liquids"," BS ISO 14887:2000, 2000, .

[208] British Standard Institution, ""Particle Size Analysis- Laser Diffraction Methods- Part 1: General Principles"," BS ISO 13320-1:1999, 1999, .

[209] Anonymous "Micromeritics AccuPyc 1330 Instruction Manual," .

[210] ASTM international, "' the Standard Practice for X-Ray Determination of Phase Content of Plasma-Sprayed Hydroxyapatite Coatings'," ASTM F 2024-00, 2000, .

[211] Fischerscope Operating Principles, "Http://www.Helmut-Fischer.com/globalfiles/DE_MMS_EN.Pdf," .

[212] Helmut-Fischer, "Fischersope Operating Manual," .

[213] Packham, D.E., 2005, "Handbook of adhesion," Wiley, .

[214] Ardhaoui, M., Naciri, M., Mullen, T., 2010, "Evaluation of Cell Behaviour on Atmospheric Plasma Deposited Siloxane and Fluorosiloxane Coatings," Journal of Adhesion Science and Technology, 24(5) pp. 889-903.

[215] Lu, L., Garcia, C. A., and Mikos, A. G., 1999, "In Vitro Degradation of Thin Poly(DL-Lactic-Co-Glycolic Acid) Films," Journal of Biomedical Materials Research, 46(2) pp. 236-244.

[216] Pascu, E. I., 2010, "Biomimetic and Biodegradable Scaffolds for Hard Tissue Engineering," Dublin City University, .

[217] Arnett, T. R., 2008, "Extracellular pH Regulates Bone Cell Function," Journal of Nutrition, 138(2) pp. 415S-418S.

[218] International Standard Organisation, "Biological Evaluation of Medical Devices-Part5: Tests for *in Vitro* Cytotoxicity," ISO10993-5, .

[219] Bahbou, M. F., Nylen, P., and Wigren, J., 2004, "Effect of Grit Blasting and Spraying Angle on the Adhesion Strength of a Plasma-Sprayed Coating," Journal of Thermal Spray Technology, 13(4) pp. 508-514.

[220] Ivosevic, M., Gupta, V., Baldoni, J. A., 2006, "Effect of Substrate Roughness on Splatting Behavior of HVOF Sprayed Polymer Particles: Modeling and Experiments," Journal of Thermal Spray Technology, 15(4) pp. 725-730.

[221] Tambe, S. P., Singh, S. K., Patri, M., 2008, "Ethylene Vinyl Acetate and Ethylene Vinyl Alcohol Copolymer for Thermal Spray Coating Application," Progress in Organic Coatings, 62(4) pp. 382-386.

[222] Ramanath, H. S., Chua, C. K., Leong, K. F., 2008, "Melt Flow Behaviour of Poly-Epsilon-Caprolactone in Fused Deposition Modelling," Journal of Materials Science-Materials in Medicine, 19(7) pp. 2541-2550.

[223] Minakov, A. A., and Schick, C., 1999, "Advanced AC Calorimetry of Polycaprolactone in Melting Region," Thermochimica Acta, 330(1-2) pp. 109-119.

[224] Immergut, E.H., and Brandrup, J., 1975, "Polymer handbook," Wiley New York, .

[225] Kweh, S. W. K., Khor, K. A., and Cheang, P., 2000, "Plasma-Sprayed Hydroxyapatite (HA) Coatings with Flame-Spheroidized Feedstock: Microstructure and Mechanical Properties," Biomaterials, 21(12) pp. 1223-1234.

[226] U.S. Food and Drug Administration, 1992, "Calcium Phosphate (Ca-P) Coating Draft Guidance for Preparation of FDA Submissions for Orthopaedic and Dental Endosseous Implants," .

[227] Gourlaouen, V., Dominguez, R., and Mendelsohn, M., 1999, "Plastic coating properties obtained by flame spraying process and their applications," Proceedings of the United Thermal Spray Conference, E. Lugscheider and P. A. Kammer, eds. DVS, Dusseldorf, pp. 841-845.

[228] Bao, Y., Gawne, D. T., and Zhang, T., 1995, "The Effect of Feedstock Particle-Size on the Heat-Transfer Rates and Properties of Thermally Sprayed Polymer-Coatings," Transactions of the Institute of Metal Finishing, 73pp. 119-124.

[229] Bento, A. C., Almond, D. P., Brown, S. R., 1996, "Thermal and Optical Characterization of the Calcium Phosphate Biomaterial Hydroxyapatite," Journal of Applied Physics, 79(9) pp. 6848-6852.

[230] Liu, L., Guo, S., Chang, J., 2008, "Surface Modification of Polycaprolactone Membrane Via Layer-by-Layer Deposition for Promoting Blood Compatibility," Journal of Biomedical Materials Research Part B-Applied Biomaterials, 87B(1) pp. 244-250.

[231] Yildirim, E. D., Besunder, R., Pappas, D., 2010, "Accelerated Differentiation of Osteoblast Cells on Polycaprolactone Scaffolds Driven by a Combined Effect of Protein Coating and Plasma Modification," Biofabrication, 2(1) pp. 014109.

[232] Chen, F., Lee, C. N., and Teoh, S. H., 2007, "Nanofibrous Modification on Ultra-Thin Poly(Epsilon-Caprolactone) Membrane Via Electrospinning," Materials Science & Engineering C-Biomimetic and Supramolecular Systems, 27(2) pp. 325-332.

[233] Li, Y., Pham, J. Q., Johnston, K. P., 2007, "Contact Angle of Water on Polystyrene Thin Films: Effects of CO2 Environment and Film Thickness," Langmuir, 23(19) pp. 9785-9793.

[234] Zhang, T., Bao, Y., Gawne, D. T., 2011, "Effect of a Moving Flame on the Temperature of Polymer Coatings and Substrates," Progress in Organic Coatings, 70(1) pp. 45-51.

[235] Hadad, M., Marot, G., Demarecaux, P., 2007, "Adhesion Tests for Thermal Spray Coatings: Correlation of Bond Strength and Interfacial Toughness," Surface Engineering, 23(4) pp. 279-283.

[236] Greving, D. J., Shadley, J. R., and Rybicki, E. F., 1994, "Effects of Coating Thickness and Residual-Stresses on the Bond Strength of Astm C633-79 Thermal Spray Coating Test Specimens," Journal of Thermal Spray Technology, 3(4) pp. 371-378.

[237] Allen, L. T., Tosetto, M., Miller, I. S., 2006, "Surface-Induced Changes in Protein Adsorption and Implications for Cellular Phenotypic Responses to Surface Interaction," Biomaterials, 27(16) pp. 3096-3108.

[238] Lee, J. H., and Lee, H. B., 1993, "A Wettability Gradient as a Tool to Study Protein Adsorption and Cell-Adhesion on Polymer Surfaces," Journal of Biomaterials Science-Polymer Edition, 4(5) pp. 467-481.

[239] Salehi, A., Tsai, S., Pawar, V., 2006, "Wettability Analysis of Orthopaedic Materials using Optical Contact Angle Methods," Bioceramics 18, Pts 1 and 2, 309-311pp. 1199-1202.

[240] Jaeger, M., Urselmann, F., Witte, F., 2008, "Osteoblast Differentiation Onto Different Biometals with an Endoprosthetic Surface Topography in Vitro," Journal of Biomedical Materials Research Part a, 86A(1) pp. 61-75.

[241] Rathbone, S., Furrer, P., Luebben, J., 2010, "Biocompatibility of Polyhydroxyalkanoate as a Potential Material for Ligament and Tendon Scaffold Material," Journal of Biomedical Materials Research Part a, 93A(4) pp. 1391-1403.

[242] Hsieh, W. C., Wada, Y., Mitobe, T., 2009, "Effect of Hydrophilic and Hydrophobic Monomers Grafting on Microbial Poly(3-Hydroxybutyrate)," Journal of the Taiwan Institute of Chemical Engineers, 40(4) pp. 413-417.

[243] Li, X., Liu, K. L., Wang, M., 2009, "Improving Hydrophilicity, Mechanical Properties and Biocompatibility of Poly[(R)-3-Hydroxybutyrate-Co-(R)-3-Hydroxyvalerate] through Blending with Poly[(R)-3-Hydroxybutyrate]-Alt-Poly(Ethylene Oxide)," Acta Biomaterialia, 5(6) pp. 2002-2012.

[244] Dowling, D. P., Miller, I. S., Ardhaoui, M., 2010, "Effect of Surface Wettability and Topography on the Adhesion of Osteosarcoma Cells on Plasma-Modified Polystyrene," Journal of Biomaterials Applications, .

[245] Schmidmaier, G., Wildemann, B., Stemberger, A., 2001, "Biodegradable Poly(D,L-Lactide) Coating of Implants for Continuous Release of Growth Factors," Journal of Biomedical Materials Research, 58(4) pp. 449-455.

[246] Benoit, M. A., Mousset, B., Delloye, C., 1997, "Antibiotic-Loaded Plaster of Paris Implants Coated with Polylactide-Co-Glycolide as a Controlled Release Delivery System for the Treatment of Bone Infections," International Orthopaedics, 21(6) pp. 403-408.

[247] Celina, M., Ottesen, D. K., Gillen, K. T., 1997, "FTIR Emission Spectroscopy Applied to Polymer Degradation," Polymer Degradation and Stability, 58(1-2) pp. 15-31.

[248] Wang, Y., Wu, G., Chen, X., 2009, "Rapid Calcification on Solution Blending of Homogenous PHBV/Collagen Composite," Journal of Applied Polymer Science, 112(2) pp. 963-970.

[249] Kemavongse, K., Prasertsan, P., Upaichit, A., 2008, "Poly-Beta-Hydroxyalkanoate Production by Halotolerant Rhodobacter Sphaeroides U7," World Journal of Microbiology & Biotechnology, 24(10) pp. 2073-2085.

[250] Asenjo, J. A., Schmidt, A. S., Andersen, P. R., 1995, "Effect of Single Nutrient Limitation of poly-β-hydroxybutyrate Molecular Weight Distribution in Alcaligens Europhus," Biotechnology and Bioengineering, 46(5) pp. 497-502.

[251] Fabbri, P., Bondioli, F., Messori, M., 2010, "Porous Scaffolds of Polycaprolactone Reinforced with in Situ Generated Hydroxyapatite for Bone Tissue Engineering," Journal of Materials Science-Materials in Medicine, 21(1) pp. 343-351.

[252] Noohom, W., Jack, K. S., Martin, D., 2009, "Understanding the Roles of Nanoparticle Dispersion and Polymer Crystallinity in Controlling the Mechanical Properties of HA/PHBV Nanocomposites," Biomedical Materials, 4(1) pp. 015003.

[253] Incardona, S., Migliaresi, C., Daniel Wagner, H., 1993, "The Mechanical Role of the fibre/matrix Transcrystalline Interphase in Carbon Fibre Reinforced j-Polymer Microcomposites," Composites Science and Technology, 47(1) pp. 43-50.

[254] Heidemann, W., Jeschkeit-Schubbert, S., Ruffieux, K., 2002, "PH-Stabilization of Predegraded PDLLA by an Admixture of Water-Soluble Sodiumhydrogenphosphate-Results of an in Vitro- and in Vivo-Study," Biomaterials, 23(17) pp. 3567-3574.

[255] Martin, C., Winet, H., and Bao, J. Y., 1996, "Acidity Near Eroding Polylactide-Polyglycolide in Vitro and in Vivo in Rabbit Tibial Bone Chambers," Biomaterials, 17(24) pp. 2373-2380.

[256] Priya, A., Nath, S., Biswas, K., 2010, "In Vitro Dissolution of Calcium Phosphate-Mullite Composite in Simulated Body Fluid," Journal of Materials Science-Materials in Medicine, 21(6) pp. 1817-1828.

[257] Coulembier, O., Degee, P., Hedrick, J. L., 2006, "From Controlled Ring-Opening Polymerization to Biodegradable Aliphatic Polyester: Especially Poly(Beta-Malic Acid) Derivatives," Progress in Polymer Science, 31(8) pp. 723-747.

[258] Zhang, R. Y., and Ma, P. X., 2004, "Biomimetic polymer/apatite Composite Scaffolds for Mineralized Tissue Engineering," Macromolecular Bioscience, 4(2) pp. 100-111.

[259] Orban, J. M., Marra, K. G., and Hollinger, J. O., 2002, "Composition Options for Tissue-Engineered Bone," Tissue Engineering, 8(4) pp. 529-539.

[260] Xiao, X., Liu, R., Huang, Q., 2009, "Preparation and Characterization of hydroxyapatite/polycaprolactone-Chitosan Composites," Journal of Materials Science-Materials in Medicine, 20(12) pp. 2375-2383.

[261] Mohammadi, M. S., Ahmed, I., Marelli, B., 2010, "Modulation of Polycaprolactone Composite Properties through Incorporation of Mixed Phosphate Glass Formulations," Acta Biomaterialia, 6(8) pp. 3157-3168.

[262] Li, H. Y., Du, R. L., and Chang, J., 2005, "Fabrication, Characterization, and in Vitro Degradation of Composite Scaffolds Based on PHBV and Bioactive Glass," Journal of Biomaterials Applications, 20(2) pp. 137-155.

[263] Petersson, I. U., Loberg, J. E. L., Fredriksson, A. S., 2009, "Semi-Conducting Properties of Titanium Dioxide Surfaces on Titanium Implants," Biomaterials, 30(27) pp. 4471-4479.

[264] Thamaraiselvi, T. V., and Rajeswari, S., "Biological Evaluation of Bioceramic Materials-a Review," Carbon, 24(31) pp. 172.

[265] Micusik, M., Omastova, M., Prokes, J., 2006, "Mechanical and Electrical Properties of Composites Based on Thermoplastic Matrices and Conductive Cellulose Fibers," Journal of Applied Polymer Science, 101(1) pp. 133-142.

[266] Basavaraja, C., Kim, D. G., Kim, W. J., 2011, "Morphology and Charge Transport Properties of Chemically Synthesized Polyaniline-Poly(Epsilon-Caprolactone) Polymer Films," Bulletin of the Korean Chemical Society, 32(3) pp. 927-933.

[267] Sanchez-Garcia, M. D., Lagaron, J. M., and Hoa, S. V., 2010, "Effect of Addition of Carbon Nanofibers and Carbon Nanotubes on Properties of Thermoplastic Biopolymers," Composites Science and Technology, 70(7) pp. 1095-1105.

[268] Lutjering, G., and Williams, J.C., 2003, "Titanium," Springer, New York, .

[269] Malberg, S., Hoglund, A., and Albertsson, A. C., 2011, "Macromolecular Design of Aliphatic Polyesters with Maintained Mechanical Properties and a Rapid, Customized Degradation Profile," Biomacromolecules, 12(6) pp. 2382-2388.

[270] Lagaron, J. M., Gimenez, E., and Saura, J. J., 2001, "Degradation of High Barrier Ethylene-Vinyl Alcohol Copolymer Under Mild Thermal-Oxidative Conditions Studied by Thermal Analysis and Infrared Spectroscopy," Polymer International, 50(6) pp. 635-642.

[271] Cool, S. M., Kenny, B., Wu, A., 2007, "Poly(3-Hydroxybutyrate-Co-3-Hydroxyvalerate) Composite Biomaterials for Bone Tissue Regeneration: In Vitro Performance Assessed by Osteoblast Proliferation, Osteoclast Adhesion and Resorption, and Macrophage Proinflammatory Response," Journal of Biomedical Materials Research Part a, 82A(3) pp. 599-610.

Appendix A- Statistical Measures

R^2

The R^2 value indicates the degree of the relationship of the response variable to the combined linear predictor variables. It is an estimate of the overall variation in the data accounted for by the model. The R^2value is calculated as follows:

$$R^2 = \frac{(SS - SSresid)}{SS}$$

The R^2 value is a number between 0 and +1. The closer the value is to one the better the model is.

Adjusted R^2

The Adjusted R^2 value is an estimate of the fraction of the overall variation in the data accounted for by the model. It is the R^2 value adjusted for the terms in the model relative to the number of points in the design.

$$R_{adj}^{\ 2} = \frac{(MS - MSresid)}{MS}$$

$MS = SS/(n-1)$; $MS_{resid} = SS_{resid}/(n-p$; n = number of experimental runs; p = number of terms in the model, including the constant

Predicted R^2

The Predicted R^2 value measures the amount of variation in new data explained by the model.

$$Predicted\ R^2 = \frac{1 - SSPRESS}{(SStotal - SSblocks)}$$

For an adequate model the Predicted R^2 and Adjusted R^2 values should be within 0.2 of each other.

Adequate Precision

The adequate precision is a measure of the range in predicted response relative to its associated error, in other words the signal to noise ratio. It should be greater than 4.

Factor Coding in Factorial Design

Design descriptions and analyses for designed experiments are best done with coded factors. Coding reduces the range of each factor to a common scale, generally -1 to +1, regardless of its relative magnitude. Scaling establishes factor levels that can be orthogonal (or nearly so). Also, it may be easier to think in terms of changes from low to high for the factors than to think about their actual values - especially when thinking about squared terms and interactions. For example, one factor may vary from 100 to 200 while another varies from 0.1 to 0.5. Typical coding has -1 as the lower level of a factor, +1 as the upper level, and 0 as the middle level. The values used for coding are called contrasts. The default contrasts generate coefficients that have simple interpretations.

After building the design, you can freely choose to display either **coded** or **actual** levels of the factors at any time from the **Display Options** menu.

Examples

1) 2-level Nominal and Ordinal Categoric Factors

	[A]
Level1	-1
Level2	1

For a two-level categorical factor the coefficient "[A]" is half the difference between the averages at the high and low values. (The same as for a two-level numeric factor.)

2) 3-level Nominal Categoric Factor

	A[1]	A[2]
Level1	1	0
Level2	0	1
Level3	-1	-1

For multi-level discrete categorical factors the first coefficient "A[1]" is the difference of level 1 from the overall average, the second coefficient "A[2]" is the difference of level 2

from the overall average and so on. The last coefficient is not independent and is equal to the overall average minus the sum of the other coefficients.

3) 3-level Ordinal Categoric Factor (equal spacing between levels)

	A[1]	A[2]
10	-1	1
20	0	-2
30	1	1

This form of contrasts is often referred to as orthogonal polynomial contrasts. Here, the coefficient "A[1]" represents the linear component, and A[2] represents the quadratic component. If there were more levels, cubic, quartic, quintic and higher polynomial level components are given.

4) 3-level Ordinal Categoric Factor (unequal spacing between levels)

	A[1]	A[2]
10	-5	3
20	-2	-4
50	7	1

The contrasts with unequal spacing have the same meaning as those with equal spacing, i.e. linear, quadratic, etc. But, as you can see, the contrast values are very different because they have to account for the odd spacing.

5) Blocks

For blocks, the default contrasts estimate the difference between the block average and the overall average. In other words, adding the block correction to the intercept estimates that block's average.

Appendix B- Sample Holder Movement

An x-y sample holder based on a pneumatic cylinder was designed by previous machine operator and used in this project. The pneumatic system controlling the sample mover is shown in the figure below.

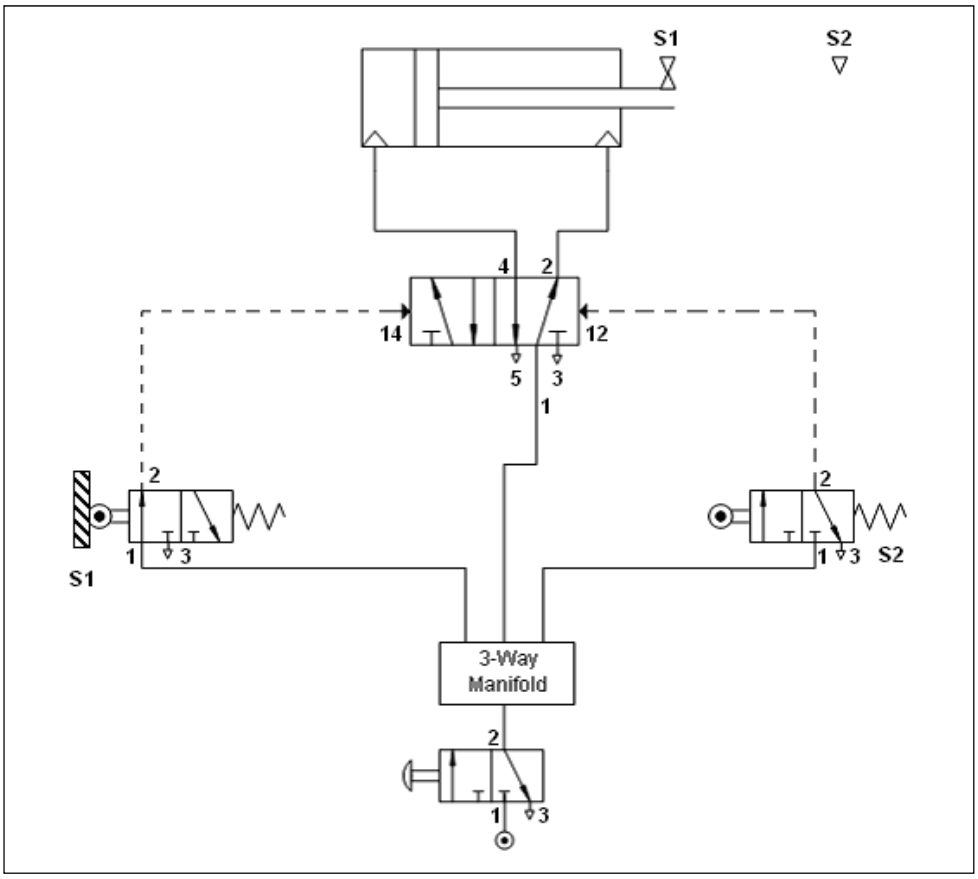

When the compressed air supply is switched on, air enters a 3-way manifold. Air flows from here to a 5/2 way valve and two spring return 3/2 way valves. The 5/2 way valve allows air to flow into one side of the pneumatic cylinder. The cylinder moves until it hits the roller switch (S2). The cylinder then moves back in the opposite direction until it hits the roller switch at the other end (S1). The speed at which the cylinder travels is controlled by valves that adjust the flow of air at each side of the cylinder.

Appendix C- Plasma Equipment Operating Instructions

Start-up

1. Ensure that both water valves are open at the wall. These supply water to cool the plasma gun and can be left open at all times unless maintenance work is being carried out.
2. Open the compressed air and argon gas valves, located on the wall behind the powder feeder at the wall. Argon is used as the primary gas. The primary gas pressure on the gauge on the control unit should be set to 75 psi.
3. Argon is also used as the powder carrying gas. The pressure for this gas also needs to be set at 75 psi. This can be checked on the gauge on the powder feeder unit.
4. The secondary gas pressure should be 50 psi. Although a secondary gas is not currently being used, there still needs to be sufficient secondary gas pressure in order for the system to operate. Argon is currently been used to supply this secondary gas pressure.
5. To switch on the control unit, turn the red and yellow 'Main Power' knob clockwise.
6. Initially the control unit will display: VENTILATION FAULT
7. This message will disappear once the pressure in the electrical component box has built-up enough.
8. The control unit will then display: E-STOP/ GASES ON
9. The powder feeder unit will display: EMERGENCY STOP
10. Press the white 'System On' button in the automatic gun operation panel on the control unit. 9MC SYSTEM READY
11. The control unit will then display:
12. The cooling water flow rate can now been seen displayed on the junction box. This is usually 11.9 l/min. If the flow rate drops too low an alarm will sound and it won't be possible to run the spray equipment.

Extraction System

1. The extraction unit should be switched on when spraying, setting up gas flow rates and setting up powder feed rates. It should be left on for a few minutes after spraying to ensure that all gases and powders are properly removed from the spray room. Ear protection should be worn when the extraction system is on.
2. To switch on the extraction system press the green start button on the side of the extraction system.
3. The extraction system light can also be turned on at the side of the extraction system.

Gas Flow Rate Set-Up

1. To set the Gas Flow Rate press the white 'Purge' button on the test panel on the control panel. Hold in this button until the following steps have been completed.
2. The control panel display will now read: SYSTEM PURGING
3. While purging, check around the gun for any water leaks. Check the nozzle and also the hoses and hose connection points. If there are leaks stop the system and check all o-rings and connections.
4. If everything is ok, check the primary gas pressure once again to ensure it is at 75 psi; adjust if necessary.
5. Set the primary gas flow rate to the required level by turning the black dial below the primary gas flow rate gauge.
6. The carrier gas flow rate can be set by turning the black dial above the carrier gas pressure gauge on the powder feeder to the required value.
7. The secondary gas flow valve should not be opened unless a secondary gas is being used.

Current

1. The current can be changed by turning the current dial. Lock the current at this value by pushing the knob on the dial.

Powder Hopper

1. Put powder into the hopper. There must be enough powder in the hopper to cover the powder pick up shaft. The weight of powder in the hopper is shown on the display.
2. To ensure that the powder does not run out during spraying, put enough powder in the hopper to cover the pick up shaft and then set the weight to zero.
3. Push the 'Set Points' button to set the powder flow rate required.
4. Enter the value required and press 'Enter'.

Powder Feeder Auto set-up

1. An auto-set-up should be run every time powder is added to the hopper, the powder feed rate is changed or the carried gas flow rate is changed. This determines the pressure required in the hopper to feed the powder at the set rate.
2. Remove the powder injector from the plasma gun and place into the powder collection pot.
3. Push the shift button on the powder feeder and then press local to set the hopper to be controlled locally.
4. Press the 'Auto Set-Up' button.
5. The display will say: WAITING FOR SIGNAL
6. Switch the black knob on the automatic gun operation panel on the control unit from preheat to spray and switch the powder feed knob on the test panel from feed off to feed on.
7. The powder feeder will run until the feed rate stabilises at the correct value. If it does not stabilise in time the auto set-up will fail and need to be run again.
8. Once auto-set-up is complete, set the powder feeder back to remote operation by pushing shift and then 'Remote'.
9. A number of alarms can be set on the powder feeder, for example an alarm can be set to come on if the spray rate drifts excessively.

Sample Mover

1. Set the spray distance to the required value by moving the sample holder in the y-direction along the sliding rails.
2. Mount the sample in the sample holder, ensuring that it is tightly clamped in place.
3. Turn on the second compressor by switching on the power at the wall and ensuring that the key is open at the back of the compressor.
4. Once the pressure has built up and the compressor cuts out, open the valve on the compressor to release any water vapour in the system.
5. Allow the pressure to build up again and turn on the sample mover by turning the red valve on the side of the extraction equipment.
6. Turn off the sample mover and ensure that it stops at one end of its stroke.

Spraying

1. Ensure that all personal protection equipment is being worn.
2. Before igniting the plasma gun, gas must be purged though the gas lines to get rid of any air, contamination or moisture that may be present.
3. Press the white 'Purge' button on the test panel on the control unit. Hold this button for 5 – 10 seconds.
4. The control panel display will now read: | SYSTEM PURGING |

5. Next press the 'Ignition' button on the test panel of the control unit to test for a spark. The control unit panel will read:

| IGNITION TEST/ COOL DOWN |

6. Hold this button for about 10 seconds, until the display reads:

| 9MC SYSTEM READY |

7. To start spraying, press the green 'Start' button in the automatic gun operation panel on the control unit.

8. The system will try three times to ignite the plasma flame. If ignition is unsuccessful the display: IGNITION FAILURE
9. If this occurs, press the emergency stop on the control unit and allow the system to cool down for about a minute. Switch on the control unit again and re-run the steps in this section.
10. When ignition occurs the current will ramp up to the set value.
11. When the current reaches the correct value the powder feed can be turned on by turning the knob from 'Preheat' to 'Spray' and turn the feed from 'Feed Off' to 'Feed On'.
12. Turn on the sample mover. Start the stop watch and spray for the required time.
13. Stop spraying by pressing the black 'Stop' button in the automatic gun operation panel on the control unit.
14. Turn off the spray and powder feed.
15. Stop the sample mover and allow the sample to cool completely before removing from the sample holder.

Turning off the equipment

1. Turn off the argon and compressed air. If hydrogen is being used the compressed air must remain on to maintain a positive pressure in the control unit and prevent hydrogen coming in contact with the electrical components
2. Turn off the control unit by turning the red 'Main Power' knob and also press the emergency stop button.
3. The powder feeder can be left on.
4. Turn off the extraction system.
5. Turn off the second compressor.

Emptying the Hopper

1. Open the powder feeder and slide the hopper out along its rails.
2. Open the catch on the lid and open the lid.
3. Place a container underneath the hopper and open the catch at the bottom of the hopper. Let the powder fall into the container.
4. Clean out the hopper with a brush and compressed air

Appendix D- Biological Analysis

Preliminary biological analysis consisted of assessment of cell viability (XTT) and osteoblast function/differentiation (alkaline phosphatise-ALP) at time points day 3 and day 7. Unfortunately, contamination of all samples occurred in the initial experiment, including the control wells. The numerous potential sources of the contamination made it impossible to identify the reason behind the fungal growth. This contamination could have been a once-off case or could be consistent. It is not common practice to isolate and identify the source of contamination for short and initial biological studies as this would take considerable amount of time and resources. A repeat was performed with the addition of antibiotics (penicillin-streptomycin and Fundizone (Amphotericin B)) to prevent further contamination.

It is important to note that the cell line used in the post-DOE biological study (osteoblast-like MG-63) was different from the one used for the preliminary biological assessment (Human Osteoblasts, HOB). Cells were initially seeded at a density of 10,000 cell per well.

Cell Viability

As previously mentioned, the samples were supposed to be incubated for a period of 3 and 7 days initially. However, the results of the XTT assay after 3 days did not yield significant cell activity. It was then decided to extend the second incubation period to 9 days.

The results obtained of the XTT assay at day 9 were unusually low and did not reflect the cell numbers in control wells (tissue culture plastic). It is unclear at this point why the readings obtained were low. Future work would involve validating that the reagents in the XTT assay were dissolving fully and functioning correctly. Viability on the surfaces could also be validated using an alternative viability assay such as Alamar Blue.

Additionally, the state of the cell line used in the experiment became a concern. In fact, even the control well with a high cell density did not yield significant data. The batch used for this study was stored in liquid nitrogen for an unknown period of time and following thawing of the cells, weeks were necessary for cells to grow and proliferate to a sufficient number for the assays. It is thought that prolonged freezing might have an effect on the

cell's health, especially if one of the steps in the cryopreservation protocol was not performed properly. Future use of the XTT assay kit or any other proliferation assays along with the MG-63 cell line could be done following an optimisation of the protocol to suit the specificities of this study.

Alkaline Phosphatase

Alkaline phosphatase is expressed during the osteoblast maturation stage. As for the XTT assay, the ALP activity after 3 days was inconclusive due to the low value obtained, including those of the control well. At day 9, the ALP activity was at a level sufficient to allow a comparison between different types of coatings to be made.

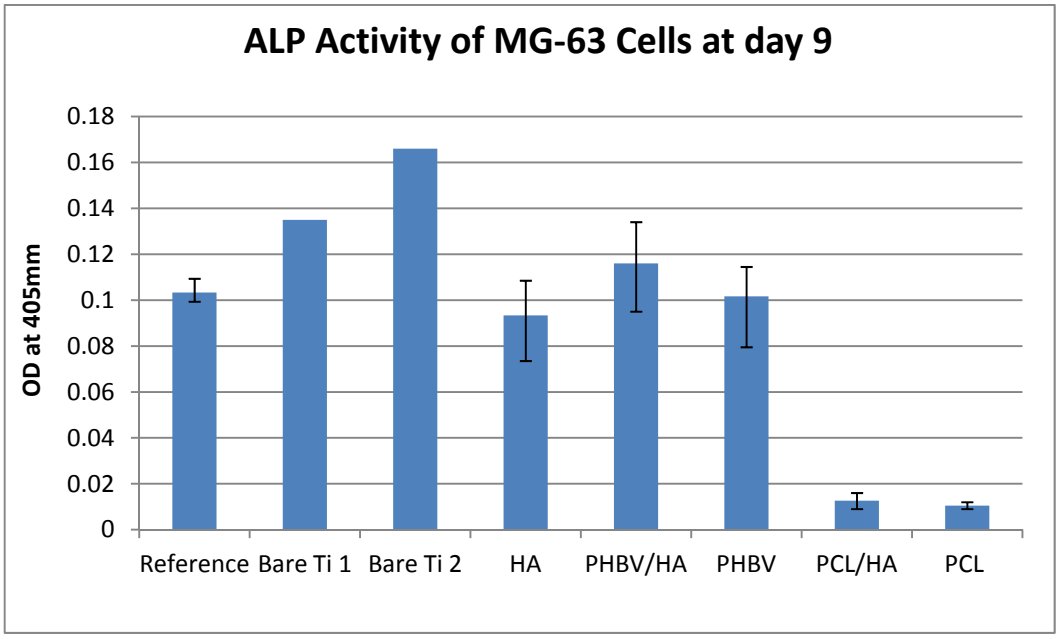

Figure 100: Alkaline phosphatase assay results after 9 days

Figure 100 shows that the PHBV based coatings performed better than the pure HA coatings and much better than the PCL based coatings, which confirms the suitability of PHBV polymers for bone replacement applications. The ALP activity on the PHBV samples was lower than that of the bare titanium sample, keeping in mind that only two Ti discs (as opposed to three samples) were used which could affect the average optical density at 450mm.

PHBV/HA showed more positive results compared to HA, PHBV, PCL/HA and PCL. Similar observations were made by Cool et al. [271] suggesting that the addition of a reinforcing ceramic phase to PHBV can vastly improve the *in vitro* cell response of PHBV biomaterials. In fact, the pro-inflammatory response was greatly reduced for PHBV/HA composite material than for pure PHBV [271]. It was also found that osteoblasts differentiated and mineralised most strongly on PHBV/HA. Further biological validation is required, this includes further replicates on the surfaces for viability and alkaline phosphatise activities as well as investigating cell morphology, osteocalcin levels and mineralisation.

Finally, further clarification of the duration effects and application of these polymers is definitely a potential for further research.